College of Engineering
Virginia Polytechnic Institute and State University
Blacksburg, Virginia 24061

May 1995

VPI-E-95-01

Load Transfer in the Stiffener-To-Skin Joints of a Pressurized Fuselage

Eric R. Johnson[1]
Naveen Rastogi[2]

Department of Aerospace and Ocean Engineering

NASA Grant NAG-1-537

Performance Period:
November 1, 1991 to April 30, 1995

Prepared for:

Structural Mechanics Branch
Structures Division
National Aeronautics and Space Administration
Langley Research Center
Hampton, VA 23681-0001

---

1. Professor, Department of Aerospace and Ocean Engineering, Virginia Polytechnic Institute and State University
2. Graduate Research Assistant, Department of Aerospace and Ocean Engineering, Virginia Polytechnic Institute and State University

ABSTRACT

Structural analyses are developed to determine the linear elastic and the geometrically nonlinear elastic response of an internally pressurized, orthogonally stiffened, composite material cylindrical shell. The configuration is a long circular cylindrical shell stiffened on the inside by a regular arrangement of identical stringers and identical rings. Periodicity permits the analysis of a unit cell model consisting of a portion of the shell wall centered over one stringer-ring joint. The stringer-ring-shell joint is modeled in an idealized manner; the stiffeners are mathematically permitted to pass through one another without contact, but do interact indirectly through their mutual contact with the shell at the joint. Discrete beams models of the stiffeners include a stringer with a symmetrical cross section and a ring with either a symmetrical or an asymmetrical open section. Mathematical formulations presented for the linear response include the effect of transverse shear deformations and the effect of warping of the ring's cross section due to torsion. These effects are important when the ring has an asymmetrical cross section because the loss of symmetry in the problem results in torsion and out-of-plane bending of the ring, and a concomitant rotation of the joint at the stiffener intersection about the circumferential axis. Data from a composite material crown panel typical of a large transport fuselage structure are used for two numerical examples. Although the inclusion of geometric nonlinearity reduces the "pillowing" of the shell, it is found that bending is localized to a narrow region near the stiffener. Including warping deformation of the ring into the analysis changes the sense of the joint rotation. Transverse shear deformation models result in increased joint flexibility.

ACKNOWLEDGEMENT

This work is supported by the Structural Mechanics Branch, NASA Langley Research Center, under grant NAG-1-537. Dr. James H. Starnes, Jr. is the technical monitor. Technical discussions with Dr. Starnes concerning the subject of this work were most helpful.

TABLE OF CONTENTS

LIST OF TABLES

LIST OF FIGURES

CHAPTER 1
INTRODUCTION

1.1 COMPOSITE MATERIALS IN PRIMARY STRUCTURES

Composite materials are being used increasingly for variety of structural applications in aerospace engineering and other related weight sensitive applications where high strength-to-weight and stiffness-to-weight ratios are required. The success of composite materials results from the ability to make use of the outstanding strength, stiffness and low specific gravity of fibres such as glass, graphite or Kevlar. When superior specific mechanical properties are combined with the unique flexibility in design and the ease of fabrication that composites offer, it is no wonder that their growth rate has far surpassed that of other materials.

Development of the state-of-the-art manufacturing techniques has made it possible to replace complicated structural components/assemblies by single co-cured or adhesively bonded composite parts, thereby minimizing the number of fasteners to be used in a structure, and hence, enhancing the structural integrity. While the use of bonded composite structures as secondary and tertiary load carrying members has been widespread in aerospace industry, their use as primary load carrying members is still very limited. Most of the applications of composites as primary structural components have been in the area of fabrication of empennage or control surfaces of an aircraft. Thus, the potential of composite materials as a primary load carrying structure, such as fuselage of an aircraft, has not been fully realized yet. One of the main reasons for this could be the lack of confidence of aerospace industry in utilizing composite materials for fuselage manufacturing, which, in turn, could be due to the lack of a full scale analysis, design, and testing

to qualify composite materials for use in the fuselage of both civil and military transport aircraft.

1.2 FUSELAGE LOADS AND DESIGN

As described in the text by Niu[1], the loads affecting fuselage design of a transport aircraft can result from flight maneuvers, landings, cabin pressurization and ground handling, etc. Fuselage (or cabin) pressurization of a transport aircraft induces hoop and longitudinal stresses in the fuselage. The fuselage internal pressure depends on the cruise altitude and the comfort desired for the flight crew and/or passengers, and can cause a pressure differential of up to 10 psi across the fuselage skin. An unstiffened, or monocoque, fuselage would carry this internal pressure load as a shell in membrane response, like a pressure vessel. However, internal longitudinal and transverse stiffeners are necessary to carry the loads resulting from flight maneuvers, landings, and ground handling, etc. The longitudinal stiffeners, called stringers or longerons, carry the major portion of the fuselage bending moment. The transverse stiffeners, called frames or rings, are spaced at regular intervals along the length of the fuselage to prevent buckling of the longitudinals and maintain cross-sectional shape of the fuselage. The presence of these internal stiffeners introduces the following two important aspects in the fuselage design of a transport aircraft:

1. The stiffeners, i.e. stringers and rings, are attached to the fuselage skin by some kind of fasteners, or perhaps bonded to it. Thus, there is a transmission of loads between the skin and the stiffeners all along their attachment lines, and at the stiffeners' intersection a local concentration of the interacting loads due to joint stiffness occurs. Understanding of the load transfer mechanism in the stiffener-to-skin joints under pressurization is necessary for determining the load capacity of these joints.

2. The presence of internal stiffeners, particularly the presence of frames or rings, prevents expansion of the fuselage skin as a membrane, and the skin bulges, or "pillows", between the stiffeners under the action of the internal presure as shown in Fig. 1.1. Hence, where the skin is restrained against its expansion as a membrane along the stiffeners, a bending boundary layer is formed.

1.3 STIFFENER-TO-SKIN JOINTS

The design of stiffener-to-skin joints was cited by Jackson et al.[2] as one of the major technology issues in utilizing graphite/epoxy composites in the fuselage of a large transport aircraft. In order to realize the full potential of advanced composites in lightweight aircraft structure, it is particularly important to ensure that the joints, either adhesively bonded or mechanically fastened, do not impose a reduced efficiency on the structure and should be cost effective as well. The use of graphite/epoxy composites in conjunction with metal fasteners in conventional, mechanically fastened joints is a critical design factor. Improper coupling of joint materials can cause serious corrosion problems to metals because of the difference in electric potential between these metals and graphite. In other words, insuring the galvanic compatibility of fastener materials with graphite composites is essential to avoid corrosion problems in the structure[3,4].

It has been established that materials such as titanium, corrosion-resistant steels, nickel and cobalt alloys can be coupled to graphite composites without such corrosive effects. In contrast, aluminum, magnesium and stainless steel are most adversely affected because of the difference in electric potential between these materials and graphite, and their use would lead to serious corrosion problems in the structure. However, fasteners made of materials such as titanium, corrosion-resistant steels, nickel and cobalt alloys are much more expensive than the more conventional fastner materials like aluminum, magnesium and stainless steel, etc. With thousands of fasteners, e.g., rivets, bolts, nuts,

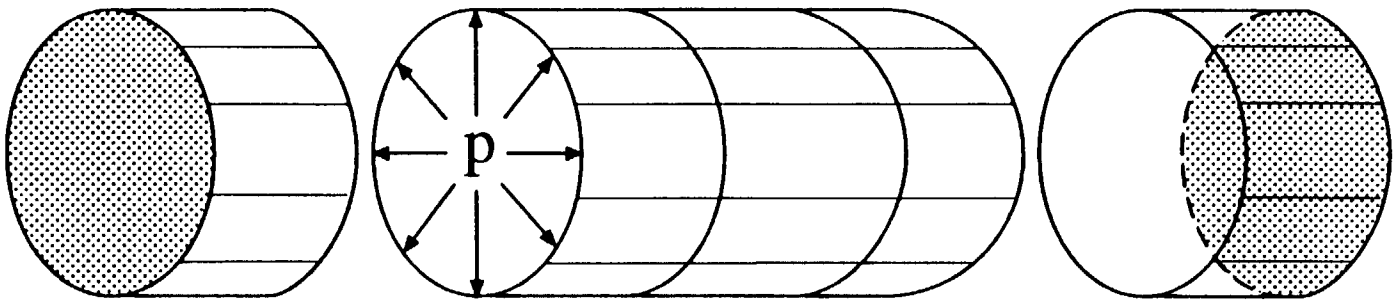

IDEALIZED STIFFENED FUSELAGE

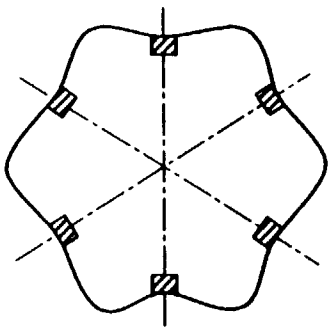

RADIAL EXPANSION
END VIEW

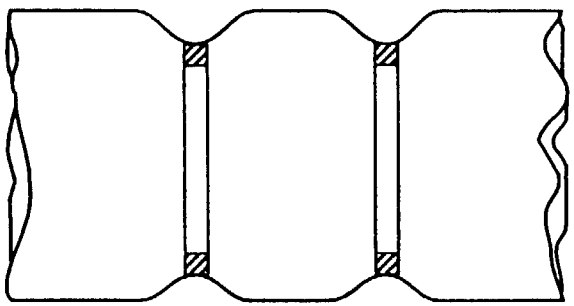

RADIAL EXPANSION
SIDE VIEW

Fig.1.1 Orthogonally stiffened cylindrical shell subjected to internal pressure.

etc. required to assemble stiffeners to the fuselage skin for a large transport aircraft, mechanically fastened joints using corrosion-resistant materials are costly and may offset the advantages of using high strength-to-weight composite materials in structures where assembly of two or more components is imperative. Niu[1] has pointed out that, in general, adhesively bonded joints are more cost efficient for lightly loaded joints, and mechanically fastened joints are more cost efficient for highly loaded joints. Thus, if the loads transferred between the stiffeners and the fuselage skin are small enough, the adhesively bonded joints can be used thereby eliminating all or most fasteners. Elimination of fasteners, or even a reduction in the number of fasteners, would enhance the use of advanced composite materials in fuselage of a transport aircraft. As an example, a graphite-epoxy crown panel for the fuselage of a large transport aircraft was recently fabricated without fasteners by co-curing the stringers and co-bonding the rings, or frames, to the skin[5,6]. Also, the curved graphite-epoxy fuselage frames were manufactured by resin transfer molding into two-dimensional braided preforms of net structural shape[7]. Clearly, the strength of the bond line is a critical issue for these primary fuselage structures made from advanced composite materials.

1.4 CONTACT PROBLEMS

As described in the monograph by Grigoluk and Tolkachev[8], contact (or load diffusion) problems occur in the theory of plates and shells when dealing with interaction of plates and shells with rigid and elastic bodies (stamps), stiffening ribs/stiffeners, and with plate-shell contacts. The class of contact problems can also include laminated plates and shells, if one introduces reactions of interaction between layers. Furthermore, they pointed out that the selection of the theory used to formulate the given contact problem may also influence the final results.

The study of load diffusion in the stiffener-to-skin joints of an orthogonally stiffened shell subjected to internal pressure is also a shell contact problem. The type of structural theory used to model the discrete elements, i.e., the shell, the stringer, and the ring, influences the distribution of the interacting loads at the shell-stiffener interface. A brief literature survey on the work done in the area of contact problems is presented in the remainder of this section.

Contact problems have always attracted scientists, academicians and designers alike because of their inherent importance for any structure analysis involving an assembly of two or more components. The first work is by Melan[9], who considered a semi-infinite plate with an infinite stiffener attached to its edge. A concentrated longitudinal force is applied to the stiffener. In 1932, Melan obtained a closed form solution for tangential forces in the plate along the line of stiffener attachment and also for the axial force in the stiffener. Buell[10], in 1948, analyzed a semi-infinite plate to which a semi-infinite stiffener is attached, loaded at the origin with a longitudinal force. An infinite series solution for the airy stress function reduced the problem to an infinite set of algebraic equations, and Buell obtained a numerical solution by reducing the set to six equations in six unknowns. A solution to Buell's problem and an identical problem for an infinite plate were obtained by Koiter[11] in 1955. Using as a Green's function the solution with a concentrated force, Koiter obtained a singular integral equation for the interacting tangential force between the stiffener and the plate. Through a series of complex mathematical steps using Mellin transformation, Koiter found the longitudinal force in the stiffener as an infinite series. Koiter's solution can serve as a criterion of exactness of Buell's numerical solution.

The load diffusion problem for a finite stiffener attached to an infinite plate was first solved by Benscooter[12] in 1949. He obtained an integro-differential equation, of the same form as the Prandtl equation for the distribution of aerodynamic forces in aircraft wing

(also known as monoplane equation), with stiffener axial force as an unknown variable. First, Benscooter expanded the variable into a series of Chebyshev polynomials of the second kind to obtain the discretized equations, and then solved them for unknown coefficients. Budiansky and Wu[13] extended Melan's problem for the case where the stiffener is rivetted to the plate at discrete points with constant spacing. Subsequent to some of these landmark works, numerous authors have studied the load diffusion problem between sheet and stiffener. An extensive biblography on the subject is given in Chapter 3 of Ref. [8].

As for circular cylindrical shells stiffened by longtudinal stiffeners, studies are few. Fischer[14] was the first to analyze an infinitely long circular cylindrical shell reinforced by equally spaced, continuously attached longitudinal stiffeners, each stiffener being loaded by a single concentrated longitudinal force (a counterpart of Melan's plate problem). Fischer accounted for bending of stiffeners and obtained a solution for the membrane shearing stress transmitted by a loaded stringer to the shell, and the axial stress developed within the stringer. Grigoluk and Tolkachev[8] also analyzed this problem but did not take into account the bending of stiffeners. A detailed biblography on some other types of shell contact problems can be found in Chapter 8 of Ref. [8].

1.5 PRESSURIZED, STIFFENED SHELLS

A literature survey on the work done in the area of stiffened shells under internal pressure suggests that in the past, only a few studies have been carried out in this area. In 1952, Flügge[15] studied the stress problems in pressurized cabins of high altitude aircraft by dividing it into two problems. First problem was concerned with curved walls of the cabin or pressure vessel, hence was called shell problem. The second problem, called the plate problem, was concerned with small rectangular panels of the cabin wall, framed by stiffeners. Of interest here are the former problems where Flügge obtained analytical

expressions for stresses in the shell and the stiffeners (i.e., stringer and ring) for a single cylinder model, and a double cylinder model, using a smeared stiffness approach. In 1958, Houghton[16] computed the stresses occuring in stringer reinforced pressurized cylindrical shells due to restraining action of the frames. He presented results showing the effect of variation of frame pitch and stiffness on the bending moment and shear force in the skins, and the hoop stress in the skins between the frames. Houghton's analysis was limited to metallic components, and did not take into account the eccentricity of stiffeners with respect to the skin. Pressure-cabin problems are described in Chapter 9 of Williams[17] 1960 text on aircraft structures. In the preface Williams justified the need for a chapter devoted to this subject on the importance of high speed civil air-transport. The effect of frames and bulkheads on the stresses in a cabin shell was considered in some detail, and it was shown how the presence of reinforcing stringers *de-localizes* the constricting effect of a frame or bulkhead. Williams analyses were also limited to metallic components, and did not take into account the eccentricity of stiffeners with respect to the skin. Wang[18], in 1970, carried out a discrete analysis of a metallic, orthogonally stiffened cylindrical shell subjected to internal pressure. Stiffener eccentricity, the normal component of interacting load between shell and stiffeners, and closed-end pressure vessel effects were taken into account. In 1985, Wang and Hsu[19] improved the earlier work by including in the analysis, a composite material shell wall, interacting shear forces between the skin and stiffeners, and a direct accounting of closed-end pressure vessel effects. In both of these works, the results were obtained for a linear elastic response and symmetric stiffeners. Skin-stiffener interactions were computed but results for them were not presented. In 1985, Boitnott[20] examined by experiment and analysis the pressure pillowing of a cylindrical composite panel clamped in a stiff fixture. Boitnott's geometrically nonlinear analysis correlated well with the experiments when panel slip from the fixture was taken into account. The

analysis showed that the boundary layer decay length decreased with increasing pressure and decreasing panel thickness.

1.6 OBJECTIVES

In the light of the foregoing discussions, it seems pertinent and timely to extend the work in the area of pressurized, stiffened shells by including in the analysis some of the features which would improve the understanding of the subject and hence, further reinforce the support for the design of a composite material fuselage for a large transport aircraft. The objectives of the present research work are to develop analyses of an orthogonally stiffened, laminated composite, cylindrical shell subjected to internal pressure. The stiffeners and shell are modeled as distinct elements in order to make available in the analyses

- the distribution of the interacting loads between the shell and stiffeners, and
- the stress concentration in the shell adjacent to the stiffeners due to "pillowing".

Other analysis issues to be addressed in support of these objectives include

- geometrically nonlinear response versus linear response, and
- the influence of a ring, or frame, with an asymmetrical open cross section on the linear elastic response.

The intent is to develop analyses that could be used for the design of stiffener-to-skin joints and the design of laminated wall construction for the skin. A potential benefit of such an analysis/design capability is (i) to use fewer expensive fasteners in the graphite/epoxy fuselage, and (ii) to obtain an optimum structural geometery (e.g. shell wall thickness and lay-up, frame and stringer stiffnesses, and stiffener spacing etc.) for an optimum interface load distribution.

1.7 PROBLEM DEFINITION

An idealized model is assumed for the semi-monocoque fuselage. This configuration is a closed-end, stiffened, pressurized shell in which closure is mathematically presumed to occur at infinity. The long circular cylindrical shell is stiffened on the inside by a regular arrangement of identical stringers and identical rings (frames). With respect to the applied internal pressure load, which is assumed spatially uniform, the model is periodic in the circumferential and longitudinal directions both in geometry and in material properties. Periodicity of this configuration permits the analysis of a portion of the shell wall centered over a generic stringer-ring joint as shown in Fig. 1.2; i.e., deformation of a structural unit cell (or repeating unit) determines the deformation of the entire stiffened shell. The radius of the middle surface of the undeformed cylindrical shell is denoted by R, and the thickness of the shell is denoted by t. Axial coordinate x and the circumferential angle θ are lines of curvature on the middle surface, and the thickness coordinate is denoted by z, with $-t/2 \leq z \leq t/2$. The origin of the surface coordinates is centered over the stiffeners' intersection so that $-l \leq x \leq l$ and $-\Theta \leq \theta \leq \Theta$, where $2l$ is the axial length, and $2R\Theta$ is the circumferential arc length of the repeating unit. The stringer is assumed to have a symmetrical cross section, and the frame is assumed to have either an asymmetrical or a symmetrical open section. Asymmetrical open section frames are commonly used as transverse stiffeners in the fuselage structure. The stiffeners are modeled as discrete beams perfectly bonded to the inside shell wall, so that the interacting loads between the stiffeners and shell wall are line load intensities. These line load intensities represent resultants of the tractions integrated across the width of the attachment flanges of the stiffeners.

Mathematical formulations for the linear elastic and a geometrically nonlinear elastic response are presented in this work. The formulations for the linear elastic response

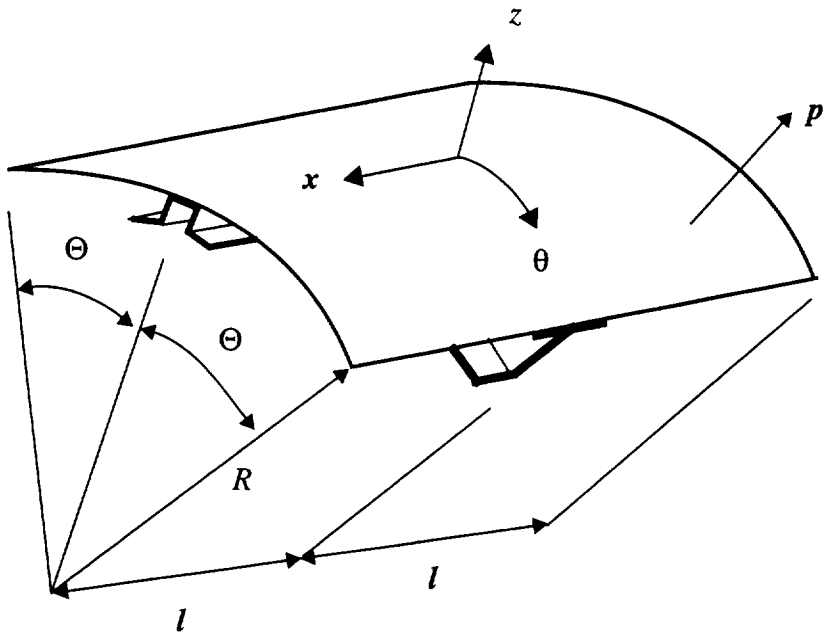

Fig. 1.2. Repeating unit of an orthogonally stiffened cylindrical shell.

include the effect of transverse shear deformations and the effect of warping deformation of the ring's cross section due to torsion. These effects are important when the ring has an asymmetrical cross section, because the loss of symmetry in the problem results in torsion of the ring, as well as out-of-plane bending, and a concomitant rotation of the joint at the stiffener intersection about the circumferential axis. For symmetric section stiffeners, the response of the unit cell (see Fig. 1.2) is symmetric about the stringer axis and the ring axis, and there is no rotation of stringer-ring-shell joint. The formulations for a geometrically nonlinear response are presented for symmetric stiffeners only, and are based on classical theory. The stringer-ring-shell joint is modeled in an idealized manner; the stiffeners are mathematically permitted to pass through one another without contact, but do interact indirectly through their mutual contact with the shell at the joint.

On the basis of the symmetry about the x-axis for the unit, only the interacting line load components tangent and normal to the stringer are included in the analysis. However, due to the ring's asymmetrical cross section, the components of line loads between shell and the ring consist of three force intensities and two moment intensities. The shell-stringer interacting force components per unit length along the contact lines are denoted by $\lambda_{xs}(x)$ for the component tangent to the stringer, and $\lambda_{zs}(x)$ for the component normal to the stringer. The three shell-ring interacting force components per unit length along the contact lines are denoted by $\lambda_{xr}(\theta)$ for the component acting in the axial direction, $\lambda_{\theta r}(\theta)$ for the component tangent to the ring, and $\lambda_{zr}(\theta)$ for the component normal to the ring. The two shell-ring interacting moment components per unit length along the contact lines are denoted by $\Lambda_{\theta r}(\theta)$ for the component tangent to the ring, and $\Lambda_{zr}(\theta)$ for the component normal to the ring. These interacting loads acting in a positive sense on the inside surface of the shell are shown in Fig. 1.3.

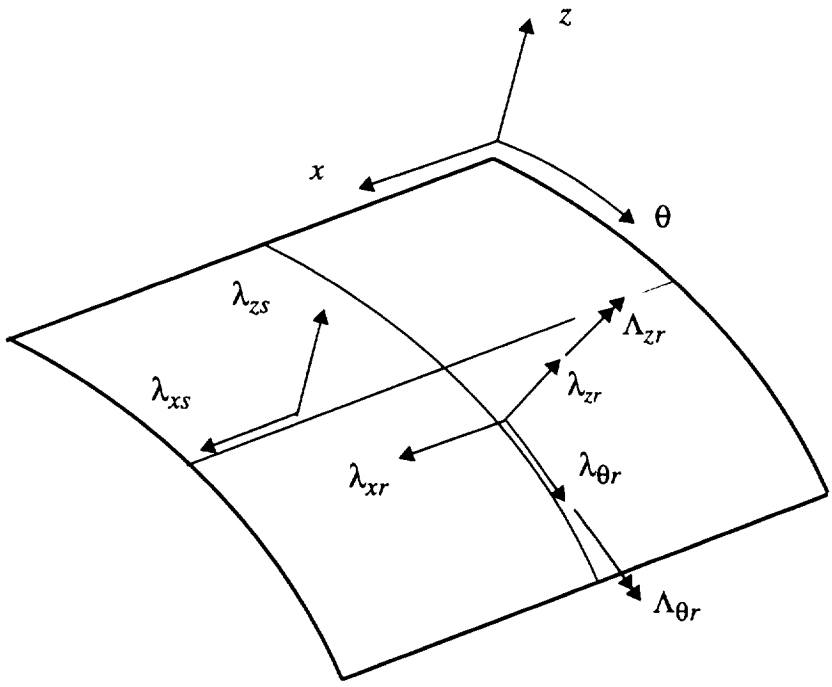

Fig. 1.3. Interacting line load intensities shown in the positive sense acting on the inside surface of the shell.

1.8 ANALYSIS APPROACH

For both the linear elastic and geometrically nonlinear elastic response of the repeating unit to internal pressure, the Ritz method is used. The principle of virtual work is applied separately to the shell, stringer and ring. Displacements are individually assumed for the shell, stringer, and the ring as Fourier Series expansions. The virtual work functionals are augmented by Lagrange multipliers to enforce kinematic constraints between the structural components of the repeating unit. As a result, point-wise displacement continuity between structural elements is achieved. The Lagrange multipliers represent the interacting line loads between the stiffeners and the shell, and are also expanded in Fourier Series. Closed-end pressure vessel effects are included. Data for the example problems are representative of the dimensions of large transport fuselage structure.

The primary advantage of using the analysis approach discussed above results from the fact that a point-wise displacement continuity is achieved between the structural elements. In commercial finite element analysis codes viz., ABAQUS[21], NASTRAN[22], etc., the interpolation functions used for the displacement fields of the structural elements (e.g., the shell and beam elements) are, in general, not the same. Thus, the continuity between the structural elements can only be satisfied at discrete points, i.e., at the nodes. Another shortcoming of these finite element codes is that they can not model the torsional warping deformation of an open section, laminated, curved beam. This is a disadvantage since the restraint of warping deformation in the ring due to continous contact with the shell results in significant circumferential normal stresses in the ring. To account for torsional warping deformation in the ring, the ring would have to be modeled as a branched shell with these finite element codes. Branched shell models of the stiffeners would significantly increase the degrees-of-freedom in the finite element model. It should be mentioned that beam models including torsional warping deformation require seven

nodal degrees of freedom between elements. The seventh degree of freedom is related to the rate of twist. However, it is standard in finite element codes to have only six nodal degrees of freedom (three displacements and three rotations) between one-dimensional elements.

CHAPTER 2
GOVERNING EQUATIONS FOR LINEAR ANALYSES

2.1 STRUCTURAL MODEL AND ASSUMPTIONS

Linear elastic analyses are carried out for a unit cell model (Fig. 1.2) defined in Section 1.7 of an internally pressurized, orthogonally stiffened, long circular cylindrical shell. The interacting line loads between the shell and stiffeners acting in a positive sense on the inside surface of the shell are shown in Fig. 1.3. For a symmetrical section ring, the repeating unit (or unit cell model) is symmetric about θ-axis as well, which implies that there is no out-of-plane bending and torsion of the ring, and consequently, no rotation of the joint at the stiffener intersection about the circumferential axis. Thus, for the symmetrical section stiffeners only the interacting line load components tangent and normal to the stiffeners are non-zero.

Mathematical formulations for the linear elastic response presented in this chapter include the effect of transverse shear deformations and the effect of warping deformation of the ring's cross section due to torsion. These effects are important when the ring has an asymmetrical cross section, because the loss of symmetry in the problem results in torsion of the ring, as well as out-of-plane bending, and a concomitant rotation of the joint at the stiffener intersection about the circumferential axis. This stringer-ring-shell joint is modeled in an idealized manner; the stiffeners are mathematically permitted to pass through one another without contact, but do interact indirectly through their mutual contact with the shell at the joint. Restraint of cross-sectional warping, as occurs here in the ring due to contact with the shell, is an important contributor to the normal stresses in thin-walled open section bars, as was demonstrated by Hoff[23]. Based on transverse shear deformation and cross-sectional warping of the ring, four structural models are defined.

The simplest model uses non-transverse-shear-deformable theory, or classical theory, and neglects warping due to torsion. The most complex model includes both effects. Models of intermediate complexity occur for inclusion of one effect without the other.

The purpose of linear elastic analyses is two fold. First, the linear elastic analysis developed in this chapter is compared with a geometrically nonlinear elastic analysis developed in Chapter 3 for the unit cell model with symmetrical cross section stiffeners. Second, the effect of skin-stringer-ring joint flexibility, and the effect of warping of the ring's cross section due to torsion, on the response are quantified. The following general assumptions, which are valid for classical as well as transverse shear deformation formulations, are made for linear elastic analyses of the unit cell model:

1. Normals to the undeformed reference surface remain straight and are inextensional.
2. Material behavior is linearly elastic.
3. The thickness normal stress is assumed to be small with respect to the normal stresses in the axial and circumferential directions, and hence it is neglected in the material law.

2.2 TRANSVERSE SHEAR DEFORMATION FORMULATIONS

2.2.1 SHELL

A consistent first order transverse shear deformation theory is developed to model the shell. Based on the assumption that the shell thickness t is relatively small and hence, does not change during loading, the displacements at an arbitrary material point in the shell are approximated by

$$U(x,\theta,z) = u(x,\theta) + z\phi_x(x,\theta) \tag{2.1}$$

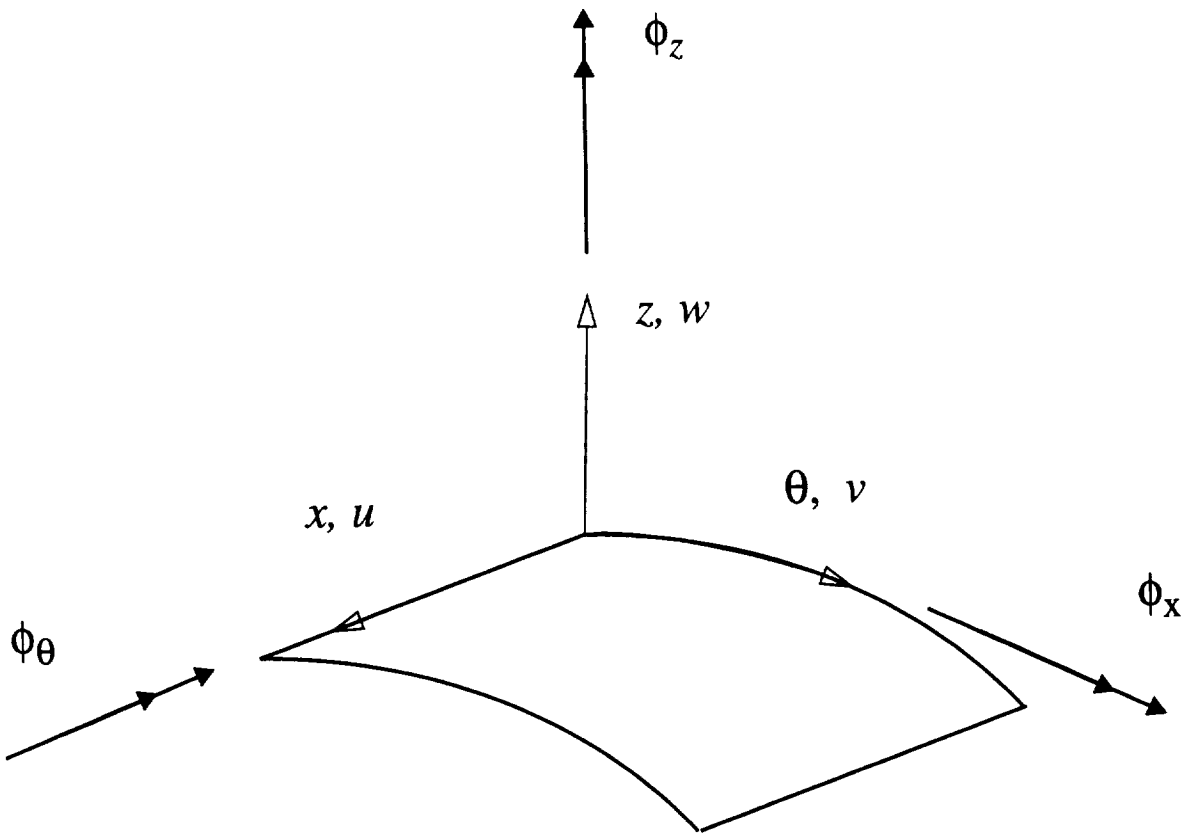

Fig. 2.1. Displacements and rotations for shell.

$$V(x,\theta,z) = v(x,\theta) + z\phi_\theta(x,\theta) \tag{2.2}$$

$$W(x,\theta,z) = w(x,\theta) \tag{2.3}$$

where $u(x,\theta)$, $v(x,\theta)$ and $w(x,\theta)$ are the displacements of the points of the reference surface, and $\phi_x(x,\theta)$ and $\phi_\theta(x,\theta)$ are the rotations of the normal to the reference surface as shown in Fig. 2.1. Assuming small displacement gradients, the three-dimensional engineering strains are related to the displacements by

$$e_{xx} = \frac{\partial U}{\partial x} \qquad e_{\theta\theta} = \frac{1}{(R+z)}\left[\frac{\partial V}{\partial \theta} + W\right] \qquad e_{zz} = \frac{\partial W}{\partial z} \tag{2.4}$$

$$e_{x\theta} = \frac{\partial V}{\partial x} + \frac{1}{(R+z)}\frac{\partial U}{\partial \theta} \tag{2.5}$$

$$e_{xz} = \frac{\partial U}{\partial z} + \frac{\partial W}{\partial x} \qquad e_{\theta z} = \frac{\partial V}{\partial z} + \frac{1}{(R+z)}\left[\frac{\partial W}{\partial \theta} - V\right] \tag{2.6}$$

in which the polar radius r in cylindrical coordinates is replaced by $R+z$. Substituting Eqs. (2.1) to (2.3) into Eqs. (2.4) to (2.6), and rearranging the terms results in the following expressions for the three-dimensional engineering strains:

$$e_{xx} = \epsilon_{xx} + z\kappa_{xx} \qquad e_{\theta\theta} = \frac{\epsilon_{\theta\theta} + z\kappa_{\theta\theta}}{(1+\frac{z}{R})} \qquad e_{zz} = 0 \tag{2.7}$$

$$e_{x\theta} = \frac{\gamma_{x\theta} + z(1+\frac{z}{2R})\bar{\kappa}_{x\theta} + \frac{z^2}{2R}\tilde{\kappa}_{x\theta}}{(1+\frac{z}{R})} \tag{2.8}$$

$$e_{xz} = \gamma_{xz} \qquad e_{\theta z} = \frac{\gamma_{\theta z}}{(1+\frac{z}{R})} \tag{2.9}$$

in which ϵ_{xx}, κ_{xx}, $\epsilon_{\theta\theta}$, $\kappa_{\theta\theta}$, $\gamma_{x\theta}$, $\bar{\kappa}_{x\theta}$, $\tilde{\kappa}_{x\theta}$, γ_{xz}, and $\gamma_{\theta z}$ are the shell strains independent of z-coordinate. These shell strains are defined in the following sub-subsection. The transverse shear strains e_{xz} and $e_{\theta z}$ given in Eqs. (2.9) were obtained through differentiation of Eqs. (2.1) to (2.3) with respect to z. However, Eqs. (2.1) to (2.3) are approximate in the z-coordinate, so that differentiating with respect to z cannot capture the distribution of the transverse shear strains through the thickness of the shell. Since the material is

assumed rigid in the z-direction ($e_{zz} = 0$), the distribution of the transverse shear strains, and consequently the distribution of the transverse shear stresses, does not influence the shell behavior. It is the integral of the transverse shear stresses through the thickness, or transverse shear resultants, that influences shell behavior. Thus, Eqs. (2.9) should be viewed as average values of the transverse shear strains, or as the transverse shear strains evaluated at the reference surface ($z = 0$).

2.2.1.1 STRAIN-DISPLACEMENT RELATIONS

In Eqs. (2.7) to (2.9), the two-dimensional, or shell, strain measures, which are independent of the z-coordinate, are defined by

$$\epsilon_{xx} = \frac{\partial u}{\partial x} \qquad \kappa_{xx} = \frac{\partial \phi_x}{\partial x} \tag{2.10}$$

$$\epsilon_{\theta\theta} = \frac{1}{R}\frac{\partial v}{\partial \theta} + \frac{w}{R} \qquad \kappa_{\theta\theta} = \frac{1}{R}\frac{\partial \phi_\theta}{\partial \theta} \tag{2.11}$$

$$\gamma_{x\theta} = \frac{\partial v}{\partial x} + \frac{1}{R}\frac{\partial u}{\partial \theta} \tag{2.12}$$

$$\bar{\kappa}_{x\theta} = \frac{\partial \phi_\theta}{\partial x} + \frac{1}{R}\frac{\partial \phi_x}{\partial \theta} + \frac{1}{R}\frac{\partial v}{\partial x} \tag{2.13}$$

$$\tilde{\kappa}_{x\theta} = \frac{\partial \phi_\theta}{\partial x} - \frac{1}{R}\frac{\partial \phi_x}{\partial \theta} - \frac{1}{R}\frac{\partial v}{\partial x} \tag{2.14}$$

$$\gamma_{xz} = \phi_x + \frac{\partial w}{\partial x} \qquad \gamma_{\theta z} = \phi_\theta - \frac{v}{R} + \frac{1}{R}\frac{\partial w}{\partial \theta} \tag{2.15}$$

If we set the (average) transverse shear strains in Eqs. (2.9) to zero, then the rotations of the normal are

$$\phi_x = -\frac{\partial w}{\partial x} \tag{2.16}$$

$$\phi_\theta = \frac{v}{R} - \frac{1}{R}\frac{\partial w}{\partial \theta} \tag{2.17}$$

so that

$$\kappa_{x\theta} = \bar{\kappa}_{x\theta} = -\frac{2}{R}\frac{\partial^2 w}{\partial x \partial \theta} + \frac{2}{R}\frac{\partial v}{\partial x} \qquad \tilde{\kappa}_{x\theta} = 0 \tag{2.18}$$

Hence, the thickness distribution of the shear strain reduces to

$$e_{x\theta} = \frac{\gamma_{x\theta} + z(1+\frac{z}{2R})\kappa_{x\theta}}{(1+\frac{z}{R})} \tag{2.19}$$

which coincides with the results of Novozhilov's[24] classical shell theory.

It is evident from Eq. (2.8) that three shell strain measures are needed to represent the distribution of the in-plane shear strain through the thickness in the transverse shear deformation shell theory. Whereas, only two shell strain measures are required in classical shell theory to represent the shearing strain distribution through the thickness (refer to Eq. (2.19)). Also it can be shown that under rigid body motions of the shell, the nine shell strain measures, given by Eqs. (2.10) through (2.15) vanish. (For Novozhilov's classical shell theory, six shell strain measures given by Eqs. (2.10-2.12) and (2.18) vanish under rigid body motions.)

2.2.1.2 VIRTUAL WORK

In the three-dimensional elasticity theory, the internal virtual work for the shell is given by

$$\delta \mathcal{W}_{int}^{shell} = \iiint_V \left[\sigma_{xx}\delta e_{xx} + \sigma_{\theta\theta}\delta e_{\theta\theta} + \sigma_{zz}\delta e_{zz} + \sigma_{x\theta}\delta e_{x\theta} + \sigma_{xz}\delta e_{xz} + \sigma_{\theta z}\delta e_{\theta z}\right] dV \tag{2.20}$$

where V denotes the volume of shell and $dV = (1+\frac{z}{R})\, dx R\, d\theta\, dz$. Substitute the variation of Eqs. (2.7) to (2.9) into Eq. (2.20), and note that the virtual strains are explicit functions of z. Integrals of the stresses with respect to z give force and moment resultants conjugate to the shell strains. Hence, the volume integral in Eq. (2.20) reduces to an area integral, and the internal virtual work becomes

$$\delta \mathcal{W}_{int}^{shell} = \iint_S \delta \vec{\epsilon}_{shell}^{T}\, \vec{\sigma}_{shell}\, dS, \tag{2.21}$$

where S denotes the area of the reference surface with $dS = dx R d\theta$. The generalized 9×1 stress vector for the shell in Eq. (2.21) is defined by

$$\vec{\sigma}_{shell} = [N_{xx}, N_{\theta\theta}, N_{\theta x}, M_{xx}, M_{\theta\theta}, \bar{M}_{x\theta}, \tilde{M}_{x\theta}, Q_x, Q_\theta]^T, \tag{2.22}$$

and the generalized strain vector for the shell is

$$\vec{\epsilon}_{shell} = [\epsilon_{xx}, \epsilon_{\theta\theta}, \gamma_{x\theta}, \kappa_{xx}, \kappa_{\theta\theta}, \bar{\kappa}_{x\theta}, \tilde{\kappa}_{x\theta}, \gamma_{xz}, \gamma_{\theta z}]^T \tag{2.23}$$

The physical stress resultants and stress couples for the shell, some of which appear in Eq. (2.22), are defined in terms of stress components of the symmetric stress tensor in cylindrical coordinates by

$$\begin{aligned}
(N_{xx},\ M_{xx}) &= \int_t (1, z)\sigma_{xx}(1 + \frac{z}{R})\ dz \\
(N_{\theta\theta},\ M_{\theta\theta}) &= \int_t (1, z)\sigma_{\theta\theta}\ dz \\
(N_{x\theta},\ M_{x\theta}) &= \int_t (1, z)\sigma_{x\theta}(1 + \frac{z}{R})\ dz \\
(N_{\theta x},\ M_{\theta x}) &= \int_t (1, z)\sigma_{\theta x}\ dz \\
Q_x &= \int_t \sigma_{xz}(1 + \frac{z}{R})\ dz \\
Q_\theta &= \int_t \sigma_{\theta z} dz
\end{aligned} \tag{2.24}$$

In Eq. (2.22), $\bar{M}_{x\theta}$ and $\tilde{M}_{x\theta}$ are the mathematical quantities conjugate to the modified twisting measures $\bar{\kappa}_{x\theta}$ and $\tilde{\kappa}_{x\theta}$, respectively, and are defined in terms of the physical stress couples by

$$\bar{M}_{x\theta} = \frac{1}{2}(M_{x\theta} + M_{\theta x}) \qquad \tilde{M}_{x\theta} = \frac{1}{2}(M_{x\theta} - M_{\theta x}) \tag{2.25}$$

The nine elements of the stress vector in Eq. (2.22) and the relations of Eq. (2.25) determine all the stress resultants and stress couples listed in Eq. (2.24) except for shear resultant $N_{x\theta}$. The shear stress resultant $N_{x\theta}$ is determined from moment equilibrium about the normal for an element of the shell. This so-called sixth equilibrium equation is

$$N_{x\theta} = N_{\theta x} + \frac{M_{\theta x}}{R} \tag{2.26}$$

Written out in full, the internal virtual work for the shell is given by

$$\delta \mathcal{W}_{int}^{shell} = \iint_S \left[N_{xx}\delta\epsilon_{xx} + N_{\theta\theta}\delta\epsilon_{\theta\theta} + N_{\theta x}\delta\gamma_{x\theta} + M_{xx}\delta\kappa_{xx} + M_{\theta\theta}\delta\kappa_{\theta\theta} + \bar{M}_{x\theta}\delta\bar{\kappa}_{x\theta} + \tilde{M}_{x\theta}\delta\tilde{\kappa}_{x\theta} + Q_x\delta\gamma_{xz} + Q_\theta\delta\gamma_{\theta z} \right] dS \tag{2.27}$$

The external virtual work for the shell is

$$\delta \mathcal{W}_{ext}^{shell} = \delta \mathcal{W}_{p}^{shell} + \delta \mathcal{W}_{\lambda}^{shell} \tag{2.28}$$

where $\delta \mathcal{W}_{p}^{shell}$ is the external virtual work due to the spatially uniform internal pressure load, and $\delta \mathcal{W}_{\lambda}^{shell}$ is the external (or augmented) virtual work due to interacting loads. The external virtual work for a cylindrical shell under uniform internal pressure, including an axial load due to the closed-end effect, is written as

$$\delta \mathcal{W}_{p}^{shell} = \iint_S p\ \delta w\ dS \quad + \quad p \int_{-\Theta}^{\Theta} \frac{R^2}{2} d\theta\ [\delta u(l,\theta) - \delta u(-l,\theta)] \tag{2.29}$$

The discussion on the augmented virtual work due to interacting loads is given in Section 2.5.

2.2.1.3 CONSTITUTIVE RELATIONS

The material law for an orthotropic lamina with one material axis in the normal direction is given by

$$\begin{Bmatrix} \sigma_{xx} \\ \sigma_{\theta\theta} \\ \sigma_{x\theta} \end{Bmatrix} = \begin{bmatrix} \bar{Q}_{11} & \bar{Q}_{12} & \bar{Q}_{16} \\ \bar{Q}_{12} & \bar{Q}_{22} & \bar{Q}_{26} \\ \bar{Q}_{16} & \bar{Q}_{26} & \bar{Q}_{66} \end{bmatrix} \begin{Bmatrix} e_{xx} \\ e_{\theta\theta} \\ e_{x\theta} \end{Bmatrix} \tag{2.30}$$

where $\bar{Q}_{ij}$ are the transformed reduced stiffnesses given in the text by Jones[25]. (The thickness normal stress is assumed to be zero in the material law.) Substitution of Eq. (2.30) into Eqs. (2.24) in conjunction with Eqs. (2.25), and use of Eqs. (2.7) to (2.9) for the three-dimensional engineering strains, results in the following linear elastic constitutive

law for a laminated composite shell wall:

$$\begin{Bmatrix} N_{xx} \\ N_{\theta\theta} \\ N_{\theta x} \\ M_{xx} \\ M_{\theta\theta} \\ \bar{M}_{x\theta} \\ \tilde{M}_{x\theta} \end{Bmatrix} = \begin{bmatrix} A_{11} & A_{12} & A_{16} & B_{11} & B_{12} & B_{16}^1 & B_{16}^2 \\ A_{12} & A_{22} & A_{26} & B_{12} & B_{22} & B_{26}^1 & B_{26}^2 \\ A_{16} & A_{26} & A_{66} & B_{61} & B_{62} & B_{66}^1 & B_{66}^2 \\ B_{11} & B_{12} & B_{61} & D_{11} & D_{12} & D_{16}^1 & D_{16}^2 \\ B_{12} & B_{22} & B_{62} & D_{12} & D_{22} & D_{26}^1 & D_{26}^2 \\ B_{16}^1 & B_{26}^1 & B_{66}^1 & D_{16}^1 & D_{26}^1 & D_{66}^{11} & D_{66}^{12} \\ B_{16}^2 & B_{26}^2 & B_{66}^2 & D_{16}^2 & D_{26}^2 & D_{66}^{12} & D_{66}^{22} \end{bmatrix} \begin{Bmatrix} \epsilon_{xx} \\ \epsilon_{\theta\theta} \\ \gamma_{x\theta} \\ \kappa_{xx} \\ \kappa_{\theta\theta} \\ \bar{\kappa}_{x\theta} \\ \tilde{\kappa}_{x\theta} \end{Bmatrix} \tag{2.31}$$

in which stiffnesses A_{ij}, B_{ij} and D_{ij} are given by

$$\begin{aligned}
(A_{11}, B_{11}, D_{11}) &= \int_t (1, z, z^2)\bar{Q}_{11}(1 + \frac{z}{R})dz \\
(A_{12}, B_{12}, D_{12}) &= \int_t (1, z, z^2)\bar{Q}_{12}dz \\
(A_{22}, B_{22}, D_{22}) &= \int_t (1, z, z^2)\bar{Q}_{22}(1 + \frac{z}{R})^{-1}dz \\
(A_{16}, B_{61}) &= \int_t (1, z)\bar{Q}_{16}dz \\
(A_{26}, B_{62}) &= \int_t (1, z)\bar{Q}_{26}(1 + \frac{z}{R})^{-1}dz \\
A_{66} &= \int_t \bar{Q}_{66}(1 + \frac{z}{R})^{-1}dz \\
B_{16}^1 &= \int_t \bar{Q}_{16}z(1 + \frac{z}{R})dz \\
B_{16}^2 &= \int_t \bar{Q}_{16}\frac{z^2}{2R}dz \\
B_{26}^1 &= \int_t \bar{Q}_{26}z(1 + \frac{z}{2R})(1 + \frac{z}{R})^{-1}dz \\
B_{26}^2 &= \int_t \bar{Q}_{26}\frac{z^2}{2R}(1 + \frac{z}{R})^{-1}dz \\
B_{66}^1 &= \int_t \bar{Q}_{66}z(1 + \frac{z}{2R})(1 + \frac{z}{R})^{-1}dz \\
B_{66}^2 &= \int_t \bar{Q}_{66}\frac{z^2}{2R}(1 + \frac{z}{R})^{-1}dz \\
D_{16}^1 &= \int_t \bar{Q}_{16}z^2(1 + \frac{z}{R})dz \\
D_{16}^2 &= \int_t \bar{Q}_{16}\frac{z^3}{2R}dz \\
D_{26}^1 &= \int_t \bar{Q}_{26}z^2(1 + \frac{z}{2R})(1 + \frac{z}{R})^{-1}dz
\end{aligned} \tag{2.32}$$

$$D_{26}^{2} = \int_t \bar{Q}_{26} \frac{z^3}{2R} (1 + \frac{z}{R})^{-1} dz$$
$$D_{66}^{11} = \int_t \bar{Q}_{66} z^2 (1 + \frac{z}{2R})^{2} (1 + \frac{z}{R})^{-1} dz$$
$$D_{66}^{12} = \int_t \bar{Q}_{66} \frac{z^3}{2R} (1 + \frac{z}{2R})(1 + \frac{z}{R})^{-1} dz$$
$$D_{66}^{22} = \int_t \bar{Q}_{66} \frac{z^4}{4R^2} (1 + \frac{z}{R})^{-1} dz$$

The lamina material law relating transverse shear stresses and strains is

$$\begin{Bmatrix} \sigma_{xz} \\ \sigma_{\theta z} \end{Bmatrix} = \begin{bmatrix} C_{44} & C_{45} \\ C_{45} & C_{55} \end{bmatrix} \begin{Bmatrix} e_{xz} \\ e_{\theta z} \end{Bmatrix} \tag{2.33}$$

where

$$C_{44} = G_{13} Cos^2\alpha + G_{23} Sin^2\alpha$$
$$C_{45} = (G_{13} - G_{23}) Cos\alpha Sin\alpha$$
$$C_{55} = G_{23} Cos^2\alpha + G_{13} Sin^2\alpha$$

in which α is the ply orientation angle. Substitution of Eq. (2.33) into the last two of Eqs. (2.24), in conjunction with Eqs. (2.9) for the transverse shear strains, results in the following linear elastic constitutive law for a laminated composite shell wall relating transverse shear resultants and strains:

$$\begin{Bmatrix} Q_x \\ Q_\theta \end{Bmatrix} = \begin{bmatrix} A_{44} & A_{45} \\ A_{45} & A_{55} \end{bmatrix} \begin{Bmatrix} \gamma_{xz} \\ \gamma_{\theta z} \end{Bmatrix} \tag{2.34}$$

The transverse shear stiffnesses, A_{44}, A_{45}, and A_{55} in Eq. (2.34) are given by

$$A_{44} = \int_t C_{44} (1 + \frac{z}{R}) dz$$
$$A_{45} = \int_t C_{45} dz \tag{2.35}$$
$$A_{55} = \int_t C_{55} (1 + \frac{z}{R})^{-1} dz$$

Since Eqs. (2.9) represent average values of the transverse shear strains, the constitutive law relating transverse shear resultants and strains, Eq. (2.34), can be viewed as

a Hooke's law based on the assumption of constant transverse shear strain distribution through the thickness. Alternatively one can obtain the constitutive law relating transverse shear resultants and strains based on the assumption of constant transverse shear stress distribution through the thickness. A detailed discussion on the subject is given in Chapter 2 of the text by Vasiliev[26]. However, both the methods result in a shear correction factor of one (as opposed to 5/6) for isotropic materials. Cohen[27] derived the transverse shear stiffnesses of laminated anisotropic shells without making either of the assumptions mentioned above. He employed Castigliano's theorem of least work to minimize the shear strain energy, and obtained the desired constitutive law, which for homogeneous isotropic materials gives a shear correction factor of 5/6.

2.2.1.4 EQUILIBRIUM EQUATIONS

The equilibrium equations for the shell can be derived using the principle of virtual work which is stated as

$$\delta \mathcal{W}_{int}^{shell} = \delta \mathcal{W}_{ext}^{shell}, \tag{2.36}$$

for every kinematically admissible displacement field. For the purpose of deriving the equilibrium equations of the shell, the contribution of the augmented virtual work due to interacting loads is neglected in Eq. (2.28) for the external virtual work. Thus, substituting Eqs. (2.27) and (2.29) for internal and external virtual work, respectively, into Eq. (2.36), using the definitions of the strain-displacement relations given by Eqs. (2.10) through (2.15), performing integration by parts, and recognizing the arbitrary nature of the first variation of the displacements, results in the following set of equilibrium equations, or Euler equations, for the shell:

$$\delta u: \quad \frac{\partial N_{xx}}{\partial x} + \frac{1}{R}\frac{\partial N_{\theta x}}{\partial \theta} = 0 \tag{2.37}$$

$$\delta v: \quad \frac{\partial N_{x\theta}}{\partial x} + \frac{1}{R}\frac{\partial N_{\theta\theta}}{\partial \theta} + \frac{1}{R}Q_{\theta} = 0 \tag{2.38}$$

$$\delta w: \quad \frac{\partial Q_x}{\partial x} + \frac{1}{R}\frac{\partial Q_\theta}{\partial \theta} - \frac{1}{R}N_{\theta\theta} + p = 0 \tag{2.39}$$

$$\delta \phi_x: \quad \frac{\partial M_{xx}}{\partial x} + \frac{1}{R}\frac{\partial M_{\theta x}}{\partial \theta} - Q_x = 0 \tag{2.40}$$

$$\delta \phi_\theta: \quad \frac{\partial M_{x\theta}}{\partial x} + \frac{1}{R}\frac{\partial M_{\theta\theta}}{\partial \theta} - Q_\theta = 0 \tag{2.41}$$

2.2.1.5 BOUNDARY CONDITIONS

The derivation of Euler equations from the principle of virtual work results in the following boundary integrals:

$$\begin{aligned} &\int_{-\Theta}^{\Theta} \left[(N_{xx} - \frac{pR}{2})\delta u + N_{x\theta}\delta v + Q_x \delta w + M_{xx}\delta\phi_x + M_{x\theta}\delta\phi_\theta \right]_{-l}^{+l} R \, d\theta \\ &+ \int_{-l}^{l} \left[N_{\theta x}\delta u + N_{\theta\theta}\delta v + Q_\theta \delta w + M_{\theta x}\delta\phi_x + M_{\theta\theta}\delta\phi_\theta \right]_{-\Theta}^{+\Theta} dx \; = 0 \end{aligned} \tag{2.42}$$

Boundary integrals in Eq. (2.42) can be made to vanish individually by specifying the boundary conditions in two ways. One way is to prescribe periodic boundary conditions; alternatively either an essential or a natural boundary condition can be prescribed. In the first case, the periodic boundary conditions at $x = \pm l$ are expressed as

$$\begin{aligned} N_{x\theta}(l,\theta) &= N_{x\theta}(-l,\theta), & \delta v(l,\theta) &= \delta v(-l,\theta) \\ Q_x(l,\theta) &= Q_x(-l,\theta), & \delta w(l,\theta) &= \delta w(-l,\theta) \\ M_{xx}(l,\theta) &= M_{xx}(-l,\theta), & \delta\phi_x(l,\theta) &= \delta\phi_x(-l,\theta) \\ M_{x\theta}(l,\theta) &= M_{x\theta}(-l,\theta), & \delta\phi_\theta(l,\theta) &= \delta\phi_\theta(-l,\theta) \quad \theta \in [-\Theta,\Theta] \end{aligned} \tag{2.43}$$

For the closed-end pressure vessel effect, prescribe

$$N_{xx}(l,\theta) = \frac{pR}{2} \;\; and \;\; N_{xx}(-l,\theta) = \frac{pR}{2} \quad \theta \in [-\Theta,\Theta] \tag{2.44}$$

Thus, $\delta u(\pm l, \theta)$ is not prescribed to vanish. Periodic conditions at $\theta = \pm\Theta$ edges are

$$\begin{aligned} N_{\theta x}(x,\Theta) &= N_{\theta x}(x,-\Theta), & \delta u(x,\Theta) &= \delta u(x,-\Theta) \\ N_{\theta\theta}(x,\Theta) &= N_{\theta\theta}(x,-\Theta), & \delta v(x,\Theta) &= \delta v(x,-\Theta) \\ Q_{\theta}(x,\Theta) &= Q_{\theta}(x,-\Theta), & \delta w(x,\Theta) &= \delta w(x,-\Theta) \\ M_{\theta\theta}(x,\Theta) &= M_{\theta\theta}(x,-\Theta), & \delta \phi_x(x,\Theta) &= \delta \phi_x(x,-\Theta) \\ M_{\theta x}(x,\Theta) &= M_{\theta x}(x,-\Theta), & \delta \phi_\theta(x,\Theta) &= \delta \phi_\theta(x,-\Theta) \quad x \in [-l,l] \end{aligned} \tag{2.45}$$

In the second case, the associated boundary conditions at $x = \pm l$ edges are to prescribe

either $N_{xx} - \frac{pR}{2}$ or u but not both,

either $N_{x\theta}$ or v but not both,

either Q_x or w but not both,

either M_{xx} or ϕ_x but not both, and

either $M_{x\theta}$ or ϕ_θ but not both.

The associated boundary conditions at $\theta = \pm\Theta$ edges are to prescribe

either $N_{\theta x}$ or u but not both,

either $N_{\theta\theta}$ or v but not both,

either Q_θ or w but not both,

either $M_{\theta x}$ or ϕ_x but not both, and

either $M_{\theta\theta}$ or ϕ_θ but not both.

2.2.2 STRINGER

Let $u_s(x)$ and $w_s(x)$ denote the axial and normal displacements, respectively, of a material point on the stringer reference axis, and let $\phi_{\theta s}(x)$ denote the rotation of normal as shown in Fig. 2.2. Thus, the axial and normal displacements of a generic material point of the stringer are given by

$$U_s(x,\xi) = u_s(x) + \xi\phi_{\theta s}(x) \tag{2.46}$$

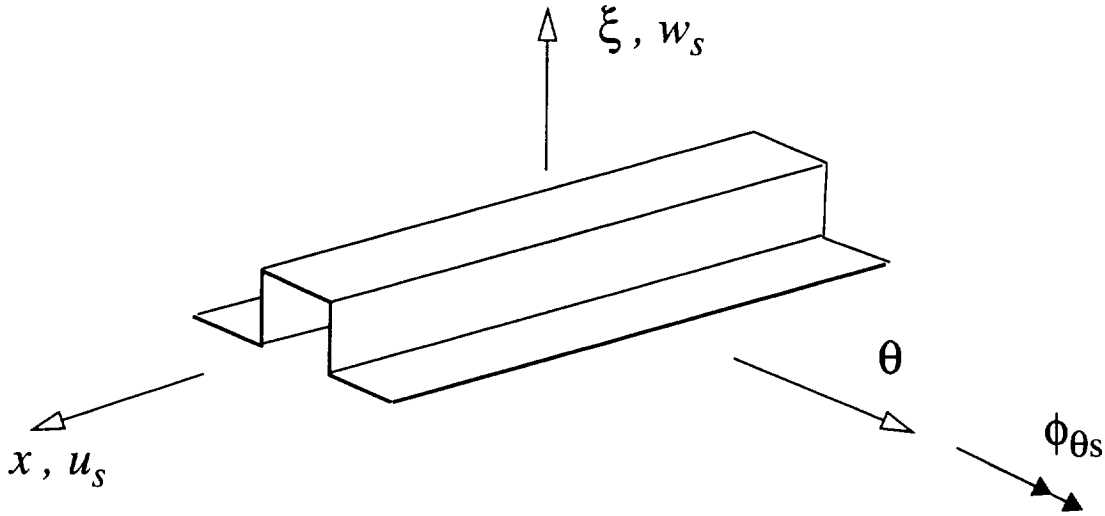

Fig. 2.2. Displacements and rotations for stringer.

$$W_s(x,\xi) = w_s(x), \tag{2.47}$$

respectively. The coordinate system (x,θ,ξ) is located at the centroid of the stringer as per the right-hand rule (see Fig. 2.2), in which ξ is the normal coordinate. Using Eqs. (2.46) and (2.47) and assuming small displacement gradients, the three-dimensional engineering strains are

$$\epsilon^s_{xx} = \epsilon_{xs} + \xi\kappa_{\theta s} \qquad e^s_{zz} = 0 \qquad e^s_{xz} = \gamma_{zs} \tag{2.48}$$

which are independent of the θ-direction coordinate because of the symmetric deformation assumption. In Eq. (2.48), the one-dimensional strain-displacement relations are defined by

$$\epsilon_{xs} = u'_s \qquad \kappa_{\theta s} = \phi'_{\theta s} \qquad \gamma_{zs} = \phi_{\theta s} + w'_s \tag{2.49}$$

in which ϵ_{xs} is the normal strain of the centroidal line, the product $\xi\kappa_{\theta s}$ is the portion of the axial normal strain due to bending, γ_{zs} is the transverse shear strain, and the prime denotes an ordinary derivative with respect to x.

The physical force and moment resultants for the stringer in terms of stress components of the symmetric stress tensor are given, in usual way, by

$$\begin{aligned}(N_{xs},\ M_{\theta s}) &= \iint_{A_s} (1,\xi)\sigma^s_{xx}\, dA_s \\ V_{zs} &= \iint_{A_s} \sigma^s_{xz}\, dA_s\end{aligned} \tag{2.50}$$

in which N_{xs} is the axial force in the stringer, $M_{\theta s}$ is the bending moment, V_{zs} is the transverse shear force, and A_s is the cross-sectional area of the stringer. Based on transverse shear deformation theory, the internal virtual work expression for the stringer is

$$\delta\mathcal{W}^{stringer}_{int} = \int_{-l}^{l} [N_{xs}\delta\epsilon_{xs} + M_{\theta s}\delta\kappa_{\theta s} + V_{zs}\delta\gamma_{zs}]dx, \tag{2.51}$$

and the Hooke's law is

$$N_{xs} = (EA)_s\epsilon_{xs} \qquad M_{\theta s} = (EI)_s\kappa_{\theta s} \qquad V_{zs} = (GA)_s\gamma_{zs} \tag{2.52}$$

2.2.3 RING

The structural model is based on transverse shear deformation theory and includes cross-sectional warping due to torsion. Warping is a distinctive feature of thin-walled, open section beams. Restraint of cross-sectional warping, as occurs here in the ring due to its contact with the shell, leads to additional longitudinal normal strains in the ring as a result of torsion. The extension of classical thin-walled, open section, curved bar theory to laminated composite materials was developed by Woodson, Johnson, and Haftka[28]. However, Woodson et al. did not consider transverse shear deformations. Most of the developments for the ring theory presented here are obtained from Woodson's dissertation[29]. The coordinate system (x, θ, ζ) is located at the centroid of the ring as per the right-handed system as shown in Fig. 2.3, in which ζ is the normal coordinate in the radial direction. Let the displacements of a material point on the ring reference axis in the x-, θ-, and ζ-directions be denoted by $u_r(\theta)$, $v_r(\theta)$, and $w_r(\theta)$, respectively. Let the rotations about the x-, θ-, and ζ-axes be denoted by $\phi_{xr}(\theta)$, $\phi_{\theta r}(\theta)$, and $\phi_{zr}(\theta)$, respectively. See Fig. 2.3 for the positive sense of these quantities. The displacements of a generic point in the cross section are related to the displacements and rotations of the point on the reference surface by the approximations

$$U_r(x, \theta, \zeta) = u_r(\theta) + \zeta \phi_{\theta r}(\theta) \tag{2.53}$$

$$V_r(x, \theta, \zeta) = v_r(\theta) + \zeta \phi_{xr}(\theta) + x \phi_{zr}(\theta) - \omega(x, \zeta) \tau_r(\theta) \tag{2.54}$$

$$W_r(x, \theta, \zeta) = w_r(\theta) - x \phi_{\theta r}(\theta) \tag{2.55}$$

The cross section of the ring is normal to the θ-axis, that is, the $x - \zeta$ plane, so that U_r and W_r are interpreted as in-plane displacement components, and V_r is the out-of-plane component. It is assumed that the cross section is rigid in its own plane. Hence, in-plane displacements in Eqs. (2.53) and (2.55) are composed of a translation of the cross-sectional

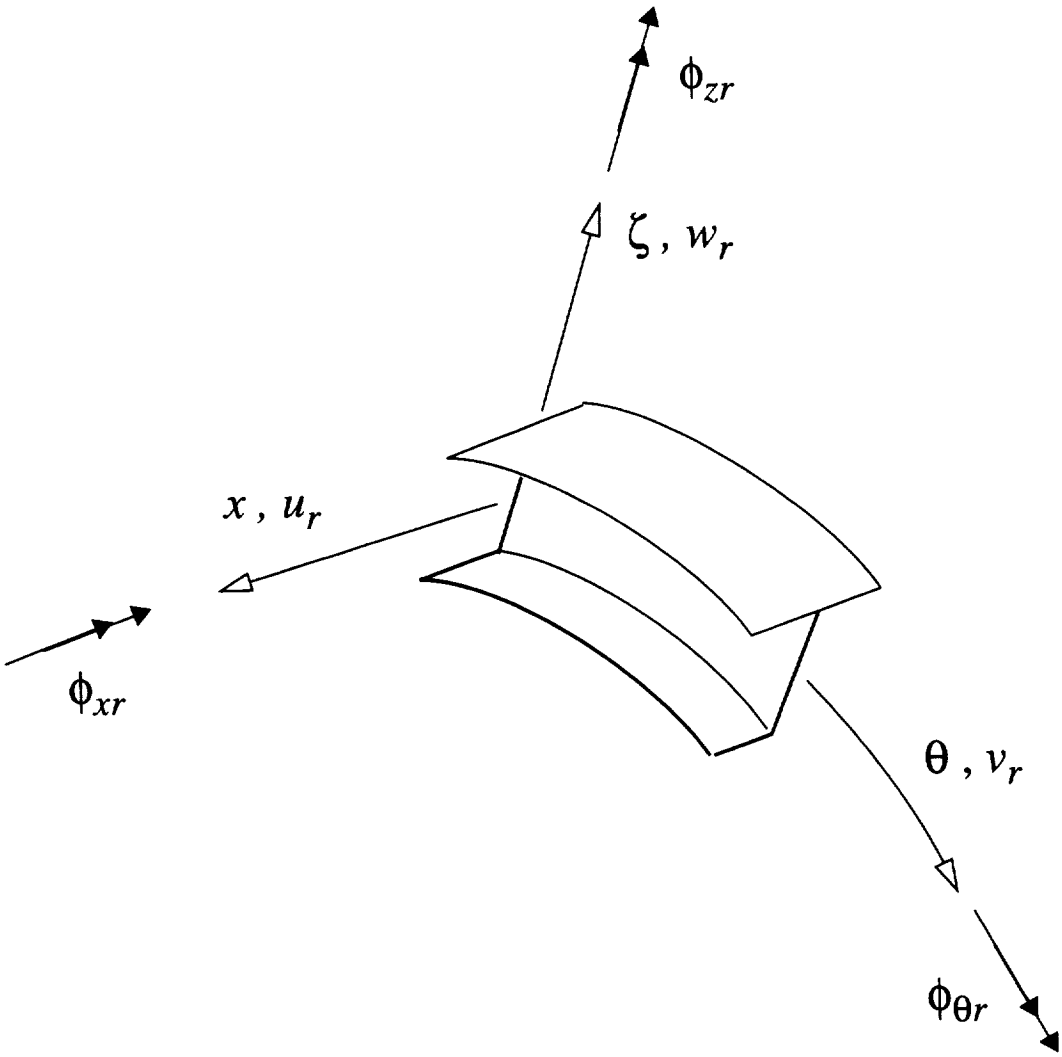

Fig. 2.3. Displacements and rotations for ring.

origin plus a small rigid body rotation $\phi_{\theta r}$ about the θ-axis. The out-of-plane displacement given by Eq. (2.54) is composed of a translation of the origin v_r, a component $\zeta\phi_{xr}$ due to bending about the x-axis, a component $x\phi_{zr}$ due to bending about the ζ-axis, and a component $-\omega\tau_r$ due to warping of the cross section out of the flexural plane. In Eq. (2.54), $\omega(x,\zeta)$ is the warping function for the ring's cross section, and $\tau_r(\theta)$ is the twist rate which is given after the next equation. The internal virtual work is

$$\delta\mathcal{W}_{int}^{ring} = \int_{-\Theta}^{\Theta} [N_{\theta r}\delta\epsilon_{\theta r} + M_{xr}\delta\kappa_{xr} + M_{zr}\delta\kappa_{zr} + T_{sr}\delta\tau_r + M_{\omega r}\delta(\dot{\tau}_r/R_0) + V_{xr}\delta\gamma_{xr} + V_{zr}\delta\gamma_{zr}]R_0\, d\theta \tag{2.56}$$

in which $N_{\theta r}$ is the circumferential force, M_{xr} is the in-plane bending moment, M_{zr} is the out-of-plane bending moment, $M_{\omega r}$ is the bimoment, T_{sr} is the St. Venant's torque, V_{xr} is transverse shear force in the x-direction, V_{zr} is transverse shear force in the ζ-direction, $\epsilon_{\theta r}$ is the circumferential normal strain of the centroidal arc, κ_{xr} is the in-plane bending rotation gradient, κ_{zr} is the out-of-plane bending rotation gradient, γ_{xr} is the transverse shear strain in x-θ plane, γ_{zr} is the transverse shear strain in θ-ζ plane, and R_0 is the radius of ring reference arc. The rotations and strain-displacement relations are

$$\begin{aligned} &\epsilon_{\theta r} = \frac{1}{R_0}(\dot{v}_r + w_r) \qquad && \kappa_{xr} = \frac{1}{R_0}\dot{\phi}_{xr} \qquad && \kappa_{zr} = \frac{1}{R_0}(\dot{\phi}_{zr} - \phi_{\theta r}) \\ &\tau_r = \frac{1}{R_0}(\dot{\phi}_{\theta r} + \phi_{zr}) \qquad && \gamma_{zr} = \phi_{xr} - \frac{1}{R_0}(v_r - \dot{w}_r) \qquad && \gamma_{xr} = \phi_{zr} + \frac{1}{R_0}\dot{u}_r \end{aligned} \tag{2.57}$$

in which the over-dot denotes an ordinary derivative with respect to θ. The material law is based on the assumption that the shear forces are decoupled from extension, bending, and torsional deformations of the ring. Thus, Hooke's law for the ring is

$$\begin{Bmatrix} N_{\theta r} \\ M_{xr} \\ M_{zr} \\ M_{\omega r} \\ T_{sr} \end{Bmatrix} = \begin{bmatrix} EA & ES_x & -ES_z & -ES_\omega & EH \\ ES_x & EI_{xx} & -EI_{zx} & -EI_{\omega x} & EH_c \\ -ES_z & -EI_{zx} & EI_{zz} & EI_{\omega z} & -EH_s \\ -ES_\omega & -EI_{\omega x} & EI_{\omega z} & EI_{\omega\omega} & -EH_q \\ EH & EH_c & -EH_s & -EH_q & GJ \end{bmatrix} \begin{Bmatrix} \epsilon_{\theta r} \\ \kappa_{xr} \\ \kappa_{zr} \\ \dot{\tau}_r/R_0 \\ \tau_r \end{Bmatrix}, \tag{2.58}$$

and

$$\begin{Bmatrix} V_{xr} \\ V_{zr} \end{Bmatrix} = \begin{bmatrix} GA_{x\theta} & GA_{xz} \\ GA_{xz} & GA_{z\theta} \end{bmatrix} \begin{Bmatrix} \gamma_{xr} \\ \gamma_{zr} \end{Bmatrix} \tag{2.59}$$

The stiffnesses in Eq. (2.58) are commonly referred to as modulus-weighted section properties. The "EH" terms are unique to laminated thin-walled beams (see Bauld and Tzeng[30]). If the laminate construction for each branch of the ring is specially orthotropic with respect to x-, θ-, and ζ-directions, then the "EH" terms are all equal to zero. The stiffness elements are evaluated from a computer code developed by Woodson. The reader is encouraged to refer to Chapters 2 and 3 of Ref. [29] for further details on this subject.

The transverse shear stiffness elements in Eq. (2.59) are given by

$$\begin{aligned} GA_{x\theta} &= [A_{55}\ h_w + \sum_{k=1}^{K} (A_{66})_k\ (b_w)_k] \\ GA_{xz} &= [A_{45}\ h_w + \sum_{k=1}^{K} (A_{45})_k\ (b_w)_k] \\ GA_{z\theta} &= [A_{66}\ h_w + \sum_{k=1}^{K} (A_{55})_k\ (b_w)_k] \end{aligned} \tag{2.60}$$

in which the transverse shear stiffnesses, A_{44}, A_{45}, and A_{55} are calculated based on the assumption of constant transverse shear strain distribution through the thickness, and are given by Eq. (2.35). In deriving the transverse shear stiffness elements given by Eqs. (2.60) above, it is assumed that cross section of the ring is made up of a vertical web and horizontal flanges. That is, the web is assumed to be parallel to the ζ-axis, and flanges are assumed to be parallel to the x-axis. In Eqs. (2.60), the parameters h_w and b_w denote the web height and flange width, respectively, and K is the total number of flanges in the ring cross section.

For structural models in which the effect of warping of the ring cross section is excluded, the contribution of the bimoment, $M_{\omega r}$, to the virtual work of the ring in Eq. (2.56) is neglected, and the fourth row and column of the stiffness matrix, Eq. (2.58), are ignored. Also, the warping function $\omega(x, \zeta)$ is taken as zero.

2.3 CLASSICAL FORMULATIONS

2.3.1 SHELL

The shell is modeled with Sanders' theory[31], in which first approximation thin shell theory is used; i.e., the effects of transverse shear and normal strains are neglected. The displacements at an arbitrary material point in the shell are approximated by Eqs. (2.1) to (2.3), in which the rotations ϕ_x and ϕ_θ are related to the displacements by Eqs. (2.16) and (2.17), respectively. Thus, transverse shear strains e_{xz} and $e_{\theta z}$ in Eqs. (2.9) vanish. For small displacement gradients, the three-dimensional engineering strains in Sanders' theory are given by Eqs. (2.7) and

$$e_{x\theta} = \frac{(1 + \frac{z}{2R} + \frac{z^2}{4R^2})\gamma_{x\theta} + z(1 + \frac{z}{2R})\kappa^s_{x\theta}}{(1 + \frac{z}{R})} \tag{2.61}$$

in which the quantity $\kappa^s_{x\theta}$ is the twisting strain measure in the Sanders' theory, which is defined in the following sub-subsection.

2.3.1.1 STRAIN-DISPLACEMENT RELATIONS

Define a generalized strain vector in terms of the shell strain measures by

$$\vec{\epsilon}_{shell} = [\epsilon_{xx}, \epsilon_{\theta\theta}, \gamma_{x\theta}, \kappa_{xx}, \kappa_{\theta\theta}, \kappa^s_{x\theta}]^T \tag{2.62}$$

The first five strain measures of the shell reference surface in Eq. (2.62) are related to the displacements by Eqs. (2.10-2.12), and the sixth strain measure, $\kappa^s_{x\theta}$, is given by

$$\kappa^s_{x\theta} = \frac{\partial \phi_\theta}{\partial x} + \frac{1}{R}\frac{\partial \phi_x}{\partial \theta} + \frac{1}{R}\phi_z \tag{2.63}$$

in which the rotation about the normal, ϕ_z, is given by

$$\phi_z = \frac{1}{2}(\frac{\partial v}{\partial x} - \frac{1}{R}\frac{\partial u}{\partial \theta}) \tag{2.64}$$

The Donnell-Mushtari-Vlasov (DMV) approximation, or quasi-shallow shell theory is obtained by neglecting the term $\frac{v}{R}$ in Eq. (2.17) for the rotation ϕ_θ, and the rotation about the normal ϕ_z in Eq. (2.63).

2.3.1.2 VIRTUAL WORK

Define a generalized stress vector in terms of the stress resultants and couples of Sanders' theory by

$$\vec{\sigma}_{shell} = [N_{xx}, N_{\theta\theta}, N^s_{x\theta}, M_{xx}, M_{\theta\theta}, M^s_{x\theta}]^T \tag{2.65}$$

such that the internal virtual work is still given by Eq. (2.21) except that the stress and strain vectors are 6×1 vectors in Sanders theory. Quantities $N^s_{x\theta}$ and $M^s_{x\theta}$ are the modified shear and twisting moment resultants. In terms of physical stress and moment resultants of the shell these are given by

$$N^s_{x\theta} = \frac{1}{2}(N_{x\theta} + N_{\theta x}) + \frac{1}{4R}(M_{x\theta} - M_{\theta x}) \tag{2.66}$$

$$M^s_{x\theta} = \frac{1}{2}(M_{x\theta} + M_{\theta x}) \tag{2.67}$$

In the Sanders' original paper[31] the term $\frac{1}{4R}(M_{x\theta} - M_{\theta x})$ in Eq. (2.66) was considered to be small as compared to $\frac{1}{2}(N_{x\theta} + N_{\theta x})$, and was, therefore, neglected. However, this approximation is not made here. For infinitesimal virtual displacements, the internal virtual work for the shell can be obtained by substituting Eqs. (2.62) and (2.65) into Eq. (2.21), which results in

$$\delta \mathcal{W}^{shell}_{int} = \iint_S [N_{xx}\delta\epsilon_{xx} + N_{\theta\theta}\delta\epsilon_{\theta\theta} + N^s_{x\theta}\delta\gamma_{x\theta} + M_{xx}\delta\kappa_{xx} + M_{\theta\theta}\delta\kappa_{\theta\theta} + M^s_{x\theta}\delta\kappa^s_{x\theta}]\, dS \tag{2.68}$$

where S denotes the area of the reference surface. The external virtual work expression for the classical shell theory is still given by Eq. (2.28).

2.3.1.3 CONSTITUTIVE RELATIONS

Consider the material law for an orthotropic lamina given by Eq. (2.30). To get the material law for the shell, substitute Eq. (2.30) into the definitions of the resultants in terms of stresses, Eqs. (2.24); substitute Eqs. (2.7) and (2.61) for the three-dimensional

strains; and then perform the integration with respect to the thickness coordinate. Using the definitions of the modified resultants in Eqs. (2.66) and (2.67) gives the final form of the material law as

$$\begin{Bmatrix} N_{xx} \\ N_{\theta\theta} \\ N^s_{x\theta} \\ M_{xx} \\ M_{\theta\theta} \\ M^s_{x\theta} \end{Bmatrix} = \begin{bmatrix} A_{11} & A_{12} & A_{16} & B_{11} & B_{12} & B_{16} \\ A_{12} & A_{22} & A_{26} & B_{12} & B_{22} & B_{26} \\ A_{16} & A_{26} & A_{66} & B_{61} & B_{62} & B_{66} \\ B_{11} & B_{12} & B_{61} & D_{11} & D_{12} & D_{16} \\ B_{12} & B_{22} & B_{62} & D_{12} & D_{22} & D_{26} \\ B_{16} & B_{26} & B_{66} & D_{16} & D_{26} & D_{66} \end{bmatrix} \begin{Bmatrix} \epsilon_{xx} \\ \epsilon_{\theta\theta} \\ \gamma_{x\theta} \\ \kappa_{xx} \\ \kappa_{\theta\theta} \\ \kappa^s_{x\theta} \end{Bmatrix} \tag{2.69}$$

where the stiffnesses $A_{11}, A_{12}, A_{22}, B_{11}, B_{12}, B_{22}, D_{11}, D_{12}$ and D_{22} in Eq. (2.69) are given by the first three of Eqs. (2.32), with the remaining stiffnesses defined by

$$\begin{aligned}
(A_{16}, B_{61}) &= \int_t (1, z)\bar{Q}_{16}[1 + \frac{z}{2R} + \frac{z^2}{4R^2}]dz \\
(A_{26}, B_{62}) &= \int_t (1, z)\bar{Q}_{26}[1 + \frac{z}{2R} + \frac{z^2}{4R^2}](1 + \frac{z}{R})^{-1}dz \\
A_{66} &= \int_t \bar{Q}_{66}[1 + \frac{z}{2R} + \frac{z^2}{4R^2}]^2(1 + \frac{z}{R})^{-1}dz \\
B_{16} &= \int_t \bar{Q}_{16}z(1 + \frac{z}{2R})dz \\
B_{26} &= \int_t \bar{Q}_{26}z(1 + \frac{z}{2R})(1 + \frac{z}{R})^{-1}dz \\
B_{66} &= \int_t \bar{Q}_{66}z[1 + \frac{z}{2R} + \frac{z^2}{4R^2}](1 + \frac{z}{2R})(1 + \frac{z}{R})^{-1}dz \\
D_{16} &= \int_t \bar{Q}_{16}z^2(1 + \frac{z}{2R})dz \\
D_{26} &= \int_t \bar{Q}_{26}z^2(1 + \frac{z}{2R})(1 + \frac{z}{R})^{-1}dz \\
D_{66} &= \int_t \bar{Q}_{66}z^2(1 + \frac{z}{2R})^2(1 + \frac{z}{R})^{-1}dz
\end{aligned} \tag{2.70}$$

2.3.2 STRINGER

The stringer is modeled with Euler-Bernoulli beam theory thereby neglecting the transverse shear strain. Hence, equating γ_{zs} in the last of Eqs. (2.49) to zero results in the following expression for $\phi_{\theta s}$:

$$\phi_{\theta s} = -w'_s \tag{2.71}$$

It may be noted that neglecting the transverse shear strain would also modify the virtual work statement given by Eq. (2.51), and the third equation in the Hooke's law, Eq. (2.52), is neglected.

2.3.3 RING

The ring is modeled with thin-walled, open section, curved bar theory developed by Woodson, Johnson, and Haftka[28]. For classical formulations, the transverse shear strains are neglected. Hence, equating γ_{xr} and γ_{zr} in the last two of Eqs. (2.57) to zero results in the following expressions for the rotations ϕ_{xr} and ϕ_{zr}.

$$\phi_{xr} = \frac{1}{R_0}(v_r - \dot{w}_r) \qquad \phi_{zr} = -\frac{1}{R_0}\dot{u}_r \tag{2.72}$$

It may be noted that neglecting the transverse shear strains would also modify the virtual work statement given by Eq. (2.56), and Hooke's law for the shear resultants, Eq. (2.59), is neglected.

2.4 DISPLACEMENT CONTINUITY

In order to maintain continuous deformation between the inside surface of the shell and stiffeners along their lines of contact, the displacements and rotations should be continuous at the shell-stiffener interface. For a symmetrical section stringer, the unit cell model is symmetric about x-axis, and the only non-zero displacements for the stringer are the axial and normal displacements. The axial and normal displacements at the top flange of the stringer in contact with the shell are obtained from Eqs. (2.46) and (2.47) for $\xi = \epsilon_s$, where ϵ_s is the radial distance from the stringer centroid to the contact line along the inside surface of the shell. Similarly, the corresponding shell displacements at the inside surface of the shell (i.e., at $z = -t/2$) are obtained from Eqs. (2.1) and

(2.3). Hence, the following displacement continuity constraints are imposed along the shell-stringer interface (i.e., $-l \leq x \leq l$, $\theta = 0$).

$$g_{xs} = u(x,0) - \frac{t}{2}\phi_x(x,0) - \left[u_s(x) + e_s\phi_{\theta s}(x)\right] = 0 \tag{2.73}$$

$$g_{zs} = w(x,0) - w_s(x) = 0 \tag{2.74}$$

The asymmetrical section ring bends out-of-plane and twists, in addition to in-plane bending and stretching along its circumference. Hence, the displacement field for the ring consists of axial, circumferential, and normal components given by Eqs. (2.53) to (2.55). From Eqs. (2.54) and (2.55), it can be observed that the circumferential and normal displacements of the ring vary along the width of the attachment flange.

Point-wise continuity of the circumferential displacement between the inside surface of the shell and the attachment flange of the ring implies

$$V(x,\theta,-t/2) = V_r(x,\theta,e_r) \qquad x \in (-b_{f1}, b_{f2}),\ \theta \in (-\Theta,\Theta) \tag{2.75}$$

in which $b_{f1} + b_{f2} = b_f > 0$ where b_f is the width of the attachment flange, and e_r is the distance from the ring reference arc to the contact line along the inside surface of the shell. Since the kinematic assumptions in the ring theory give V_r as an explicit linear function of x, Eq. (2.54), and the x-distribution of the shell displacement V, Eq. (2.2), is not known apriori, pointwise satisfaction of Eq. (2.75) across the width of the attachment flange cannot be achieved. To proceed, the shell displacement is approximated in a Taylor series in x about $x = 0$. That is,

$$V(x,\theta,-t/2) = V(0,\theta,-t/2) + x\frac{\partial V}{\partial x}|_{x=0} + O(x^2) \tag{2.76}$$

Substituting Eq. (2.76) into Eq. (2.75), the continuity of the circumferential displacement across the width of the attachment flange can be achieved through terms of order x. Thus, $V(0,\theta,-t/2) = V_r(0,\theta,e_r)$ leads to

$$g_{\theta r} = v(0,\theta) - \frac{t}{2}\phi_\theta(0,\theta) - \left[v_r(\theta) + e_r\phi_{xr}(\theta) - \omega_0\tau_r(\theta)\right] = 0, \tag{2.77}$$

and $x\frac{\partial V}{\partial x}|_{x=0} = V_r(x,\theta,e_r) - V_r(0,\theta,e_r)$ leads to

$$G_{zr} = \left[\frac{\partial v}{\partial x}|_{x=0} - \frac{t}{2}\frac{\partial \phi_\theta}{\partial x}|_{x=0}\right] - \left[\phi_{zr}(\theta) - \omega_1 \tau_r(\theta)\right] = 0 \tag{2.78}$$

The constraint $G_{zr} = 0$ imposed through Eq. (2.78) also implies that the rotation about z-axis of the shell's line element tangent to x-curve, $\frac{\partial V}{\partial x}$, equals the rotation of the ring around ζ-axis along their contact line. In Eqs. (2.77) and (2.78), parameters ω_0 and ω_1 are the constant coefficients in the contour warping function, $\omega(x,\zeta) = \omega_0 + x\omega_1$, for the attachment flange of the ring. (Thickness warping is neglected and ζ =constant along the flange contour.) For structural models in which the effect of warping of the ring cross section is excluded, the contour warping function $\omega(x,\zeta)$ is taken as zero.

Similarly, point-wise continuity of the normal displacement between the inside surface of the shell and the attachment flange of the ring implies

$$W(x,\theta,-t/2) = W_r(x,\theta,e_r) \qquad x \in (-b_{f1}, b_{f2}),\ \theta \in (-\Theta,\Theta) \tag{2.79}$$

Since the kinematic assumptions in the ring theory give W_r as an explicit linear function of x, Eq. (2.55), and the x-distribution of the shell displacement W, Eq. (2.3), is not known apriori, pointwise satisfaction of Eq. (2.79) across the width of the attachment flange cannot be achieved. To proceed, the shell displacement is approximated in a Taylor series in x about $x = 0$. That is,

$$W(x,\theta,-t/2) = W(0,\theta,-t/2) + x\frac{\partial W}{\partial x}|_{x=0} + O(x^2) \tag{2.80}$$

Substituting Eq. (2.80) into Eq. (2.79) the continuity of the normal displacement across the width of the attachment flange can be achieved through terms of order x. Thus, $W(0,\theta,-t/2) = W_r(0,\theta,e_r)$ leads to

$$g_{zr} = w(0,\theta) - w_r(\theta) = 0 \tag{2.81}$$

and $x\frac{\partial W}{\partial x}|_{x=0} = W_r(x,\theta,e_r) - W_r(0,\theta,e_r)$ leads to

$$G_{\theta r} = \frac{\partial w}{\partial x}|_{x=0} + \phi_{\theta r}(\theta) = 0 \tag{2.82}$$

The constraint $G_{\theta r} = 0$ imposed through Eq. (2.82) also implies that the rotation about θ-axis of the shell's line element tangent to x-curve, $-\frac{\partial W}{\partial x}$, is equal to the twist of the ring, $\phi_{\theta r}$, along the contact line.

Point-wise continuity of the axial displacement between the inside surface of the shell and the attachment flange of the ring implies

$$U(x,\theta,-t/2) = U_r(x,\theta,e_r) \qquad x \in (-b_{f1}, b_{f2}),\ \theta \in (-\Theta,\Theta) \tag{2.83}$$

Since the kinematic assumptions in the ring theory give U_r independent of x, Eq. (2.53), and the shell displacement U, Eq. (2.1), is an arbitrary function of x, pointwise satisfaction of Eq. (2.83) across the width of the attachment flange can be achieved only through terms of order x^0. Thus, $U(0,\theta,-t/2) = U_r(0,\theta,e_r)$ leads to

$$g_{xr} = u(0,\theta) - \frac{t}{2}\phi_x(0,\theta) - \left[u_r(\theta) + e_r\phi_{\theta r}(\theta)\right] = 0 \tag{2.84}$$

In order to include the axial load sharing between the shell and stringer due to closed-end pressure vessel effects directly into the analysis, a seperate constraint is imposed. This constraint is that the elongation of the shell at $\theta = 0$, $z = 0$ and the elongation of the stringer at $\xi = 0$ are the same; i.e.

$$\left[U(l,0,0) - U(-l,0,0)\right] - \left[U_s(l,0) - U_s(-l,0)\right] = 0 \tag{2.85}$$

Substituting Eqs. (2.1) and (2.46) into Eq. (2.85) leads to

$$\left[u(l,0) - u(-l,0)\right] - \left[u_s(l) - u_s(-l)\right] = 0 \tag{2.86}$$

2.5 AUGMENTED VIRTUAL WORK FOR THE ASSEMBLY

Inter-element continuity is enforced by augmenting the virtual work functional with the integrals of Lagrange multipliers functions times the variations in the displacement constraints. Refering to Fig. 1.3 the Lagrange multipliers are interpreted as the components of the interacting line loads between the stiffeners and the shell, and are defined positive if acting on the inside surface of the shell in positive coordinate directions. Thus, for the shell, the augmented (or external) virtual work due to the interacting loads is

$$\begin{aligned}\delta \mathcal{W}_{\lambda}^{shell} = & \int_{-l}^{l} \left\{ \lambda_{xs}(x)\left[\delta u(x,0) - \frac{t}{2}\delta\phi_x(x,0)\right] + \lambda_{zs}(x)\delta w(x,0) \right\} dx \\ & + \int_{-\Theta}^{\Theta} \left\{ \lambda_{xr}(\theta)\left[\delta u(0,\theta) - \frac{t}{2}\delta\phi_x(0,\theta)\right] + \lambda_{\theta r}(\theta)\left[\delta v(0,\theta) - \frac{t}{2}\delta\phi_\theta(0,\theta)\right] \right. \\ & \left. + \lambda_{zr}(\theta)\delta w(0,\theta) - \Lambda_{\theta r}(\theta)\delta\left(\frac{\partial w}{\partial x}\Big|_{x=0}\right) + \Lambda_{zr}(\theta)\delta\left(\frac{\partial v}{\partial x}\Big|_{x=0} - \frac{t}{2}\frac{\partial \phi_\theta}{\partial x}\Big|_{x=0}\right) \right\} * \\ & \left(R - \frac{t}{2}\right) d\theta - Q[\delta u(l,0) - \delta u(-l,0)]\end{aligned} \tag{2.87}$$

The axial force Q in Eq. (2.87) is an additional Lagrange multiplier that accounts for axial load sharing between the stringer and shell. Similarly, for the stringer, the augmented (or external) virtual work due to the interacting loads is

$$\begin{aligned}\delta \mathcal{W}_{\lambda}^{stringer} = & -\int_{-l}^{l} \left\{ \lambda_{xs}(x)\left[\delta u_s(x) + e_s\delta\phi_{\theta s}(x)\right] + \lambda_{zs}(x)\delta w_s(x) \right\} dx \\ & + Q[\delta u_s(l) - \delta u_s(-l)]\end{aligned} \tag{2.88}$$

and, for the ring is given by

$$\begin{aligned}\delta \mathcal{W}_{\lambda}^{ring} = & -\int_{-\Theta}^{\Theta} \left\{ \lambda_{xr}(\theta)\left[\delta u_r(\theta) + e_r\delta\phi_{\theta r}(\theta)\right] + \lambda_{\theta r}(\theta)\left[\delta v_r(\theta) + e_r\delta\phi_{xr}(\theta) - \omega_0\delta\tau_r(\theta)\right] \right. \\ & \left. + \lambda_{zr}(\theta)\delta w_r(\theta) + \Lambda_{\theta r}(\theta)\delta\phi_{\theta r}(\theta) + \Lambda_{zr}(\theta)\left[\delta\phi_{zr}(\theta) - \omega_1\delta\tau_r(\theta)\right] \right\}\left(1 + \frac{e_r}{R_0}\right) * \\ & R_0\, d\theta\end{aligned} \tag{2.89}$$

The displacement constraints (Eqs. (2.73), (2.74), (2.77), (2.78), (2.81), (2.82), (2.84) and (2.86)) are enforced by vanishing of the inner product of these equations with the variations in the Lagrange multiplier functions. The variational form of these constraints are

$$\int_{-l}^{l} \left[\delta\lambda_{xs} g_{xs} + \delta\lambda_{zs} g_{zs}\right] \, dx \;=\; 0 \tag{2.90}$$

$$\int_{-\Theta}^{\Theta} \left[\delta\lambda_{xr} g_{xr} + \delta\lambda_{\theta r} g_{\theta r} + \delta\lambda_{zr} g_{zr} + \delta\Lambda_{\theta r} G_{\theta r} + \delta\Lambda_{zr} G_{zr}\right] \, (R_0 + \epsilon_r) \, d\theta \;=\; 0 \tag{2.91}$$

$$\delta Q \left\{ \left[u(l,0) - u(-l,0)\right] - \left[u_s(l) - u_s(-l)\right] \right\} \;=\; 0 \tag{2.92}$$

CHAPTER 3
GOVERNING EQUATIONS FOR NONLINEAR ANALYSIS

3.1 ANALYTICAL MODEL AND ASSUMPTIONS

A geometrically nonlinear elastic analysis is carried out for the orthogonally-stiffened cylindrical shell subjected to internal pressure. The structural repeating unit (or unit cell model) of Fig. 1.2 is analyzed to obtain response of the entire structure. The shell is modeled with Sander's nonlinear theory of thin shells, and the stiffeners are modeled with a nonlinear Euler-Bernoulli beam theory. The purpose of nonlinear elastic analysis is twofold: First, the distributions of interacting loads between the shell wall and the stiffeners are obtained and compared with those obtained from a geometrically linear elastic analysis. Second, the influence of geometric nonlinearity on the the stress concentration in the shell adjacent to the stiffeners due to "pillowing" is studied.

Only stiffeners with symmetrical cross sections are considered for the nonlinear response. Hence there is no out-of-plane bending and torsion of the ring, and no rotation of the joint at the stiffener intersection about the circumferential axis. Also, on the basis of the symmetry about the x- and θ-axes for the repeating unit, only the interacting line load components tangent and normal to the stiffeners are included in the analysis. The shell-stringer interacting force components per unit length along the contact lines are denoted by $\lambda_{xs}(x)$ for the component tangent to the stringer, and $\lambda_{zs}(x)$ for the component normal to the stringer. The two shell-ring interacting load components per unit length along the contact lines are denoted by $\lambda_{\theta r}(\theta)$ for the component tangent to the ring and $\lambda_{zr}(\theta)$ for the component normal to the ring. These interacting loads acting in a positive sense on the inside surface of the shell are shown in Fig. 1.3. In this chapter nonlinear formulations

are presented for the shell and stiffeners based on classical theory. The following general assumptions are made for nonlinear elastic analysis of the repeating unit:

1. Normals to the undeformed reference surface remain straight and normal to the deformed reference surface, and are inextensional.
2. Material behavior is linearly elastic.
3. The thickness normal stress is assumed to be small with respect to the normal stresses in the axial and circumferential directions, and hence it is neglected in the material law.

3.2 SHELL

3.2.1 STRAIN-DISPLACEMENT RELATIONS

Sanders[32] nonlinear theory of thin shells is employed to model the shell. The generalized strain vector for the shell is given by Eq. (2.62). Assuming the strains are small and rotations are moderately small, the membrane strain-displacement relations are

$$\begin{aligned} \epsilon_{xx} &= \frac{\partial u}{\partial x} + \frac{1}{2}\phi_x^2 + \frac{1}{2}\phi_z^2 \\ \epsilon_{\theta\theta} &= \frac{1}{R}\frac{\partial v}{\partial \theta} + \frac{w}{R} + \frac{1}{2}\phi_\theta^2 - \frac{1}{2}\phi_z^2 \\ \gamma_{x\theta} &= \frac{\partial v}{\partial x} + \frac{1}{R}\frac{\partial u}{\partial \theta} + \phi_x\phi_\theta \end{aligned} \tag{3.1}$$

in which the rotations ϕ_x, ϕ_θ and ϕ_z are given by Eqs. (2.16), (2.17) and (2.64), respectively. The change in the normal curvature components, κ_{xx}, $\kappa_{\theta\theta}$, and $\kappa_{x\theta}^s$ in terms of the shell rotations are linear and are given by Eqs. (2.10), (2.11) and (2.63), respectively. The Donnell-Mushtari-Vlasov (DMV) approximation, or quasi-shallow shell theory, is obtained by neglecting the rotation about the normal in the strains of Eqs. (3.1) and (2.63), and

the term $\frac{v}{R}$ in rotation ϕ_θ of Eq. (2.17). In this work, it is assumed that the contribution of the rotation about the normal to the strains is negligible for the shell. However, the DMV approximation is not assumed initially.

3.2.2 INTERNAL VIRTUAL WORK

The generalized stress vector in terms of the stress resultants and couples of Sanders' theory is defined by Eq. (2.65), and the internal virtual work for the shell in deformed state is given by Eq. (2.68). However, the stress resultants and stress couples are now defined in terms of second Piola-Kirchhoff stress tensor, which is based on the undeformed configuration of the body. Substituting for strains from Eqs. (3.1), κ_{xx} from (2.10), $\kappa_{\theta\theta}$ from (2.11), and $\kappa^s_{x\theta}$ from (2.63) into Eq. (2.68), in conjuction with Eqs. (2.16) and (2.17) for the definitions of rotations, results in the following expression for the internal virtual work for the shell:

$$\begin{aligned}\delta \mathcal{W}_{int}^{shell} = \iint_S \Big\{ & N_{xx}\ \delta(\frac{\partial u}{\partial x}) + \frac{N^s_{x\theta}}{R}\ \delta(\frac{\partial u}{\partial \theta}) + \Big[-\frac{N_{\theta\theta}}{R}(\frac{1}{R}\frac{\partial w}{\partial \theta} - \frac{v}{R}) - \frac{N^s_{x\theta}}{R}\frac{\partial w}{\partial x}\Big]\ \delta v \\ & + \Big[N^s_{x\theta} + \frac{M^s_{x\theta}}{R}\Big]\ \delta(\frac{\partial v}{\partial x}) + \Big[\frac{N_{\theta\theta}}{R} + \frac{M_{\theta\theta}}{R^2}\Big]\ \delta(\frac{\partial v}{\partial \theta}) + \frac{N_{\theta\theta}}{R}\ \delta w - M_{xx}\ \delta(\frac{\partial^2 w}{\partial x^2}) \\ & - \frac{M_{\theta\theta}}{R^2}\ \delta(\frac{\partial^2 w}{\partial \theta^2}) - \frac{2M^s_{x\theta}}{R}\ \delta(\frac{\partial^2 w}{\partial \theta \partial x}) + \Big[N_{xx}\frac{\partial w}{\partial x} + N^s_{x\theta}(\frac{1}{R}\frac{\partial w}{\partial \theta} - \frac{v}{R})\Big]\ \delta(\frac{\partial w}{\partial x}) \\ & + \Big[\frac{N_{\theta\theta}}{R}(\frac{1}{R}\frac{\partial w}{\partial \theta} - \frac{v}{R}) + \frac{N^s_{x\theta}}{R}\frac{\partial w}{\partial x}\Big]\ \delta(\frac{\partial w}{\partial \theta})\Big\}\ dS\end{aligned} \tag{3.2}$$

3.2.3 EXTERNAL VIRTUAL WORK

Mathematically the stiffened shell is considered closed at $x = \pm\infty$. The work done by hydrostatic pressure on an enclosed volume can be derived from a potential energy functional, since hydrostatic pressure is a conservative load. However, the infinite volume is inconvenient to deal with. Instead, a repeating volume element of the structure that is of finite size can be considered, and the potential energy functional for it can be derived.

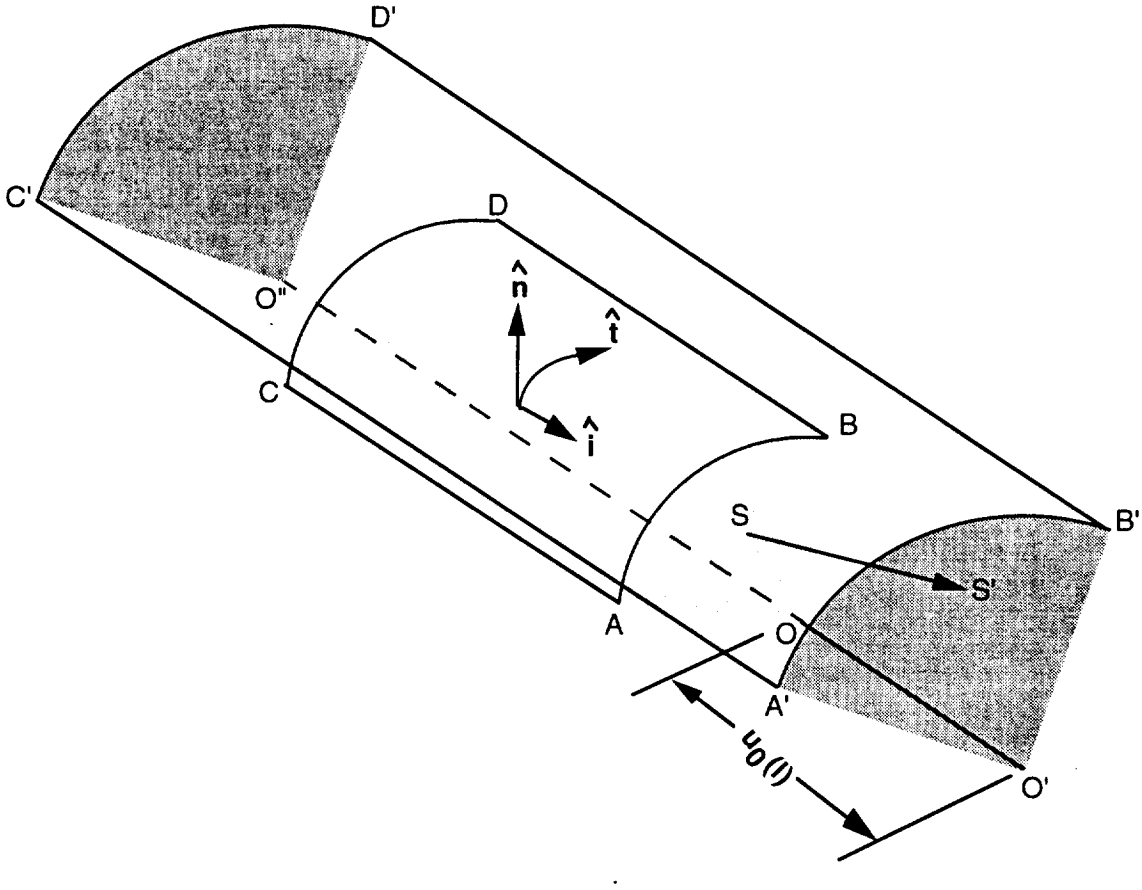

Fig. 3.1 Enclosed volume of a repeating unit.

An enclosed volume to contain the pressurized medium can be modeled by joining the edges of the repeating unit to the axis of revolution of the cylinder as shown in Fig. 3.1. The shaded portions are assumed to represent diaphragms (or end caps) enclosing the so-formed pie-shaped volume. These diaphragms do not resist deformation of the repeating unit, but act to transmit loads normal to the edges of the repeating unit due to the internal pressure. Under the action of uniform internal pressure, the right cylindrical sector expands to acquire larger volume. Thus, for the deformed volume of Fig. 3.1, the external virtual work for the shell due to internal pressure is written as

$$\delta \mathcal{W}_p^{shell} = \delta \mathcal{W}_{ps}^{shell} + \delta \mathcal{W}_{pd}^{shell} \tag{3.3}$$

where $\delta \mathcal{W}_{ps}^{shell}$ is the virtual work done by the internal pressure acting on the deformed panel area $A'B'C'D'$, and $\delta \mathcal{W}_{pd}^{shell}$ is the virtual work done by the internal pressure acting on the deformed diaphragm areas $O'A'B'$ and $O''C'D'$. The virtual work done by the internal pressure acting on the deformed panels $O'A'C'O''$ and $O'B'D'O''$ is zero due to the periodicity of displacement boundary conditions at $\theta = \pm\Theta$.

Expression for $\delta \mathcal{W}_{ps}^{shell}$

Consider a material point at P on the undeformed reference surface of the shell that goes to point P' on the deformed surface. Let the position vector of point P be $\vec{\mathbf{R}}$ and of point P' be $\vec{\mathbf{R}}^*$, and further let the displacement vector from point P to P' be $\vec{\mathbf{U}}$, as shown in Fig. 3.2(a). In terms of components along the directions of unit vectors $\hat{\mathbf{i}}$, $\hat{\mathbf{t}}(\theta)$, and $\hat{\mathbf{n}}(\theta)$ of a generic point on the undeformed surface, these vectors are represented as

$$\vec{\mathbf{R}} = x\ \hat{\mathbf{i}} + R\ \hat{\mathbf{n}}(\theta) \tag{3.4}$$

$$\vec{\mathbf{U}} = u(x,\theta)\ \hat{\mathbf{i}} + v(x,\theta)\ \hat{\mathbf{t}}(\theta) + w(x,\theta)\ \hat{\mathbf{n}}(\theta) \tag{3.5}$$

$$\vec{\mathbf{R}}^* = \vec{\mathbf{R}} + \vec{\mathbf{U}} \tag{3.6}$$

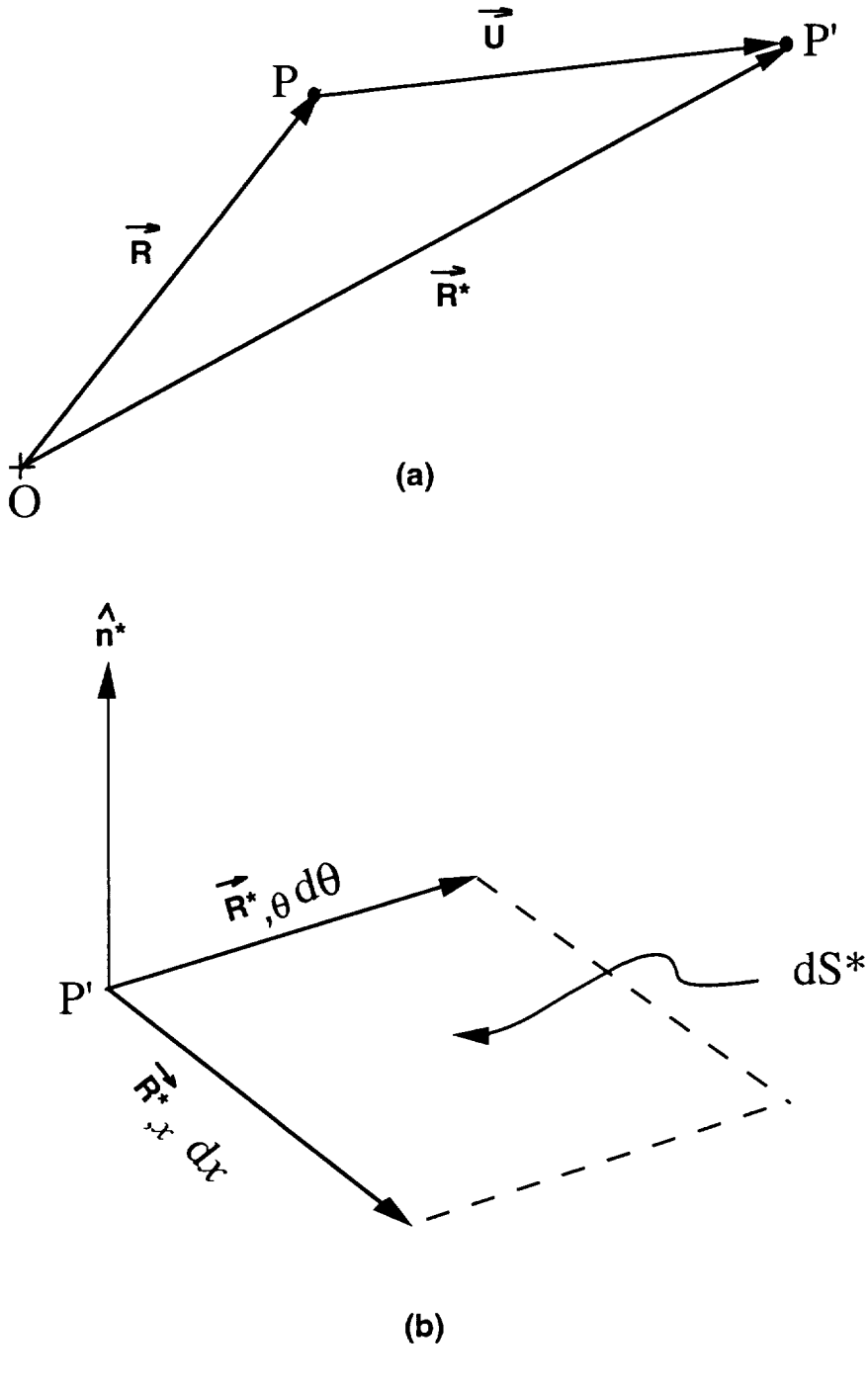

Fig. 3.2 Position vector and elemental area of the deformed upper surface.

Using the geometric property of the cross products of position vectors (Fig. 3.2(b)), an elemental area dS^* of the deformed surface can be written as

$$dS^*\ \hat{\mathbf{n}}^* \;=\; \frac{\partial \vec{\mathbf{R}}^*}{\partial x}\,dx \;\times\; \frac{\partial \vec{\mathbf{R}}^*}{\partial \theta}\,d\theta \tag{3.7}$$

where $\hat{\mathbf{n}}^*$ is the unit vector normal to the deformed surface element. Substituting Eqs. (3.4) and (3.5) into Eq. (3.6), using the resulting expression for $\vec{\mathbf{R}}^*$ in Eq. (3.7), and noting that $\frac{\partial \hat{\mathbf{n}}}{\partial \theta} = \hat{\mathbf{t}}$ and $\frac{\partial \hat{\mathbf{t}}}{\partial \theta} = -\hat{\mathbf{n}}$, the following expression for the elemental area of the deformed surface is obtained.

$$dS^*\ \hat{\mathbf{n}}^* \;=\; \begin{vmatrix} \hat{\mathbf{i}} & \hat{\mathbf{t}} & \hat{\mathbf{n}} \\ 1+\frac{\partial u}{\partial x} & \frac{\partial v}{\partial x} & \frac{\partial w}{\partial x} \\ \frac{1}{R}\frac{\partial u}{\partial \theta} & 1+\frac{1}{R}(\frac{\partial v}{\partial \theta}+w) & \frac{1}{R}(\frac{\partial w}{\partial \theta}-v) \end{vmatrix} dS \tag{3.8}$$

where $dS = R d\theta\, dx$ is the elemental area of the undeformed surface. For the hydrostatic pressure p acting on the deformed surface $A'B'C'D'$, the external virtual work is given by

$$\delta \mathcal{W}_{ps}^{shell} = \iint_{S^*} (p\ dS^*\ \hat{\mathbf{n}}^*) \bullet \delta \vec{\mathbf{U}} \tag{3.9}$$

where $\delta\vec{\mathbf{U}} = \delta u(x,\theta)\,\hat{\mathbf{i}} + \delta v(x,\theta)\,\hat{\mathbf{t}}(\theta) + \delta w(x,\theta)\,\hat{\mathbf{n}}(\theta)$ is the virtual (infinitesimal) displacement vector, and S^* is the area of the deformed reference surface. Upon substituting Eq. (3.8) into Eq. (3.9) and carrying out the algebra, the following expression for the first component of external virtual work is obtained:

$$\begin{aligned}\delta \mathcal{W}_{ps}^{shell} =& p\iint_S \Big\{ \Big[\frac{1}{R}(\frac{\partial w}{\partial \theta} - v)\frac{\partial v}{\partial x} - \big[1+\frac{1}{R}(\frac{\partial v}{\partial \theta}+w)\big]\frac{\partial w}{\partial x}\Big]\delta u + \Big[\frac{1}{R}\frac{\partial u}{\partial \theta}\frac{\partial w}{\partial x} - \frac{1}{R}(\frac{\partial w}{\partial \theta} \\ & - v)\big(1+\frac{\partial u}{\partial x}\big)\Big]\ \delta v + \Big[\big(1+\frac{\partial u}{\partial x}\big)\big[1+\frac{1}{R}(\frac{\partial v}{\partial \theta}+w)\big] - \frac{1}{R}\frac{\partial u}{\partial \theta}\frac{\partial v}{\partial x}\Big]\ \delta w \Big\}\ dS\end{aligned} \tag{3.10}$$

in which S denotes the area of the undeformed reference surface. Equation (3.10) is expanded and the terms are rearranged to obtain the following intermediate expression for the first component of external virtual work:

$$\begin{aligned}\delta \mathcal{W}_{ps}^{shell} =& p\iint_S \Big\{ \delta\Big[\frac{1}{2R}(v^2+w^2)(1+\frac{\partial u}{\partial x}) + w(\frac{\partial u}{\partial x} + \frac{1}{R}\frac{\partial v}{\partial \theta}) + w\Big] - \frac{\partial w}{\partial x}(1+\frac{w}{R})\delta u \\ & + \frac{1}{R}\Big(\frac{\partial v}{\partial x}\frac{\partial w}{\partial \theta} - \frac{\partial v}{\partial \theta}\frac{\partial w}{\partial x}\Big)\delta u + \frac{1}{R}\Big(\frac{\partial w}{\partial x}\frac{\partial u}{\partial \theta} - \frac{\partial w}{\partial \theta}\frac{\partial u}{\partial x}\Big)\delta v + \frac{1}{R}\Big(\frac{\partial u}{\partial x}\frac{\partial v}{\partial \theta} - \frac{\partial u}{\partial \theta}\frac{\partial v}{\partial x}\Big)\delta w \\ & - \Big[\frac{1}{2R}(v^2+w^2)+w\Big]\delta\Big(\frac{\partial u}{\partial x}\Big) - \frac{v}{R}\frac{\partial v}{\partial x}\delta u - \frac{w}{R}\delta\Big(\frac{\partial v}{\partial \theta}\Big) - \frac{1}{R}\frac{\partial w}{\partial \theta}\delta v\Big\} dS\end{aligned} \tag{3.11}$$

The terms containing derivatives of the virtual displacements in Eq. (3.11) are integrated by parts, and then the terms are further rearranged to obtain the following expression for the first component of external virtual work functional:

$$\begin{aligned}\delta \mathcal{W}_{ps}^{shell} =& p\iint_S \delta\Big[\frac{1}{2R}(v^2+w^2)(1+\frac{\partial u}{\partial x}) + w(\frac{\partial u}{\partial x}+\frac{1}{R}\frac{\partial v}{\partial \theta}) + \frac{1}{3R}(\frac{\partial v}{\partial x}\frac{\partial w}{\partial \theta}-\frac{\partial v}{\partial \theta}\frac{\partial w}{\partial x})u \\ &+ \frac{1}{3R}(\frac{\partial w}{\partial x}\frac{\partial u}{\partial \theta}-\frac{\partial w}{\partial \theta}\frac{\partial u}{\partial x})v + \frac{1}{3R}(\frac{\partial u}{\partial x}\frac{\partial v}{\partial \theta}-\frac{\partial u}{\partial \theta}\frac{\partial v}{\partial x})w + w\Big] dS \\ &+ p\int_{-l}^{l}\Big\{\frac{1}{3}\Big[w\frac{\partial v}{\partial x}-v\frac{\partial w}{\partial x}\Big]\ \delta u + \Big[-w+\frac{1}{3}(u\frac{\partial w}{\partial x}-w\frac{\partial u}{\partial x})\Big]\ \delta v \\ &+ \frac{1}{3}\Big[v\frac{\partial u}{\partial x}-u\frac{\partial v}{\partial x}\Big]\ \delta w\Big\}_{-\Theta}^{+\Theta} dx \\ &+ p\int_{-\Theta}^{\Theta}\Big\{\Big[-w-\frac{1}{2R}(v^2+w^2)+\frac{1}{3R}(v\frac{\partial w}{\partial \theta}-w\frac{\partial v}{\partial \theta})\Big]\ \delta u + \frac{1}{3R}(w\frac{\partial u}{\partial \theta} \\ &- u\frac{\partial w}{\partial \theta})\ \delta v + \frac{1}{3R}(u\frac{\partial v}{\partial \theta}-v\frac{\partial u}{\partial \theta})\ \delta w\Big\}_{-l}^{+l} R\, d\theta\end{aligned} \tag{3.12}$$

Expression for $\delta \mathcal{W}_{pd}^{shell}$

The stiffened shell has a periodic symmetry about its axis of revolution in the sense that a rotation of the structure through integer multiplies of 2Θ brings the structure into self-coincidence. That is, after a rotation through 2Θ about the axis of revolution the stiffened shell is indistinguishable from its original position. Since the pressure load is spatially uniform, the deformed structure exhibits the same periodic symmetry about the axis of revolution. That is, a rotation of the deformed stiffened shell through an integer multiple of 2Θ about the axis of revolution brings the deformed shell into self-coincidence.

The θ-curves of the shell's reference surface at $x = \pm l$, both in undeformed and deformed states, serve to define the end diaphragms. In the undeformed state the θ-curves are circles and the end diaphragms are circular areas of radius R. The diaphragms in the deformed state are defined by the displacement of diametrical lines. Deformed images of diametrical lines remain straight and pass through the axis of revolution. Consider a

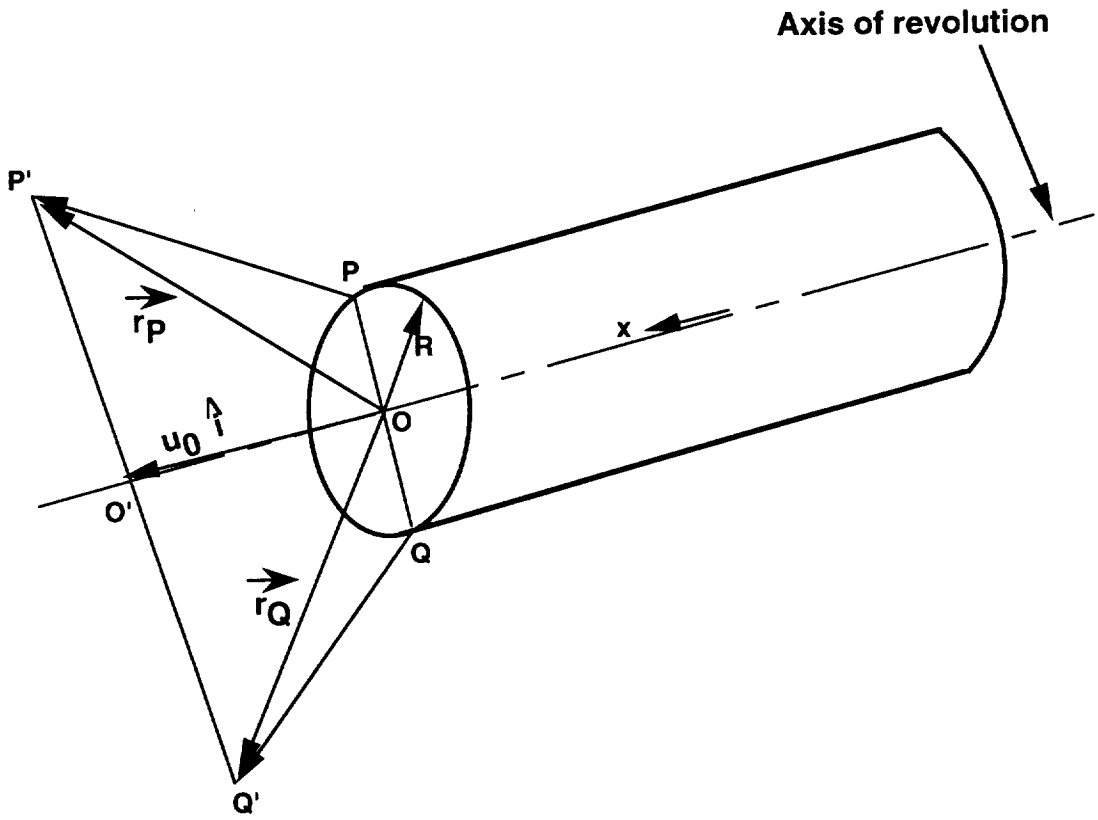

Fig. 3.3 Image of diameter POQ in the deformed state is P'O'Q' with O' on the axis of revolution.

typical diameter PQ in the undeformed diaphragm as shown in Fig. 3.3. The material point at P displaces to P' and the material point Q displaces to Q'. The displacements of particles P and Q are such that the vector $\vec{P'Q'}$ passes through the axis of revolution at point O'. The deformed image of every diametrical is a straight line through the same point on the axis of revolution. Thus, the point O' on the axis of revolution is common to every displaced diametrical line. The displacement of the center of the diaphragm from O to O' is denoted by $u_0\hat{\mathbf{i}}$. The position vectors of points P' and Q' relative to point O are

$$\vec{\mathbf{r_P}} = u_P\ \hat{\mathbf{i}} + v_P\ \hat{\mathbf{t}}(\theta) + (R + w_P)\ \hat{\mathbf{n}}(\theta) \tag{3.13}$$

$$\vec{\mathbf{r_Q}} = u_Q\ \hat{\mathbf{i}} - v_Q\ \hat{\mathbf{t}}(\theta) - (R + w_Q)\ \hat{\mathbf{n}}(\theta) \tag{3.14}$$

in which unit vectors $\hat{\mathbf{t}}(\theta)$ and $\hat{\mathbf{n}}(\theta)$ are tangent and normal to the θ-curve at P. (Note that point Q is on the opposite end of the diameter so its tangent and normal are $-\hat{\mathbf{t}}(\theta)$ and $-\hat{\mathbf{n}}(\theta)$, respectively.) The displacement of the center of the diaphragm is determined by the fact that points P', O', and Q' lie on a straight line. In vector notation this straight line condition is

$$(\vec{\mathbf{r_P}} - u_0\ \hat{\mathbf{i}}) \times (\vec{\mathbf{r_Q}} - u_0\ \hat{\mathbf{i}}) = 0 \tag{3.15}$$

Substituting Eqs. (3.13) and (3.14) into (3.15), and carrying out the cross product results in two independent conditions, which are

$$\frac{u_Q - u_0}{u_P - u_0} = -\frac{R + w_Q}{R + w_P} \tag{3.16}$$

$$\frac{v_Q}{v_P} = \frac{R + w_Q}{R + w_P} \tag{3.17}$$

Solve Eq. (3.16) to get

$$u_0 = f_1\ u_P + f_2\ u_Q \tag{3.18}$$

where

$$f_1 = \frac{R + w_Q}{2R + w_P + w_Q} \tag{3.19}$$

$$f_2 = \frac{R + w_P}{2R + w_P + w_Q} \tag{3.20}$$

From Eqs. (3.19) and (3.20), it can be seen that the sum $f_1 + f_2 = 1$. Equation (3.18) shows that the displacement of the center of the diaphragm can be written in terms of the displacements of material points on the opposite ends of the diameter of the undeformed diaphragm. Since all deformed diametrical lines pass through O', displacement u_0 is independent of θ.

Since displacement u_0 is independent of θ, the periodicity of the deformation pattern of the θ-curve can be used to write u_0 in terms of the displacements of points on the θ-curve in the first unit cell. Consider an odd number of unit cells, such as $N_r = 3$ as shown in Fig. 3.4(a), and an even number of unit cells, such as $N_r = 4$ as shown in Fig. 3.4(b). For the case of $N_r = 3$, identify point P as C and point Q as F. A clockwise rotation of $2\Theta = 2\pi/3$ brings diameter CF to position EB, and the conditions of self-coincidence implies

$$u_F = u_B \quad , v_F = v_B \quad , w_F = w_B \tag{3.21}$$

where point B is at the stiffener ($\theta = 0$) in the first unit. Using Eq. (3.18) the displacement of the center of the diaphragm can be written as

$$u_0 = f_1\ u(\Theta) + f_2\ u(0), \quad N_r\ odd \tag{3.22}$$

with

$$f_1 = \frac{R + w(0)}{2R + w(\Theta) + w(0)}$$

$$f_2 = \frac{R + w(\Theta)}{2R + w(\Theta) + w(0)}$$

in which displacements at C correspond to $\theta = \Theta$ and displacements at B correspond to $\theta = 0$ in the first unit. For the case of $N_r = 4$, diametrically oppposite points must have the same displacement components due to periodicity. That is, a rotation of diameter CG

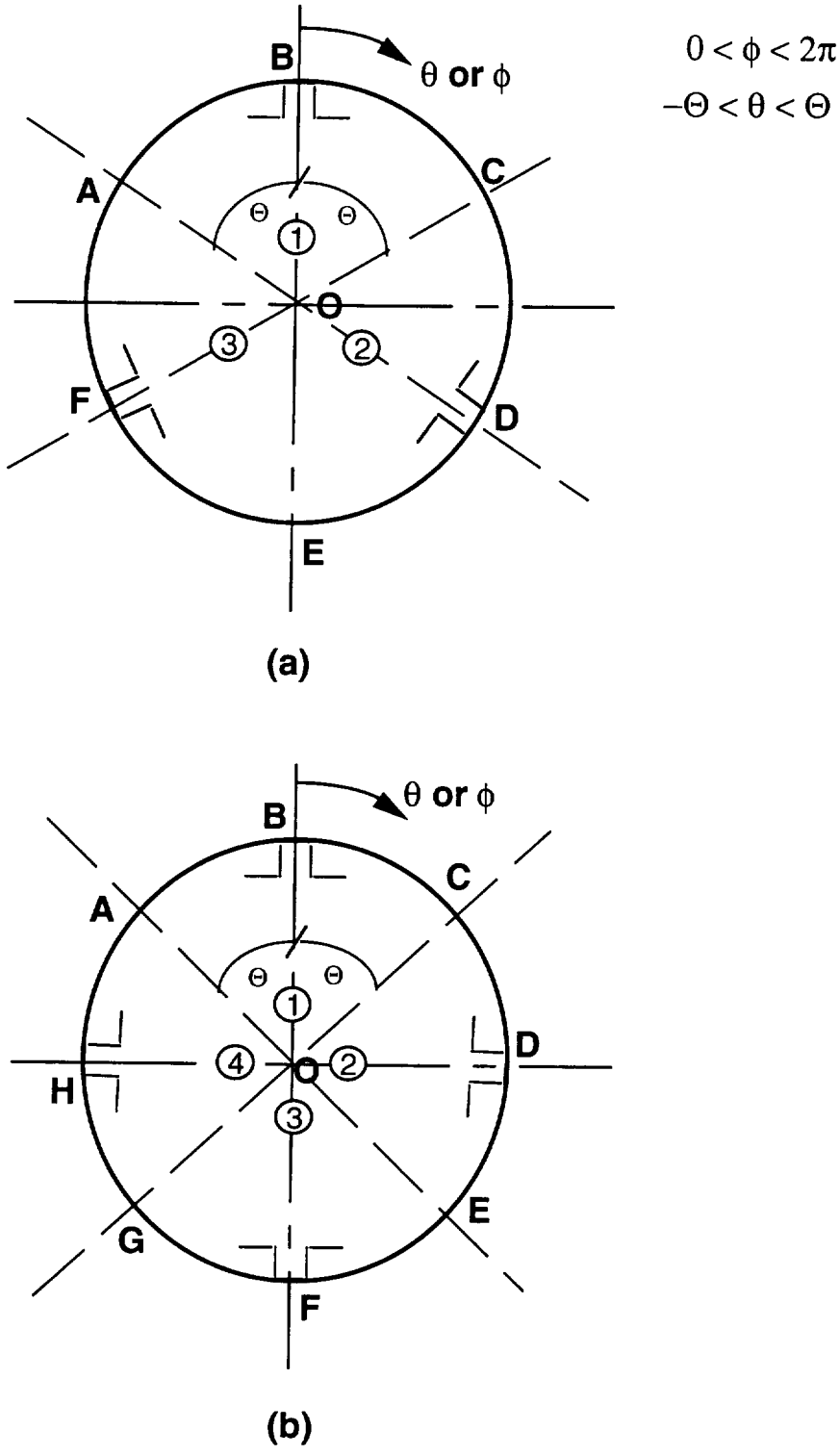

Fig. 3.4 Stiffened shell of (a) three, and (b) four unit cells.

in Fig. 3.4(b) through $N_r/2$ multiples of 2Θ, i.e., π radians, implies $u_C = u_G$, $v_C = v_G$, and $w_C = w_G$, with $\theta = \Theta$ for point C in the first unit. Identify points C and G with P and Q, respectively, in Eq. (3.18) such that the periodicity condition gives $u_0 = u(\Theta)$. Similar considerations for diameter BF connecting the two stringers leads to $u_0 = u(0)$. Therefore, for even number of unit cells one gets

$$u_0 = u(\Theta) = u(0), \quad N_r \ even \tag{3.23}$$

The condition for displacement u_0 for N_r odd is more complex than for N_r even.

Consider a point S in the circular sector OAB of the diaphragm at $x = l$ as shown in Fig. 3.1. The polar coordinates of S are r and θ with $0 \leq r \leq R$ and $-\Theta \leq \theta \leq \Theta$. The particle at S displaces to point S' in the deformation. The position vector of point S' relative to point O is

$$\vec{\mathbf{r}}^*(l, r, \theta) = r\ \hat{\mathbf{n}}(\theta) + \vec{\mathbf{u}}(l, r, \theta) \tag{3.24}$$

in which $r\ \hat{\mathbf{n}}(\theta)$ is the position vector of point S, and $\vec{\mathbf{u}}(l, r, \theta)$ is the displacement vector of S. Since the deformed image of a diameter is a straight line, the displacement vector for point S can be interpolated by

$$\vec{\mathbf{u}}(l, r, \theta) = \frac{r}{R}\left[u(l, \theta)\ \hat{\mathbf{i}} + v(l, \theta)\ \hat{\mathbf{t}}(\theta) + w(l, \theta)\ \hat{\mathbf{n}}(\theta)\right] + (1 - \frac{r}{R})u_0(l)\ \hat{\mathbf{i}} \tag{3.25}$$

in which $u_0(l)$ is the axial displacement of the center of the diaphragm at $x = l$, and it is given by Eq. (3.22) if N_r is odd and Eq. (3.23) if N_r is even. At $r = R$ the displacement vector for the diaphragm coincides with displacement vector of the shell's reference surface at $x = l$. The virtual work of the pressure acting on the deformed diaphragm $O'A'B'$ referenced to the undeformed diaphragm OAB is

$$\delta \mathcal{W}_{pd}^{shell}\Big|_{at\ x=l} = \int_{-\Theta}^{\Theta}\int_{0}^{R} p\ (\frac{\partial \vec{\mathbf{r}}^*}{\partial \theta}\ d\theta\ \times\ \frac{\partial \vec{\mathbf{r}}^*}{\partial r}\ dr)_{x=l}\ \bullet\ \delta \vec{\mathbf{u}}(l, r, \theta) \tag{3.26}$$

Substituting Eqs. (3.24) and (3.25) into Eq. (3.26) results in the following expression for the internal virtual work.

$$\delta W_{pd}^{shell}\Big|_{at\ x=l} = \int_{-\Theta}^{\Theta}\int_{0}^{R} p \begin{vmatrix} \delta u_0 + \frac{r}{R}[\delta u(l,\theta) - \delta u_0] & \frac{r}{R}\delta v & \frac{r}{R}\delta w \\ \frac{1}{R}\frac{\partial u}{\partial \theta} & 1 + \frac{1}{R}(\frac{\partial v}{\partial \theta} + w) & \frac{1}{R}(\frac{\partial w}{\partial \theta} - v) \\ \frac{1}{R}[u(l,\theta) - u_0] & \frac{v}{R} & 1 + \frac{w}{R} \end{vmatrix}_{x=l} r dr\ d\theta \tag{3.27}$$

A similar procedure is used on the circular sector of the undeformed diaphragm at $x = -l$. Note that the displacement of the center of the diaphragm at $x = -l$ is $u_0(-l)$, and it is given by either Eq. (3.22) or Eq. (3.23) as long as the displacements of the θ-curve at $x = -l$ are used in these formulas. The external virtual work of the hydrostatic pressure on the deformed sector $O''C'D'$ is

$$\delta W_{pd}^{shell}\Big|_{at\ x=-l} = -\int_{-\Theta}^{\Theta}\int_{0}^{R} p\ (\frac{\partial \vec{\mathbf{r}^*}}{\partial \theta}\ d\theta\ \times\ \frac{\partial \vec{\mathbf{r}^*}}{\partial r}\ dr)_{x=-l} \bullet \delta \vec{\mathbf{u}}(-l, r, \theta) \tag{3.28}$$

where l is replaced by -l in Eqs. (3.24) and (3.25). The total external virtual work of the pressure on the diaphragms is the sum of the virtual work of the pressure on each of them. Expanding the determinate in Eq. (3.27) and performing integration with respect to polar radius r (since r appears explicitly in the integrand), and following a similar procedure for the virtual work done by the pressure acting on the end diaphragm $O''C'D'$ (Eq. (3.28)), the second component of the external virtual work is written as

$$\begin{aligned} \delta W_{pd}^{shell} = p \int_{-\Theta}^{\Theta} \Big\{ & \Big[R + 2w + \frac{1}{R}(v^2 + w^2) + \frac{1}{R}\ (w\frac{\partial v}{\partial \theta} - v\frac{\partial w}{\partial \theta}) + \frac{\partial v}{\partial \theta}\Big]\ (\frac{1}{3}\delta u + \frac{1}{6}\delta u_0) \\ & + \frac{1}{3R}\Big[(\frac{\partial w}{\partial \theta} - v)(u - u_0) - \frac{\partial u}{\partial \theta}(R + w)\Big]\ \delta v \\ & + \frac{1}{3R}\Big[v\frac{\partial u}{\partial \theta} - (u - u_0)(R + w + \frac{\partial v}{\partial \theta})\Big]\ \delta w \Big\}_{-l}^{+l} R\ d\theta \end{aligned} \tag{3.29}$$

The total external virtual work for the shell due to internal pressure can now be obtained by substituting Eqs. (3.12) and (3.29) into Eq. (3.3). In this substitution process,

the line integrals at edges $x = \pm l$ from Eqs. (3.12) and (3.29) combine and simplify. (Several terms combine to add to zero, and integration by parts in θ are performed to eliminate derivatives of the virtual displacements. Periodicity of the displacements at $\theta = \pm\Theta$ result in vanishing of the boundary terms in the integration by parts.) After these manipulations, the following expression for the total external virtual work for shell results:

$$\begin{aligned}
\delta W_p^{shell} =& p\iint_S \delta\Big[\frac{1}{2R}(v^2+w^2)(1+\frac{\partial u}{\partial x}) + w(\frac{\partial u}{\partial x}+\frac{1}{R}\frac{\partial v}{\partial \theta}) + \frac{1}{3R}(\frac{\partial v}{\partial x}\frac{\partial w}{\partial \theta} - \frac{\partial v}{\partial \theta}\frac{\partial w}{\partial x})u \\
&+ \frac{1}{3R}(\frac{\partial w}{\partial x}\frac{\partial u}{\partial \theta} - \frac{\partial w}{\partial \theta}\frac{\partial u}{\partial x})v + \frac{1}{3R}(\frac{\partial u}{\partial x}\frac{\partial v}{\partial \theta} - \frac{\partial u}{\partial \theta}\frac{\partial v}{\partial x})w + w\Big] dS + p\int_{-l}^{l}\Big\{\frac{1}{3}\Big[w\frac{\partial v}{\partial x} \\
&- v\frac{\partial w}{\partial x}\Big]\ \delta u + \Big[-w + \frac{1}{3}(u\frac{\partial w}{\partial x} - w\frac{\partial u}{\partial x})\Big]\ \delta v + \frac{1}{3}\Big[v\frac{\partial u}{\partial x} - u\frac{\partial v}{\partial x}\Big]\ \delta w\Big\}_{-\Theta}^{+\Theta} dx \\
&+ \delta\left\{p\int_{-\Theta}^{\Theta}\Big[(R+\frac{\partial v}{\partial \theta})(\frac{u}{3}+\frac{u_0}{6}) + \frac{1}{6R}(w\frac{\partial v}{\partial \theta} - v\frac{\partial w}{\partial \theta})\ u_0 \right. \\
&\left. - \Big[\frac{w}{3} + \frac{1}{6R}(v^2+w^2)\Big](u-u_0)\Big]\ R\ d\theta\right\}_{-l}^{+l}
\end{aligned} \tag{3.30}$$

On the basis of periodicity of the shell's displacements at $\theta = \pm\Theta$ edges, it can be shown that the first of the line integrals in Eq. (3.30) vanishes, and the final result for the external work functional for the shell under hydrostatic pressure is

$$\begin{aligned}
W_{ext}^{shell} =& p\iint_S \Big[w + \frac{1}{2R}(v^2+w^2)(1+\frac{\partial u}{\partial x}) + w(\frac{\partial u}{\partial x}+\frac{1}{R}\frac{\partial v}{\partial \theta}) + \frac{1}{3R}(\frac{\partial v}{\partial x}\frac{\partial w}{\partial \theta} - \frac{\partial v}{\partial \theta}\frac{\partial w}{\partial x})u \\
&+ \frac{1}{3R}(\frac{\partial w}{\partial x}\frac{\partial u}{\partial \theta} - \frac{\partial w}{\partial \theta}\frac{\partial u}{\partial x})v + \frac{1}{3R}(\frac{\partial u}{\partial x}\frac{\partial v}{\partial \theta} - \frac{\partial u}{\partial \theta}\frac{\partial v}{\partial x})w\Big]\ dS \\
&+ \ p\int_{-\Theta}^{\Theta}\Big[(R+\frac{\partial v}{\partial \theta})(\frac{u}{3}+\frac{u_0}{6}) + \frac{1}{6R}(w\frac{\partial v}{\partial \theta} - v\frac{\partial w}{\partial \theta})\ u_0 \\
&- \Big[\frac{w}{3} + \frac{1}{6R}(v^2+w^2)\Big](u-u_0)\Big]_{-l}^{+l} R\ d\theta
\end{aligned} \tag{3.31}$$

3.3 STRINGER

For a symmetrical cross section, the internal virtual work statement for the stringer is

$$\delta \mathcal{W}_{int}^{stringer} = \int_{-l}^{l} [N_{xs}\delta\epsilon_{xs} + M_{\theta s}\delta\kappa_{\theta s}]dx \tag{3.32}$$

in which N_{xs} is the axial force in the stringer, $M_{\theta s}$ is the bending moment, ϵ_{xs} is the extensional normal strain of the centroidal line, and $\kappa_{\theta s}$ is the change in curvature of the centroidal line. Based on Euler-Bernoulli nonlinear beam theory, the strain-displacement relations for stringer are

$$\epsilon_{xs} = u'_s + \frac{1}{2}(w'_s)^2 \qquad \kappa_{\theta s} = -w''_s \tag{3.33}$$

in which the prime denotes an ordinary derivative with respect to x. Substituting Eq. (3.33) into Eq. (3.32) results in the following expression for internal virtual work for the stringer.

$$\delta \mathcal{W}_{int}^{stringer} = \int_{-l}^{l} \left[N_{xs}\ \delta(\frac{\partial u_s}{\partial x}) + N_{xs}\frac{\partial w_s}{\partial x}\ \delta(\frac{\partial w_s}{\partial x}) - M_{\theta s}\ \delta(\frac{\partial^2 w_s}{\partial x^2}) \right] dx \tag{3.34}$$

Hooke's law for the stringer is

$$N_{xs} = (EA)_s\epsilon_{xs} \qquad M_{\theta s} = (EI)_s\kappa_{\theta s} \tag{3.35}$$

3.4 RING

For a ring with symmetrical cross section, there is no out-of-plane bending and torsion. Hence, the statement of internal virtual work for the ring is

$$\delta \mathcal{W}_{int}^{ring} = \int_{-\Theta}^{\Theta} [N_{\theta r}\delta\epsilon_{\theta r} + M_{xr}\delta\kappa_{xr}]R_0\ d\theta \tag{3.36}$$

in which $N_{\theta r}$ is the circumferential force, M_{xr} is the bending moment, $\epsilon_{\theta r}$ is the circumferential normal strain of the reference arc, κ_{xr} is the change in curvature of the reference arc, and R_0 is the radius of ring reference arc. Based on small strains and moderate rotations, and the kinematic relations for the ring are

$$\begin{aligned} \epsilon_{\theta r} &= \frac{1}{R_0}(\dot{v}_r + w_r) + \frac{1}{2}\phi_{xr}^2 \\ \kappa_{xr} &= \frac{1}{R_0}\dot{\phi}_{xr} \\ \phi_{xr} &= \frac{1}{R_0}(v_r - \dot{w}_r) \end{aligned} \tag{3.37}$$

in which the over-dot denotes an ordinary derivative with respect to θ. Substituting Eqs. (3.37) into Eq. (3.36) results in the following expression for internal virtual work for the ring:

$$\begin{aligned} \delta \mathcal{W}_{int}^{ring} = \int_{-\Theta}^{\Theta} \Bigg\{ & \frac{N_{\theta r}}{R_0}\left(\frac{v_r}{R_0} - \frac{1}{R_0}\frac{\partial w_r}{\partial \theta}\right)\delta v_r + \left[\frac{N_{\theta r}}{R_0} + \frac{M_{xr}}{R_0^2}\right]\delta\left(\frac{\partial v_r}{\partial \theta}\right) + \frac{N_{\theta r}}{R_0}\,\delta w_r \\ & + \frac{N_{\theta r}}{R_0}\left(\frac{1}{R_0}\frac{\partial w_r}{\partial \theta} - \frac{v_r}{R_0}\right)\delta\left(\frac{\partial w_r}{\partial \theta}\right) - \frac{M_{xr}}{R_0^2}\,\delta\left(\frac{\partial^2 w_r}{\partial \theta^2}\right)\Bigg\} R_0\, d\theta \end{aligned} \tag{3.38}$$

Hooke's law for the ring is

$$N_{\theta r} = (EA)_r \epsilon_{\theta r} \qquad M_{xr} = (EI)_r \kappa_{xr} \tag{3.39}$$

3.5 INCREMENTAL VIRTUAL WORK

The internal and external virtual work functionals obtained above contain terms that are nonlinear in the displacements times virtual displacements of the first degree. Newton's method is employed to solve the nonlinear equilibrium equations that result from the principle of virtual work. It is convenient to derive the incremental virtual work functionals for each structural element for implementation of the update procedure in Newton's method. At fixed values of external loads, consider replacing the (actual)

displacement field in the virtual work functional of an element by an approximation. Let this approximation be a known displacement field plus a small incremental displacement field. The approximation is substituted into the virtual work functional of the element and the functional is linearized in the incremental displacement field. As an example of the replacement procedure, the case of shell is explained in detail. Let the shell displacement field

$$\{\vec{u}\} \longrightarrow \{\vec{u}\} + \{\Delta\vec{u}\} \tag{3.40}$$

in which $\{\vec{u}\}$ on the right hand side of Eq. (3.40) is assumed to be known and $\{\Delta\vec{u}\}$ is an unknown small increment. As a result of replacement illustrated by Eq. (3.40), the strains and curvatures become

$$\{\vec{\epsilon}\} \longrightarrow \{\vec{\epsilon}\} + \{\Delta\vec{\epsilon}\} \tag{3.41}$$

$$\{\vec{\kappa}\} \longrightarrow \{\vec{\kappa}\} + \{\Delta\vec{\kappa}\} \tag{3.42}$$

in which $\{\Delta\vec{\epsilon}\}$ and $\{\Delta\vec{\kappa}\}$ are linear in $\{\Delta\vec{u}\}$. The stress and moment resultants are replaced as

$$\{\vec{N}\} \longrightarrow \{\vec{N}\} + \{\Delta\vec{N}\} \tag{3.43}$$

$$\{\vec{M}\} \longrightarrow \{\vec{M}\} + \{\Delta\vec{M}\} \tag{3.44}$$

in which $\{\Delta\vec{N}\}$ and $\{\Delta\vec{M}\}$ are determined by the constitutive law (Eq. (2.69)) by using incremental strains and curvatures; viz., $\{\Delta\vec{\epsilon}\}$ and $\{\Delta\vec{\kappa}\}$.

The virtual displacements are not incremented since they are any of a set of kinematically admissible (test) functions and it is only the (actual) displacements (in the space of trial functions) that are being determined by iteration. Consequently,

$$\delta\,(\Delta\vec{u}) = 0 \tag{3.45}$$

Substituting the replacements (Eqs. (3.40) through (3.44)) in the virtual work functional (Eq. (3.2) or (3.30)), and linearizing in the increments results in the incremental virtual work functionals. The above procedure is repeated for the stiffeners as well to obtain respective incremental virtual work functionals.

3.5.1 SHELL

The linearized incremental strains and curvatures for shell are obtained by following the incremental procedure described above. Substituting Eq. (3.40) to (3.42) into Eqs. (3.1), (2.10), (2.11), and (2.63) in conjunction with Eqs. (2.16) and (2.17), results in the following linearized incremental strains and curvatures for shell:

$$\Delta\epsilon_{xx} = \frac{\partial \Delta u}{\partial x} + (\frac{\partial w}{\partial x})(\frac{\partial \Delta w}{\partial x}) \tag{3.46}$$

$$\Delta\epsilon_{\theta\theta} = \frac{1}{R}\frac{\partial \Delta v}{\partial \theta} + \frac{\Delta w}{R} + (\frac{1}{R}\frac{\partial w}{\partial \theta} - \frac{v}{R})(\frac{1}{R}\frac{\partial \Delta w}{\partial \theta} - \frac{\Delta v}{R}) \tag{3.47}$$

$$\Delta\gamma_{x\theta} = \frac{\partial \Delta v}{\partial x} + \frac{1}{R}\frac{\partial \Delta u}{\partial \theta} + (\frac{\partial \Delta w}{\partial x})(\frac{1}{R}\frac{\partial w}{\partial \theta} - \frac{v}{R}) + (\frac{\partial w}{\partial x})(\frac{1}{R}\frac{\partial \Delta w}{\partial \theta} - \frac{\Delta v}{R}) \tag{3.48}$$

$$\Delta\kappa_{xx} = -\frac{\partial^2 \Delta w}{\partial x^2} \tag{3.49}$$

$$\Delta\kappa_{\theta\theta} = -\frac{1}{R^2}\frac{\partial^2 \Delta w}{\partial \theta^2} + \frac{1}{R^2}\frac{\partial \Delta v}{\partial \theta} \tag{3.50}$$

$$\Delta\kappa^s_{x\theta} = -\frac{2}{R}\frac{\partial^2 \Delta w}{\partial x \partial \theta} + \frac{1}{R}\frac{\partial \Delta v}{\partial x} \tag{3.51}$$

Similarly following the replacement procedure explained above, from Eq. (3.2) the linearized incremental internal virtual work for the shell is obtained as

$$\begin{aligned}
\delta(\Delta \mathcal{W}^{shell}_{int}) = \iint_S \Big\{ & \Delta N_{xx}\delta(\frac{\partial u}{\partial x}) + \frac{\Delta N^s_{x\theta}}{R}\delta(\frac{\partial u}{\partial \theta}) - \Big[\frac{\Delta N_{\theta\theta}}{R}(\frac{1}{R}\frac{\partial w}{\partial \theta} - \frac{v}{R}) + \frac{\Delta N^s_{x\theta}}{R}\frac{\partial w}{\partial x} \\
& + \frac{N_{\theta\theta}}{R}(\frac{1}{R}\frac{\partial \Delta w}{\partial \theta} - \frac{\Delta v}{R}) + \frac{N^s_{x\theta}}{R}\frac{\partial \Delta w}{\partial x}\Big]\delta v + \Big[\Delta N^s_{x\theta} + \frac{\Delta M^s_{x\theta}}{R}\Big]\delta(\frac{\partial v}{\partial x}) \\
& + \Big[\frac{\Delta N_{\theta\theta}}{R} + \frac{\Delta M_{\theta\theta}}{R^2}\Big]\delta(\frac{\partial v}{\partial \theta}) + \frac{\Delta N_{\theta\theta}}{R}\delta w - \Delta M_{xx}\delta(\frac{\partial^2 w}{\partial x^2}) - \frac{\Delta M_{\theta\theta}}{R^2}\delta(\frac{\partial^2 w}{\partial \theta^2}) \\
& - \frac{2\Delta M^s_{x\theta}}{R}\delta(\frac{\partial^2 w}{\partial \theta \partial x}) + \Big[\Delta N_{xx}\frac{\partial w}{\partial x} + \Delta N^s_{x\theta}(\frac{1}{R}\frac{\partial w}{\partial \theta} - \frac{v}{R}) + N^s_{x\theta}(\frac{1}{R}\frac{\partial \Delta w}{\partial \theta} \\
& - \frac{\Delta v}{R}) + N_{xx}\frac{\partial \Delta w}{\partial x}\Big]\delta(\frac{\partial w}{\partial x}) + \Big[\frac{\Delta N_{\theta\theta}}{R}(\frac{1}{R}\frac{\partial w}{\partial \theta} - \frac{v}{R}) + \frac{\Delta N^s_{x\theta}}{R}\frac{\partial w}{\partial x} \\
& + \frac{N^s_{x\theta}}{R}\frac{\partial \Delta w}{\partial x} + \frac{N_{\theta\theta}}{R}(\frac{1}{R}\frac{\partial \Delta w}{\partial \theta} - \frac{\Delta v}{R})\Big]\delta(\frac{\partial w}{\partial \theta})\Big\}\, dS,
\end{aligned} \tag{3.52}$$

and from Eq. (3.30), the linearized incremental external virtual work for the shell due to internal pressure load is obtained as

$$\begin{aligned}
\delta(\Delta W_p^{shell}) =& p \iint_S \Big\{ \frac{1}{3R}\Big[\frac{\partial \Delta v}{\partial x}\frac{\partial w}{\partial \theta} - \frac{\partial \Delta v}{\partial \theta}\frac{\partial w}{\partial x} + \frac{\partial v}{\partial x}\frac{\partial \Delta w}{\partial \theta} - \frac{\partial v}{\partial \theta}\frac{\partial \Delta w}{\partial x}\Big]\,\delta u + \Big[\,\Delta w \\
&+ \frac{1}{R}(v\Delta v + w\Delta w) + \frac{1}{3R}(\Delta w\frac{\partial v}{\partial \theta} - v\frac{\partial \Delta w}{\partial \theta} + w\frac{\partial \Delta v}{\partial \theta} - \Delta v\frac{\partial w}{\partial \theta})\Big]\delta(\frac{\partial u}{\partial x}) \\
&+ \frac{1}{3R}\Big[v\frac{\partial \Delta w}{\partial x} - \Delta w\frac{\partial v}{\partial x} + \Delta v\frac{\partial w}{\partial x} - w\frac{\partial \Delta v}{\partial x}\Big]\,\delta(\frac{\partial u}{\partial \theta}) + \Big[\frac{\Delta v}{R}\,(1+\frac{\partial u}{\partial x}) \\
&+ \frac{v}{R}\,\frac{\partial \Delta u}{\partial x} + \frac{1}{3R}\,(\frac{\partial \Delta w}{\partial x}\frac{\partial u}{\partial \theta} - \frac{\partial \Delta w}{\partial \theta}\frac{\partial u}{\partial x} + \frac{\partial w}{\partial x}\frac{\partial \Delta u}{\partial \theta} - \frac{\partial w}{\partial \theta}\frac{\partial \Delta u}{\partial x})\Big]\delta v \\
&+ \frac{1}{3R}\Big[\Delta u\frac{\partial w}{\partial \theta} - w\frac{\partial \Delta u}{\partial \theta} + u\frac{\partial \Delta w}{\partial \theta} - \Delta w\frac{\partial u}{\partial \theta}\Big]\delta(\frac{\partial v}{\partial x}) + \Big[\frac{\Delta w}{R} + \frac{1}{3R}(w\frac{\partial \Delta u}{\partial x} \\
&- \Delta u\frac{\partial w}{\partial x} + \Delta w\frac{\partial u}{\partial x} - u\frac{\partial \Delta w}{\partial x})\Big]\delta(\frac{\partial v}{\partial \theta}) + \Big[(1+\frac{w}{R})\frac{\partial \Delta u}{\partial x} + (1+\frac{\partial u}{\partial x})\frac{\Delta w}{R} \\
&+ \frac{1}{R}\,\frac{\partial \Delta v}{\partial \theta} + \frac{1}{3R}\,(\frac{\partial \Delta u}{\partial x}\frac{\partial v}{\partial \theta} - \frac{\partial \Delta u}{\partial \theta}\frac{\partial v}{\partial x} + \frac{\partial u}{\partial x}\frac{\partial \Delta v}{\partial \theta} - \frac{\partial u}{\partial \theta}\frac{\partial \Delta v}{\partial x})\Big]\,\delta w \\
&+ \frac{1}{3R}\Big[\Delta v\frac{\partial u}{\partial \theta} - u\frac{\partial \Delta v}{\partial \theta} + v\frac{\partial \Delta u}{\partial \theta} - \Delta u\frac{\partial v}{\partial \theta}\Big]\delta(\frac{\partial w}{\partial x}) + \frac{1}{3R}\Big[\Delta u\frac{\partial v}{\partial x} - v\frac{\partial \Delta u}{\partial x} \\
&+ u\frac{\partial \Delta v}{\partial x} - \Delta v\frac{\partial u}{\partial x}\Big]\delta(\frac{\partial w}{\partial \theta})\Big\}\,dS + \delta\Big\{p\int_{-\Theta}^{\Theta}\frac{1}{6R}\,\Big[\,(w\frac{\partial \Delta v}{\partial \theta} - \Delta v\frac{\partial w}{\partial \theta} \\
&+ \Delta w\frac{\partial v}{\partial \theta} - v\frac{\partial \Delta w}{\partial \theta})u_0 + (w\frac{\partial v}{\partial \theta} - v\frac{\partial w}{\partial \theta})\Delta u_0 + \frac{\partial \Delta v}{\partial \theta}(\frac{u}{3} + \frac{u_0}{6}) \\
&+ \frac{\partial v}{\partial \theta}(\frac{\Delta u}{3} + \frac{\Delta u_0}{6}) - \Big[\frac{\Delta w}{3} + \frac{1}{3R}(v\Delta v + w\Delta w)\Big](u - u_0) \\
&- \Big[\frac{w}{3} + \frac{1}{6R}(v^2 + w^2)\Big](\Delta u - \Delta u_0)\Big]\,R\,d\theta\Big\}_{-l}^{+l}
\end{aligned} \tag{3.53}$$

It may be noted that Eq. (3.53) leads to a symmetric load stiffness since constant pressure acting on a fully enclosed volume is a conservative force system.

3.5.2 STRINGER

Following the incremental replacement procedure Eq. (3.33) results in the following linearized incremental strains and curvatures for the stringer:

$$\Delta\epsilon_{xs} = \frac{\partial \Delta u_s}{\partial x} + (\frac{\partial w_s}{\partial x})(\frac{\partial \Delta w_s}{\partial x}) \tag{3.54}$$

$$\Delta\kappa_{xs} = -\frac{\partial^2 \Delta w_s}{\partial x^2} \tag{3.55}$$

Simularly, from Eq. (3.34) the linearized incremental internal virtual work for the stringer is obtained as

$$\delta(\Delta \mathcal{W}_{int}^{stringer}) = \int_{-l}^{l} \Big[\Delta N_{xs}\ \delta(\frac{\partial u_s}{\partial x}) + (\Delta N_{xs}\frac{\partial w_s}{\partial x} + N_{xs}\frac{\partial \Delta w_s}{\partial x})\ \delta(\frac{\partial w_s}{\partial x}) - \Delta M_{xs}\ \delta(\frac{\partial^2 w_s}{\partial x^2})\Big]\ dx \tag{3.56}$$

3.5.3 RING

The application of incremental replacement procedure to Eq. (3.37) results in the following linearized incremental strains and curvatures for the ring:

$$\Delta\epsilon_{\theta r} = \frac{1}{R_0}\frac{\partial \Delta v_r}{\partial \theta} + \frac{\Delta w_r}{R_0} + (\frac{1}{R_0}\frac{\partial w_r}{\partial \theta} - \frac{v_r}{R_0})(\frac{1}{R_0}\frac{\partial \Delta w_r}{\partial \theta} - \frac{\Delta v_r}{R_0}) \tag{3.57}$$

$$\Delta\kappa_{xr} = \frac{1}{R_0^2}\frac{\partial \Delta v_r}{\partial \theta} - \frac{1}{R_0^2}\frac{\partial^2 \Delta w_r}{\partial \theta^2} \tag{3.58}$$

Similarly, from Eq. (3.38) the linearized incremental internal virtual work for the ring is obtained as

$$\begin{aligned}\delta(\Delta \mathcal{W}_{int}^{ring}) = \int_{-\Theta}^{\Theta} \Big\{ &\Big[\frac{\Delta N_{\theta r}}{R_0}(\frac{v_r}{R_0} - \frac{1}{R_0}\frac{\partial w_r}{\partial \theta}) + \frac{N_{\theta r}}{R_0}(\frac{\Delta v_r}{R_0} - \frac{1}{R_0}\frac{\partial \Delta w_r}{\partial \theta})\Big]\ \delta v_r \\ &+ \Big[\frac{\Delta N_{\theta r}}{R_0} + \frac{\Delta M_{xr}}{R_0^2}\Big]\ \delta(\frac{\partial v_r}{\partial \theta}) + \frac{\Delta N_{\theta r}}{R_0}\ \delta w_r + \Big[\frac{\Delta N_{\theta r}}{R_0}(\frac{1}{R_0}\frac{\partial w_r}{\partial \theta} - \frac{v_r}{R_0}) \\ &+ \frac{N_{\theta r}}{R_0}(\frac{1}{R_0}\frac{\partial \Delta w_r}{\partial \theta} - \frac{\Delta v_r}{R_0})\Big]\ \delta(\frac{\partial w_r}{\partial \theta}) - \frac{\Delta M_{xr}}{R_0^2}\ \delta(\frac{\partial^2 w_r}{\partial \theta^2})\Big\}\ R_0\ d\theta\end{aligned} \tag{3.59}$$

3.6 DISPLACEMENT CONTINUITY

For the symmetrical cross section stiffeners, the repeating unit is symmetric about x- and θ-axes, and the only non-zero displacements for the stiffeners are the axial and

normal displacements. For a symmetrical cross section, there is no out-of-plane bending and torsion of the ring. Thus, axial displacement of the points on the reference arc of the ring, U_r, in Eq. (2.53) is zero. In addition the rotations about θ- and ζ-axes, $\phi_{\theta r}$ and ϕ_{zr}, in Eqs. (2.54) and (2.55) for the circumferential and normal displacements of the ring, are set to zero. Hence, for the symmetrical cross section stiffeners, the displacement continuity constraints imposed between the shell and stringer at their interface are given by Eqs. (2.73) and (2.74), and the constraints imposed between the shell and ring at their interface are given by Eqs. (2.77) and (2.81). Note that in Eq. (2.77) the twist rate τ_r is equal to zero for a symmetrical cross section ring.

The advantage of enforcing the displacement continuty constraints, as opposed to the strain compatibility constraints (as was done by Wang and Hsu[19]), between the discrete elements is more evident in the nonlinear analysis. The displacement based continuity constraints result in equations which are linear in displacement and rotations of the elements (Eqs. (2.73), (2.77), etc.). On the other hand the strain based compatibility constraints would yield nonlinear equations in terms of the displacements and rotations of the structural elements (see e.g., Eqs. (3.1), (3.33) and (3.37)).

3.7 AUGMENTED VIRTUAL WORK TERMS

Based on the discussion for the displacement continuity constraints in the foregoing section, the augmented (or external) virtual work terms for the shell due to the interacting loads are given by

$$\begin{aligned}\delta \mathcal{W}_{\lambda}^{shell} = & \int_{-l}^{l} \left\{ \lambda_{xs}(x)\left[\delta u(x,0) - \frac{t}{2}\delta\phi_x(x,0)\right] + \lambda_{zs}(x)\delta w(x,0) \right\} dx \\ & + \int_{-\Theta}^{\Theta} \left\{ \lambda_{\theta r}(\theta)\left[\delta v(0,\theta) - \frac{t}{2}\delta\phi_\theta(0,\theta)\right] + \lambda_{zr}(\theta)\delta w(0,\theta) \right\} (R - \frac{t}{2}) d\theta \\ & - Q[\delta u(l,0) - \delta u(-l,0)]\end{aligned} \tag{3.60}$$

Similarly, the augmented (or external) virtual work terms for the ring due to the interacting loads are

$$\delta W_{\lambda}^{ring} = -\int_{-\Theta}^{\Theta} \left\{ \lambda_{\theta r}(\theta)\left[\delta v_r(\theta) + e_r \delta\phi_{xr}(\theta)\right] + \lambda_{zr}(\theta)\delta w_r(\theta) \right\} \left(1 + \frac{e_r}{R_0}\right) R_0 \, d\theta \qquad (3.61)$$

The augmented (or external) virtual work for the stringer due to the interacting loads is still given by Eq. (2.88). The variational form of the constraints in the nonlinear analysis are

$$\begin{aligned} \int_{-l}^{l} \left[\delta\lambda_{xs} g_{xs} + \delta\lambda_{zs} g_{zs}\right] dx &= 0 \\ \int_{-\Theta}^{\Theta} \left[\delta\lambda_{\theta r} g_{\theta r} + \delta\lambda_{zr} g_{zr}\right](R_0 + e_r)\, d\theta &= 0 \\ \delta Q\left\{\left[u(l,0) - u(-l,0)\right] - \left[u_s(l) - u_s(-l)\right]\right\} &= 0 \end{aligned} \qquad (3.62)$$

CHAPTER 4
FOURIER APPROXIMATIONS AND SOLUTION PROCEDURE

4.1 INTRODUCTION

The structural model is periodic in the circumferential and longitudinal directions both in geometry and in material properties. With respect to the applied internal pressure load, which is assumed spatially uniform, the model is periodic in the circumferential direction. For a closed-end pressurized shell, in which closure is mathematically presumed to occur at $x = \pm\infty$, there is an axial stretching that corresponds to a non-periodic axial displacement field. However, for each equal length segment of the shell obtained by sectioning it perpendicular to the x-axis, the total axial force is the same. Thus, the elongation of each segment is the same. These periodic conditions and uniform axial extension due to a closed-end pressure load permit definition of a structural repeating unit or unit cell model as shown in Fig. 1.2.

The periodic nature of the repeating unit or unit cell model requires that the stress and moment resultants, and the conjugate displacements and rotations for the discrete elements are also periodic in nature so that the repeating units, when placed together, form the complete stiffened cylindrical shell model. An analogy to this approach can be a jigsaw puzzle with "fully interlocking" identical pieces. This implies that the boundary conditions for the repeating unit are periodic in nature. The periodicity of the forces and displacements at the edges of the repeating unit (or in other words, the periodicity of boundary conditions) is ensured by assuming a Fourier Series solution to the linear elastic and nonlinear elastic response of the repeating unit. The Ritz method is utilized and the principle of virtual work is applied separately to each structural element. Displacements

are seperately assumed for the shell, stringer and ring. The periodic portions of the displacements and rotations are represented by truncated Fourier Series having fundamental periods in the stringer and ring spacing. The non-periodic portions of the displacements due to axial stretching are represented by simple terms in x. The Fourier Series reflect symmetry about the x-axis only for the repeating unit since the ring can be either symmetrical or asymmetrical in cross section. In this chapter the assumed Fourier Series approximations for the actual, virtual and incremental (for nonlinear analysis only) displacement fields, and the actual and virtual interacting line load intensities are presented. The system of discrete equations is obtained and their solution procedure is outlined.

4.2 DISPLACEMENTS AND ROTATIONS APPROXIMATIONS

4.2.1 SHELL

For the shell, actual displacements of the middle surface (see Fig. 2.1) are represented as

$$u(x,\theta) = \frac{q_0 x}{2l} + \sum_{m=1}^{M}\sum_{n=0}^{N} u_{1mn} Sin(\alpha_m x) Cos(\beta_n \theta) + \sum_{m=1}^{M}\sum_{n=1}^{N} u_{2mn} Cos(\alpha_m x) Cos(\beta_n \theta) \tag{4.1}$$

$$v(x,\theta) = \sum_{m=0}^{M}\sum_{n=1}^{N} v_{1mn} Cos(\alpha_m x) Sin(\beta_n \theta) + \sum_{m=1}^{M}\sum_{n=1}^{N} v_{2mn} Sin(\alpha_m x) Sin(\beta_n \theta) \tag{4.2}$$

$$w(x,\theta) = \sum_{m=0}^{M}\sum_{n=0}^{N} w_{1mn} Cos(\alpha_m x) Cos(\beta_n \theta) + \sum_{m=1}^{M}\sum_{n=1}^{N} w_{2mn} Sin(\alpha_m x) Cos(\beta_n \theta), \tag{4.3}$$

and rotations of the normal are

$$\phi_x(x,\theta) = \sum_{m=1}^{M}\sum_{n=0}^{N} \phi_{x1mn} Sin(\alpha_m x) Cos(\beta_n \theta) + \sum_{m=1}^{M}\sum_{n=1}^{N} \phi_{x2mn} Cos(\alpha_m x) Cos(\beta_n \theta) \tag{4.4}$$

$$\phi_\theta(x,\theta) = \sum_{m=0}^{M}\sum_{n=1}^{N} \phi_{\theta 1mn} Cos(\alpha_m x) Sin(\beta_n \theta) + \sum_{m=1}^{M}\sum_{n=1}^{N} \phi_{\theta 2mn} Sin(\alpha_m x) Sin(\beta_n \theta) \tag{4.5}$$

in which $\alpha_m = \frac{m\pi}{l}$ and $\beta_n = \frac{n\pi}{\Theta}$ where m and n are non-negative integers. Coefficient q_0 in the axial displacement field of the shell represents elongation caused by either an axial mechanical load or due to closed-end pressure vessel effects. Note that some terms in the truncated Fourier Series of Eqs. (4.1-4.5) have been omitted. The coefficients of the omitted terms are u_{200}, u_{2m0}, u_{20n}, w_{2m0}, ϕ_{x200}, ϕ_{x2m0}, and ϕ_{x20n}, in which $m \in S_M$ and $n \in S_N$ where $S_M = \{1, 2, ..., M\}$ and $S_N = \{1, 2, ..., N\}$. The rationale for their omission is discussed in Section 4.4.

The test space of the virtual displacements and rotations is the same space used for actual displacements and rotations. The virtual displacements are represented as

$$\delta u(x,\theta) \in \{\frac{\delta q_0 x}{2l}, \delta u_{1p0} Sin(\alpha_p x), \delta u_{1pq} Sin(\alpha_p x) Cos(\beta_q \theta), \delta u_{2pq} Cos(\alpha_p x) Cos(\beta_q \theta)\} \tag{4.6}$$

$$\delta v(x,\theta) \in \{\delta v_{10q} Sin(\beta_q \theta), \delta v_{1pq} Cos(\alpha_p x) Sin(\beta_q \theta), \delta v_{2pq} Sin(\alpha_p x) Sin(\beta_q \theta)\} \tag{4.7}$$

$$\begin{aligned} \delta w(x,\theta) \in \{&\delta w_{100}, \delta w_{1p0} Cos(\alpha_p x), \delta w_{10q} Cos(\beta_q \theta), \delta w_{1pq} Cos(\alpha_p x) Cos(\beta_q \theta), \\ &\delta w_{2pq} Sin(\alpha_p x) Cos(\beta_q \theta)\}, \end{aligned} \tag{4.8}$$

and the virtual rotations of the normal are

$$\delta \phi_x(x,\theta) \in \{\delta \phi_{x1p0} Sin(\alpha_p x), \delta \phi_{x1pq} Sin(\alpha_p x) Cos(\beta_q \theta), \delta \phi_{x2pq} Cos(\alpha_p x) Cos(\beta_q \theta)\} \tag{4.9}$$

$$\delta \phi_\theta(x,\theta) \in \{\delta \phi_{\theta 10q} Sin(\beta_q \theta), \delta \phi_{\theta 1pq} Cos(\alpha_p x) Sin(\beta_q \theta), \delta \phi_{\theta 2pq} Sin(\alpha_p x) Sin(\beta_q \theta)\} \tag{4.10}$$

in which $\alpha_p = \frac{p\pi}{l}$ and $\beta_q = \frac{q\pi}{\Theta}$ where $p \in S_M$ and $q \in S_N$.

4.2.2 STRINGER

The actual displacements of the centroidal line of stringer (see Fig. 2.2) are

$$u_s(x) = \frac{q_1 x}{2l} + \sum_{m=1}^{M} u_{s1m} Sin(\alpha_m x) + \sum_{m=1}^{M} u_{s2m} Cos(\alpha_m x) \tag{4.11}$$

$$w_s(x) = \sum_{m=1}^{M} w_{s1m} Sin(\alpha_m x) + \sum_{m=1}^{M} w_{s2m} Cos(\alpha_m x), \tag{4.12}$$

and the rotation of the normal of the stringer about the θ-axis is

$$\phi_{\theta s}(x) = \sum_{m=1}^{M} \phi_{\theta s1m} Sin(\alpha_m x) + \sum_{m=1}^{M} \phi_{\theta s2m} Cos(\alpha_m x) \tag{4.13}$$

where the coeffcients u_{s20} , w_{s20} and $\phi_{\theta s20}$ are omitted. Coefficient q_1 in the axial displacement field of the stringer represents elongation caused by either an axial mechanical load or due to closed-end pressure vessel effects.

The virtual displacements of the centroidal line of stringer are

$$\delta u_s(x) \in \{\frac{\delta q_1 x}{2l}, \delta u_{s1p} Sin(\alpha_p x), \delta u_{s2p} Cos(\alpha_p x)\} \tag{4.14}$$

$$\delta w_s(x) \in \{\delta w_{s1p} Sin(\alpha_p x), \delta w_{s2p} Cos(\alpha_p x)\}, \tag{4.15}$$

and the virtual rotation of the normal of the stringer about the θ-axis is

$$\delta \phi_{\theta s}(x) \in \{\delta \phi_{\theta s1p} Sin(\alpha_p x), \delta \phi_{\theta s2p} Cos(\alpha_p x)\} \tag{4.16}$$

where $p \in S_M$.

4.2.3 RING

The actual displacements of the reference circle of the ring (see Fig. 2.3) are

$$u_r(\theta) = \sum_{n=1}^{N} u_{rn} Cos(\beta_n \theta) \tag{4.17}$$

$$v_r(\theta) = \sum_{n=1}^{N} v_{rn} Sin(\beta_n \theta) \tag{4.18}$$

$$w_r(\theta) = \sum_{n=0}^{N} w_{rn} Cos(\beta_n \theta), \tag{4.19}$$

and rotations are

$$\phi_{xr}(\theta) = \sum_{n=1}^{N} \phi_{xrn} Sin(\beta_n \theta) \tag{4.20}$$

$$\phi_{\theta r}(\theta) = \sum_{n=1}^{N} \phi_{\theta rn} Cos(\beta_n \theta) \tag{4.21}$$

$$\phi_{zr}(\theta) = \sum_{n=1}^{N} \phi_{zrn} Sin(\beta_n \theta) \tag{4.22}$$

where the coeffcients u_{r0} and $\phi_{\theta r0}$ are omitted.

The virtual displacements of the reference circle of the ring are

$$\delta u_r(\theta) \in \{\delta u_{rq} Cos(\beta_q \theta)\} \tag{4.23}$$

$$\delta v_r(\theta) \in \{\delta v_{rq} Sin(\beta_q \theta)\} \tag{4.24}$$

$$\delta w_r(\theta) \in \{\delta w_{r0}, \delta w_{rq} Cos(\beta_q \theta)\}, \tag{4.25}$$

and the virtual rotations are

$$\delta\phi_{xr}(\theta) \in \{\delta\phi_{xrq} Sin(\beta_q \theta)\} \tag{4.26}$$

$$\delta\phi_{\theta r}(\theta) \in \{\delta\phi_{\theta rq} Cos(\beta_q \theta)\} \tag{4.27}$$

$$\delta\phi_{zr}(\theta) \in \{\delta\phi_{zrq} Sin(\beta_q \theta)\} \tag{4.28}$$

where $q \in S_N$.

4.3 INTERACTING LOAD APPROXIMATIONS

4.3.1 SHELL-STRINGER

The distributions of the actual interacting line loads between the shell and stringer (see Fig. 1.3), or Lagrange multipliers, are taken as

$$\lambda_{xs}(x) = \sum_{m=1}^{M} \lambda_{xs1m} Sin(\alpha_m x) + \sum_{m=1}^{M} \lambda_{xs2m} Cos(\alpha_m x) \tag{4.29}$$

$$\lambda_{zs}(x) = \sum_{m=1}^{M} \lambda_{zs1m} Sin(\alpha_m x) + \sum_{m=1}^{M} \lambda_{zs2m} Cos(\alpha_m x) \tag{4.30}$$

where the coefficients λ_{x2s0} and λ_{z2s0} are omitted.

The test space of the virtual interacting loads is the same space used for actual interacting load approximations. The shell-stringer virtual interacting loads are represented as

$$\delta\lambda_{xs}(x) \in \left\{\delta\lambda_{xs1p} Sin(\alpha_p x), \delta\lambda_{xs2p} Cos(\alpha_p x)\right\} \tag{4.31}$$

$$\delta\lambda_{zs}(x) \in \left\{\delta\lambda_{zs1p} Sin(\alpha_p x), \delta\lambda_{zs2p} Cos(\alpha_p x)\right\}, \quad p \in S_M \tag{4.32}$$

4.3.2 SHELL-RING

The distributions of actual interacting line loads between the shell and ring (see Fig. 1.3) are taken as

$$\lambda_{xr}(\theta) = \sum_{n=1}^{N} \lambda_{xrn} Cos(\beta_n \theta) \tag{4.33}$$

$$\lambda_{\theta r}(\theta) = \sum_{n=1}^{N} \lambda_{\theta rn} Sin(\beta_n \theta) \tag{4.34}$$

$$\lambda_{zr}(\theta) = \sum_{n=0}^{N} \lambda_{zrn} Cos(\beta_n \theta) \tag{4.35}$$

$$\Lambda_{\theta r}(\theta) = \sum_{n=1}^{N} \Lambda_{\theta rn} Cos(\beta_n \theta) \tag{4.36}$$

$$\Lambda_{zr}(\theta) = \sum_{n=1}^{N} \Lambda_{zrn} Sin(\beta_n \theta) \tag{4.37}$$

where the coefficients λ_{xr0} and $\Lambda_{\theta r0}$ are omitted.

The test space of the virtual interacting loads is the same space used for the actual interacting load approximations. The distribution of the shell-ring virtual interacting loads are taken as

$$\delta\lambda_{xr}(\theta) \in \left\{\delta\lambda_{xrq} Cos(\beta_q \theta)\right\} \tag{4.38}$$

$$\delta\lambda_{\theta r}(\theta) \in \left\{\delta\lambda_{\theta rq} Sin(\beta_q \theta)\right\} \tag{4.39}$$

$$\delta\lambda_{zr}(\theta) \in \left\{\delta\lambda_{zr0}, \delta\lambda_{zrq} Cos(\beta_q \theta)\right\} \tag{4.40}$$

$$\delta\Lambda_{\theta r}(\theta) \in \left\{\delta\Lambda_{\theta rq} Cos(\beta_q \theta)\right\} \tag{4.41}$$

$$\delta\Lambda_{zr}(\theta) \in \left\{\delta\Lambda_{zrq} Sin(\beta_q \theta)\right\}, \quad q \in S_N \tag{4.42}$$

4.4 TERMS OMITTED IN THE FOURIER SERIES

Terms omitted in the truncated Fourier Series for the displacements, rotations, and interacting loads are determined from the rigid body equilibrium conditions for the ring and stringer, and from the displacement continuity conditions between the shell and stiffeners. The external virtual work for the stringer and ring must vanish for any possible rigid body motions of these elements.

4.4.1 RIGID BODY EQUILIBRIUM FOR RING

Consider the ring in its entirety, that is, as made up of an integer number of repeating units around its circumference. Let ϕ be the global coordinate such that $0 \leq \phi \leq 2\pi$ (see Fig. 3.4). The global coordinate ϕ is related to the local coordinate θ in the i^{th} repeating unit by $\phi = \phi_i + \theta$, $i = 1, ..., N_r$ where N_r is the total number of repeating units and $\phi_i = (i-1)\frac{2\pi}{N_r}$. Rigid body motion of the ring is considered as a translation of its center point O to O' plus an infinitesimal rotation about point O'. The displacement of a generic point P in the ring is then given by

$$\vec{\mathbf{U}}_{Rigid} = \vec{\mathbf{U}}_{Translation} + \vec{\mathbf{U}}_{Rotation} \tag{4.43}$$

The ring is referred to a fixed cartesian system (x, y, z) with unit basis vectors $\hat{\mathbf{i}}$, $\hat{\mathbf{j}}$, and $\hat{\mathbf{k}}$ as shown in Fig. 4.1. Also it is convenient to use cylindrical coordinates $(x, \phi, R_0 + \zeta)$

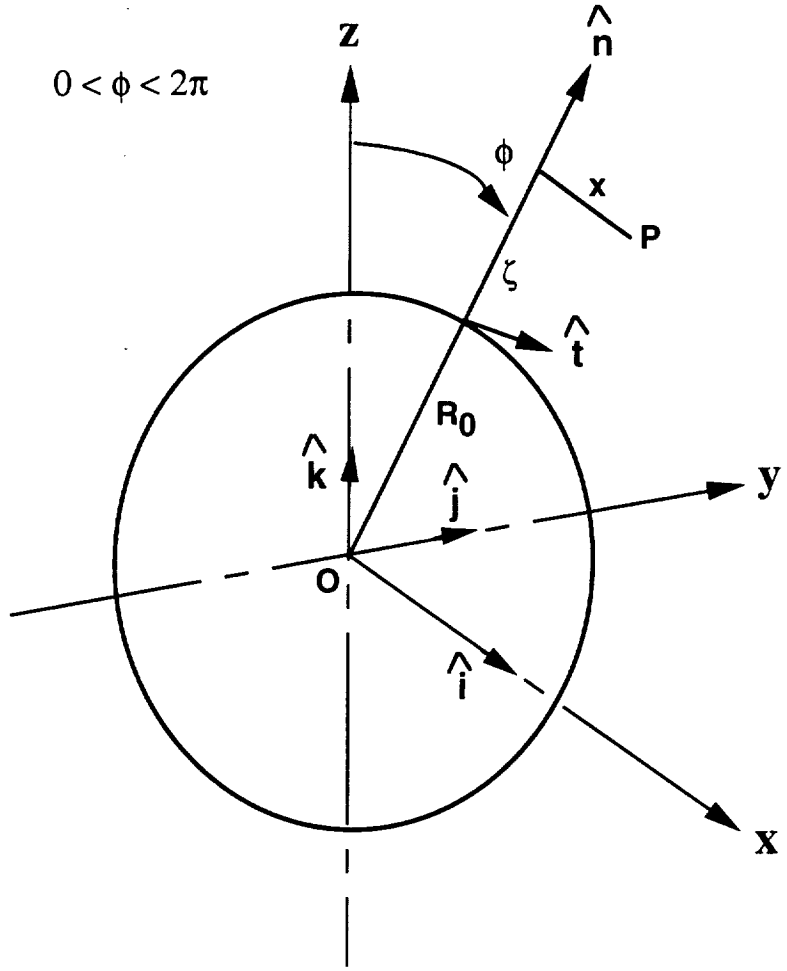

Fig. 4.1 Cylindrical coordinates (x, ϕ, $R_0+\zeta$) of a typical point P in the ring.

with unit vectors $\hat{\mathbf{i}}$, $\hat{\mathbf{t}}(\phi)$, and $\hat{\mathbf{n}}(\phi)$ as shown in Fig. 4.1. The translational displacement of point O is given by $\vec{\mathbf{U}}_{Translation} = U_x\hat{\mathbf{i}} + U_y\hat{\mathbf{j}} + U_z\hat{\mathbf{k}}$. For infinitesimal rotations, the rotation can be represented as a vector $\vec{\Omega} = \Omega_x\hat{\mathbf{i}} + \Omega_y\hat{\mathbf{j}} + \Omega_z\hat{\mathbf{k}}$. The displacement of P relative to O due to rotation is

$$\vec{\mathbf{U}}_{Rotation} = \vec{\Omega} \times \vec{\mathbf{P}} \tag{4.44}$$

where $\vec{\mathbf{P}} = x\ \hat{\mathbf{i}} + (R_0 + \zeta)\ Sin\phi\ \hat{\mathbf{j}} + (R_0 + \zeta)\ Cos\phi\ \hat{\mathbf{k}}$. Thus, the total displacement vector in cartesian components becomes

$$\begin{aligned}\vec{\mathbf{U}}_{Rigid} = &[U_x + (R_0 + \zeta)\Omega_y Cos\phi - (R_0 + \zeta)\Omega_z Sin\phi]\ \hat{\mathbf{i}} \\ &+ [U_y - (R_0 + \zeta)\Omega_x Cos\phi + x\Omega_z]\ \hat{\mathbf{j}} \\ &+ [U_z + (R_0 + \zeta)\Omega_x Sin\phi - x\Omega_y]\ \hat{\mathbf{k}}\end{aligned} \tag{4.45}$$

In Chapter 2, the displacement vector of a generic point P is represented in cylindrical coordinates as

$$\vec{\mathbf{U}}_{Ring} = U_r(x, \phi, \zeta)\hat{\mathbf{i}} + V_r(x, \phi, \zeta)\hat{\mathbf{t}}(\phi) + W_r(x, \phi, \zeta)\hat{\mathbf{n}}(\phi) \tag{4.46}$$

where the cylindrical coordinate components, U_r, V_r and W_r, are given by Eqs. (2.53) to (2.55). Note that the local polar angle θ has been replaced by the global polar angle ϕ. The direction cosines between the unit vectors in cartesian and cylindrical coordinates are

	$\hat{\mathbf{i}}$	$\hat{\mathbf{j}}$	$\hat{\mathbf{k}}$
$\hat{\mathbf{i}}$	1	0	0
$\hat{\mathbf{t}}$	0	Cosϕ	-Sinϕ
$\hat{\mathbf{n}}$	0	Sinϕ	Cosϕ

Thus, $\vec{\mathbf{U}}_{Rigid}$ in cartesian components, Eq. (4.45), can be transformed to cylindrical components, and then like components can be equated between it and Eq. (4.46). As a result of this process the displacements of the reference arc of the ring become

$$\begin{aligned}u_r &= U_x + R_0(\Omega_y Cos\phi - \Omega_z Sin\phi) \\ v_r &= U_y Cos\phi - U_z Sin\phi - R_0\Omega_x \\ w_r &= U_y Sin\phi + U_z Cos\phi,\end{aligned} \tag{4.47}$$

and the (infintesimal) rotations become

$$\begin{aligned}\phi_{xr} &= -\Omega_x \\ \phi_{\theta r} &= \Omega_y Cos\phi - \Omega_z Sin\phi \\ \phi_{zr} &= \Omega_y Sin\phi + \Omega_z Cos\phi\end{aligned} \tag{4.48}$$

From the last two of Eqs. (4.48), the rate of twist τ_r as given by Eq. (2.57) vanishes. It may be noted that the strains and changes in the curvatures in Eqs. (2.57) also vanish identically for all values of U_x, U_y, U_z, Ω_x, Ω_y, and Ω_z.

Substitution of displacements and rotations from Eqs. (4.47) and (4.48) above into the external virtual work for the ring, Eq. (2.89), results in

$$\delta W_{\lambda}^{Rigid} = -\left[F_{xr}\delta U_x + F_{yr}\delta U_y + F_{zr}\delta U_z + C_{xr}\delta\Omega_x + C_{yr}\delta\Omega_y + C_{zr}\delta\Omega_z\right] \tag{4.49}$$

where

$$F_{xr} = \int_0^{2\pi} \lambda_{xr}\ (R_0 + \epsilon_r)\ d\phi \tag{4.50}$$

$$F_{yr} = \int_0^{2\pi} \left[\lambda_{\theta r}\ Cos\phi + \lambda_{zr}\ Sin\phi\right]\ (R_0 + \epsilon_r)\ d\phi \tag{4.51}$$

$$F_{zr} = \int_0^{2\pi} \left[\lambda_{zr}\ Cos\phi - \lambda_{\theta r}\ Sin\phi\right]\ (R_0 + \epsilon_r)\ d\phi \tag{4.52}$$

$$C_{xr} = \int_0^{2\pi} \lambda_{\theta r}\ (R_0 + \epsilon_r)^2\ d\phi \tag{4.53}$$

$$C_{yr} = \int_0^{2\pi} \left\{[R_0\lambda_{xr} + \Lambda_{\theta r}]Cos\phi + \Lambda_{zr}Sin\phi\right\}(R_0 + \epsilon_r)\ d\phi \tag{4.54}$$

$$C_{zr} = \int_0^{2\pi} \left\{ -[R_0\lambda_{xr} + \Lambda_{\theta r}]Sin\phi + \Lambda_{zr}Cos\phi\right\}(R_0 + \epsilon_r)\ d\phi \tag{4.55}$$

Equation (4.49) represents the external virtual work for the complete ring, and is obtained by replacing the local polar angle θ in Eq. (2.89) by the global polar angle ϕ. Since the

external virtual work for the ring in Eq. (4.49) must vanish for any possible rigid body motions, the components of the force and moment resultants defined in Eqs. (4.50-4.55) should vanish individually; i.e., $F_{xr} = F_{yr} = F_{zr} = C_{xr} = C_{yr} = C_{zr} = 0$. Consider the force resultant in y-direction for the complete ring as given by Eq. (4.51). Substituting $\phi = \phi_i + \theta$ and writing the integral as a sum over all units, one gets

$$F_{yr} = \sum_{i=1}^{N_r} [F_t Cos\phi_i + F_n Sin\phi_i] \tag{4.56}$$

in which

$$F_t = \int_{-\Theta}^{\Theta} \left[\lambda_{\theta r}\, Cos\theta + \lambda_{zr}\, Sin\theta\right] (R_0 + \epsilon_r)\, d\theta$$

$$F_n = \int_{-\Theta}^{\Theta} \left[\lambda_{zr}\, Cos\theta - \lambda_{\theta r}\, Sin\theta\right] (R_0 + \epsilon_r)\, d\theta$$

In the i^{th} unit the force component F_t is tangent, and component F_n is normal, to the ring at $\phi = \phi_i$. Since the magnitudes of the components F_t and F_n are the same for each repeating unit, Eq. (4.56) can be rewritten as

$$F_{yr} = F_t \sum_{i=1}^{N_r} Cos\phi_i + F_n \sum_{i=1}^{N_r} Sin\phi_i \tag{4.57}$$

For the complete ring $\sum_{i=1}^{N_r} Cos\phi_i = \sum_{i=1}^{N_r} Sin\phi_i = 0$. Hence, the total force resultant F_{yr} is equal to zero. Similarly, it can be shown that the force component F_{zr} in Eq. (4.52), moment component C_{yr} (Eq. (4.54)), moment component C_{zr} (Eq. (4.55)), all vanish for a complete ring. Thus, the rigid body motions that lead to non-trivial equilibrium conditions are the force and moment resultants in the x-direction. These resultants must vanish for each repeating unit. Hence, the non-trivial x-direction equilibrium equations are

$$\int_{-\Theta}^{\Theta} \lambda_{xr}(\theta)\, (R_0 + \epsilon_r)\, d\theta = 0 \tag{4.58}$$

and

$$\int_{-\Theta}^{\Theta} \lambda_{\theta r}(\theta)\, (R_0 + \epsilon_r)^2\, d\theta = 0 \tag{4.59}$$

4.4.2 RIGID BODY EQUILIBRIUM FOR STRINGER

For the stringer the rigid body motions are spatially uniform x-direction and z-direction displacements. (A rigid body rotation of the stringer in the x-z plane is not considered since this motion would violate longitudinal periodicity of the repeating units.) Vanishing of the external virtual work for an arbitrary rigid body displacement of the stringer in the axial direction leads to the x-direction equilibrium equation

$$\int_{-l}^{l} \lambda_{xs}(x)\, dx = 0 \tag{4.60}$$

Similarly, the equilibrium equation for a rigid body displacement of the stringer in the z-direction is

$$\int_{-l}^{l} \lambda_{zs}(x)\, dx = 0 \tag{4.61}$$

4.4.3 TERMS OMITTED

Equilibrium Eqs. (4.58), (4.60) and (4.61) imply that coefficients

$$\lambda_{xr0} = 0 \qquad \lambda_{xs20} = 0 \qquad \lambda_{zs20} = 0 \tag{4.62}$$

in the Fourier Series for the interacting loads, and these conditions have been taken into account in Eqs. (4.33), (4.29), and (4.30). The sine series for $\lambda_{\theta r}$ given in Eq. (4.34) satisfies the equilibrium condition given in Eq. (4.59).

Consider the variational form of the constraints, Eqs. (2.90) and (2.91), for the spatially uniform components of the virtual interacting line loads. These equations are

$$\Big[u_{200} - \frac{t}{2}\phi_{x200} + \sum_{n=1}^{N}(u_{20n} - \frac{t}{2}\phi_{x20n}) - (u_{s20} + e_s\phi_{\theta s20})\Big]\delta\lambda_{xs20} = 0 \tag{4.63}$$

$$\Big[\sum_{n=0}^{N} w_{10n} - w_{s20}\Big]\delta\lambda_{zs20} = 0 \tag{4.64}$$

$$\left[u_{200} - \frac{t}{2}\phi_{x200} + \sum_{m=1}^{M}(u_{2m0} - \frac{t}{2}\phi_{x2m0}) - (u_{r0} + \epsilon_r\phi_{\theta r0})\right]\delta\lambda_{xr0} = 0 \qquad (4.65)$$

Since these equations are satisfied on the basis that $\delta\lambda_{xs20} = 0$, $\delta\lambda_{zs20} = 0$ and $\delta\lambda_{xr0} = 0$, consistent with Eq. (4.62), the bracketed terms in Eqs. (4.63) to (4.65) do not necessarily vanish. The implication that these bracketed terms in Eqs. (4.63) to (4.65) do not vanish is that displacement continuity conditions are not satisfied pointwise. Pointwise continuity can be achieved by taking each Fourier coefficient appearing in the bracketed terms of Eqs. (4.63) to (4.65) to be individually zero. Fourier Series given in Eqs. (4.1), (4.4), (4.11), (4.13), (4.17), and (4.21) reflect this choice. Moreover, Fourier coefficients u_{200}, u_{s20}, and u_{r0} represent rigid body displacement in the axial direction for the shell, stringer, and ring, respectively, and setting them to zero can be justified on the basis that rigid body displacement does not contribute to the deformation of the structural elements. Since Fourier coefficient w_{s20} represents rigid body displacement of the stringer in the z-direction, it would seem that it should be set to zero as well. However, to maintain continuity between the stringer and the shell in the z-direction, the condition

$$\sum_{n=0}^{N} w_{10n} - w_{s20} = 0 \qquad (4.66)$$

is imposed to determine w_{s20} after obtaining the solution for the displacement components that deform the shell; i.e., Fourier coefficients w_{10n}, $n = 1, ..., N$, are taken to be non-zero independent degrees of freedom since the stringer coefficient w_{s20} is not a part of the solution vector.

Finally, consider the constraint equation associated with $\delta\Lambda_{\theta r0}$, the spatially uniform component of the interacting moment intensity, which is omitted in the series given by Eq. (4.36). Derived from Eq. (2.91), this constraint equation is

$$\left[\sum_{m=1}^{M} \alpha_m w_{2m0} + \phi_{\theta r0}\right]\delta\Lambda_{\theta r0} = 0 \qquad (4.67)$$

The constant component of the twist, $\phi_{\theta r0}$, is equated to zero from the considerations associated with Eq. (4.65). Consequently, a non-zero value of the uniform component of the interacting moment intensity, $\Lambda_{\theta r0} \neq 0$, would not contribute to the equilibrium of the ring, since $\Lambda_{\theta r0}$ and $\phi_{\theta r0}$ are conjugate variables in the external work for the ring (refer to Eq. (2.89)). Since $\phi_{\theta r0} = 0$, it is necessary that $\Lambda_{\theta r0} = 0$ to achieve consistent conditions for the torsional and out-of-plane bending equilibrium of the ring. With $\delta\Lambda_{\theta r0} = 0$ in Eq. (4.67), the bracketed term does not necessarily vanish, and as a result pointwise rotational continuity betwen the shell and the ring is not assured. Pointwise rotational continuity is achieved if the coefficients $w_{2m0} = 0$, $m = 1, ..., M$, as is done in the Fourier Series for the normal displacement of the shell given by Eq. (4.3).

4.5 DISCRETE EQUATIONS AND THEIR SOLUTION

The Ritz method is used to obtain the system of discrete equations. The principle of virtual work is applied separately to the shell, stringer, and ring. The virtual work functionals are augmented by Lagrange multipliers to enforce kinematic constraints between the structural components of the repeating unit. Discrete equations for the linear analyses are solved directly. For the nonlinear analysis an iterative solution procedure is employed.

4.5.1 LINEAR ANALYSES

The approximations in Eqs. (4.1) through (4.28) for the actual and virtual displacements, and Eqs. (4.29) through (4.42) for the actual and virtual interacting loads are substituted into the virtual work functionals for each structural element, and also substituted into the variational form of displacement continuity constraints. Then integration over the space is performed. This process results in a $10MN + 13M + 14N + 6$ system of equations for the transverse shear deformation model and $6MN + 10M + 11N + 6$ system

of equations for the classical model, governing the displacements and the interacting loads. These governing equations are of the form

$$\begin{bmatrix} K_{11} & 0 & 0 & B_{11} & B_{12} & B_{13} \\ 0 & K_{22} & 0 & B_{21} & 0 & B_{23} \\ 0 & 0 & K_{33} & 0 & B_{32} & 0 \\ B_{11}^T & B_{21}^T & 0 & 0 & 0 & 0 \\ B_{12}^T & 0 & B_{32}^T & 0 & 0 & 0 \\ B_{13}^T & B_{23}^T & 0 & 0 & 0 & 0 \end{bmatrix} \begin{Bmatrix} \hat{u}_{shell} \\ \hat{u}_{str} \\ \hat{u}_{ring} \\ \hat{\lambda}_{str} \\ \hat{\lambda}_{ring} \\ Q \end{Bmatrix} = \begin{Bmatrix} F_{11} \\ 0 \\ 0 \\ 0 \\ 0 \\ 0 \end{Bmatrix} \tag{4.68}$$

in which submatrices K_{11}, K_{22} and K_{33} are the stiffness matrices for the shell, stringer, and ring, respectively, obtained from their respective internal virtual work statements. The submatrices $B_{ij}, i,j = 1,2,3$, in Eq. (4.68) are determined from the external (or augmented) virtual work terms involving the interacting loads, and the constraint Eqs. (2.73), (2.74), (2.77), (2.78), (2.81), (2.82), (2.84) and (2.86). The vector on the right-hand-side of Eq. (4.68) is the force vector, determined from the external virtual work terms involving pressure. The constraint equations correspond to the last three rows of the partitioned matrix in Eq. (4.68). The non-zero elements of the matrices K_{ij}, B_{ij} and F_{11} for the transverse shear deformation and classical models are given in Appendices A and B, respectively. The symbolic manipulation software *Mathematica* is used to derive these submatrices. The discrete vectors of unknown variables (i.e. shell and stiffeners' displacements, and shell-stiffener interacting loads) in Eq. (4.68) for the transverse shear deformation model and classical model are given in the following two sub-subsections.

4.5.1.1 TRANSVERSE SHEAR DEFORMATION MODEL

The discrete displacement vector for the shell is the $(10MN + 3M + 3N + 2) \times 1$ vector

$$\hat{u}_{shell} = \left[\hat{u}_0^T, \hat{u}_1^T, ..., \hat{u}_M^T\right]^T \tag{4.69}$$

in which subvectors are

$$\hat{u}_0 = \left[q_0, w_{100}, v_{101}, w_{101}, \phi_{\theta 101}, ..., v_{10N}, w_{10N}, \phi_{\theta 10N}\right]^T \tag{4.70}$$

$$\hat{u}_m = \big[u_{1m0}, w_{1m0}, \phi_{x1m0}, u_{1m1}, u_{2m1}, v_{1m1}, v_{2m1}, w_{1m1}, w_{2m1}, \phi_{x1m1}, \phi_{x2m1},$$
$$\phi_{\theta 1m1}, \phi_{\theta 2m1}, ..., u_{1mN}, u_{2mN}, v_{1mN}, v_{2mN}, w_{1mN}, w_{2mN}, \phi_{x1mN}, \tag{4.71}$$
$$\phi_{x2mN}, \phi_{\theta 1mN}, \phi_{\theta 2mN}\big]^T$$
$$\text{where } m = 1, ..., M$$

The $(6M + 1) \times 1$ discrete displacement vector for the stringer and $(6N + 1) \times 1$ vector for the ring are

$$\hat{u}_{str} = \big[q_1, u_{s11}, u_{s21}, w_{s11}, w_{s21}, \phi_{\theta s11}, \phi_{\theta s21}, ..., u_{s1M}, u_{s2M},$$
$$w_{s1M}, w_{s2M}, \phi_{\theta s1M}, \phi_{\theta s2M}\big]^T \tag{4.72}$$

$$\hat{u}_{ring} = \big[w_{r0}, u_{r1}, v_{r1}, w_{r1}, \phi_{xr1}, \phi_{\theta r1}, \phi_{zr1}, ..., u_{rN}, v_{rN}, w_{rN}, \phi_{xrN}, \phi_{\theta rN}, \phi_{zrN}\big]^T \tag{4.73}$$

in which the term w_{s0} for the stringer has been omitted as discussed in reference to Eq. (4.66). The $4M \times 1$ discrete interacting loads vector for the shell-stringer interface and $(5N + 1) \times 1$ vector for the shell-ring interface are

$$\hat{\lambda}_{str} = \big[\lambda_{xs11}, \lambda_{xs21}, \lambda_{zs11}, \lambda_{zs21}, ..., \lambda_{xs1M}, \lambda_{xs2M}, \lambda_{zs1M}, \lambda_{zs2M}\big]^T \tag{4.74}$$

$$\hat{\lambda}_{ring} = \big[\lambda_{zr0}, \lambda_{xr1}, \lambda_{\theta r1}, \lambda_{zr1}, \Lambda_{\theta r1}, \Lambda_{zr1}, ..., \lambda_{xrN}, \lambda_{\theta rN}, \lambda_{zrN}, \Lambda_{\theta rN}, \Lambda_{zrN}\big]^T \tag{4.75}$$

4.5.1.2 CLASSICAL MODEL

The discrete displacement vector for the shell is the $(6MN + 2M + 2N + 2) \times 1$ vector

$$\hat{u}_{shell} = \big[\hat{u}_0^T, \hat{u}_1^T, ..., \hat{u}_M^T\big]^T \tag{4.76}$$

in which subvectors are

$$\hat{u}_0 = \big[q_0, w_{100}, v_{101}, w_{101}, ..., v_{10N}, w_{10N}\big]^T \tag{4.77}$$

$$\hat{u}_m = \big[u_{1m0}, w_{1m0}, u_{1m1}, u_{2m1}, v_{1m1}, v_{2m1}, w_{1m1}, w_{2m1}, ..., u_{1mN}, u_{2mN},$$
$$v_{1mN}, v_{2mN}, w_{1mN}, w_{2mN}\big]^T \tag{4.78}$$

where $m = 1, ..., M$

The $(4M + 1) \times 1$ discrete displacement vector for the stringer and $(4N + 1) \times 1$ vector for the ring are

$$\hat{u}_{str} = \left[q_1, u_{s11}, u_{s21}, w_{s11}, w_{s21}, ..., u_{s1M}, u_{s2M}, w_{s1M}, w_{s2M}\right]^T \tag{4.79}$$

$$\hat{u}_{ring} = \left[w_{r0}, u_{r1}, v_{r1}, w_{r1}, \phi_{\theta r1}, ..., u_{rN}, v_{rN}, w_{rN}, \phi_{\theta rN}\right]^T \tag{4.80}$$

The $4M \times 1$ discrete interacting loads vector for the shell-stringer interface and $(5N+1) \times 1$ vector for the shell-ring interface are the same as for the shear deformation model and are given by Eqs. (4.74) and (4.75).

The stiffness submatrices K_{11}, K_{22} and K_{33} in Eq. (4.68) are symmetric. From Appendices A and B, it may be noted that the elements of the shell stiffness matrix K_{11} are sparsely populated because of the orthogonality of the Fourier Series. The structure of K_{11} is block diagonal; i.e., nonzero elements occur for index p of the test function equal to index m of the trial function, and index q of the test function equal to index n of the trial function. See Fig. 4.2. Furthermore, there is a decoupling of the elements obtained from the displacement and rotation approximations using single and double Fourier series. This special nature of the shell stiffness matrix K_{11} makes it possible to invert the matrix in blocks (i.e., as blocks of 2×2 or 6×6 submatrices, etc.) instead of inverting the matrix as a whole (i.e., as $(6MN + 2M + 2N + 2) \times (6MN + 2M + 2N + 2)$ matrix). This results in considerable saving of the CPU time. As an example consider the linear analysis with Fourier Series approximations truncated at 8 harmonics in x- and θ-directions, i.e., $M = N = 8$. This results in 418×418 K_{11} matrix for the classical structural model. It takes 20 seconds of CPU time on IBM 3090 machine when the shell stiffness matrix K_{11} is inverted in blocks compared to 71 seconds of CPU time on the same computer when the matrix is inverted as a whole.

$$[K_{11}] = \begin{array}{c} \begin{array}{cccccccccccc} q_{10} & w_{10i} & u_{1m0} & w_{1m0} & v_{10n} & w_{10n} & u_{1mn} & u_{2mn} & v_{1mn} & v_{2mn} & w_{1mn} & w_{2mn} \end{array} \\ \begin{bmatrix} K_{11}(1,1) & K_{11}(1,2) & 0 & 0 & 0 & 0 & 0 & 0 & 0 & 0 & 0 & 0 \\ K_{11}(1,2) & K_{11}(2,2) & 0 & 0 & 0 & 0 & 0 & 0 & 0 & 0 & 0 & 0 \\ 0 & 0 & K_{11}(3,3) & K_{11}(3,4) & 0 & 0 & 0 & 0 & 0 & 0 & 0 & 0 \\ 0 & 0 & K_{11}(3,4) & K_{11}(4,4) & 0 & 0 & 0 & 0 & 0 & 0 & 0 & 0 \\ 0 & 0 & 0 & 0 & K_{11}(5,5) & K_{11}(5,6) & 0 & 0 & 0 & 0 & 0 & 0 \\ 0 & 0 & 0 & 0 & K_{11}(5,6) & K_{11}(6,6) & 0 & 0 & 0 & 0 & 0 & 0 \\ 0 & 0 & 0 & 0 & 0 & 0 & K_{11}(7,7) & K_{11}(7,8) & K_{11}(7,9) & K_{11}(7,10) & K_{11}(7,11) & K_{11}(7,12) \\ 0 & 0 & 0 & 0 & 0 & 0 & K_{11}(7,8) & K_{11}(8,8) & K_{11}(8,9) & K_{11}(8,10) & K_{11}(8,11) & K_{11}(8,12) \\ 0 & 0 & 0 & 0 & 0 & 0 & K_{11}(7,9) & K_{11}(8,9) & K_{11}(9,9) & K_{11}(9,10) & K_{11}(9,11) & K_{11}(9,12) \\ 0 & 0 & 0 & 0 & 0 & 0 & K_{11}(7,10) & K_{11}(8,10) & K_{11}(9,10) & K_{11}(10,10) & K_{11}(10,11) & K_{11}(10,12) \\ 0 & 0 & 0 & 0 & 0 & 0 & K_{11}(7,11) & K_{11}(8,11) & K_{11}(9,11) & K_{11}(10,11) & K_{11}(11,11) & K_{11}(11,12) \\ 0 & 0 & 0 & 0 & 0 & 0 & K_{11}(7,12) & K_{11}(8,12) & K_{11}(9,12) & K_{11}(10,12) & K_{11}(11,12) & K_{11}(12,12) \end{bmatrix} \end{array}$$

Fig. 4.2 Structure of the shell stiffness submatrix [K_{11}] for classical model, linear analysis, and for generic values of indices *m* and *n*.

Equation (4.68) is first solved for the displacements in terms of interacting loads, then this solution is substituted into the constraint equations to determine the interacting loads. Thus, the total solution is obtained. An LU decomposition procedure is used to invert the blocks in the stiffness submatrices, K_{11}, K_{22} and K_{33}.

4.5.2 NONLINEAR ANALYSIS

As stated earlier, the nonlinear analysis is performed for the repeating unit with symmetrical section stiffeners only. On the basis of symmetry of the repeating unit about x- and θ-axes, the displacements and interacting loads approximations are modified for the nonlinear analysis. In Eqs. (4.1) through (4.3) for shell displacements, in Eqs. (4.11) and (4.12) for stringer displacements, in Eqs. (4.17) and (4.20) to (4.22) for ring displacements, in Eqs. (4.29) and (4.30) for the shell-stringer interacting loads, and in Eqs. (4.33), (4.36) and (4.37) for the shell-ring interacting loads, the coefficients u_{2mn}, v_{2mn}, w_{2mn}, u_{s2m}, w_{s1m}, u_{rn}, ϕ_{xrn}, $\phi_{\theta rn}$, ϕ_{zrn}, λ_{xs2m}, λ_{zs1m}, λ_{xrn}, $\Lambda_{\theta rn}$, and Λ_{zrn}, all are set to zero where $m = 1, 2, ... M$ and $n = 1, 2, ... N$. Note that the corresponding coefficients in the virtual displacements and interacting load approximations (Eqs. (4.6-4.8), (4.14), (4.15), (4.23), (4.26-4.28), (4.31), (4.32), (4.38), (4.41), and (4.42)) for the shell and stiffeners are also set to zero. These modified approximations for the displacements are substituted into the actual and the incremental virtual work functionals derived for each structural element in Section 3.5. The incremental displacements have the same functional forms as the actual displacements, with the amplitudes denoted by the prefix Δ. The integration over space is performed after substitution for the Lagrange multipliers, or interacting loads, and after substitution for each virtual displacement. This process results in a $3MN + 6M + 6N + 6$ system of equations governing the increment in displacements (indicated by a Δ preceding the displacement subvector symbol) and the Lagrange multipliers. The

governing equations are of the form

$$[C]\begin{Bmatrix} \Delta\hat{u}_{shell} \\ \Delta\hat{u}_{str} \\ \Delta\hat{u}_{r} \\ \hat{\lambda}_{str} \\ \hat{\lambda}_{r} \\ Q \end{Bmatrix} = \begin{bmatrix} R_{shell}(\hat{u}_{shell};\, p) \\ -R_{str}(\hat{u}_{str}) \\ -R_{r}(\hat{u}_{r}) \\ 0 \\ 0 \\ 0 \end{bmatrix} \tag{4.81}$$

where the system matrix $[C]$ is given by

$$[C] = \begin{bmatrix} K_{11}(\hat{u}_{shell}) - pL(\hat{u}_{shell}) & 0 & 0 & B_{11} & B_{12} & B_{13} \\ 0 & K_{22}(\hat{u}_{str}) & 0 & B_{21} & 0 & B_{23} \\ 0 & 0 & K_{33}(\hat{u}_{r}) & 0 & B_{32} & 0 \\ B_{11}^{T} & B_{21}^{T} & 0 & 0 & 0 & 0 \\ B_{12}^{T} & 0 & B_{32}^{T} & 0 & 0 & 0 \\ B_{13}^{T} & B_{23}^{T} & 0 & 0 & 0 & 0 \end{bmatrix} \tag{4.82}$$

Submatrices K_{11}, K_{22} and K_{33} are the tangent stiffness matrices for the shell, stringer, and ring, respectively, that are functions of the displacements. These matrices are obtained from their respective incremental internal virtual work statements. The matrix L results from the incremental external virtual work functional for the hydrostatic pressure, Eq. (3.53), and is a function of displacements as well. The submatrices $B_{ij}, i, j = 1, 2, 3$, in Eq. (4.82) are determined from the external virtual work terms involving the Lagrange multipliers, and the constraint Eqs. (2.73), (2.74), (2.77) and (2.81). These B_{ij} submatrices are not functions of the displacements. The vector on the right-hand-side of Eq. (4.81) is the residual force vector. The subvectors of R_{shell}, R_{str}, and R_r of the residual force vector are obtained from the internal and external virtual work (due to internal pressure, Eq. (3.30)) statements of the respective structural element. The constraint equations correspond to the last three rows of the partitioned matrix in Eq. (4.82). The elements of submatrices K_{ij} and L are given in Appendix C, and the elements of subvectors R_{shell}, R_{str} and R_r are given in Appendix D. The elements of submatrices B_{ij} are obtained from those given in Appendix B for the classical model by neglecting the elements corresponding to the coefficients set to zero based on the symmetry of the stiffeners.

The discrete displacement vector for the shell in Eq. (4.81) is the $(3MN + 2M + 2N + 2) \times 1$ vector

$$\hat{u}_{shell} = \left[\hat{u}_0^T, \hat{u}_1^T, ..., \hat{u}_M^T\right]^T \tag{4.83}$$

in which the subvectors are

$$\begin{aligned} \hat{u}_0 &= \left[q_0, w_{00}, v_{01}, w_{01}, ..., v_{0N}, w_{0N}\right]^T \\ \hat{u}_m &= \left[u_{m0}, w_{m0}, u_{m1}, v_{m1}, w_{m1}, ..., u_{mN}, v_{mN}, w_{mN}\right]^T \end{aligned} \tag{4.84}$$

where $m = 1, ..., M$. In Eq. (4.81) the $(2M + 1) \times 1$ discrete displacement vector for the stringer and $(2N + 1) \times 1$ vector for the ring are

$$\begin{aligned} \hat{u}_{str} &= \left[q_1, u_{s1}, w_{s1}, ..., u_{sM}, w_{sM}\right]^T \\ \hat{u}_r &= \left[w_{r0}, v_{r1}, w_{r1}, ..., v_{rN}, w_{rN}\right]^T \end{aligned} \tag{4.85}$$

The discrete vectors of the Lagrange multipliers are

$$\begin{aligned} \hat{\lambda}_{str} &= \left[\lambda_{xs1}, \lambda_{zs1}, ..., \lambda_{xsM}, \lambda_{zsM}\right]^T \\ \hat{\lambda}_r &= \left[\lambda_{zr0}, \lambda_{\theta r1}, \lambda_{zr1}, ..., \lambda_{\theta rN}, \lambda_{zrN}\right]^T \end{aligned} \tag{4.86}$$

The iterative method of solution is based on Eq. (4.81). At a fixed value of the pressure p, a sequence of displacements is defined by adding an increment to the previous member of the sequence to determine the next member in the sequence. For a good initial displacement estimate, the sequence converges to the displacement solution of the nonlinear problem. The initial estimate used here is the converged solution at the last pressure load step. The update procedure to determine the increment is based on the modified Newton method. In the modified Newton method the matrices K_{11}, K_{22} and K_{33}, and L in Eq. (4.82) are only computed for the initial displacement in the sequence, and are not updated for each new member in the sequence. As shown in Eqs. (4.81) and (4.82) the constraints are applied to the increments in the displacements. If the initial estimate of the displacement satisfies these constraint equations and the increments satisfy

these same equations, then the final displacement in the sequence will satisfy these same equations.

The convergence of the solution at a fixed load step implies that the equilibrium of the repeating unit is attained at that load step. Thus, at the converged solution the residual defined by $\delta \mathcal{W}_{ext} - \delta \mathcal{W}_{int} = \delta \hat{u}^T R$, and the change in displacements $\Delta \hat{u}$ should be sufficiently small. A reasonable criterion for convergence test can be to minimize $\Delta \hat{u}^T R$, where the virtual displacements are replaced by the (admissible) incremental displacement vector. An error function defined as $\Delta \hat{u}^T R$ is used to check the convergence against a preset tolerance, i.e., $\Delta \hat{u}^T R \leq TOL$ at the converged solution. In the present analysis, this error function is formulated as

$$\begin{aligned} \Delta \hat{u}^T R = & ABS\left[\Delta \hat{u}_{shell}^T [R_{shell} - B_{11}\hat{\lambda}_{str} - B_{12}\hat{\lambda}_r - B_{13}Q]\right] \\ & + ABS\left[\Delta \hat{u}_{str}^T [-R_{str} - B_{21}\hat{\lambda}_{str} - B_{23}Q]\right] \\ & + ABS\left[\Delta \hat{u}_r^T [-R_r - B_{32}\hat{\lambda}_r]\right] \end{aligned} \tag{4.87}$$

The stiffness submatrices $(K_{11} - pL)$, K_{22} and K_{33} in Eq. (4.82) are symmetric. From Appendix C, it may be noted that the elements of the stiffness matrix for the shell, K_{11}, are densely populated inspite of orthogonality of the series. Furthermore, in the nonlinear analysis there is a coupling of the elements obtained from the displacement approximations using single and double Fourier Series. Thus, the shell stiffness matrix $(K_{11} - pL)$ cannot be inverted in the blocks as is done in the case of linear analysis. Instead, the matrix is now required to be inverted as a whole (i.e., as $(3MN + 2M + 2N + 2) \times (3MN + 2M + 2N + 2)$ matrix), and hence, is computationally more expensive. Equation (4.81) is first solved for the displacements in terms of interacting loads, then this solution is substituted into the constraint equations to determine the interacting loads. Thus, the total solution is obtained. An LU decomposition procedure is used to invert the stiffness submatrices.

4.5.3 VERIFICATION OF NUMERICAL SOLUTION

Separate FORTRAN computer programs are written for the linear and nonlinear analyses. In each program several checks on the numerical results are coded to establish necessary conditions for the solution accuracy. These are

1. The solution for the Fourier coefficients for the displacements and interacting loads are substituted into the left-hand side of the Eq. (4.68) to compute the force vector. This computed force vector is compared to the input force vector to check the accuracy of the numerical solution to Eq. (4.68).

2. From free body diagrams of the shell, stringer, and ring, overall equilibrium conditions are established for each. These overall equilibrium conditions are evaluated using the numerical solution to check if they are satisfied.

3. Pointwise equilibrium equations, or the Euler equations for the functionals, are not necessarily satisfied by the Ritz method. However, for the stringer and ring in the present analysis, the Ritz solution is an exact solution of the Euler equations as well. Consequently, the Euler equations for the stiffeners are programmed and evaluated at many points using the numerical solution to assess accuracy.

4. For the nonlinear analysis the accuracy of the numerical results at each load step is ensured by checking the error function defined by Eq. (4.87) against a preset tolerance. At the converged solution the left-hand and right-hand sides of Eq. (4.81) are individually equal to zero, and this is verified by the error function given by Eq. (4.87). Furthermore, for the converged solution at final load step, the final displacements in the sequence are substituted into the displacement constraint equations at the shell-stiffener interface to verify them.

All numerical results presented in the following chapters satisfy these checks on numerical accuracy.

CHAPTER 5
A UNIT CELL MODEL WITH SYMMETRIC STIFFENERS

5.1 INTRODUCTION

Numerical results are obtained for a linear elastic and a geometrically nonlinear elastic response of the unit cell model subjected to internal pressure. The stiffeners are assumed to have symmetrical cross sections. The purpose of the linear elastic analysis is two fold: First, the results obtained are used to validate the structural model employed in the analysis by comparing to the results presented by Wang and Hsu[19]. Second, these results for the linear elastic response are subsequently used to compare with a geometrically nonlinear elastic response. Data used in the example are representative of the dimensions and cabin pressure of a large transport fuselage structure.

5.2 NUMERICAL DATA

Numerical data for the example are R = 117.5 in., $2l$ = 20 in., $2R\Theta$ = 5.8 in., t = 0.075 in., R_0 = 113.72 in., e_s = 1.10 in., e_r = 3.78 in., $(EA)_r = 0.592 \times 10^7$ lb., $(EI)_r = 0.269 \times 10^8$ lb-in^2., $(EA)_s = 0.404 \times 10^7$ lb., $(EI)_s = 0.142 \times 10^8$ lb-in^2., and with the shell wall stiffness matrices given by

$$A = \begin{bmatrix} 0.664 & 0.221 & 0 \\ 0.221 & 0.577 & 0 \\ 0 & 0 & 0.221 \end{bmatrix} \times 10^6 \; lb/in. \qquad B = 0$$

$$D = \begin{bmatrix} 262 & 159 & 4.33 \\ 159 & 210 & 4.33 \\ 4.33 & 4.33 & 159 \end{bmatrix} lb\ in.$$

This data was originally used in an example by Wang and Hsu[19]. In their analysis, Wang and Hsu neglected the contribution of bend-twist coupling terms D_{16} and D_{26} in

the bending stiffness matrix of shell. This implies that the shell wall is assumed to be specially orthotropic. The present analysis is also based on the same assumption. All the results presented for this example are for an internal pressure $p = 10$ psi. The Fourier Series are truncated at $M = N = 16$ (unless otherwise indicated), and this results in 966 degrees of freedom (or equations to be solved) in the structural model. Since $2\Theta = 2.83^{o}$, the shell in this example is shallow and the DMV shell theory should be adequate. It is found that the numerical results using Sanders theory with the rotation about the normal neglected and the numerical results using DMV theory were essentially the same.

5.3 VALIDATION OF STRUCTURAL MODEL

The results obtained from the linear elastic analysis are compared with those obtained by Wang and Hsu[19] to validate the structural model. They presented the results for the normal displacement and strains of shell, which are limited to linear analysis. Wang and Hsu included the interacting loads in their analysis but did not present results for them. The distributions of the shell's normal displacement w in the circumferential and axial directions are shown in Figs. 5.1 and 5.2, respectively, for the linear analysis. The w-distributions shown for the linear analysis compare very well with those presented by Wang and Hsu (see Fig. 5 in Ref. [19]). The distributions of the circumferential and axial normal strains on the inner and outer surfaces of the shell from the linear analysis are shown in Figs. 5.3 and 5.4, respectively. The values of the ϵ_{xx} and $\epsilon_{\theta\theta}$ strains compare very well to those presented by Wang and Hsu (see Figs. 6 and 7 in Ref. [19]), except in one respect. The exception is that the circumferential distribution of the axial strain ϵ_{xx} at $x = -l$ (Fig. 5.4) does not exhibit a decrease in value as the stringer is approached. Wang and Hsu's results, however, show ϵ_{xx} (Fig. 6 in Ref. [19]) decreasing to nearly zero as the stringer is approached along the circumference. Several changes to the shell displacement approximations were attempted, but any of these attempts could not give

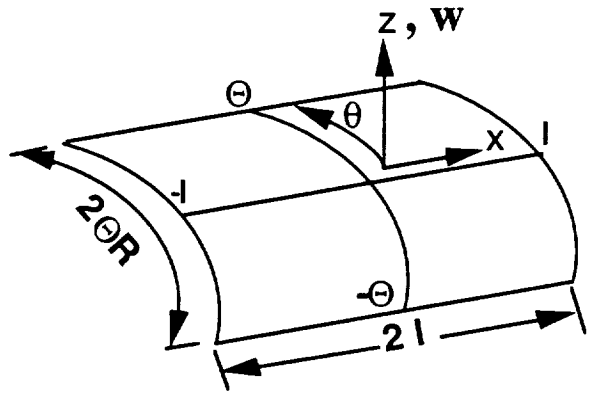

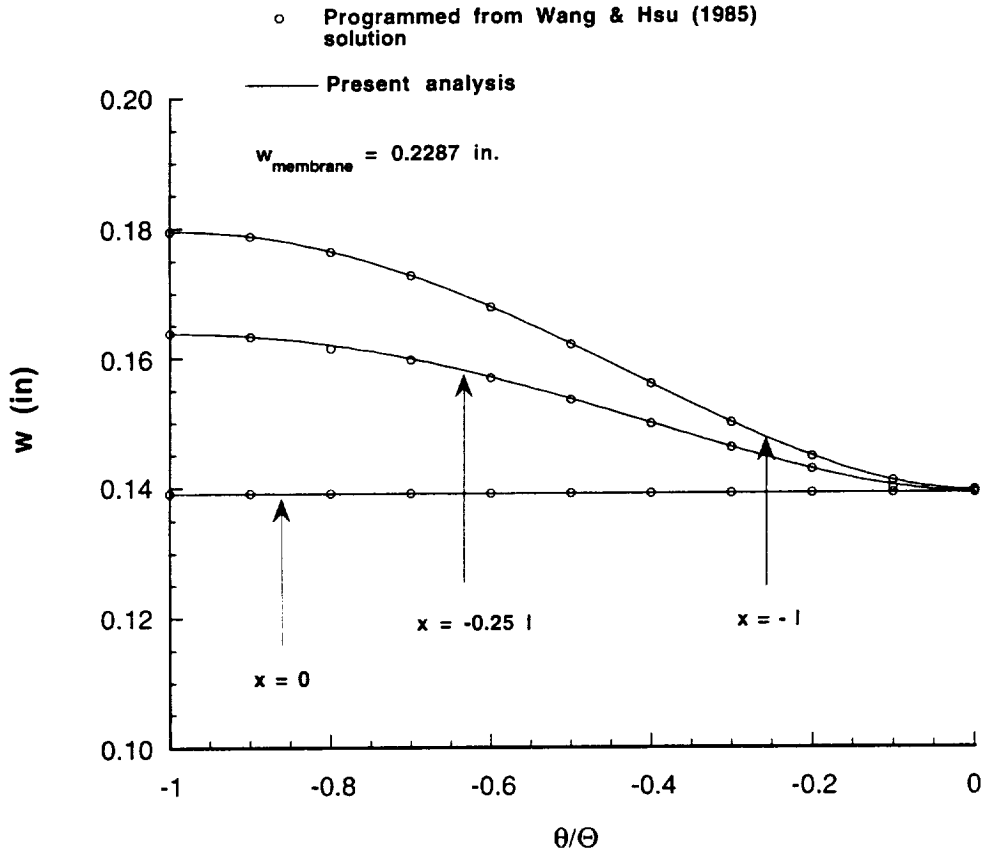

Fig. 5.1 Circumferential distribution of the shell's normal displacement from the linear analysis at 10 psi.

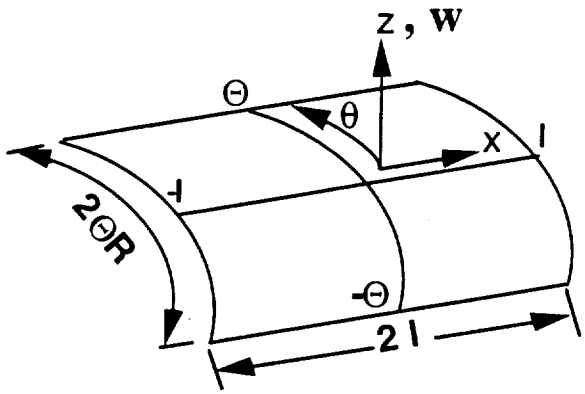

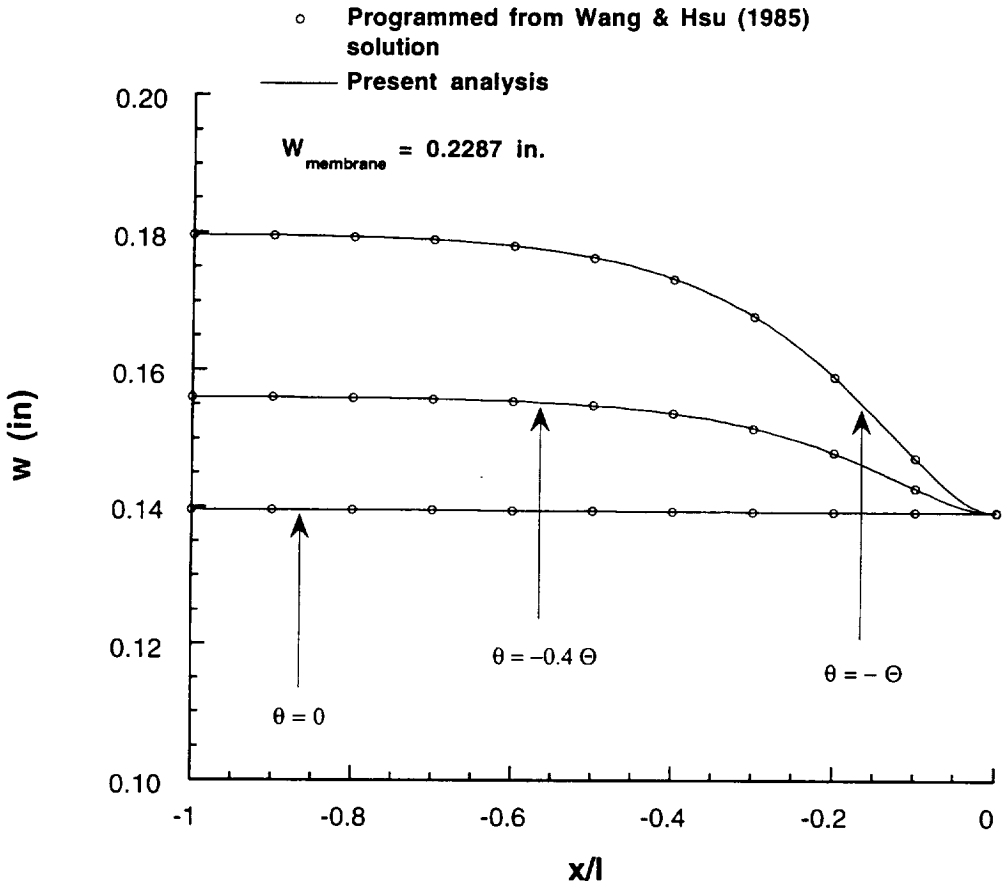

Fig. 5.2 Axial distribution of the shell's normal displacement from the linear analysis at 10 psi.

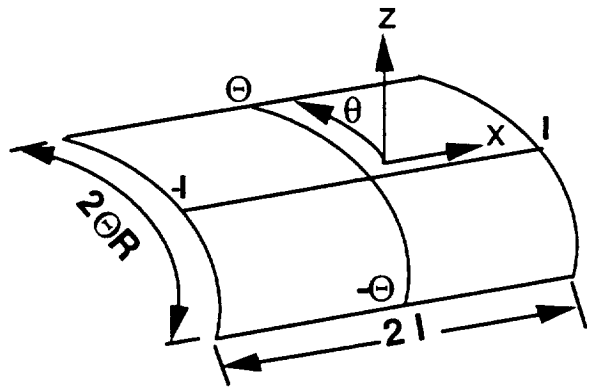

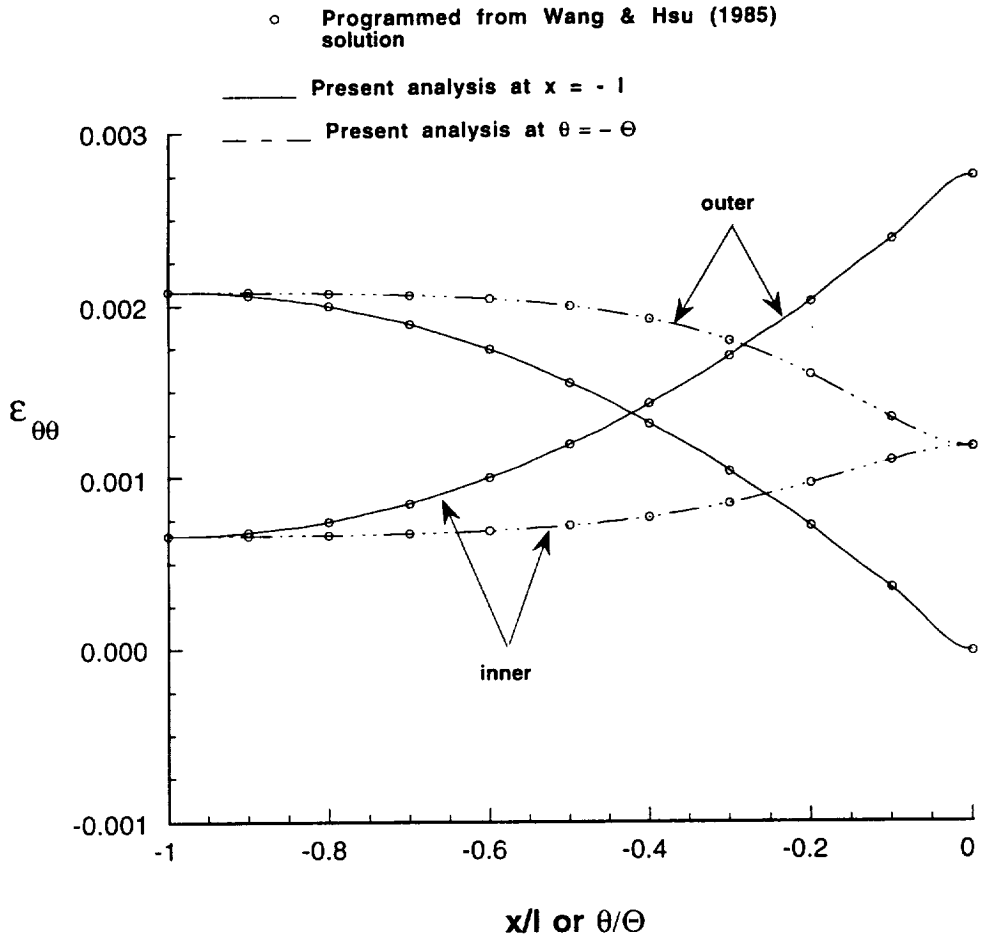

Fig. 5.3 Circumferential normal strain on the inner and outer shell surfaces from the linear analysis at 10 psi.

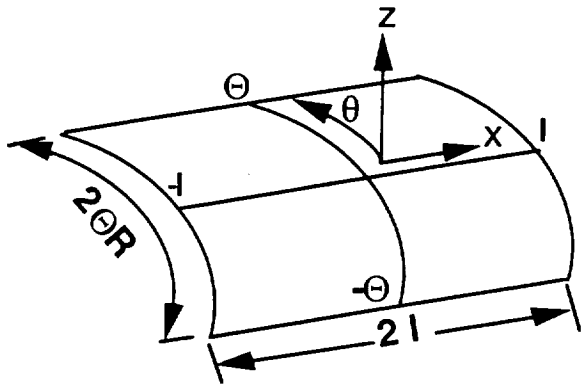

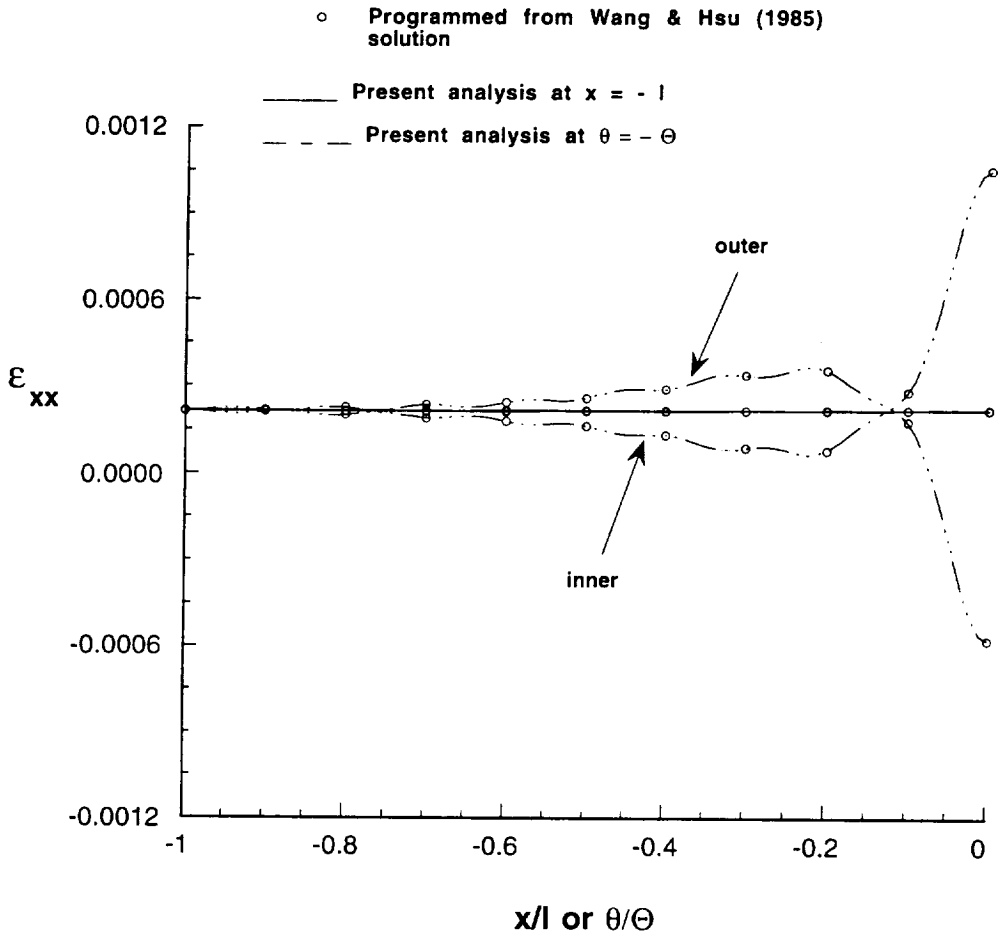

Fig. 5.4 Axial normal strain on the inner and outer shell surfaces from the linear analysis at 10 psi.

a solution showing a decrease in the axial normal strain at the stringer. As a last resort Wang and Hsu's solution was programmed. However, as shown in Figs. 5.1 to 5.4, the solution thus obtained only reconfirmed the results obtained from the current analysis, and did not show a decrease in the axial normal strain at the stringer.

5.4 LINEAR RESPONSE VERSUS NONLINEAR RESPONSE

5.4.1 PILLOWING

Circumferential distributions of the normal displacement w for the shell are shown in Fig. 5.1 for the linear analysis and in Fig. 5.5 for the nonlinear analysis. Axial distributions of the normal displacement for the shell are shown in Fig. 5.2 for the linear analysis and in Fig. 5.6 for the nonlinear analysis. For reference, the normal displacement for the unstiffened shell, or membrane reponse, is $w = 0.2287$ inches for the linear analysis, and $w = 0.2290$ inches for the nonlinear analysis. The presence of the stiffeners reduces the normal displacements from these membrane values as is shown in these figures. The pillowing effect is much more pronounced for the linear analysis (Figs. 5.1 and 5.2) than for the nonlinear analysis (Figs. 5.5 and 5.6). The largest normal displacement occurs midway between the stiffeners, and this value for the linear analysis is 0.1796 inches while it is 0.1541 inches when geometric nonlinearity is included. The minimum normal displacement occurs at the stiffener intersection, and its value is 0.1392 inches in the linear analysis and 0.1490 inches in the nonlinear analysis. Normal displacements along the stiffeners vary only slightly from their values at the intersection for both analyses. Thus, including geometric nonlinearity in the analysis increases the minimum value of the normal displacement of the shell and decreases its maximum value, which is an indication that pillowing is reduced in the nonlinear response.

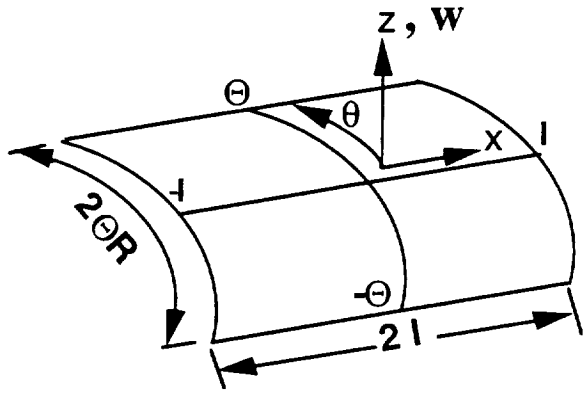

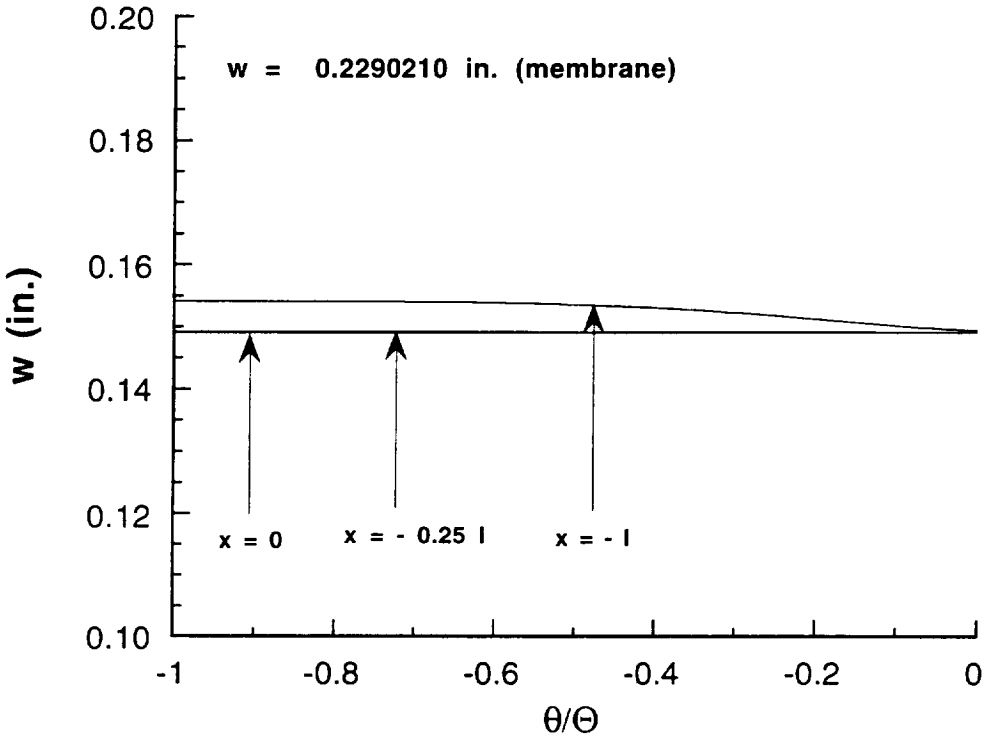

Fig. 5.5 Circumferential distribution of the shell's normal displacement from the nonlinear analysis at 10 psi.

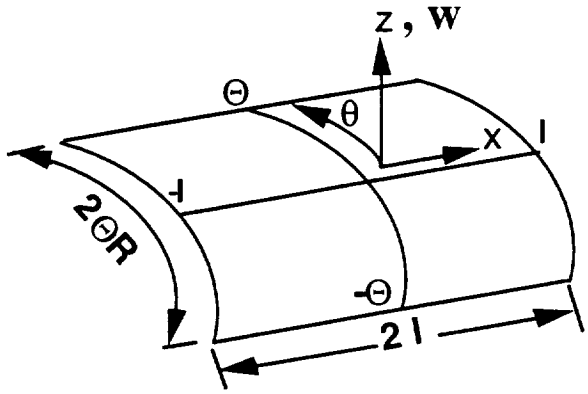

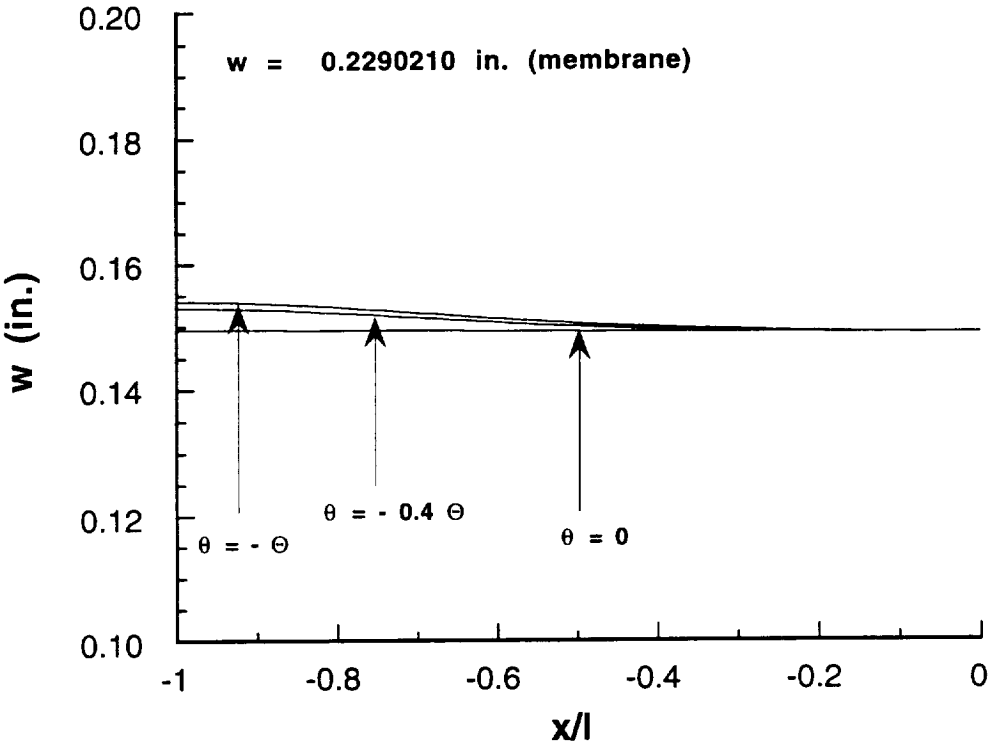

Fig. 5.6 Axial distribution of the shell's normal displacement from the nonlinear analysis at 10 psi.

The circumferential and axial normal strain distributions on the inner and outer surfaces of the shell also show the reduced pillowing effect in the nonlinear analysis. See Figs. 5.7 and 5.8. The circumferential bending strain (difference in $\epsilon_{\theta\theta}$ between the inner and outer surfaces) is maximum at the stringer midway between the rings (Figs. 5.3 and 5.7), and axial bending strain is maximum at the ring midway between the stringers (Figs. 5.4 and 5.8). These maximum bending strains are substantially reduced in the geometrically nonlinear response.

5.4.2 BENDING BOUNDARY LAYER

Compare the circumferential normal strain distributions midway between the ring stiffeners ($x = \pm l$) from the linear analysis (Fig. 5.3) to the nonlinear analysis (Fig. 5.7). The bending strain magnitudes, which are differences between the outer and inner normal strain values, are less in the nonlinear response than in the linear response. In the linear analysis the shell exhibits bending over its entire circumference. In nonlinear analysis the shell behaves like a membrane in the central portion with bending confined to a narrow zone, or boundary layer, adjacent to the stringer. Since the bending is confined to a narrow zone near the stringer, the strain gradients are larger in the nonlinear response than in the linear response. These observations are confirmed by plotting the circumferential bending moment $M_{\theta\theta}$ and the circumferential transverse shear resultant Q_θ versus θ/Θ at $x = -l$ as is done in Figs. 5.9 and 5.10, respectively. The bending moment magnitude is less in the nonlinear analysis compared to the linear analysis. Moreover, for the nonlinear analysis the bending moment is significantly different from zero only in the boundary layer. This is similar to the distributions of the circumferential strains. By the shell equilibrium, the transverse shear resultant Q_θ is proportional to the derivative (gradient) of bending moment, $\partial M_{\theta\theta}/\partial\theta$. Because the bending moment gradients, or the strain gradients, in the nonlinear analysis are larger than in the linear analysis, the transverse shear resultant

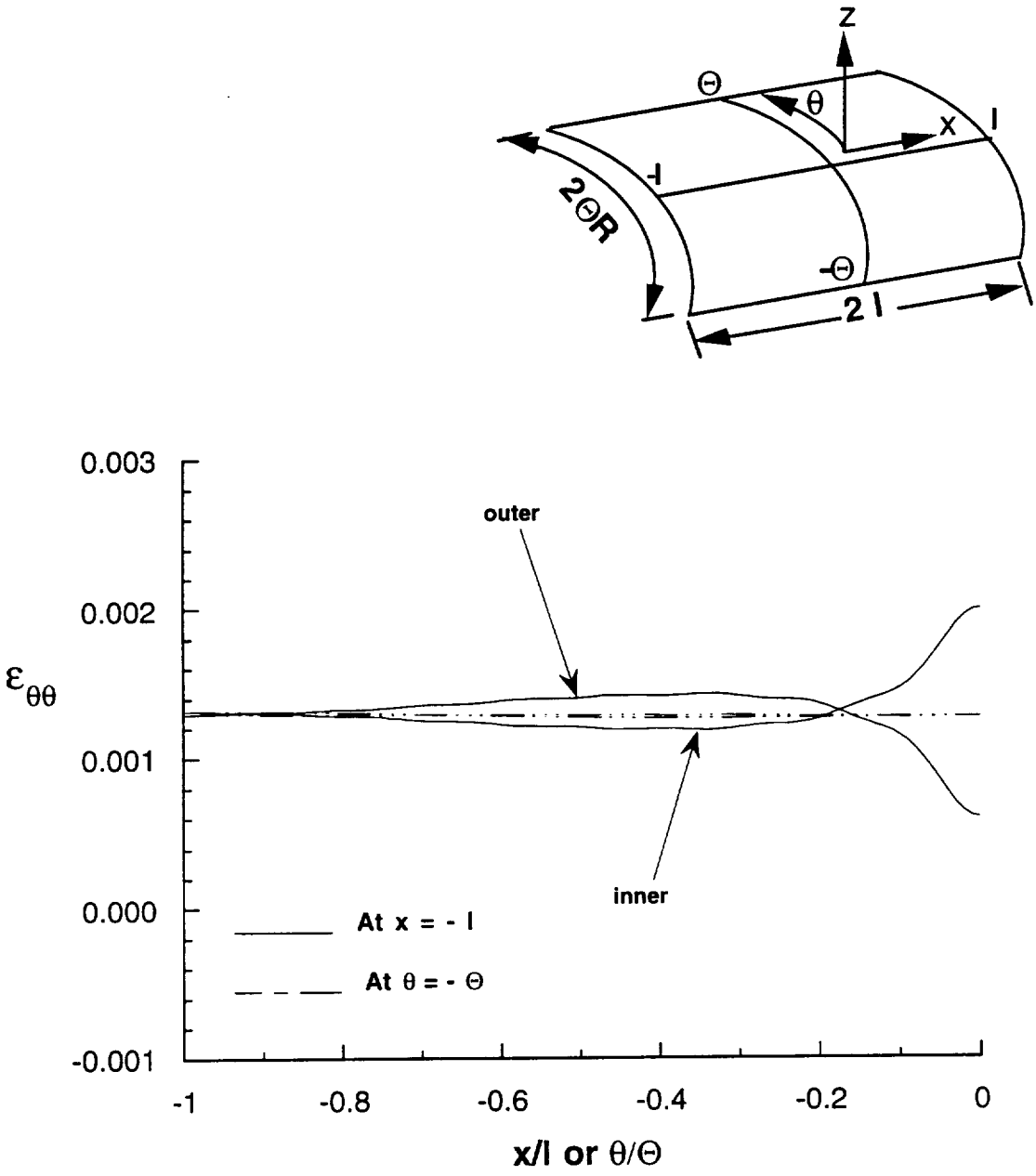

Fig. 5.7 Circumferential normal strain on the inner and outer shell surfaces from the nonlinear analysis at 10 psi.

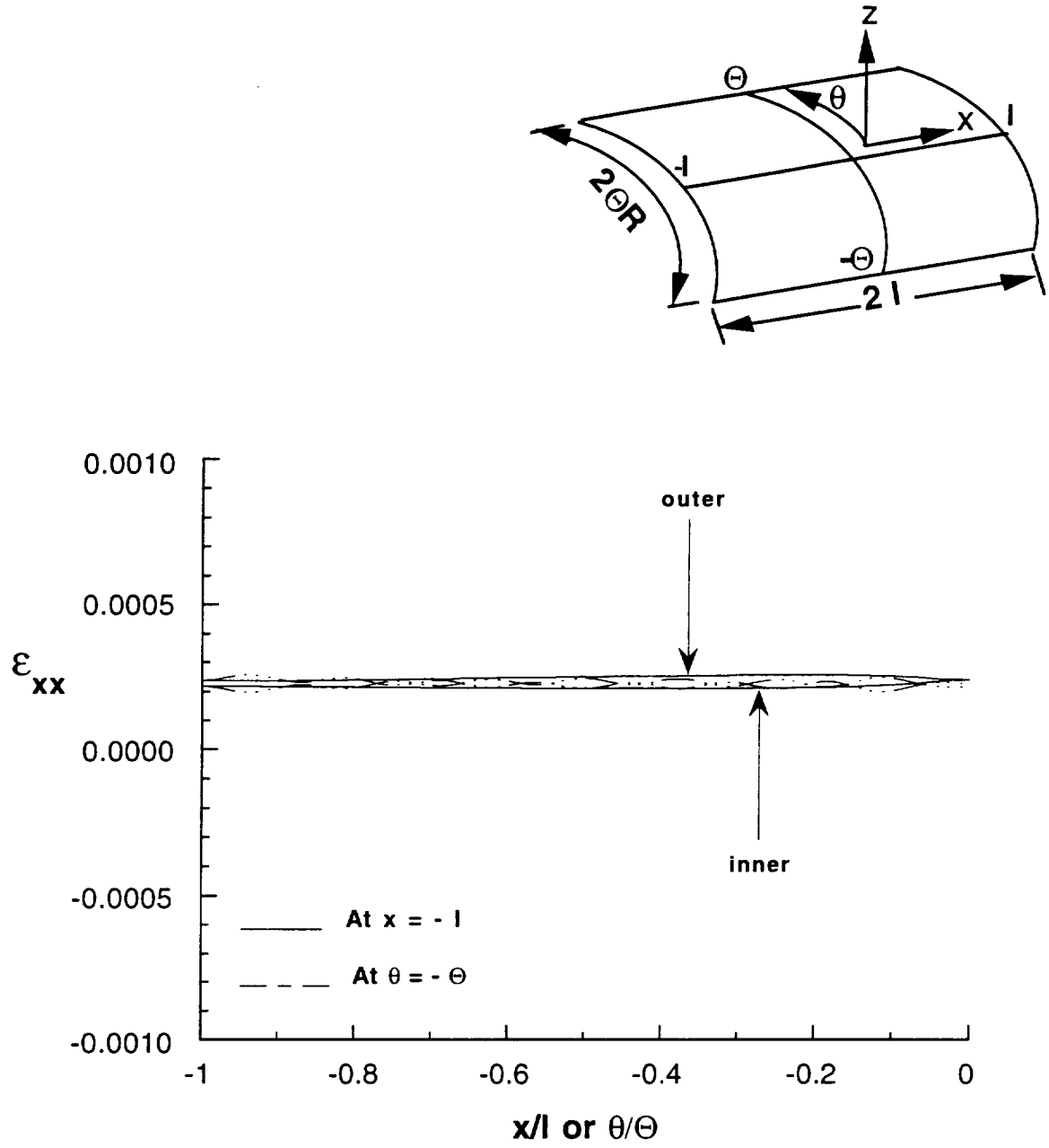

Fig. 5.8 Axial normal strain on the inner and outer shell surfaces from the nonlinear analysis at 10 psi.

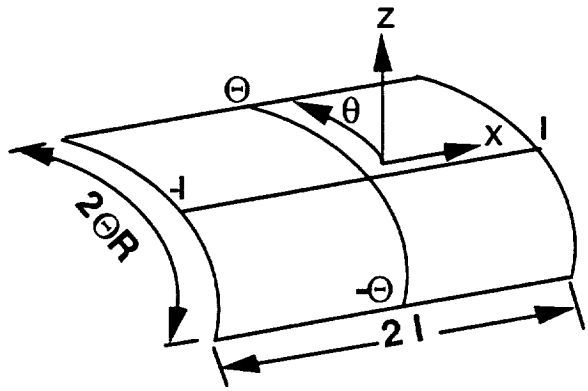

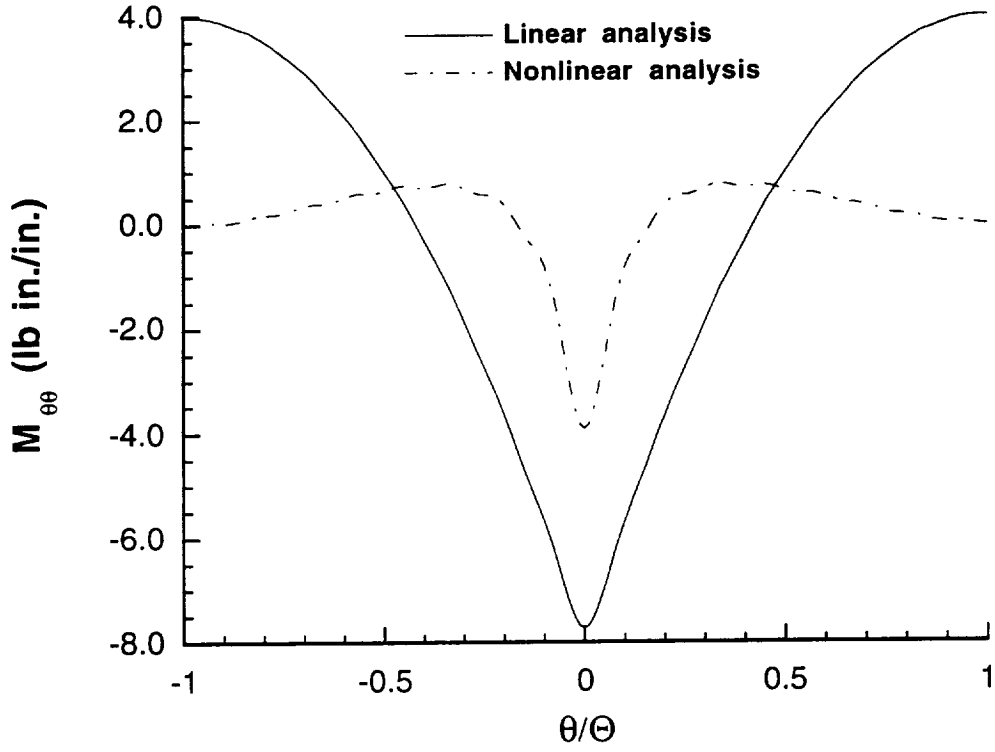

Fig. 5.9 Distribution of the shell's circumferential bending moment midway between the rings (x=-l) at 10 psi.

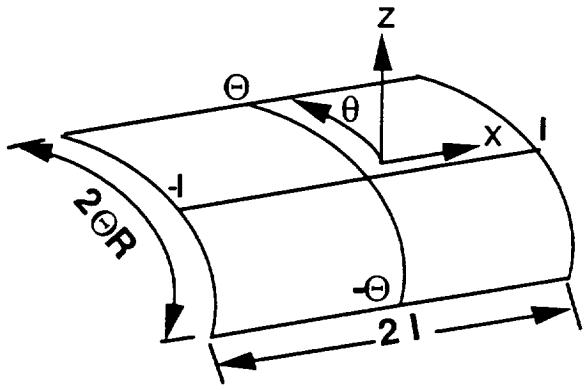

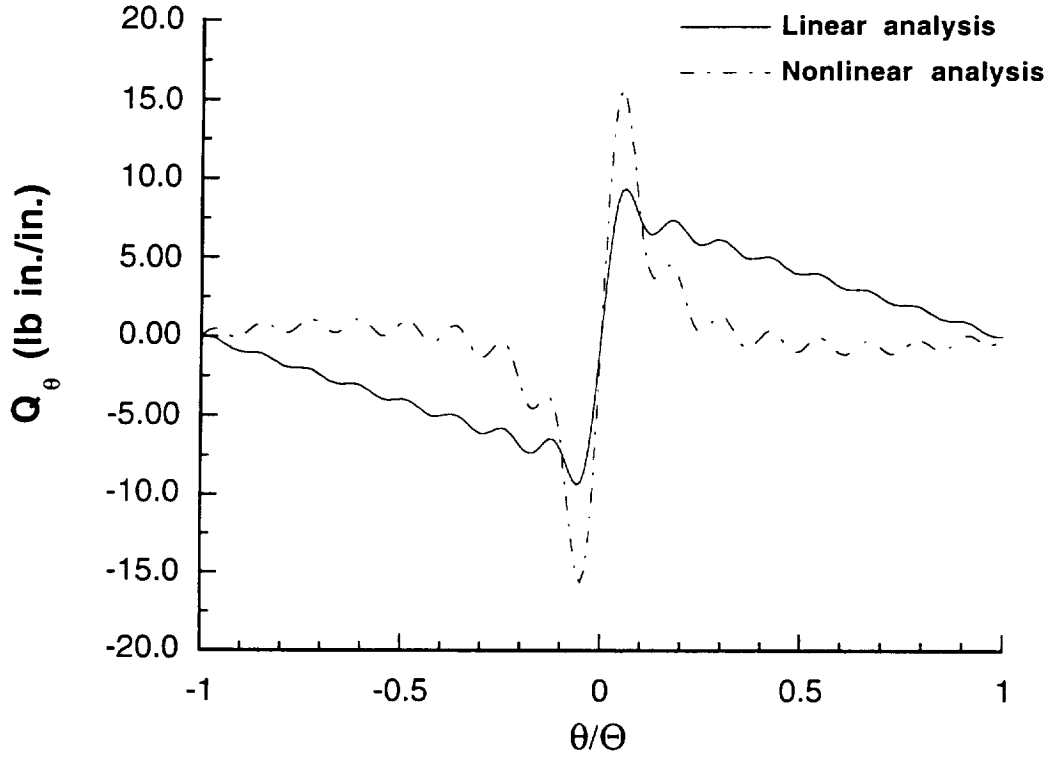

Fig. 5.10 Distribution of the shell's circumferential transverse shear resultant midway between the rings (x=-l) at 10 psi.

has a larger magnitude in the nonlinear analysis than in the linear analysis as is shown in Fig. 5.10. A larger transverse shear resultant in the nonlinear analysis means that the interlaminar shear stresses are larger in the nonlinear analysis than in the linear analysis. Thus, while pillowing is reduced in the nonlinear response, the confinement of bending to a boundary layer near the stringer results in larger interlaminar shear stresses near the stringer in the nonlinear response than in the linear response. These features of the nonlinear response are consistent with the results found by Boitnott[20].

5.4.3 INTERACTING LOAD DISTRIBUTIONS

The distributions of the interacting line loads between the ring and the shell are shown in Figs. 5.11 and 5.12. The distributions of the circumferential component, $\lambda_{\theta r}$, are antisymmetric about the origin, and $\lambda_{\theta r}$ has reduced magnitudes due to the geometrically nonlinear effect. As shown in Fig. 5.12, the distributions of the normal component of the interacting load, λ_{zr}, are symmetric about the origin, attain extremum at the origin, and exhibit severe gradients at the origin. The negative value of λ_{zr} at the origin indicates that the action of the ring is to pull the shell radially inward against the action of the pressure to expand the shell outward. The peak normal load intensity is changed from -1,674 lb/in. in the linear analysis to -1,045 lb/in. in the nonlinear analysis.

The distributions of the interacting line loads between the stringer and the shell are shown in Figs. 5.13 and 5.14. The distributions of the tangential component, λ_{xs}, are antisymmetric about the origin and λ_{xs} has reduced magnitudes due to the geometrically nonlinear effect as shown in Fig. 5.13. The distributions of the normal component, λ_{zs}, are symmetric about the origin as shown in Fig. 5.14. The normal component λ_{zs} is maximum at the origin and has a steep gradient there. The maximum value of normal component is reduced from 484.7 lb/in. in the linear analysis to 320.3 lb/in. in the

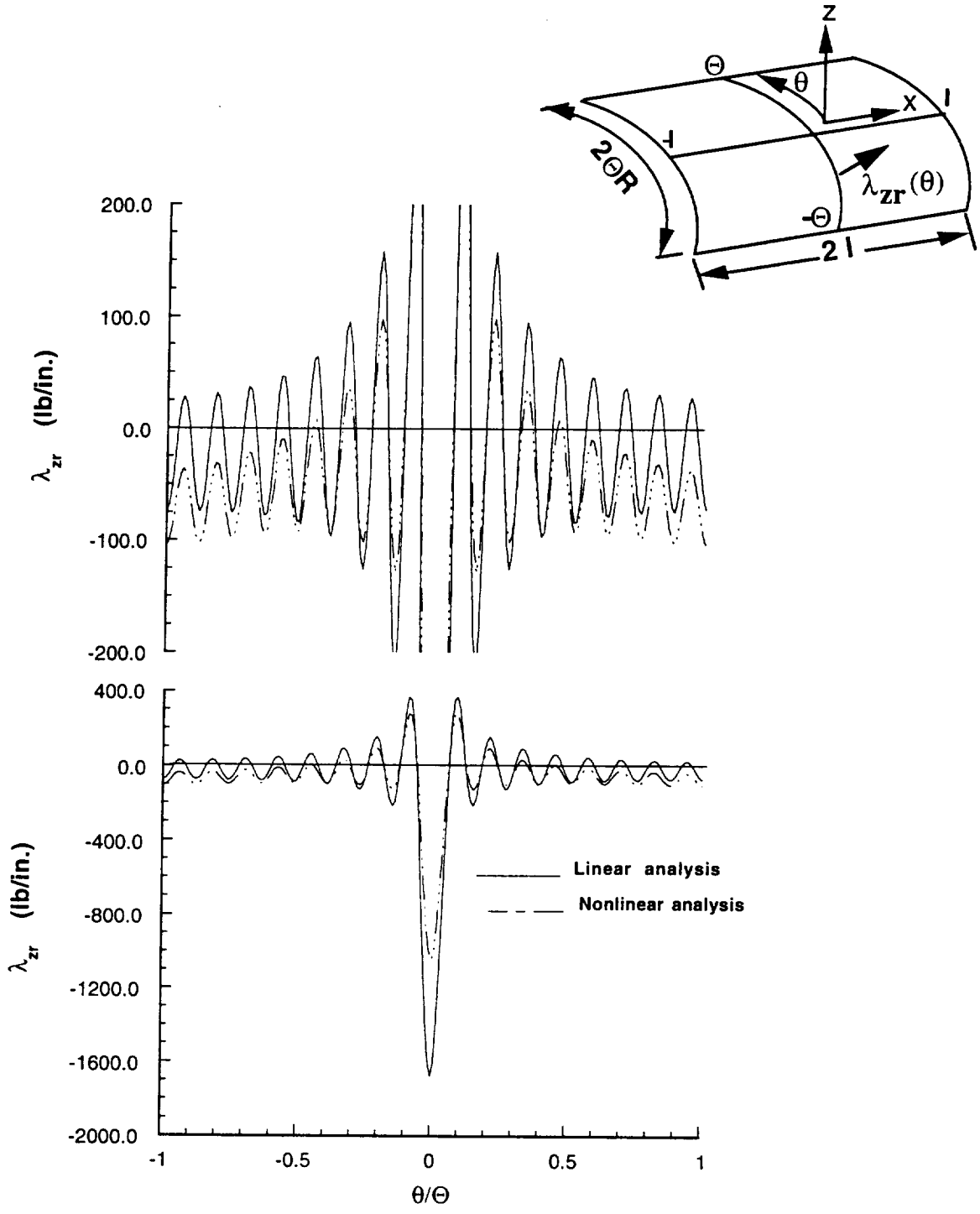

Fig. 5.12 Normal component of the line load acting on the shell due to the ring at 10 psi.

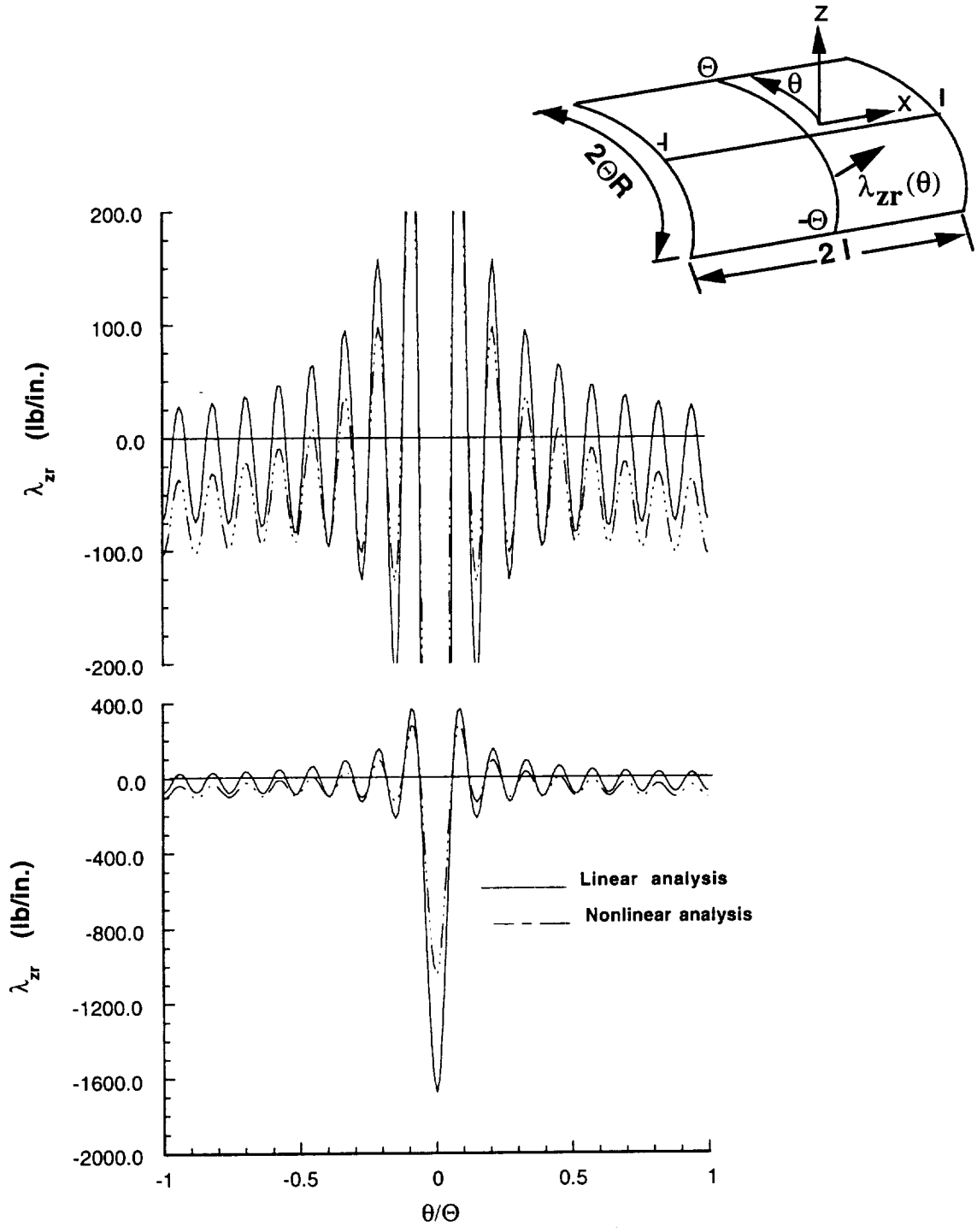

Fig. 5.12 Normal component of the line load acting on the shell due to the ring at 10 psi.

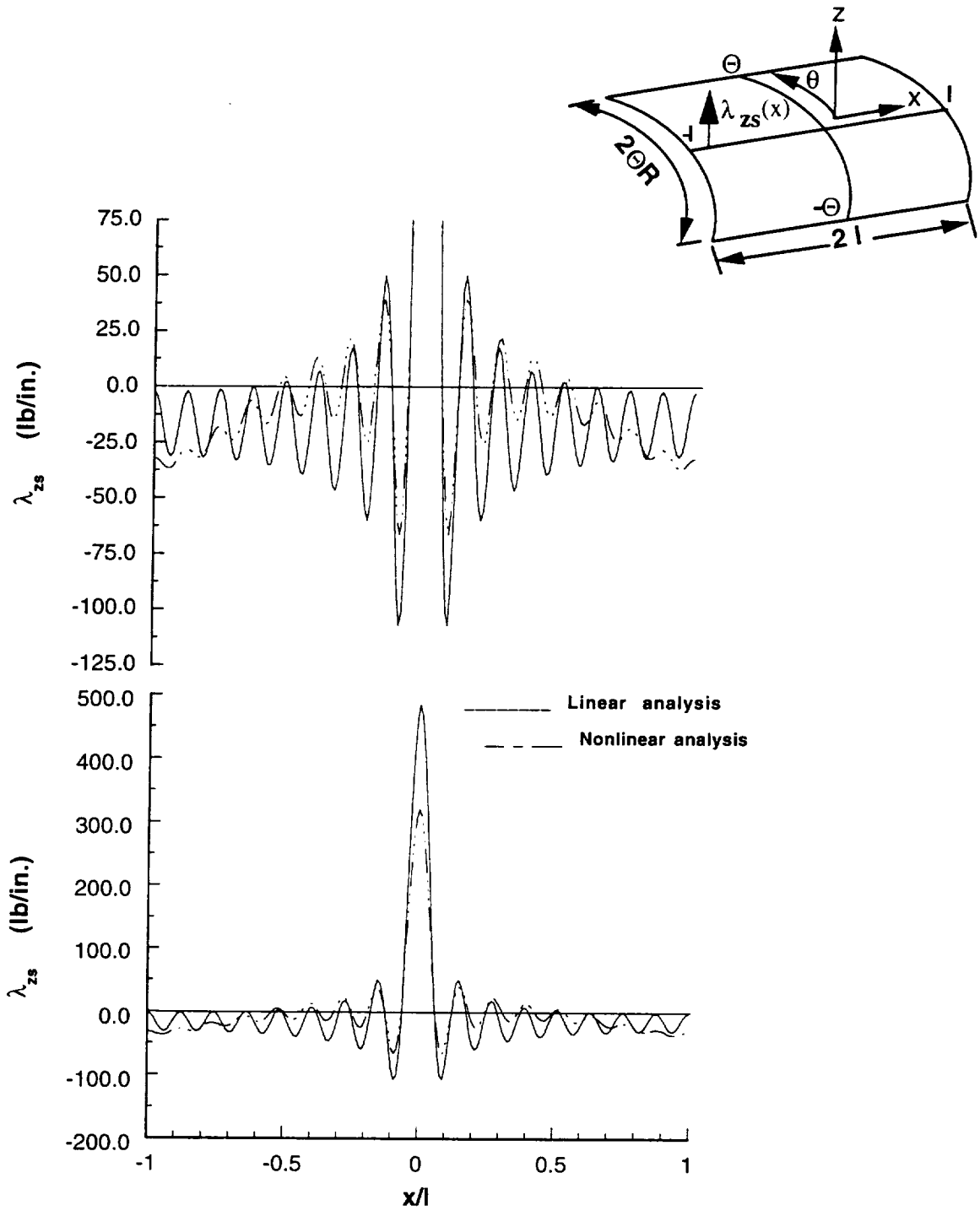

Fig. 5.14 Normal component of the line load acting on the shell due to the stringer at 10 psi.

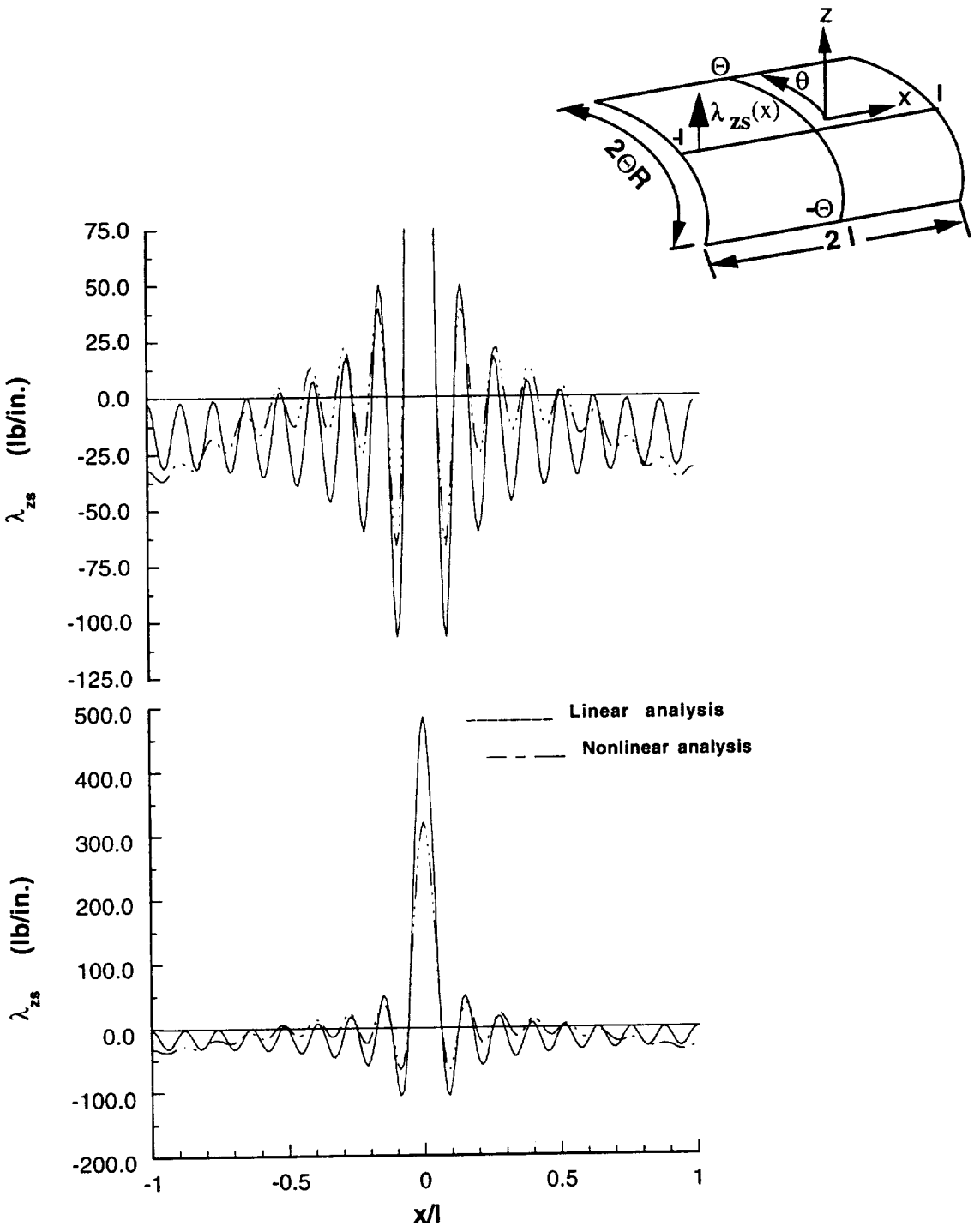

Fig. 5.14 Normal component of the line load acting on the shell due to the stringer at 10 psi.

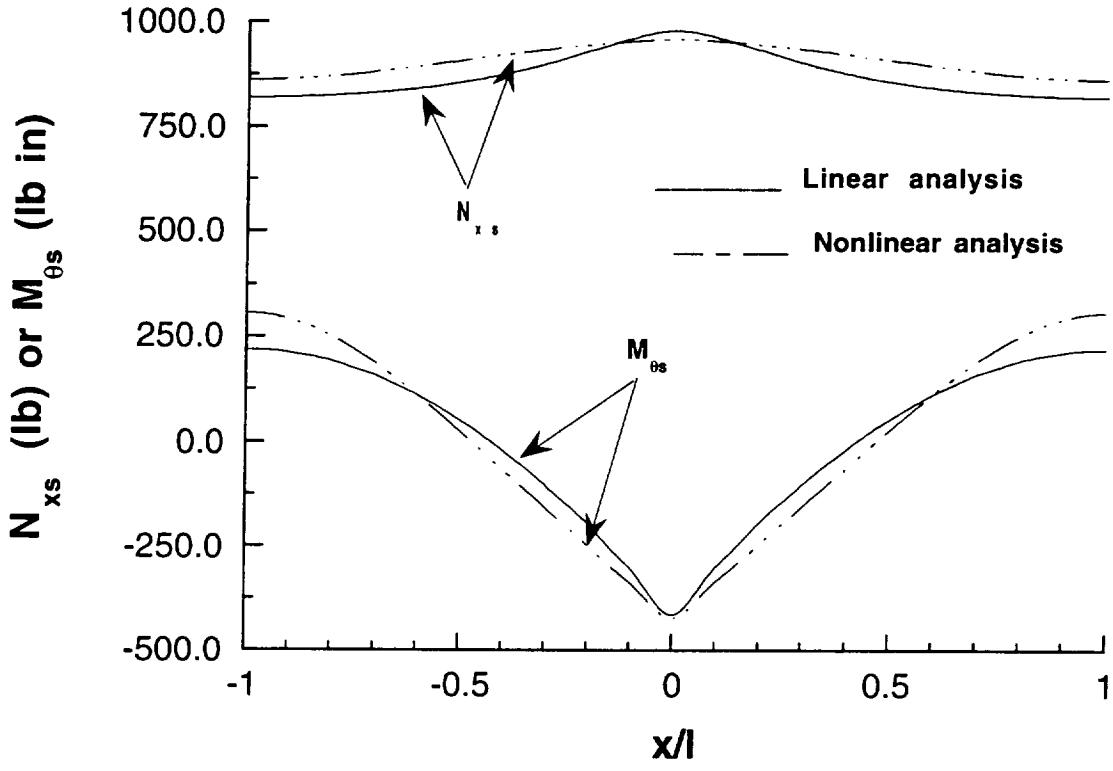

Fig. 5.15 Stringer axial force and bending moment distributions at 10 psi.

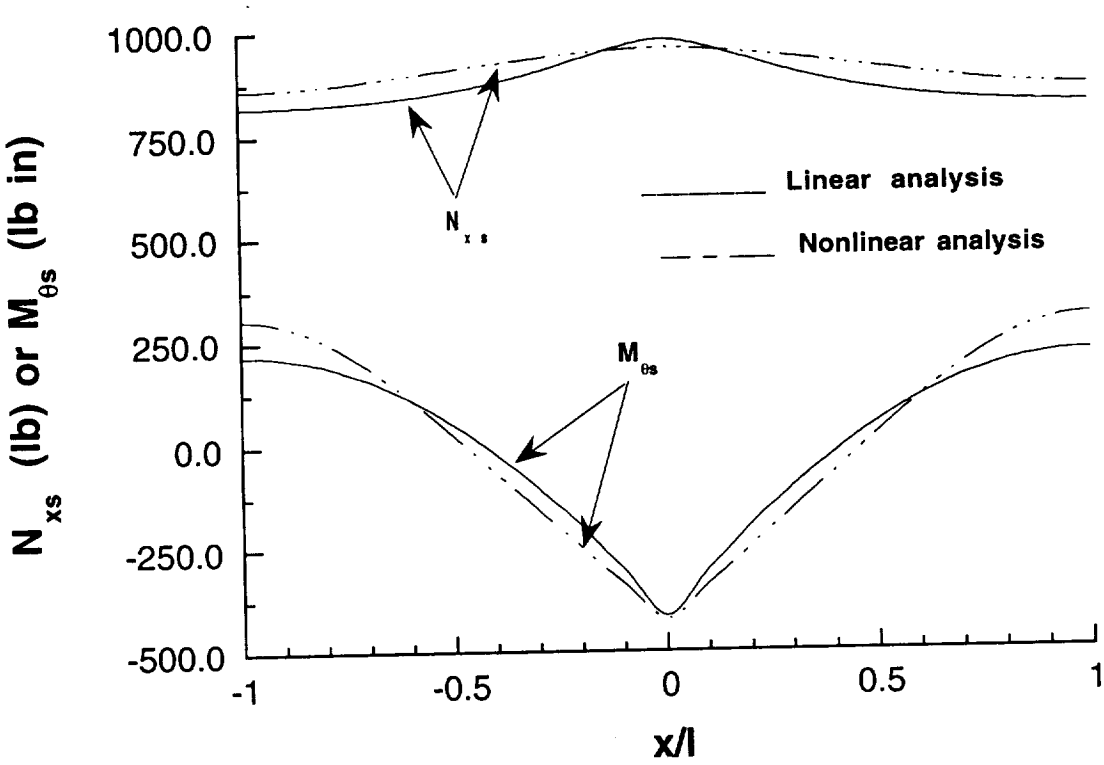

Fig. 5.15 Stringer axial force and bending moment distributions at 10 psi.

magnitude of the interacting normal load intensity at the stiffener intersection as M and N increase. The total normal load intensity acting on the shell at the stiffener intersection is denoted by λ_z, where $\lambda_z = \lambda_{zr}(0) + \lambda_{zs}(0)$. This value is -1,190 lb/in. from the linear analysis and is changed to -725 lb/in. in the nonlinear analysis for $M = N = 16$. A normalized value of λ_z is plotted versus increasing M and N values, with $M = N$, in Fig. 5.17 for the linear analysis, and in Fig. 5.18 for the nonlinear analysis. The normalization factor, λ_{zmax}, is simply the value of λ_z for the largest values of M and N considered in each analysis. As shown in figures, λ_z is steadily increasing with an increasing number of terms in the truncated Fourier Series. Consequently, the series for λ_z does not exhibit, in the range of M and N considered, a convergent behavior. In spite of the fact that the normal load intensity at the stiffener intersection is exhibiting singular behavior, the *total* radial resultant load at the stiffener intersection converges rapidly with increasing values of M and N as shown in Figs. 5.17 and 5.18. The total radial resultant plotted in these figures is defined by

$$F_z = \int_{-\Theta}^{\Theta} \left[\lambda_{zr}\, Cos\theta - \lambda_{\theta r}\, Sin\theta\right] (R_0 + e_r)\, d\theta, \tag{5.1}$$

since the resultant from the stringer vanishes by Eq. (4.61). (A more general approach to the resultants at the stiffener intersection is discussed in subsection 6.3.2.) From the linear analysis $F_z = -357.5$ lbs, and from the nonlinear analysis $F_z = -382.8$ lbs. Since the applied radial load due to internal pressure acting on the repeating unit is 1,160 lbs (= 10 psi$\times$20 in.$\times$5.8 in.), the ring resists about 30.8% of this applied load in the linear response, and this percentage is increased to 33% in the nonlinear response. The remaining portion of the applied radial pressure load is carried by the shell.

magnitude of the interacting normal load intensity at the stiffener intersection as M and N increase. The total normal load intensity acting on the shell at the stiffener intersection is denoted by λ_z, where $\lambda_z = \lambda_{zr}(0) + \lambda_{zs}(0)$. This value is -1,190 lb/in. from the linear analysis and is changed to -725 lb/in. in the nonlinear analysis for $M = N = 16$. A normalized value of λ_z is plotted versus increasing M and N values, with $M = N$, in Fig. 5.17 for the linear analysis, and in Fig. 5.18 for the nonlinear analysis. The normalization factor, λ_{zmax}, is simply the value of λ_z for the largest values of M and N considered in each analysis. As shown in figures, λ_z is steadily increasing with an increasing number of terms in the truncated Fourier Series. Consequently, the series for λ_z does not exhibit, in the range of M and N considered, a convergent behavior. In spite of the fact that the normal load intensity at the stiffener intersection is exhibiting singular behavior, the *total* radial resultant load at the stiffener intersection converges rapidly with increasing values of M and N as shown in Figs. 5.17 and 5.18. The total radial resultant plotted in these figures is defined by

$$F_z = \int_{-\Theta}^{\Theta} \left[\lambda_{zr}\, Cos\theta - \lambda_{\theta r}\, Sin\theta\right] (R_0 + e_r)\, d\theta, \tag{5.1}$$

since the resultant from the stringer vanishes by Eq. (4.61). (A more general approach to the resultants at the stiffener intersection is discussed in subsection 6.3.2.) From the linear analysis $F_z = -357.5$ lbs, and from the nonlinear analysis $F_z = -382.8$ lbs. Since the applied radial load due to internal pressure acting on the repeating unit is 1,160 lbs (= 10 psi$\times$20 in.$\times$5.8 in.), the ring resists about 30.8% of this applied load in the linear response, and this percentage is increased to 33% in the nonlinear response. The remaining portion of the applied radial pressure load is carried by the shell.

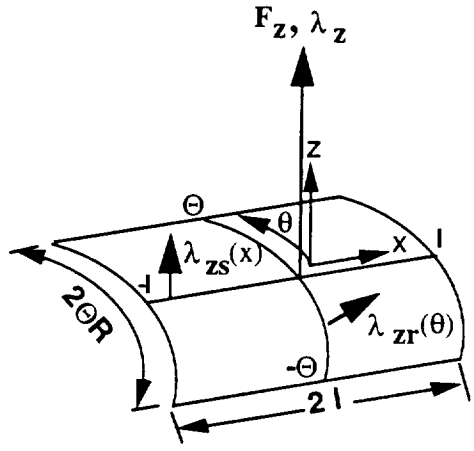

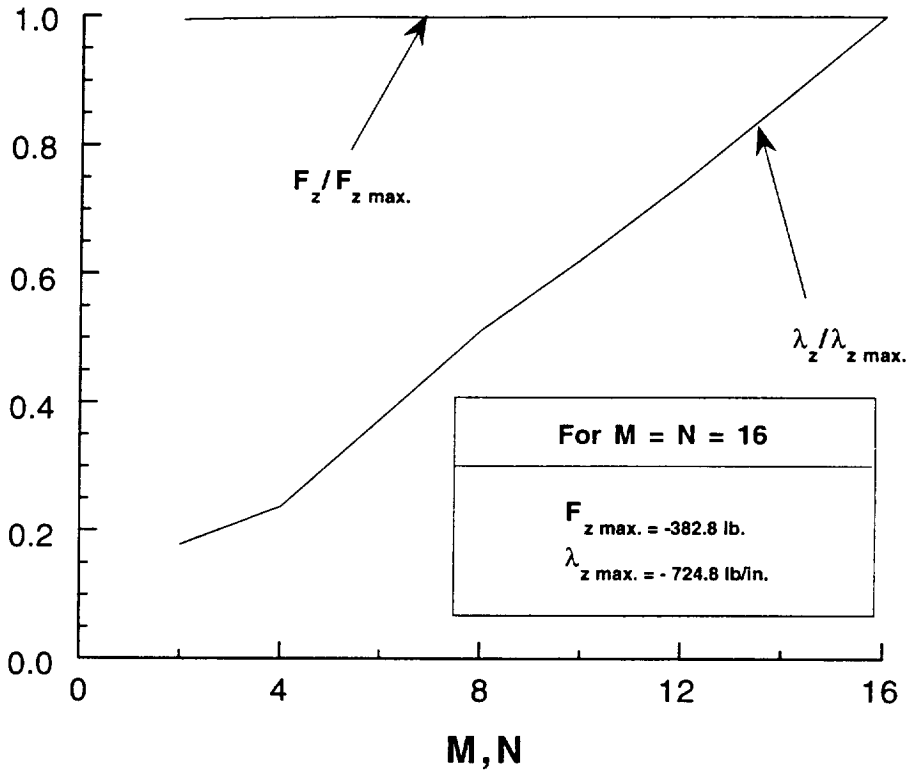

Fig. 5.18 Normal load intensity λ_z and total normal load F_z at the stiffener intersection for increasing number of harmonics in the nonlinear analysis at 10 psi.

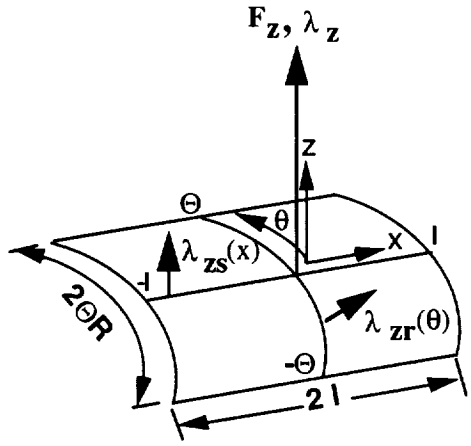

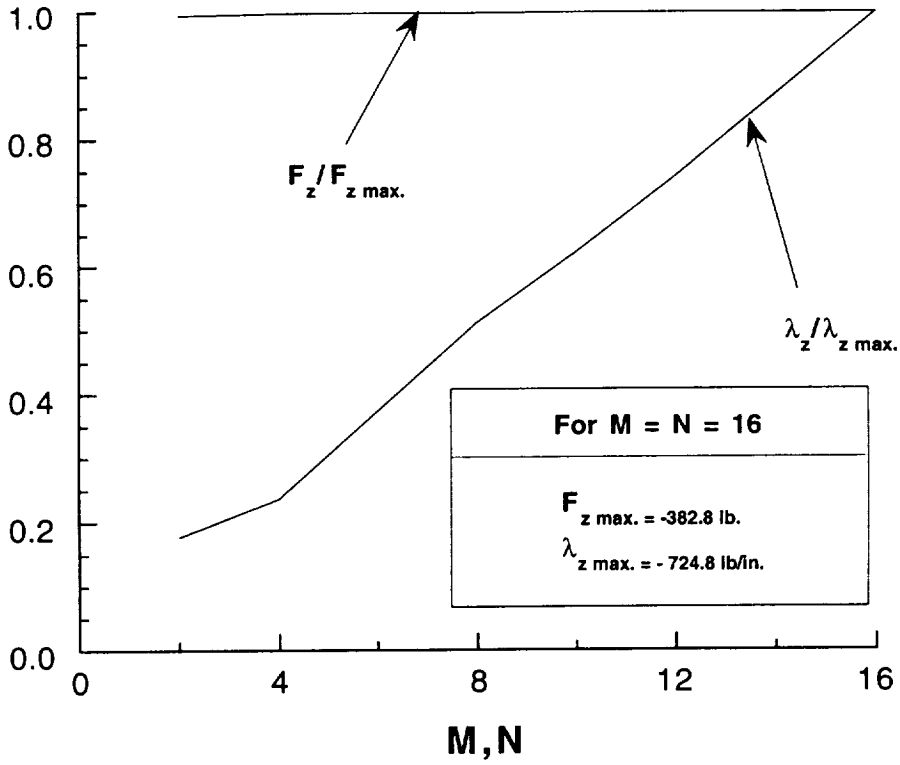

Fig. 5.18 Normal load intensity λ_z and total normal load F_z at the stiffener intersection for increasing number of harmonics in the nonlinear analysis at 10 psi.

of geometric nonlinearity into the analysis. The axial force carried by the stringer due to the closed-end pressure vessel effect is increased in the nonlinear analysis with respect to its value in the linear analysis. Also, the circumferential force carried by the ring is increased in the nonlinear analysis with respect to its value in the linear analysis. Thus, the stiffeners resist an increased portion of the internal pressure load, accompanied by a commensurate decrease in the load carried by the shell, when geometric nonlinearity is included into the analysis.

of geometric nonlinearity into the analysis. The axial force carried by the stringer due to the closed-end pressure vessel effect is increased in the nonlinear analysis with respect to its value in the linear analysis. Also, the circumferential force carried by the ring is increased in the nonlinear analysis with respect to its value in the linear analysis. Thus, the stiffeners resist an increased portion of the internal pressure load, accompanied by a commensurate decrease in the load carried by the shell, when geometric nonlinearity is included into the analysis.

$$D = \begin{bmatrix} 474.937 & 256.071 & 45.074 & 0 \\ 256.071 & 615.194 & 54.003 & -0.47 \times 10^{-5} \\ 45.074 & 54.003 & 276.965 & -0.75 \times 10^{-5} \\ 0 & -0.47 \times 10^{-5} & -0.75 \times 10^{-5} & 0.75 \times 10^{-5} \end{bmatrix} lb\ in.$$

The elements of the transverse shear stiffness matrix in Eq. (2.34) are

$$A_{44} = A_{55} = 0.69264 \times 10^5\ lb/in., \quad A_{45} = 0$$

The bending and stretching-bending coupling submatrices for classical model are given by

$$D = \begin{bmatrix} 474.937 & 256.071 & 0 \\ 256.071 & 615.194 & 0 \\ 0 & 0 & 276.965 \end{bmatrix} lb\ in. \qquad B = 0$$

The extensional stiffness submatrix A is essentially the same for classical theory and the transverse shear deformation theory.

Cross sections of the stiffeners and their dimensions are shown in Fig. 6.1. The stringer is an inverted hat section laminated from twelve plies of AS4/938 graphite-epoxy tow prepreg with a $[\pm 45, 0_2, 90, \pm 15, 90, 0_2, \pm 45]_T$ lay up and total thickness of 0.0888 in. The stiffnesses in Hooke's law for the stringer in Eq. (2.52) are

$$(EA)_s = 0.6675 \times 10^7 lb, \quad (EI)_s = 0.2141 \times 10^7 lb\ in.^2, \quad (GA)_s = 0.843 \times 10^6 lb$$

The frame, or ring, is a 2-D braided graphite-epoxy J-section consisting of 0^o and 90^o tows. The wall thickness is 0.141 inches, and the elastic modulii are assumed to be $E_1 = 7.76 \times 10^6 lb/in.^2$, $E_2 = 8.02 \times 10^6 lb/in.^2$, $G_{12} = G_{13} = G_{23} = 1.99 \times 10^6 lb/in.^2$, and $\nu_{12} = 0.187$. Using the ring material properties and the cross-sectional dimensions, the stiffness matrix for the ring in Eq. (2.58) is computed from the computer code developed by Woodson[29]. The non-zero stiffnesses are

$$EA = 0.9088 \times 10^7 lb, \quad EI_{xx} = 3.915 \times 10^7 lb\ in.^2, \quad EI_{zz} = 0.1867 \times 10^7 lb\ in.^2$$

$$EI_{zx} = 0.2993 \times 10^7 lb\ in.^2, \quad EI_{\omega x} = -1.322 \times 10^7 lb\ in.^3, \quad GJ = 0.1346 \times 10^5 lb\ in.^2$$

$$D = \begin{bmatrix} 474.937 & 256.071 & 45.074 & 0 \\ 256.071 & 615.194 & 54.003 & -0.47 \times 10^{-5} \\ 45.074 & 54.003 & 276.965 & -0.75 \times 10^{-5} \\ 0 & -0.47 \times 10^{-5} & -0.75 \times 10^{-5} & 0.75 \times 10^{-5} \end{bmatrix} lb\ in.$$

The elements of the transverse shear stiffness matrix in Eq. (2.34) are

$$A_{44} = A_{55} = 0.69264 \times 10^5\ lb/in., \qquad A_{45} = 0$$

The bending and stretching-bending coupling submatrices for classical model are given by

$$D = \begin{bmatrix} 474.937 & 256.071 & 0 \\ 256.071 & 615.194 & 0 \\ 0 & 0 & 276.965 \end{bmatrix} lb\ in. \qquad B = 0$$

The extensional stiffness submatrix A is essentially the same for classical theory and the transverse shear deformation theory.

Cross sections of the stiffeners and their dimensions are shown in Fig. 6.1. The stringer is an inverted hat section laminated from twelve plies of AS4/938 graphite-epoxy tow prepreg with a $[\pm 45, 0_2, 90, \pm 15, 90, 0_2, \pm 45]_T$ lay up and total thickness of 0.0888 in. The stiffnesses in Hooke's law for the stringer in Eq. (2.52) are

$$(EA)_s = 0.6675 \times 10^7 lb, \quad (EI)_s = 0.2141 \times 10^7 lb\ in.^2, \quad (GA)_s = 0.843 \times 10^6 lb$$

The frame, or ring, is a 2-D braided graphite-epoxy J-section consisting of 0^o and 90^o tows. The wall thickness is 0.141 inches, and the elastic modulii are assumed to be $E_1 = 7.76 \times 10^6 lb/in.^2$, $E_2 = 8.02 \times 10^6 lb/in.^2$, $G_{12} = G_{13} = G_{23} = 1.99 \times 10^6 lb/in.^2$, and $\nu_{12} = 0.187$. Using the ring material properties and the cross-sectional dimensions, the stiffness matrix for the ring in Eq. (2.58) is computed from the computer code developed by Woodson[29]. The non-zero stiffnesses are

$$EA = 0.9088 \times 10^7 lb, \quad EI_{xx} = 3.915 \times 10^7 lb\ in.^2, \quad EI_{zz} = 0.1867 \times 10^7 lb\ in.^2$$

$$EI_{zx} = 0.2993 \times 10^7 lb\ in.^2, \quad EI_{\omega x} = -1.322 \times 10^7 lb\ in.^3, \quad GJ = 0.1346 \times 10^5 lb\ in.^2$$

$$EI_{\omega\omega} = 1.705 \times 10^7 lb\ in.^4, \quad EI_{\omega z} = -0.1865 \times 10^6 lb\ in.^3$$

$$GA_{x\theta} = GA_{z\theta} = 0.2396 \times 10^7\ lb$$

All the results presented are for an internal pressure $p = 10$ psi, and the Fourier Series are truncated at twenty-four terms in the x- and θ-directions ($M = N = 24$). Based on $M = N = 24$, the transverse shear deformation model consists of a total of 6414 degress of freedom, and classical model consists of 3966 degress of freedom.

6.3 INFLUENCE OF AN ASYMMETRICAL SECTION RING

6.3.1 INTERACTING LOAD DISTRIBUTIONS

The distributions of the interacting line load intensities between the stiffeners and the shell are shown in Figs. 6.2 through 6.8. The effects of transverse shear deformations and of warping deformation of the ring's cross section due to torsion on the magnitudes of the interacting line loads are summarized in Table 6.1. For the component λ_{xs} tangent to the stringer (Fig. 6.2), there are only small differences in the distributions as predicted by the four structural models. However, the peak value of the component normal to the stringer, λ_{zs}, is reduced in the transverse shear deformation models with respect to its peak value in the classical models (Fig. 6.3 and Table 6.1).

The distributions of axial force intensity, λ_{xr}, between the ring and shell predicted by the classical and shear deformation models with warping are nearly the same (Fig. 6.4). However, the distributions of this force intensity predicted by the classical and shear deformation models without warping have significant differences. Thus, this interacting load intensity is more sensitive to the inclusion or exclusion of warping of the ring cross section into the structural model. As shown in Fig. 6.5, the differences in the results for circumferential force intensity, $\lambda_{\theta r}$, between the ring and shell from the four models are

$$EI_{\omega\omega} = 1.705 \times 10^7 lb\ in.^4, \quad EI_{\omega z} = -0.1865 \times 10^6 lb\ in.^3$$

$$GA_{x\theta} = GA_{z\theta} = 0.2396 \times 10^7\ lb$$

All the results presented are for an internal pressure $p = 10$ psi, and the Fourier Series are truncated at twenty-four terms in the x- and θ-directions ($M = N = 24$). Based on $M = N = 24$, the transverse shear deformation model consists of a total of 6414 degress of freedom, and classical model consists of 3966 degress of freedom.

6.3 INFLUENCE OF AN ASYMMETRICAL SECTION RING

6.3.1 INTERACTING LOAD DISTRIBUTIONS

The distributions of the interacting line load intensities between the stiffeners and the shell are shown in Figs. 6.2 through 6.8. The effects of transverse shear deformations and of warping deformation of the ring's cross section due to torsion on the magnitudes of the interacting line loads are summarized in Table 6.1. For the component λ_{xs} tangent to the stringer (Fig. 6.2), there are only small differences in the distributions as predicted by the four structural models. However, the peak value of the component normal to the stringer, λ_{zs}, is reduced in the transverse shear deformation models with respect to its peak value in the classical models (Fig. 6.3 and Table 6.1).

The distributions of axial force intensity, λ_{xr}, between the ring and shell predicted by the classical and shear deformation models with warping are nearly the same (Fig. 6.4). However, the distributions of this force intensity predicted by the classical and shear deformation models without warping have significant differences. Thus, this interacting load intensity is more sensitive to the inclusion or exclusion of warping of the ring cross section into the structural model. As shown in Fig. 6.5, the differences in the results for circumferential force intensity, $\lambda_{\theta r}$, between the ring and shell from the four models are

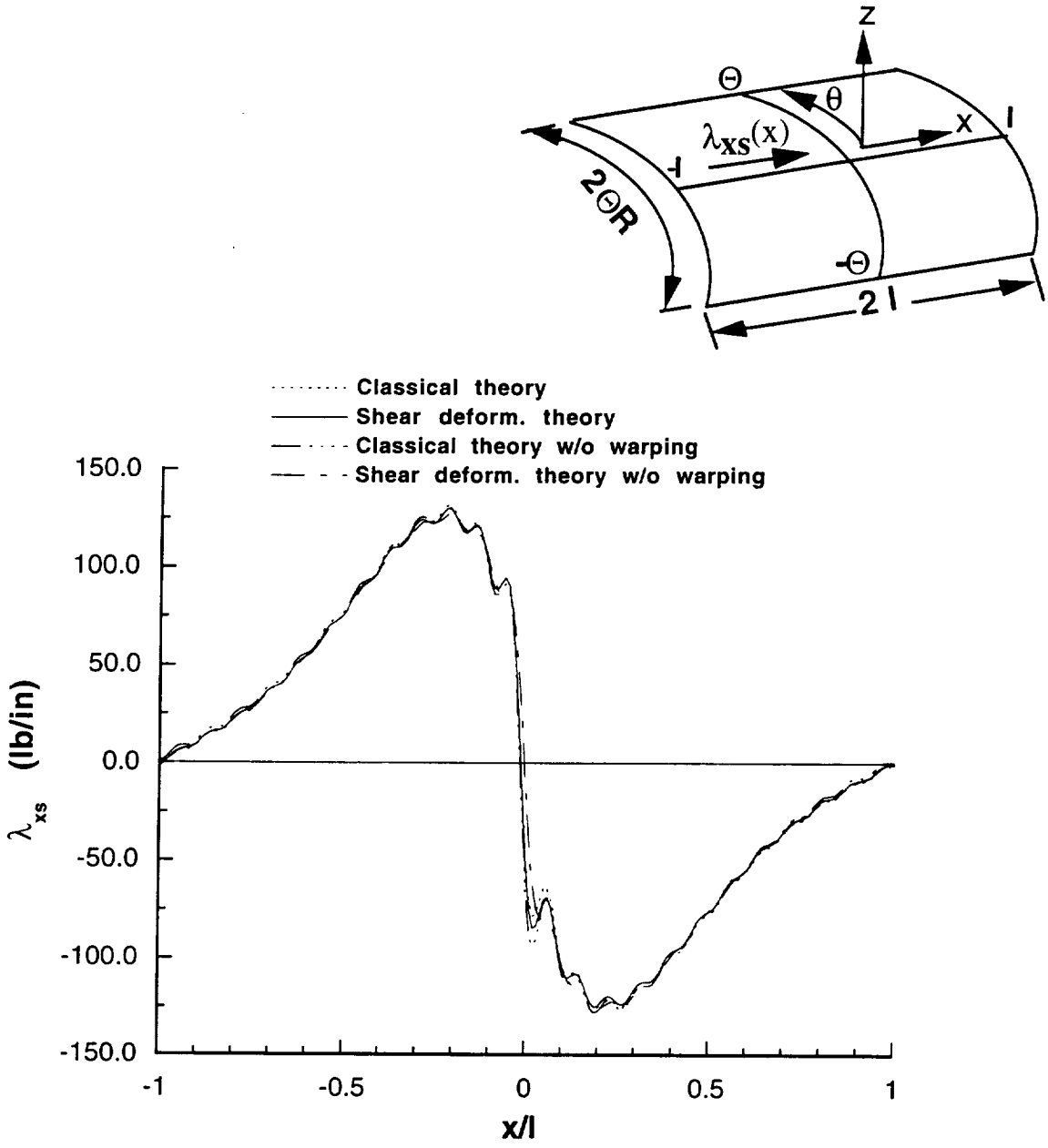

Fig. 6.2 Stringer-shell tangential force intensity in axial direction at 10 psi.

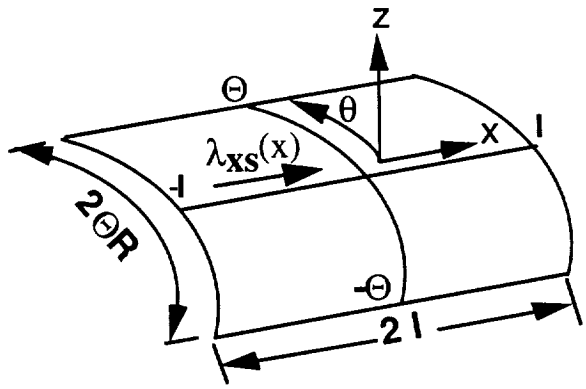

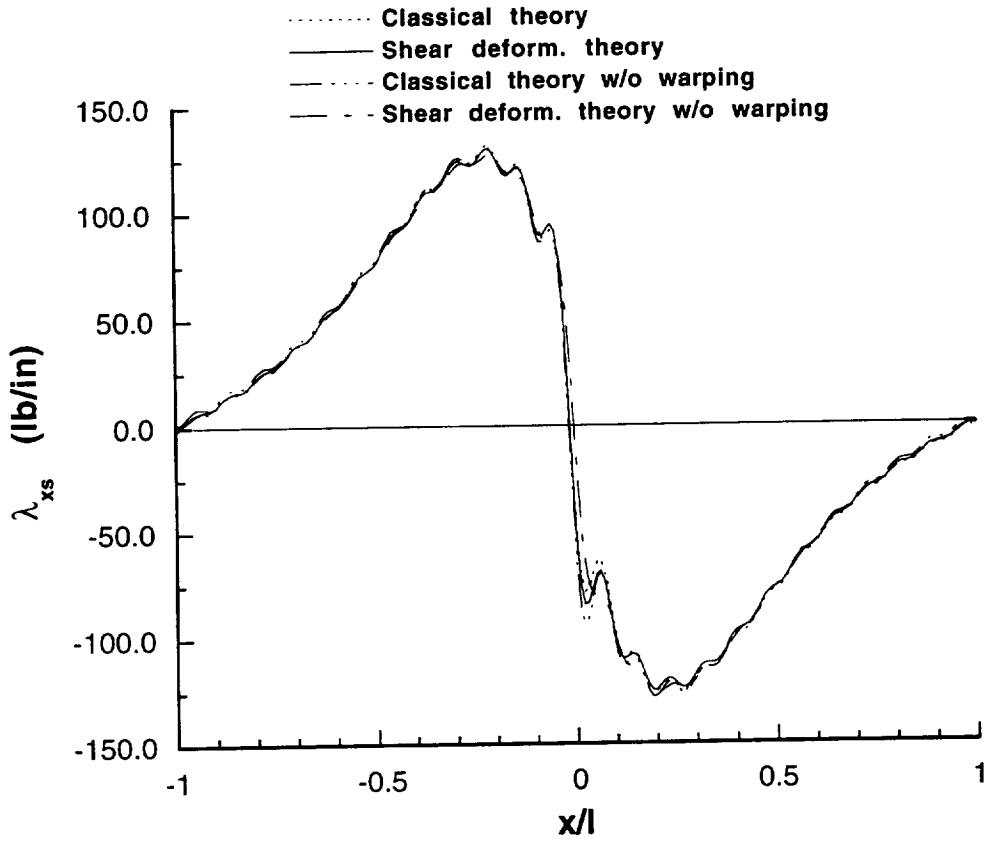

Fig. 6.2 Stringer-shell tangential force intensity in axial direction at 10 psi.

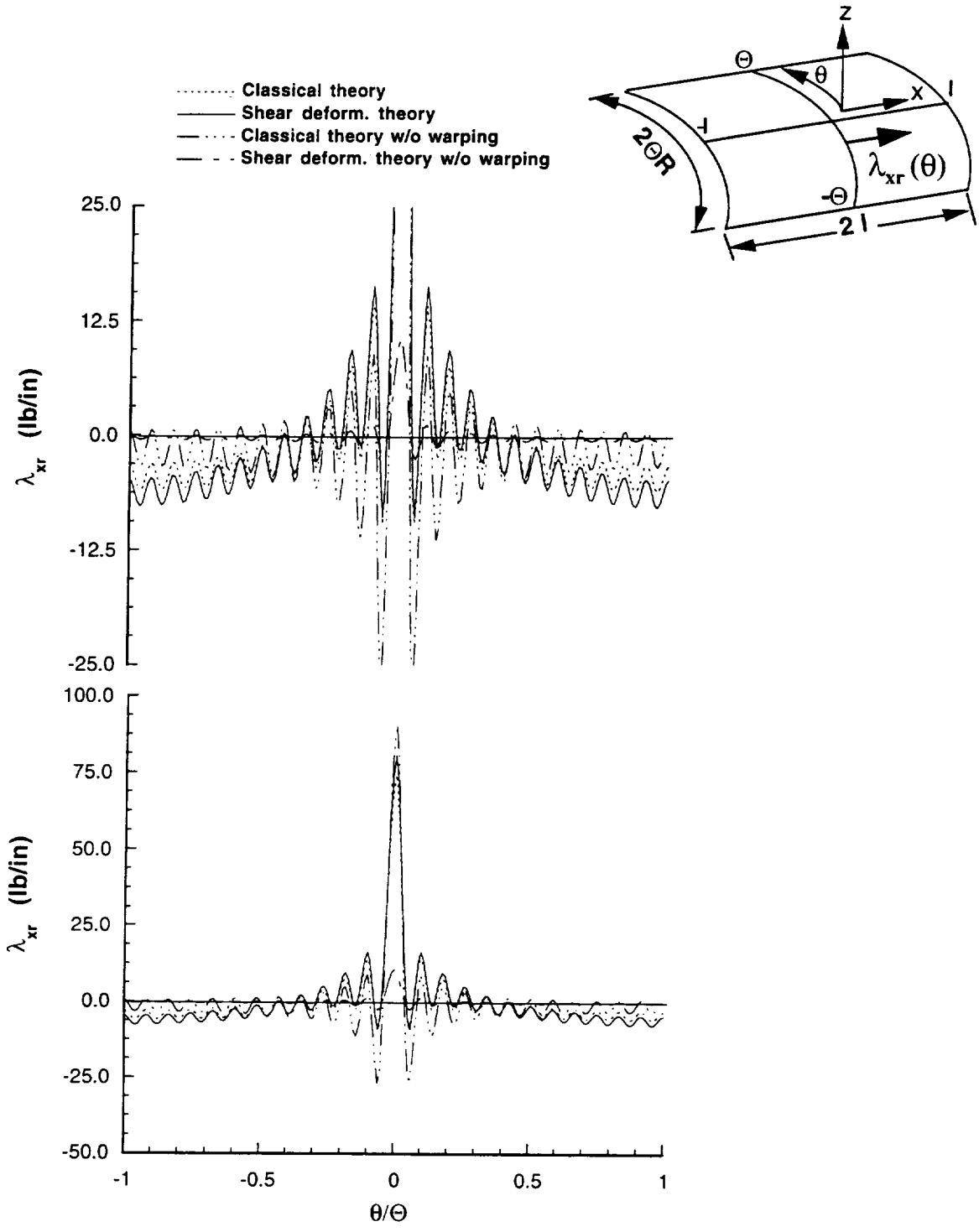

Fig. 6.4 Ring-shell axial force intensity in circumferential direction at 10 psi.

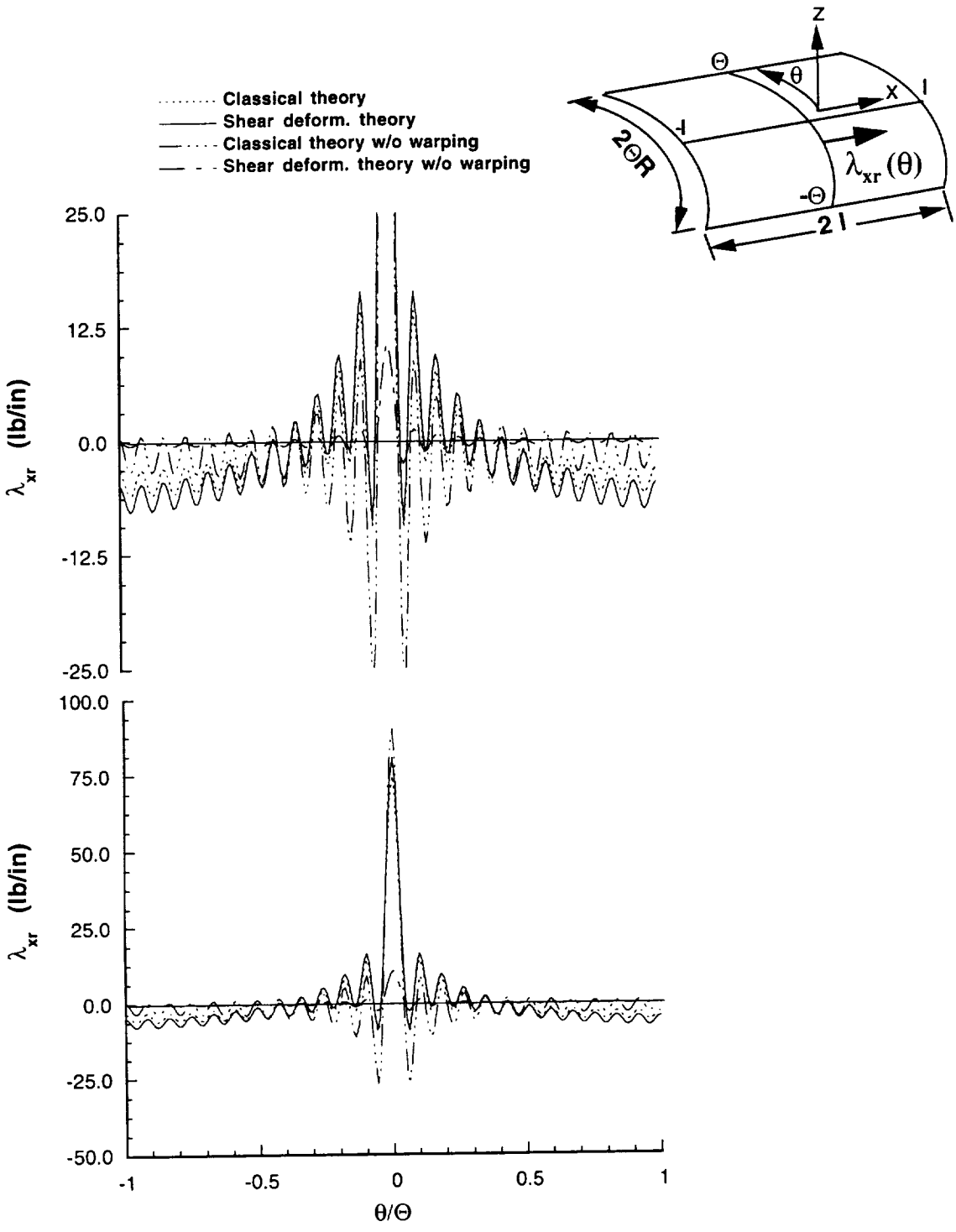

Fig. 6.4 Ring-shell axial force intensity in circumferential direction at 10 psi.

small, except in the vicinity of the stiffener intersection where the effects of including the transverse shear deformation into the models are manifested. However, the differences in $\lambda_{\theta r}$ occur over one wave length of the highest frequency i.e., $\Delta\theta/\Theta = 2/24$. Differences occuring over the shortest wavelength may not be significant; more terms in the Fourier series are required to verify this. The distributions of the normal force intensity, λ_{zr}, between the ring and shell predicted by the four models are essentially the same (Fig. 6.6). The distributions of the circumferential moment component, $\Lambda_{\theta r}$, predicted by the classical models have higher magnitudes as compared to shear deformation models (Fig. 6.7 and Table 6.1). Also note the change in sign of $\Lambda_{\theta r}$ distributions in the vicinity of the joint as a result of inclusion of warping into the models. The classical theory predicts much larger magnitudes of normal moment component, Λ_{zr}, compared to the transverse shear deformation theory for the models in which warping is included (Fig. 6.8 and Table 6.1). However, the reverse is true for the structural models with no warping. Also, there is a change in sign in the distributions of Λ_{zr} for classical models with and without warping effects.

The distribution of the normal component of the traction across the width of the attachment flange of the ring is represented by line force intensity λ_{zr} and line moment intensity $\Lambda_{\theta r}$. The values of λ_{zr} are nearly the same in the classical and transverse shear deformation models (Fig. 6.6), but magnitudes of $\Lambda_{\theta r}$ are substantially *decreased* in the transverse shear deformation models with respect to the classical models (Fig. 6.7). Thus, the asymmetry of the normal traction across the flange width of the ring is *decreased* in the transverse shear deformation models with respect to the classical models.

The distribution of the circumferential component of the traction across the width of the attachment flange of the ring is represented by line force intensity $\lambda_{\theta r}$ and line moment intensity Λ_{zr}. The values of $\lambda_{\theta r}$ are nearly the same in the classical and transverse shear

small, except in the vicinity of the stiffener intersection where the effects of including the transverse shear deformation into the models are manifested. However, the differences in $\lambda_{\theta r}$ occur over one wave length of the highest frequency i.e., $\Delta\theta/\Theta = 2/24$. Differences occuring over the shortest wavelength may not be significant; more terms in the Fourier series are required to verify this. The distributions of the normal force intensity, λ_{zr}, between the ring and shell predicted by the four models are essentially the same (Fig. 6.6). The distributions of the circumferential moment component, $\Lambda_{\theta r}$, predicted by the classical models have higher magnitudes as compared to shear deformation models (Fig. 6.7 and Table 6.1). Also note the change in sign of $\Lambda_{\theta r}$ distributions in the vicinity of the joint as a result of inclusion of warping into the models. The classical theory predicts much larger magnitudes of normal moment component, Λ_{zr}, compared to the transverse shear deformation theory for the models in which warping is included (Fig. 6.8 and Table 6.1). However, the reverse is true for the structural models with no warping. Also, there is a change in sign in the distributions of Λ_{zr} for classical models with and without warping effects.

The distribution of the normal component of the traction across the width of the attachment flange of the ring is represented by line force intensity λ_{zr} and line moment intensity $\Lambda_{\theta r}$. The values of λ_{zr} are nearly the same in the classical and transverse shear deformation models (Fig. 6.6), but magnitudes of $\Lambda_{\theta r}$ are substantially *decreased* in the transverse shear deformation models with respect to the classical models (Fig. 6.7). Thus, the asymmetry of the normal traction across the flange width of the ring is *decreased* in the transverse shear deformation models with respect to the classical models.

The distribution of the circumferential component of the traction across the width of the attachment flange of the ring is represented by line force intensity $\lambda_{\theta r}$ and line moment intensity Λ_{zr}. The values of $\lambda_{\theta r}$ are nearly the same in the classical and transverse shear

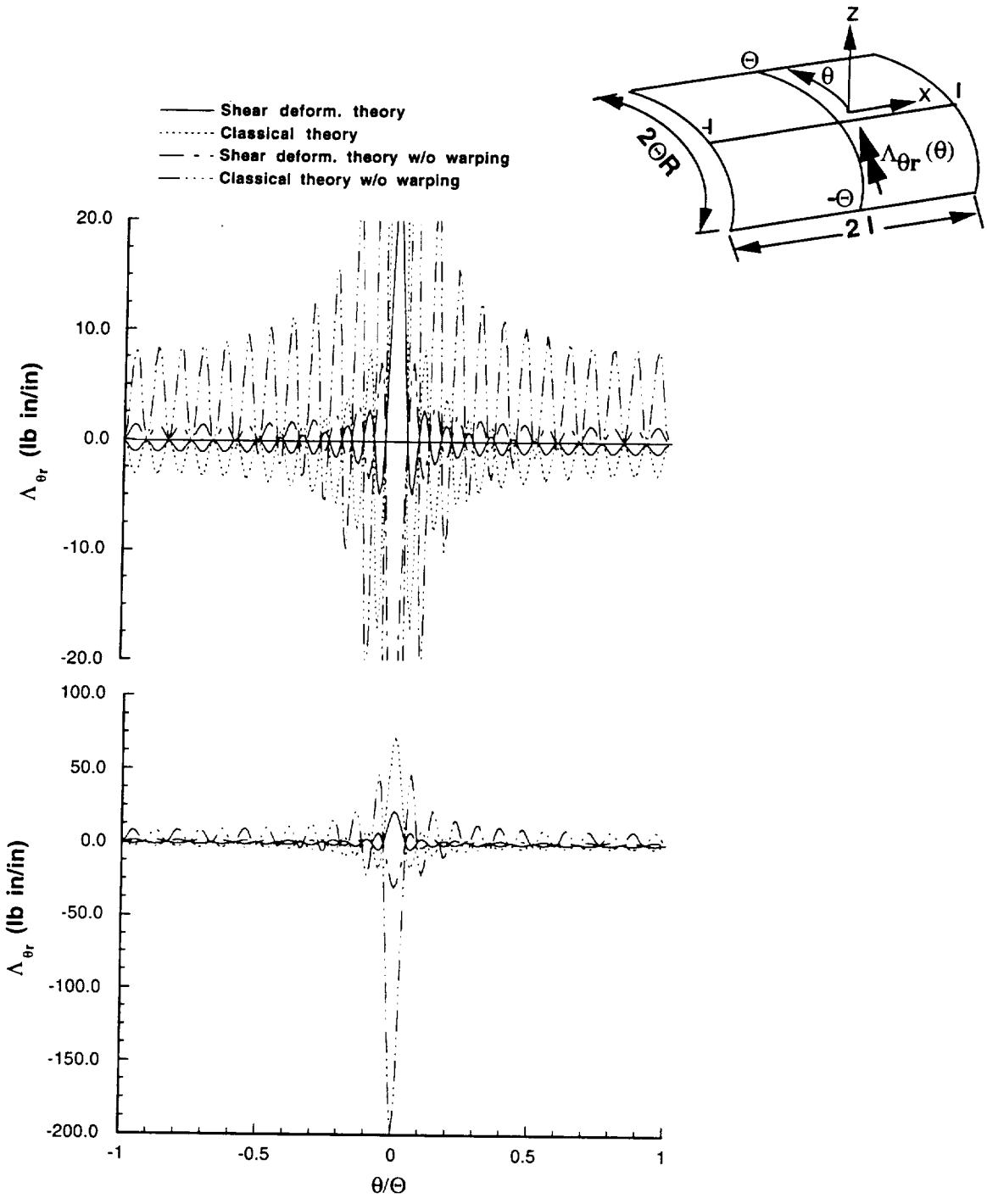

Fig. 6.7 Ring-shell tangential moment intensity in circumferential direction at 10 psi.

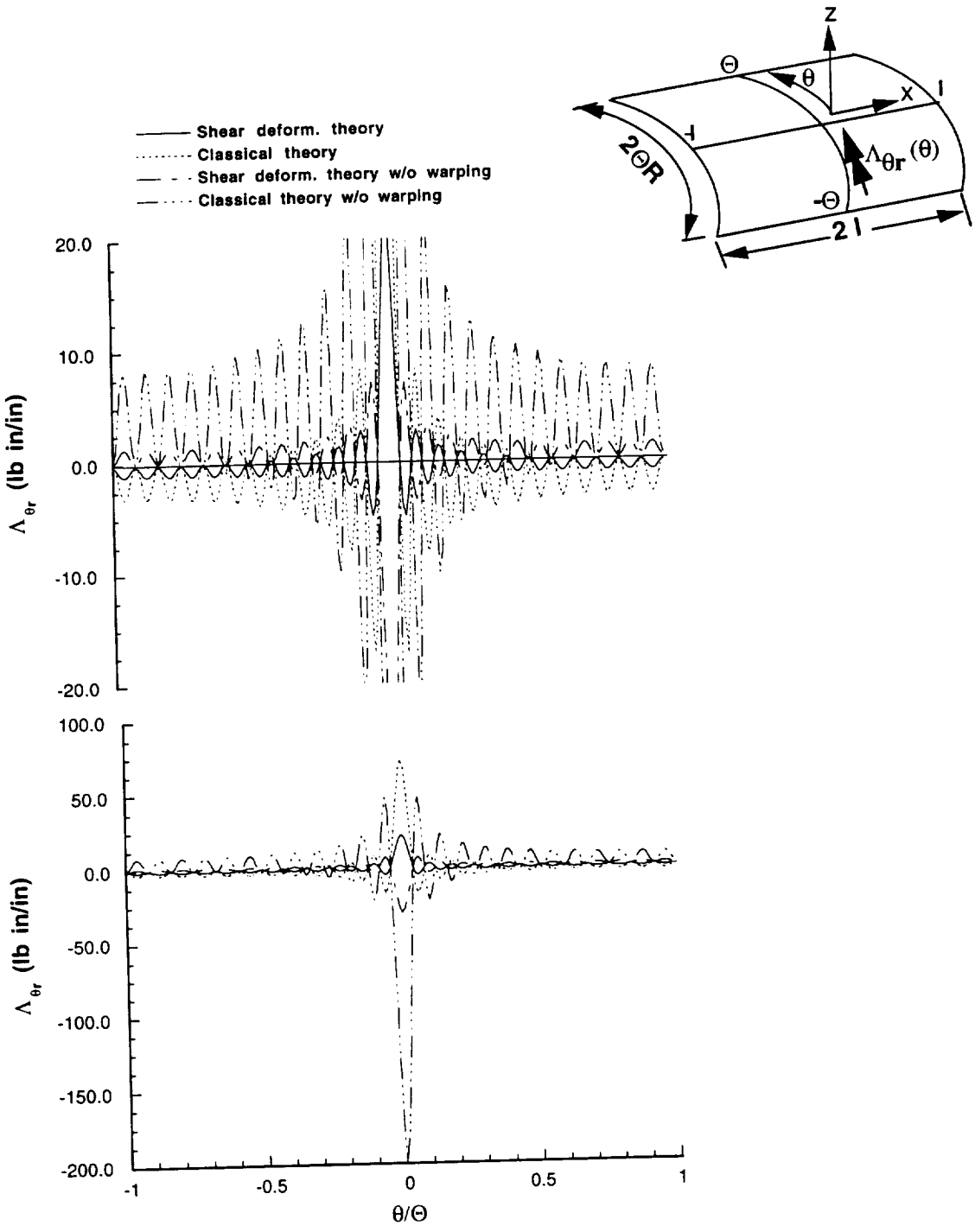

Fig. 6.7 Ring-shell tangential moment intensity in circumferential direction at 10 psi.

deformation models (Fig. 6.5). However, the magnitude of Λ_{zr} is substantially *increased* in the transverse shear deformation model with respect to the classical model with warping excluded, and is substantially *decreased* in the transverse shear deformation model with respect to the classical model with warping included (Fig. 6.8). Thus, the asymmetry of the circumferential traction across the flange width of the ring is *increased* in the transverse shear deformation model with respect to the classical model without warping, and is *decreased* in the transverse shear deformation model with respect to the classical model with warping.

The inclusion of transverse shear deformation and warping of ring's cross section into the analyses influences the distributions and magnitudes of interacting line load components λ_{zs}, λ_{xr}, $\lambda_{\theta r}$, $\Lambda_{\theta r}$, and Λ_{zr}. The distributions of interacting line load components λ_{xs} and λ_{zr} remain essentially the same. The cause of sensitivity to transverse shear deformations is two-fold: First, the tangential displacements of the shell along the contact lines are *de-coupled* from the out-of-plane rotations of the reference surface of the shell, and for the stiffeners the longitudinal displacements along the contact lines are *de-coupled* from the rotations of the longitudinal reference axes. Second, in the transverse shear deformation model, the torsional rotation of the ring at the shell-stringer-ring joint is *de-coupled* from the in-plane bending rotation of the stringer at the joint, thereby allowing for increased joint flexibility. In the classical model, the torsional rotation of the ring at the joint is constrained to be the same as the bending rotation of the stringer (see Fig. 6.9). The values of these joint rotations for the four structural models are given in Table 6.2. Notice from Table 6.2 that the sense of the rotation changes if warping is included, and that the transverse shear deformation results in a torsional rotation of the ring that is about twice as much as the bending rotation of the stringer.

deformation models (Fig. 6.5). However, the magnitude of Λ_{zr} is substantially *increased* in the transverse shear deformation model with respect to the classical model with warping excluded, and is substantially *decreased* in the transverse shear deformation model with respect to the classical model with warping included (Fig. 6.8). Thus, the asymmetry of the circumferential traction across the flange width of the ring is *increased* in the transverse shear deformation model with respect to the classical model without warping, and is *decreased* in the transverse shear deformation model with respect to the classical model with warping.

The inclusion of transverse shear deformation and warping of ring's cross section into the analyses influences the distributions and magnitudes of interacting line load components λ_{zs}, λ_{xr}, $\lambda_{\theta r}$, $\Lambda_{\theta r}$, and Λ_{zr}. The distributions of interacting line load components λ_{xs} and λ_{zr} remain essentially the same. The cause of sensitivity to transverse shear deformations is two-fold: First, the tangential displacements of the shell along the contact lines are *de-coupled* from the out-of-plane rotations of the reference surface of the shell, and for the stiffeners the longitudinal displacements along the contact lines are *de-coupled* from the rotations of the longitudinal reference axes. Second, in the transverse shear deformation model, the torsional rotation of the ring at the shell-stringer-ring joint is *de-coupled* from the in-plane bending rotation of the stringer at the joint, thereby allowing for increased joint flexibility. In the classical model, the torsional rotation of the ring at the joint is constrained to be the same as the bending rotation of the stringer (see Fig. 6.9). The values of these joint rotations for the four structural models are given in Table 6.2. Notice from Table 6.2 that the sense of the rotation changes if warping is included, and that the transverse shear deformation results in a torsional rotation of the ring that is about twice as much as the bending rotation of the stringer.

Table 6.2 Rotations About The Circumferential Axis At The Stiffener Intersection.

Description of the Rotation of the Structural Component	Rotations in 10^{-5} radians			
	Classical Theory		Transverse Shear Theory	
	No Warping	Warping	No Warping	Warping
Shell normal $\phi_x(0, 0)$	- 2.56	2.58	-1.06	2.65
Ring twist $\phi_{\theta r}(0)$	- 2.56	2.58	-2.67	3.64
Stringer normal $\phi_{\theta s}(0)$	- 2.56	2.58	-0.29	1.85

Table 6.2 Rotations About The Circumferential Axis At The Stiffener Intersection.

Description of the Rotation of the Structural Component	Rotations in 10^{-5} radians			
	Classical Theory		Transverse Shear Theory	
	No Warping	Warping	No Warping	Warping
Shell normal $\phi_x(0, 0)$	- 2.56	2.58	-1.06	2.65
Ring twist $\phi_{\theta r}(0)$	- 2.56	2.58	-2.67	3.64
Stringer normal $\phi_{\theta s}(0)$	- 2.56	2.58	-0.29	1.85

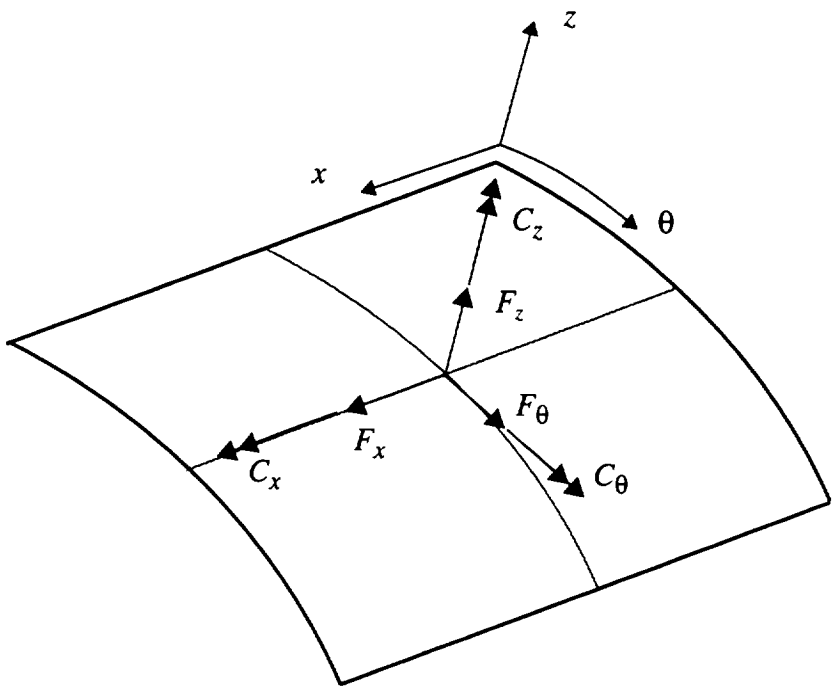

Fig. 6.10.Components of the resultant of the interacting line load intensities acting on the inside wall of the shell at the origin.

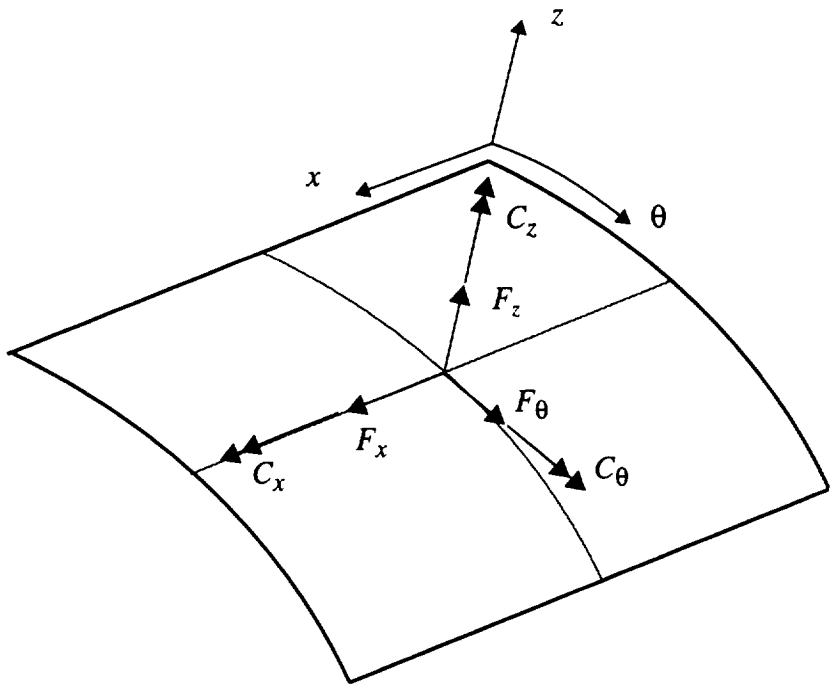

Fig. 6.10.Components of the resultant of the interacting line load intensities acting on the inside wall of the shell at the origin.

Table 6.3 Resultants At Stiffener Intersection.

Components of the Resultant	Classical Theory		Transverse Shear Theory	
	No Warping	Warping	No Warping	Warping
C_θ from stringer, lb-in.	- 1.1696	- 0.0921	- 0.2953	- 0.7797
C_θ from ring, lb-in.	1.627	5.645	1.363	6.0192
C_θ total, lb-in.	0.457	5.5526	1.0676	5.2396
F_z, lb.	- 564.06	- 564.56	- 562.27	- 563.15

Table 6.3 Resultants At Stiffener Intersection.

Components of the Resultant	Classical Theory		Transverse Shear Theory	
	No Warping	Warping	No Warping	Warping
C_θ from stringer, lb-in.	- 1.1696	- 0.0921	- 0.2953	- 0.7797
C_θ from ring, lb-in.	1.627	5.645	1.363	6.0192
C_θ total, lb-in.	0.457	5.5526	1.0676	5.2396
F_z, lb.	- 564.06	- 564.56	- 562.27	- 563.15

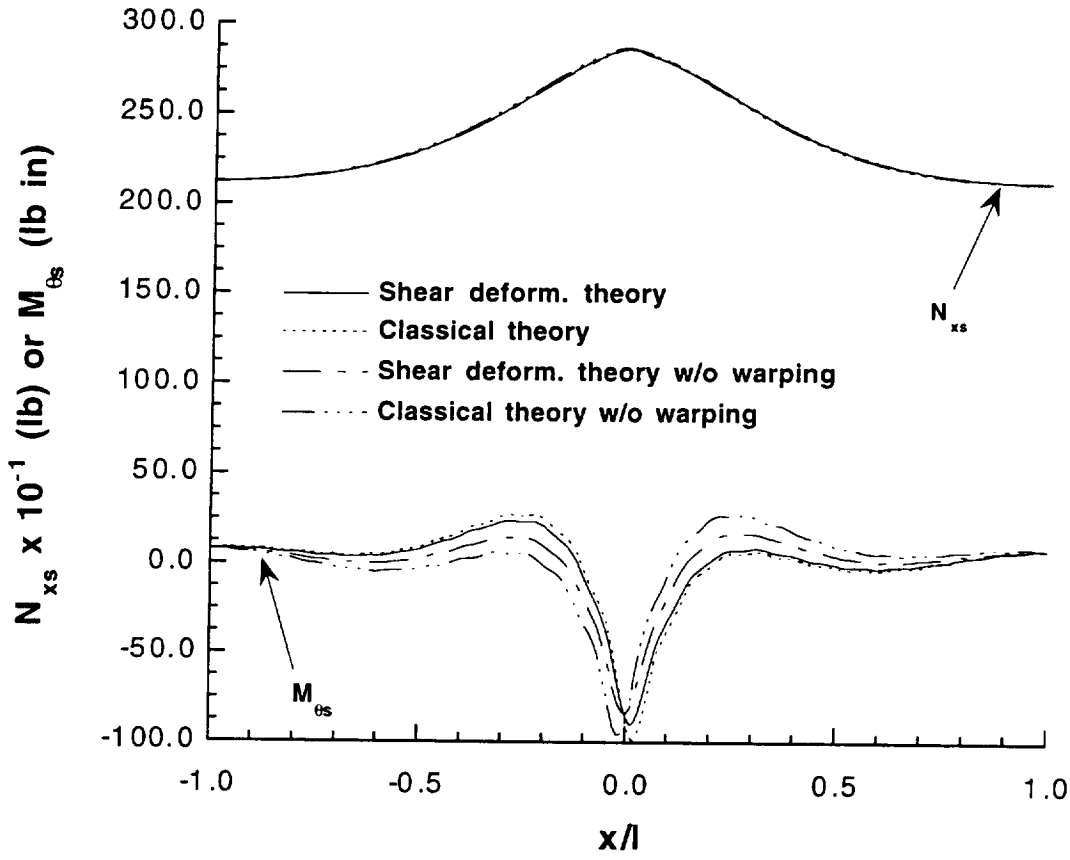

Fig. 6.11 Stringer axial force and bending moment distribution at 10 psi.

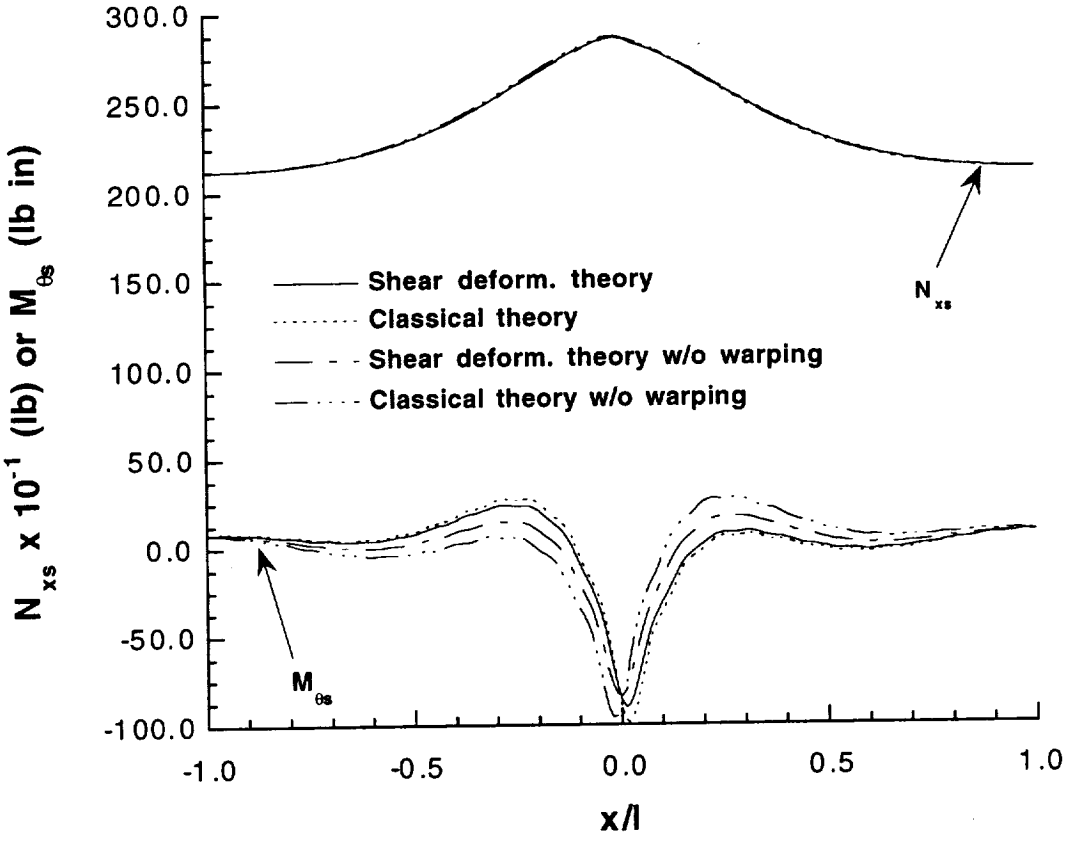

Fig. 6.11 Stringer axial force and bending moment distribution at 10 psi.

asymmetric about the origin. Only small differences are predicted by the four structural models in the distribution of V_{zs}.

The distributions of the circumferential force and in-plane bending moment in the ring are shown in Fig. 6.13. The differences in these distributions predicted by the four models are very small. The distributions of the in-plane shear force, V_{zr}, in the ring predicted by the four structural models have negligible differences, as shown in Fig. 6.14. The out-of-plane bending moment M_{zr} and torque T_r in the ring are more sensitive to the change in models as shown Fig. 6.15. The distributions of the out-of-plane bending moment are symmetric about the origin, and their magnitudes predicted by the models with warping included are substantially larger as compared to their magnitudes predicted by the models without warping. The distributions of total torque, T_r $(= T_{sr} - \dot{M}_{\omega r}/R_0)$, are antisymmetric about the origin. As shown in Fig. 6.15, the torque has reduced magnitudes in the transverse shear deformation model compared to the classical model when warping is included. The torque predicted by the models without warping is St. Venant's torque T_{sr}, and this is negligible as shown in Fig. 6.15. The distributions of out-of-plane shear force, V_{xr}, in the ring are shown in Fig. 6.16, and these distributions are antisymmetric about the origin. The magnitudes of V_{xr} predicted by the transverse shear deformation model are larger compared to the classical model when warping is included. However the reverse is true for the V_{xr} distributions without warping. The distributions for $M_{\theta s}$, M_{zr}, T_r and V_{xr} shown in Figs. 6.11, 6.15 and 6.16, respectively, indicate that these stiffener actions are sensitive to both transverse shear deformations and warping deformations.

6.3.5 SHELL RESPONSE

The distribution of the normal displacement along x-curve midway between the stringers ($\theta = -\Theta$), and along the θ-curve midway between the rings ($x = -l$), are

asymmetric about the origin. Only small differences are predicted by the four structural models in the distribution of V_{zs}.

The distributions of the circumferential force and in-plane bending moment in the ring are shown in Fig. 6.13. The differences in these distributions predicted by the four models are very small. The distributions of the in-plane shear force, V_{zr}, in the ring predicted by the four structural models have negligible differences, as shown in Fig. 6.14. The out-of-plane bending moment M_{zr} and torque T_r in the ring are more sensitive to the change in models as shown Fig. 6.15. The distributions of the out-of-plane bending moment are symmetric about the origin, and their magnitudes predicted by the models with warping included are substantially larger as compared to their magnitudes predicted by the models without warping. The distributions of total torque, T_r $(= T_{sr} - \dot{M}_{\omega r}/R_0)$, are antisymmetric about the origin. As shown in Fig. 6.15, the torque has reduced magnitudes in the transverse shear deformation model compared to the classical model when warping is included. The torque predicted by the models without warping is St. Venant's torque T_{sr}, and this is negligible as shown in Fig. 6.15. The distributions of out-of-plane shear force, V_{xr}, in the ring are shown in Fig. 6.16, and these distributions are antisymmetric about the origin. The magnitudes of V_{xr} predicted by the transverse shear deformation model are larger compared to the classical model when warping is included. However the reverse is true for the V_{xr} distributions without warping. The distributions for $M_{\theta s}$, M_{zr}, T_r and V_{xr} shown in Figs. 6.11, 6.15 and 6.16, respectively, indicate that these stiffener actions are sensitive to both transverse shear deformations and warping deformations.

6.3.5 SHELL RESPONSE

The distribution of the normal displacement along x-curve midway between the stringers ($\theta = -\Theta$), and along the θ-curve midway between the rings ($x = -l$), are

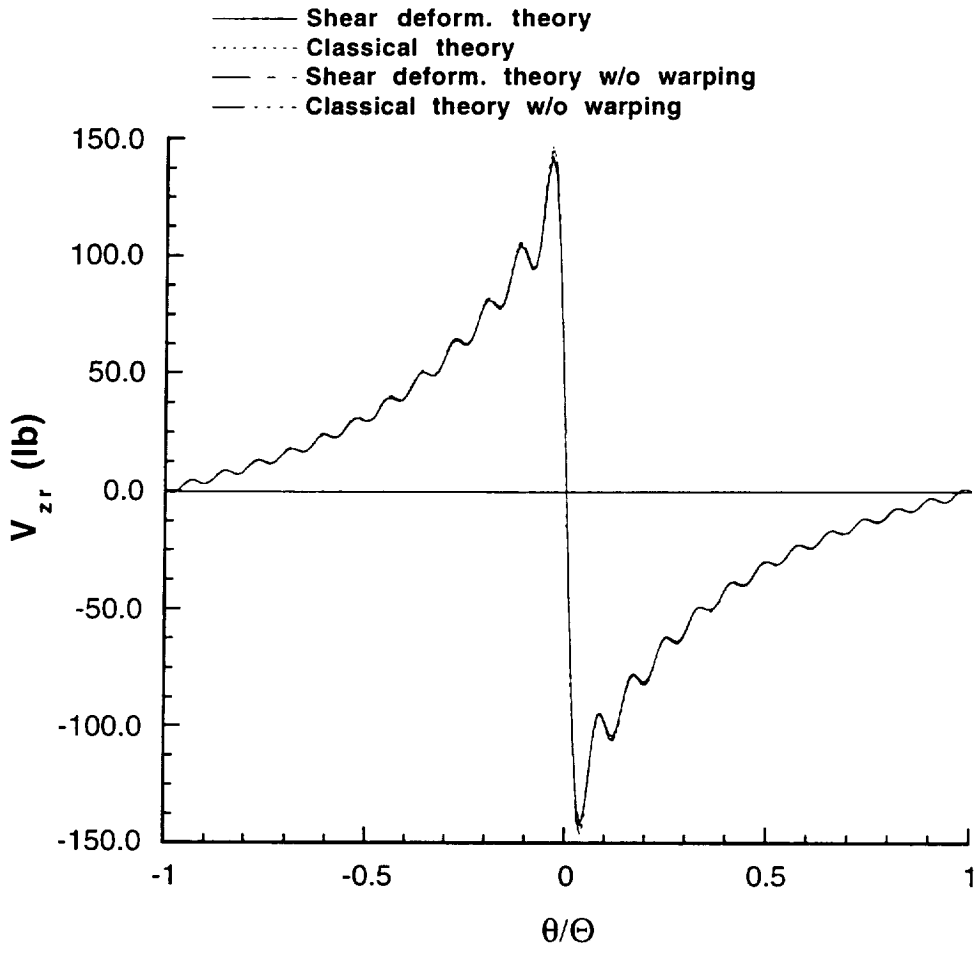

Fig. 6.14 Ring in-plane shear force distribution at 10 psi.

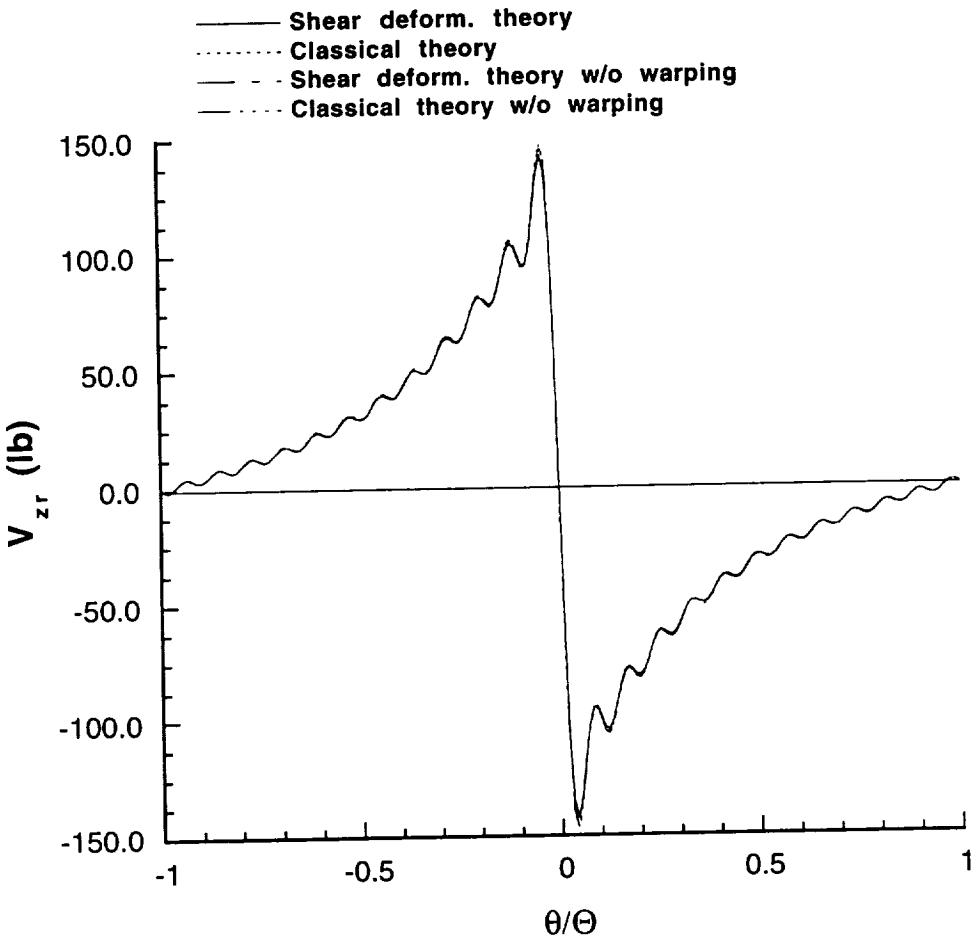

Fig. 6.14 Ring in-plane shear force distribution at 10 psi.

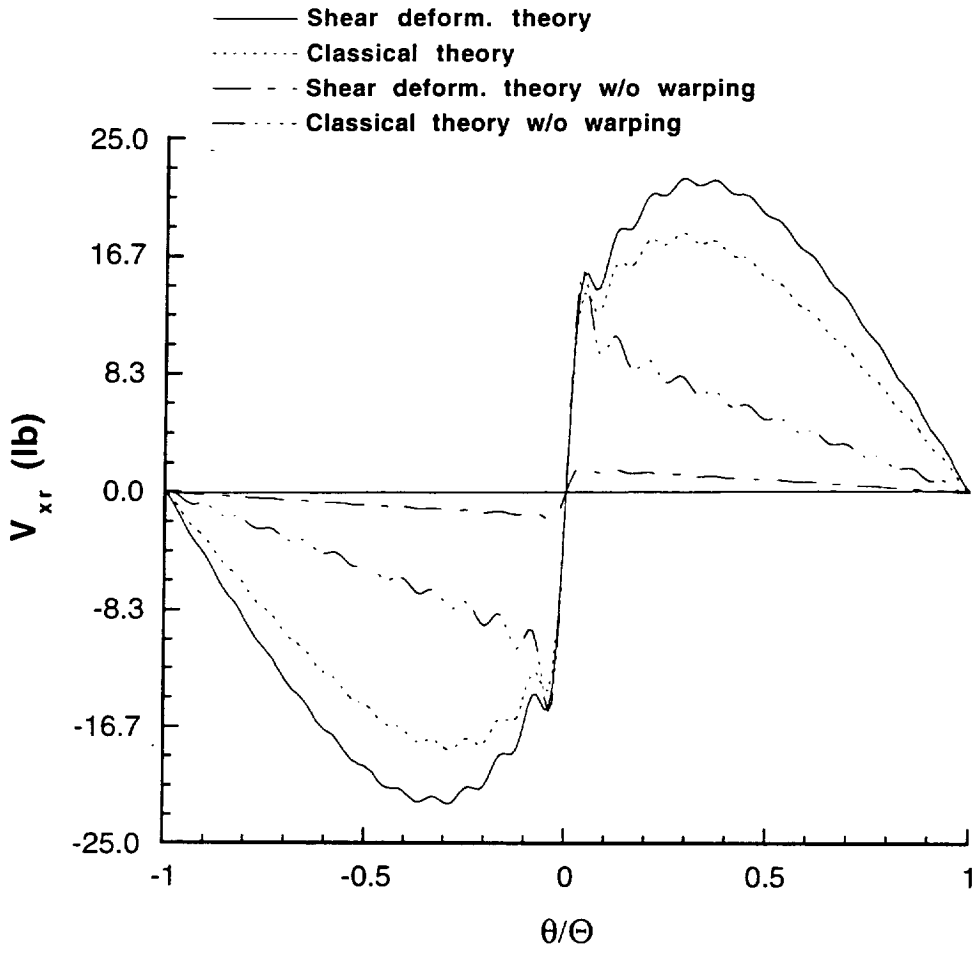

Fig. 6.16 Ring out-of-plane shear force distribution at 10 psi.

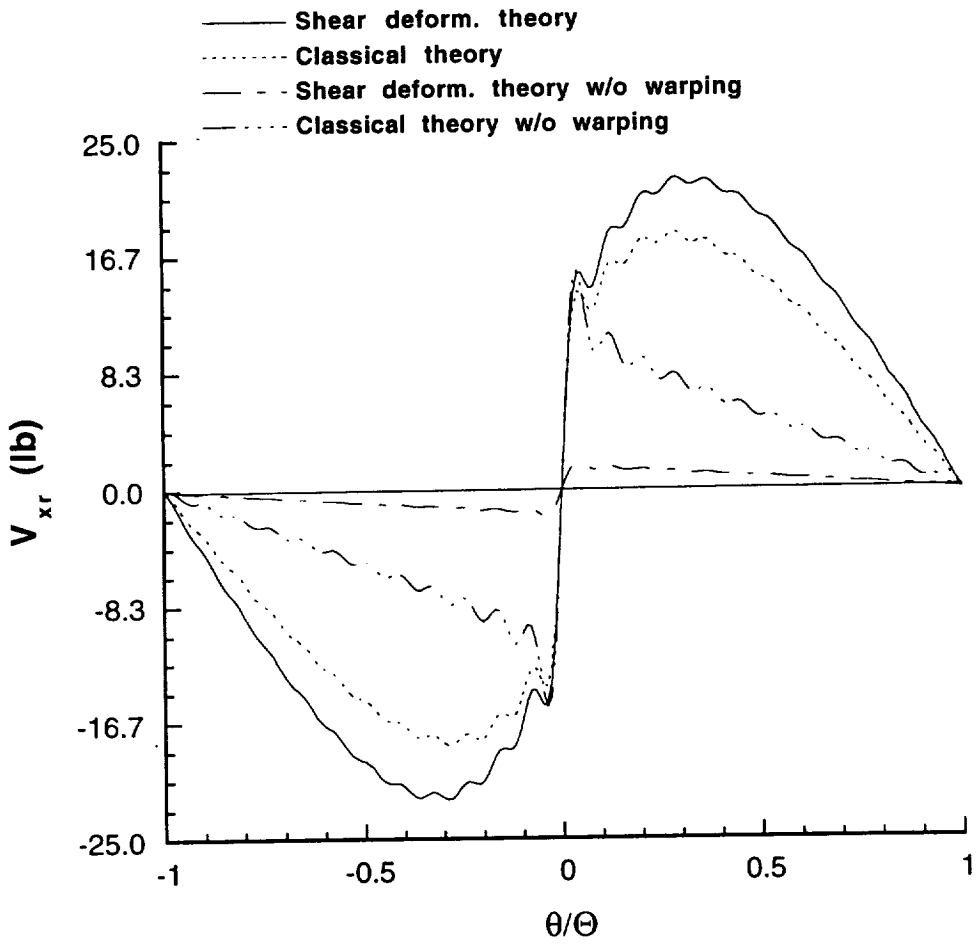

Fig. 6.16 Ring out-of-plane shear force distribution at 10 psi.

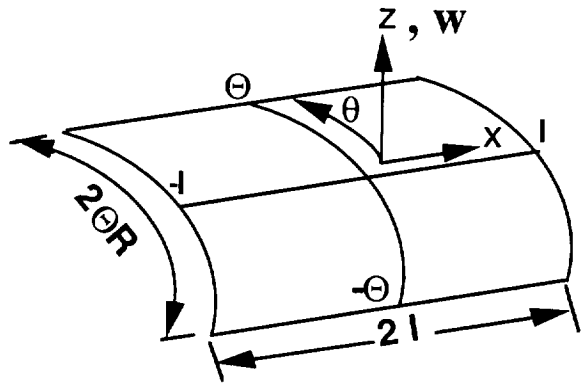

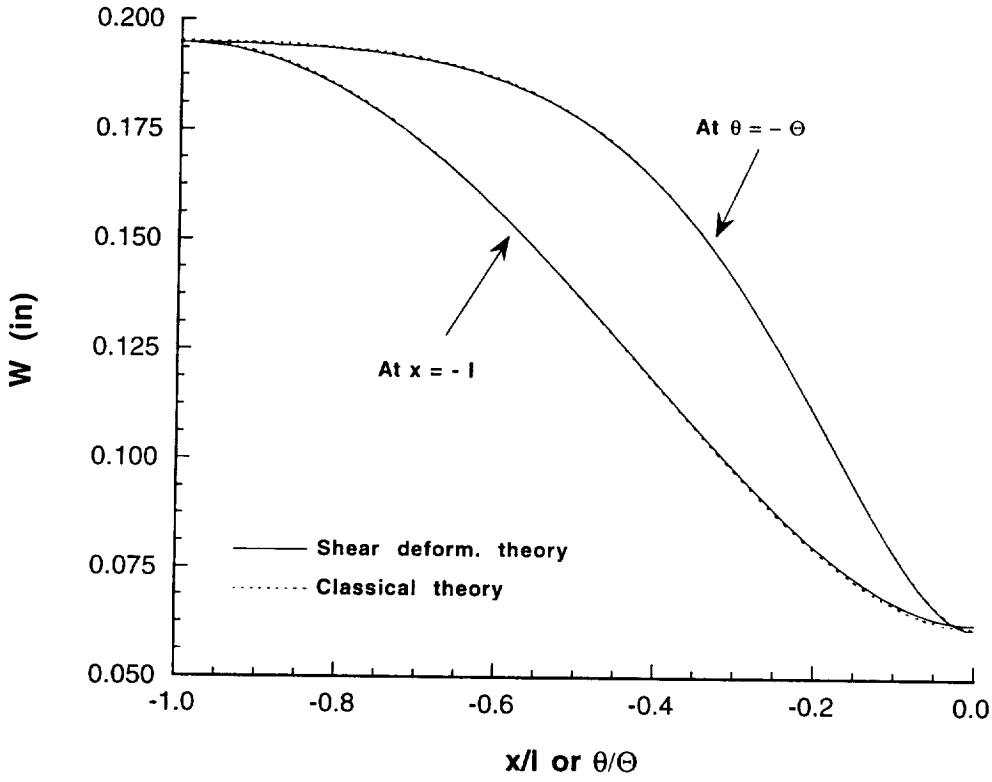

Fig. 6.17 Distributions of shell's normal displacement at 10 psi.

shown in Fig. 6.17. As depicted in this figure, there is a negligible difference between the results from the transverse shear deformation model and classical model (warping of the ring is included in both models). Also, there is negligible difference in the axial and circumferential normal strain distributions between the two models as shown in Figs. 6.18 and 6.19. Thus, the normal displacement and in-plane normal strains for the shell are not significantly influenced by the inclusion of either transverse shear deformations or warping deformation of the ring into the structural models, in part because the shell is very thin for the example studied ($R/t = 1268$).

6.4 A RING WITH SYMMETRICAL CROSS SECTION

As a benchmark for comparing the transverse shear deformation model with the classical model, analyses were performed for a ring with symmetric cross section. In this case the changes made to the numerical example under discussion are to set the bending-coupling stiffeness EI_{zx}, the out-of-plane bending-to-warping coupling stiffness $EI_{\omega x}$, and the contour warping function parameter ω_0 of the ring, all to zero. Consequently, the θ-axis, as well as the x-axis, are axes of symmetry for the repeating unit in terms of geometry, load, and material properties. Symmetry about the θ-axis implies there is no out-of-plane bending and torsion of the ring; i.e., $u_r(\theta) = \phi_{\theta r}(\theta) = \phi_{zr}(\theta) = \lambda_{xr}(\theta) = \Lambda_{\theta r}(\theta) = \Lambda_{zr}(\theta) = 0$ for $-\Theta \leq \theta \leq \Theta$. Thus, for the symmetrical section stiffeners only the interacting line load components tangent and normal to the stiffeners are non-zero. Since there is no torsion, warping of the ring cross section does not play any role in the analyses.

The distributions of the tangential interacting load intensity between the shell and ring are shown in Fig. 6.20. The differences in the results from the two models are small except in the vicinity of the stiffener intersection. The peak magnitude of $\lambda_{\theta r}$ in the transverse shear deformation model is smaller than the peak value for $\lambda_{\theta r}$ in the classical

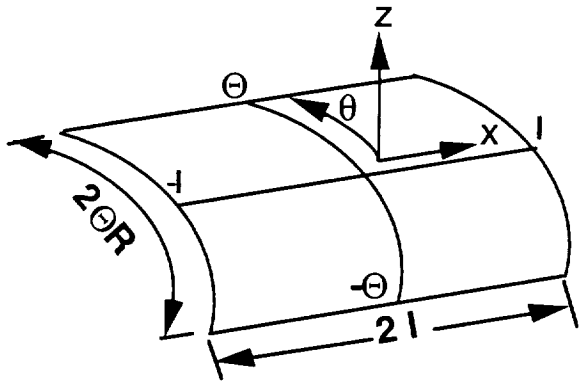

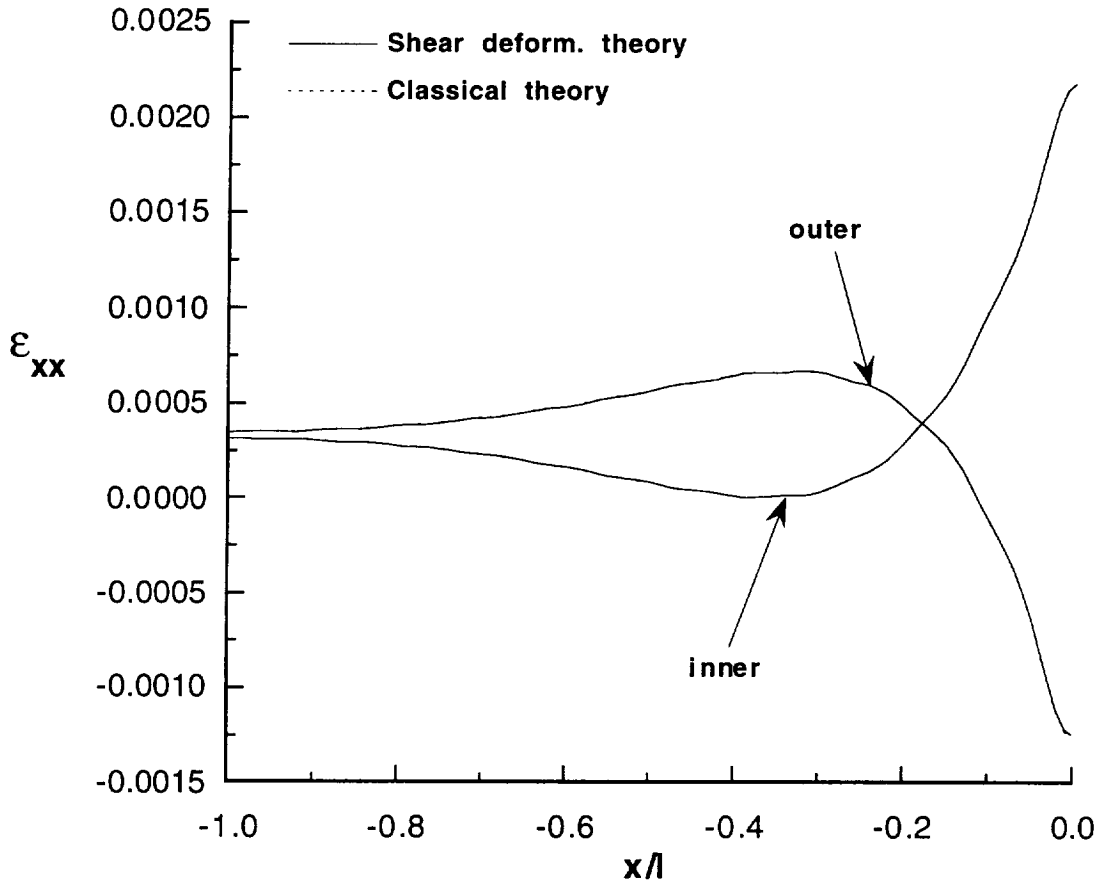

Fig. 6.18 Distributions of the axial normal strain on the inner and outer shell surfaces midway between the stringers (θ=-Θ) at 10 psi.

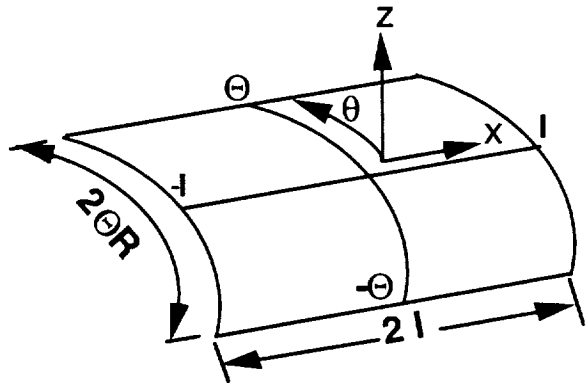

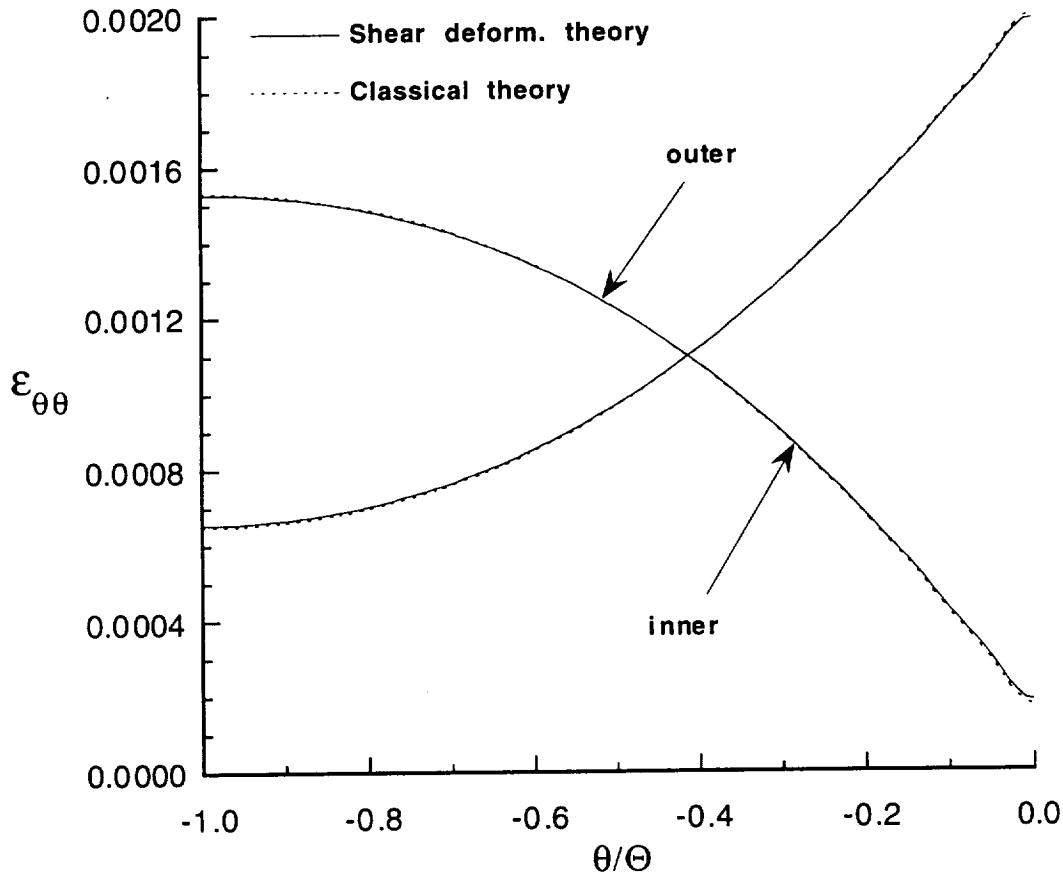

Fig. 6.19 Distributions of the circumferential normal strain on the inner and outer shell surfaces midway between the rings (x=-l) at 10 psi.

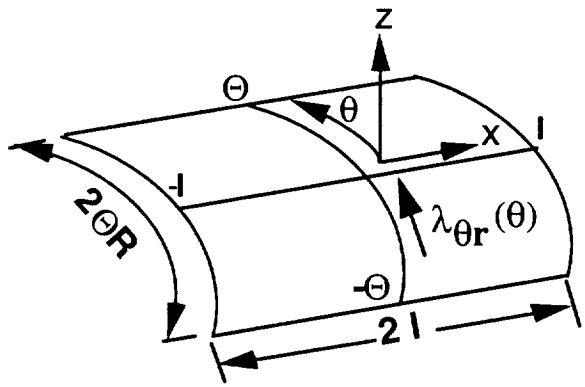

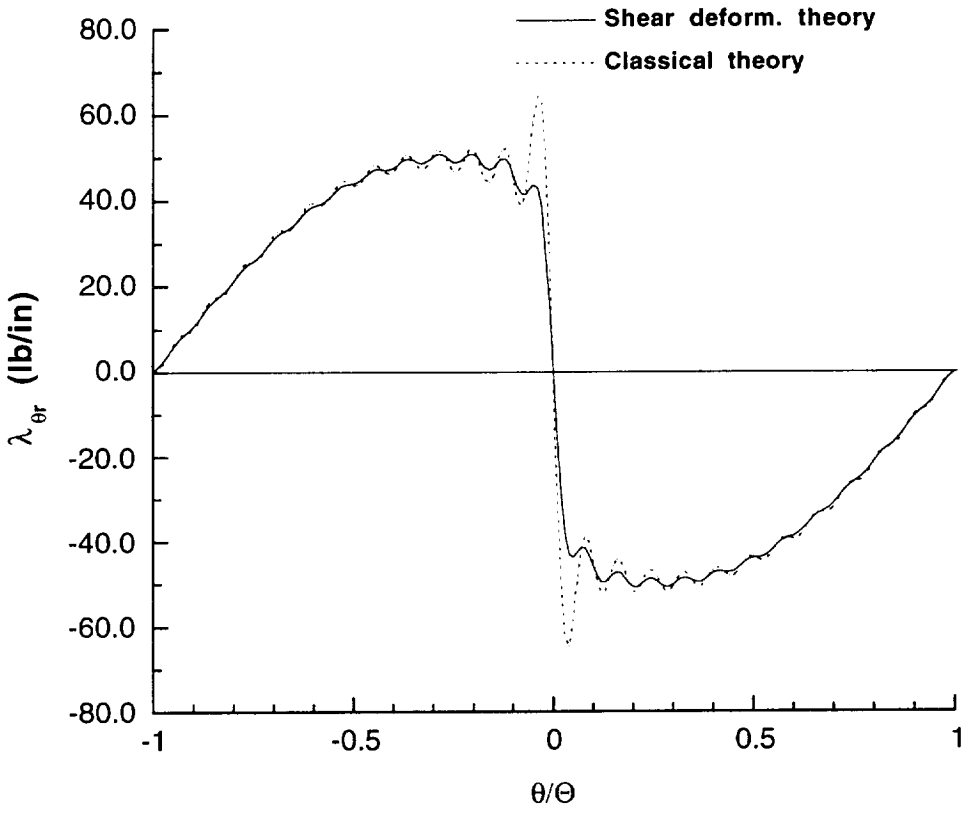

Fig. 6.20 Ring-shell tangential force intensity in circumferential direction for a ring with symmetrical cross section at 10 psi.

model (50.8 lb/in versus 64.5 lb/in.). However, this difference occurs over one wave length of the highest harmonic retained in the analysis, and may not be significant. The distributions of the tangential and normal interacting load intensities between the shell and stringer, and the normal load intensity between the shell and ring are not significantly different in the two models.

For a symmetrical cross section ring, in Eqs. (6.1) through (6.6) $F_x = F_\theta = C_x = C_\theta = C_z = 0$. The only non-zero component of the force resultant is the radial force F_z. The values of F_z computed from the classical and transverse shear deformation models are -563.72 lb. and -561.89 lb., respectively.

6.5 SUMMARY OF RESULTS

The asymmetrical section ring complicated the analysis of the unit cell, since symmetry about the plane of the ring is lost. Out-of-plane bending and torsion of the ring occur as well as a rotation of the shell-stringer-ring joint about the circumferential axis. Inclusion of transverse shear deformations, and warping deformation of the ring's cross section due to torsion, into the mathematical model significantly influenced several aspects of the response.

The sense of the rotations of the structural elements at the joint is changed with the inclusion of warping deformation in the ring, and the twist rotation of the ring at the joint increases by 40% with the inclusion of transverse shear deformation, as is shown in Table 6.2. That is, joint flexibility increases since element rotations at the joint are de-coupled by using transverse shear deformation models.

The interacting loads that are strongly affected by the structural modeling are those components associated with the asymmetric response. These are the axial force intensity λ_{xr}, the normal moment intensity Λ_{zr}, and the tangential moment intensity $\Lambda_{\theta r}$, between

the ring and shell. At the joint the magnitude of λ_{xr} is increased by the inclusion of warping and reduced by the inclusion of transverse shear (Fig. 6.4). The normal moment intensity Λ_{zr} is a measure of the asymmetry in the distribution of the circumferential traction across the width of the ring's attachment flange. The sense of Λ_{zr} is changed when both transverse shear and warping are included, and its magnitudes are reduced by the transverse shear effect (Fig. 6.8). However, the magnitude of the resultant of the circumferential traction across the flange width of the ring, as measured by the line load intensity $\lambda_{\theta r}$, is only moderately affected by the changes in the structural models (Fig. 6.5). The tangential moment intensity $\Lambda_{\theta r}$ is a measure of the asymmetry in the distribution of the normal traction across the width of the ring's attachment flange. At the joint, the sense of $\Lambda_{\theta r}$ is changed by the inclusion of warping deformation and additionally its magnitude is reduced by the inclusion of transverse shear deformation (Fig. 6.7). However, the magnitude of the resultant of the normal traction across the flange width, as measured by the line load intensity λ_{zr}, is essentially unaffected by changes in the structural models (Fig. 6.6).

The distributions of the normal actions between the shell and stiffeners (λ_{zs}, λ_{zr}, and $\Lambda_{\theta r}$) all show significant magnitudes only in the vicinity of the joint, with much smaller magnitudes away from the joint. In fact, they all appear to exhibit singular behavior at the joint, but only finite magnitudes are represented by the truncated series approximations. The distributions of the actions tangent to the stiffeners (λ_{xs}, $\lambda_{\theta r}$, and Λ_{zr}), on the other hand, have small magnitudes in the vicinity of the joint and larger magnitudes away from the joint. These tangential actions do not exhibit singular behavior. (These results are similar to those found for the symmetric stiffeners problem discussed in Chapter 5.)

In spite of the singular behavior of the line load intensities associated with the normal actions, the resultant of these distributions resolved at the joint converge relatively quickly

with the number of terms retained in the series approximations. The resultant consists of a radial force F_z and a moment C_θ about the circumeferential axis. F_z represents the action of the stiffeners to pull the shell radially inward against the pressure load, and C_θ is primarily due to asymmetry in the actions between the ring and shell. Force F_z is essentially unaffected by the structural modeling (Table 6.3), and its magnitude for the example studied is about 17% of the total pressure load carried by the unit cell. The remaining pressure load is carried by the shell itself. The moment C_θ is very sensitive to the structural modeling, in particular to the effect of warping as shown in Table 6.3. This moment C_θ vanishes for a completely symmetric problem.

The out-of-plane bending moment and torque in the ring are very sensitive to the structural modeling, as might be expected. The magnitudes of the both the out-of-plane bending moment and torque increase with the inclusion of warping and transverse shear into the mathematical model (Fig. 6.15). However, the shell's normal displacement and strains are insensitive to the changes in the structural models for the very thin shell ($R/t = 1268$) used in the numerical example.

CHAPTER 7
CONCLUDING REMARKS

7.1 SUMMARY

Structural analyses are developed to determine the linear elastic and geometrically nonlinear elastic response of an internally pressurized, orthogonally stiffened cylindrical shell. The structural configuration is of a long circular cylindrical shell stiffened on the inside by a regular arrangement of identical stringers and identical rings. Periodicity of this configuration permits the analysis of a unit cell model consisting of a portion of the shell wall centered over one stringer-ring joint; i.e., deformation of a structural unit cell determines the deformation of the entire stiffened shell. See Fig. 1.1. The stringer-ring-shell joint is modeled in an idealized manner; the stiffeners are mathematically permitted to pass through one another without contact, but do interact indirectly through their mutual contact with the shell at the joint. The stiffeners are modeled as discrete beams. The stringer is assumed to have a symmetrical cross section and the ring either a symmetric or an asymmetric open section.

The formulations presented for the linear elastic response include the effect of transverse shear deformations and the effect of warping of the ring's cross section due to torsion. These effects are important when the ring has an asymmetrical cross section, because the loss of symmetry in the problem results in torsion of the ring, as well as out-of-plane bending, and a concomitant rotation of the joint at the stiffener intersection about the circumferential axis. Restraint of cross-sectional warping, as occurs here in the ring due to contact with the shell, is an important contributor to the normal stresses in thin-walled open section bars. Based on transverse shear deformations and cross-sectional warping

of the ring, four structural models are defined. The simplest model uses non-transverse-shear-deformable theory, or classical theory, and neglects warping due to torsion. The most complex model includes both effects. Models of intermediate complexity occur for inclusion of one effect without the other. The formulations presented for the geometrically nonlinear response take into consideration only the symmetrical cross section of stiffeners, and are based on classical structural theories.

For all the structural models, the response of the unit cell under internal pressure is obtained by utilizing the Ritz method. Displacements are assumed as truncated Fourier Series plus simple terms in the axial coordinate to account for the closed-end pressure vessel effect. Equilibrium is imposed by virtual work. Pointwise displacement continuity between the shell and stiffeners is achieved by Lagrange multipliers which represent the interacting line load distributions between the stiffeners and the inside shell wall (see Fig. 1.2). Data from a composite material crown panel typical of a large transport fuselage are used for two numerical examples. The first numerical example is used to validate the structural model, and also to compare the linear response and geometrically nonlinear response of the unit cell model with symmetrical section stiffeners. In the second numerical example the linear elastic response of the unit cell model with an asymmetrical cross section ring is analyzed.

7.2 CONCLUDING REMARKS

7.2.1 EFFECT OF GEOMETRIC NONLINEARITY

It is found that the spatial distribution of the normal displacements of the cylindrical shell are more uniform, and the bending strains are reduced, in the geometrically nonlinear elastic analysis with respect to what is predicted by the linear elastic analysis. That is, pillowing of the skin is reduced by the inclusion of geometric nonlinearity into the analysis.

However, in the nonlinear analysis the most severe circumferential bending is confined to a narrow boundary layer adjacent to the stringer midway between the rings, and the interior portion of the shell behaves as a membrane. In the linear analysis the bending occurs over the entire circumference of the shell. The development of the bending boundary layer due to the inclusion of geometric nonlinearity into the analysis causes an increase in the circumferential transverse shear resultant in the shell adjacent to the stringer compared to the linear analysis. Increased interlaminar shear stresses can be expected as a result of the increased transverse shear resultant.

The axial force carried by the stringer due to the closed-end pressure vessel effect is increased in the nonlinear analysis with respect to its value in the linear analysis. Also, the circumferential force carried by the ring is increased in the nonlinear analysis with respect to its value in the linear analysis. Thus, the stiffeners resist an increased portion of the internal pressure load, accompanied by a commensurate decrease in the load carried by the shell, when geometric nonlinearity is included into the analysis.

7.2.2 INFLUENCE OF AN ASYMMETRICAL SECTION RING

The asymmetrical section ring complicated the analysis of the unit cell, since symmetry about the plane of the ring is lost. Inclusion of transverse shear deformations, and warping deformation of the ring's cross section due to torsion, into the mathematical model significantly influenced several aspects of the response. The interacting loads that are strongly affected by the structural modeling are those components associated with the asymmetric response. These are the axial force intensity λ_{xr}, the normal moment intensity Λ_{zr}, and the tangential moment intensity $\Lambda_{\theta r}$ between the ring and shell. At the joint the magnitude of λ_{xr} is increased by the inclusion of warping and reduced by the inclusion of transverse shear (Fig. 6.4). The normal moment intensity Λ_{zr} is a measure of the asymmetry in the distribution of the circumferential traction across the width of

the ring's attachment flange. The sense of Λ_{zr} is changed when both transverse shear and warping are included, and its magnitudes are reduced by the transverse shear effect (Fig. 6.8). However, the magnitude of the resultant of the circumferential traction across the flange width of the ring, as measured by the line load intensity $\lambda_{\theta r}$, is only moderately affected by the changes in the structural models (Fig. 6.5). The tangential moment intensity $\Lambda_{\theta r}$ is a measure of the asymmetry in the distribution of the normal traction across the width of the ring's attachment flange. At the joint, the sense of $\Lambda_{\theta r}$ is changed by the inclusion of warping deformation and additionally its magnitude is reduced by the inclusion of transverse shear deformation (Fig. 6.7). However, the magnitude of the resultant of the normal traction across the flange width, as measured by the line load intensity λ_{zr}, is essentially unaffected by changes in the structural models (Fig. 6.6).

The sense of the rotations of the structural elements at the joint is changed with the inclusion of warping deformation in the ring, and the twist rotation of the ring at the joint increases by 40% with the inclusion of transverse shear deformation, as is shown in Table 6.2. That is, joint flexibility increases since element rotations at the joint are de-coupled by using transverse shear deformation models.

The out-of-plane bending moment and torque in the ring are very sensitive to the structural modeling, as might be expected. The magnitudes of the both the out-of-plane bending moment and torque increase with the inclusion of warping and transverse shear into the mathematical model (Fig. 6.15). However, the distributions and magnitudes of the normal displacement and strains of the shell midway between the stiffeners are unaffected by the change in the structural models.

7.2.3 SINGULARITY AT THE SHELL-STRINGER-RING JOINT

The distributions of the normal actions between the shell and stiffeners (λ_{zs}, λ_{zr}, and $\Lambda_{\theta r}$) all show significant magnitudes only in the vicinity of the joint, with much smaller magnitudes away from the joint. In fact, they all appear to exhibit singular behavior at the joint, but only finite magnitudes are represented by the truncated series approximations. The distributions of the actions tangent to the stiffeners (λ_{xs}, $\lambda_{\theta r}$, and Λ_{zr}), on the other hand, have small magnitudes in the vicinity of the joint and larger magnitudes away from the joint. These tangential actions do not exhibit singular behavior. In spite of the singular behavior of the line load intensities associated with the normal actions, the resultant of these distributions resolved at the joint converge relatively quickly with the number of terms retained in the series approximations (e.g., see Fig. 5.17). The resultant consists of a radial force F_z and a moment C_θ about the circumferential axis (see Fig. 6.10). F_z represents the action of the stiffeners to pull the shell radially inward against the pressure load, and C_θ is primarily due to asymmetry in the actions between the ring and shell. The magnitude of force F_z represents the portion of the total pressure load carried by the stiffeners. The remaining pressure load is carried by the shell itself. Force F_z is essentially unaffected by the structural modeling (Table 6.3). The moment C_θ is very sensitive to the structural modeling, in particular to the effect of warping as shown in Table 6.3. This moment C_θ vanishes for a completely symmetric problem.

The series for the interacting normal load intensity λ_{zr} at the stiffener intersection does not appear to converge even in the geometrically nonlinear analysis. However, the Fourier Series for the total radial resultant load carried by the stiffeners, which is resolved at the intersection, exhibits rapid convergence in the geometrically nonlinear analysis (see Fig. 5.18). The total radial resultant load carried by the stiffeners is slightly increased in the geometrically nonlinear analysis with respect to its value in the linear analysis.

7.3 RECOMMENDATIONS FOR FUTURE WORK

The analysis could be extended to include the important load cases of torsion and bending in addition to internal pressure. Torsion of the stiffened shell is equivalent to a shear load of the unit cell, and this loading case corresponds to an antisymmetric deformation pattern of the unit cell model. Bending is somewhat more complex since the displacement field has period of 2π rather than the periodicity of the stringer spacing.

Singular solutions can be investigated to improve the solution methodology. To begin with, the simplest configuration can be analyzed; i.e., consider the linear response of a classical structural model with symmetric section stiffeners. This problem can be reformulated in terms of four integral equations in which the unknowns are the magnitudes of the interacting load components $\lambda_{xs}(x)$, $\lambda_{zs}(x)$, $\lambda_{\theta r}(\theta)$, and $\lambda_{zr}(\theta)$. These integral equations are associated with either the tangential or normal displacement constraints between the shell and stiffeners. The kernels to these equations are Green's functions (or influence functions), which are displacement solutions to the shell, stringer, and ring problems under the actions of concentrated forces. This approach is appealing because the solution reduces to solving for the interacting load components in integral expressions along the contact lines rather than solving for the displacements and interacting loads over the entire solution domain. The difficulty with this approach is in obtaining the Green's functions, and solving singular integral equations that may result from the contact problems.

REFERENCES

[1]Niu, M. C-Y., *Airframe Structural Design*, Conmilit Press Ltd., Hong Kong, 1988, pp. 520-526.

[2]Jackson, A. C., Campion, M. C., and Pei, G., "Study of Utilization of Advanced Composites in Fuselage Structures of Large Transports," *NASA Contractor Report 172404*, Contract NAS1-17415, September, 1984.

[3]Rouse, N. E., "Making Reliable Joints in Composites," *Machine Design*, March, 1985, pp 79-82.

[4]Cole, R. T., Batch, E. J., and Potter, J., "Fasteners for Composite Structures," *Composites*, Vol. 13, 1982, pp. 233-240.

[5]Ilcewicz, L. B., Smith, P. J., and Horton, R. E., "Advanced Composites Fuselage Technology," *Proceedings of the Third NASA/DoD Advanced Composites Technology Conference*, NASA CP-3178, 1992, pp. 97-156.

[6]Swanson, G. D., Ilcewicz, L. B., Walker, T. H., Graesser, D., Tuttle, M., and Zabinsky, Z., "Local Design Optimization for Composite Transport Fuselage Crown Panels," *Proceedings of the Second NASA/DoD Advanced Composites Technology Conference*, NASA CP-3154, 1992, pp. 243-262.

[7]Jackson, A. C., "Development of Textile Composite Preforms for Aircraft Structures," *Proceedings of the AIAA/ASME/ASCE/AHS/ASC 35th Structures, Structural Dynamics and Materials Conference* (Hilton Head, SC), Part 2, AIAA, Washington, D.C., April 1994, pp. 1008-1012.

[8]Grigoluk, E., and Tolkachev, V., *Contact Problems in the Theory of Plates and shells*, Mir Publishers, Moscow, English Translation, 1987, pp. 5, 129-191, 328-395.

[9]Melan, E., "Ein Beitrag zur Theorie geschweisster Verbindungen," *Ing.-Arch.*, Vol. 3, No. 2, 1932, pp. 123-129.

[10]Buell, E. L., " On the Distribution of Plane Stress in a Semi-infinite Plate with Partially Stiffened Edge," *Journal of Math and Physics*, Vol. 26, No. 4, 1948, pp. 223-233.

[11]Koiter, W. T., "Diffusion of Load from a Stiffener into a Sheet," *Quarterly Journal of Mechanics and Applied Math.*, Vol. 8, No. 2, 1955, pp. 164-178.

[12]Benscoter, S. U., "Analysis of a Single Stiffener on an Infinite Sheet," *Journal of Applied Mechanics*, Vol. 16, No. 3, 1949, pp. 242-246.

[13]Budiansky, B., and Wu, Tai Te, "Transfer of Load to a Sheet from a Rivet-attached Stiffener," *Journal of Math and Physics*, Vol. 40, No. 2, 1961, pp. 142-162.

[14]Fischer, F. J., "Stress Diffusion from Axially Loaded Stiffeners into Cylindrical Shells," *International Journal of Solids & Structures*, Vol. 4, 1968, pp. 1181-1201.

[15]Flügge, W., "Stress Problems in Pressurized Cabins," *NACA Technical Note 2612*, 1952.

[16]Houghton, D. S., "The Influence of Frame Pitch and Stiffness on the Stress Distribution in Pressurized Cylinders," *CoA Note No. 79*, The College of Aeronautics, Cranfield, February, 1958.

[17]Williams, D., "Pressure-Cabin Problems," *An Introduction to the Theory of Aircraft Structures*, Edward Arnold Ltd., 1960, pp. 283-321.

[18]Wang, J. T-S., "Orthogonally Stiffened Cylindrical Shells Subjected to Internal Pressure," *AIAA Journal*, Vol. 8, March, 1970, pp. 455-461.

[19]Wang, J. T-S., and Hsu, T-H., "Discrete Analysis of Orthogonally Stiffened Composite Cylindrical Shell," *AIAA Journal*, Vol. 23, No. 11, 1985, pp. 1753-1761.

[20]Boitnott, R. L., "Nonlinear Response and Failure Characteristics of an Internally Pressurized Composite Cylindrical Panels," *Doctoral Dissertation*, Engineering Science and Mechanics Department, Virginia Polytechnic Institute and State University, Blacksburg, Virginia, March 1985, pp. 82-97, 104-117.

[21] *The ABAQUS Theory Manual*, Version 5.3, Hibbitt, Karlsson and Sorensen, Inc., Rhode Island, 1993.

[22] MacNeal, R. H., *The NASTRAN Theoretical Manual*, The MacNeal-Schwendler Corporation, California, 1972.

[23] Hoff, N. J., "The Applicablity of Saint-Venant's Principle to Airplane Structures," *Journal of Aeronautical Science*, Vol. 12, 1945, pp. 455-460.

[24] Novozhilov, V. V., *Thin Shell Theory*, Noordhoff Ltd., The Netherlands, 1964, pp. 23.

[25] Jones, R. M., *Mechanics of Composite Materials*, Scripta Book Co., Washington DC, 1975, pp. 51, 154, 155.

[26] Vasiliev, V. V., *Mechanics of Composite Structures*, Taylor & Francis Ltd., Washington DC, 1993, pp. 62-71.

[27] Cohen, G. A., "Transverse Shear Stiffness of Laminated Anisotropic Shells," *Computer Methods in Applied Mechanics and Engineering*, Vol. 13, 1978, pp. 205-220.

[28] Woodson, M. B., Johnson, E. R., and Haftka, R. T., "A Vlasov Theory for Laminated Composite Circular Beams with Thin-walled Open Sections," *Proceedings of the AIAA/ASME/ASCE/AHS/ASC 34th Structures, Structural Dynamics and Materials Conference* (LaJolla, CA), Part 5, AIAA, Washington, D.C., April 1993, pp. 2742-2760.

[29] Woodson, M. B., "Optimal Design of Composite Fuselage Frames for Crashworthiness," *Doctoral Dissertation*, Department of Aerospace and Ocean Engineering, Virginia Polytechnic Institute and State University, Blacksburg, Virginia, December 1994, pp. 17-71.

[30] Bauld, N. R., Jr., and Tzeng, L., "A Vlasov Theory for Fiber-Reinforced Beams with Thin-walled Open Cross-Sections," *International Journal of Solids & Structures*, Vol. 20, No. 3, 1984, pp. 277-297.

[31]Sanders, J. L., "An Improved First-Approximation Theory for Thin Shells," *NASA Technical Report R-24*, June, 1959.

[32]Sanders, J. L., "Nonlinear Theories for Thin Shells," *Quarterly of Applied Mathematics*, Vol. 21, No. 1, 1963, pp. 21-36.

[33]Minguet, P. J., Fedro, M., O'Brien, T. K., Martin, R., Ilcewicz, L., Awerbuch, J., and Wang, A., "Development of a Structural Test Simulating Pressure Pillowing Effects in a Bonded Skin/Stringer/Frame Configuration," *Proceedings of the Fourth NASA/DoD Advanced Composites Technology Conference*, NASA CP-3229, 1993, pp. 863-880.

NOMENCLATURE

A_{ij}	Laminate extensional stiffness
B_{ij}	Laminate extension-bending coupling stiffness
D_{ij}	Laminate bending stiffness
e_r	Eccentricity of ring
e_s	Eccentricity of stringer
e_{xx}, $e_{\theta\theta}$, e_{zz}	Three-dimensional engineering normal strains
$e_{x\theta}$, $e_{\theta z}$, e_{xz}	Three-dimensional engineering shear strains
m	Harmonic in axial direction
M	Number of harmonics in axial direction
$M_{\omega r}$	Ring bimoment
$M_{\theta s}$	Stringer bending moment
M_{xr}	Ring in-plane bending moment
M_{xx}, $M_{\theta\theta}$, $M_{\theta x}$, $M_{x\theta}$	Stress couples of shell theory
$M^s_{x\theta}$	Stress couple of Sanders' theory of shells
$\bar{M}_{\theta x}$, $\tilde{M}_{x\theta}$	Modified stress couples of transverse shear deformation shell theory
M_{zr}	Ring out-of-plane bending moment
n	Harmonic in circumferential direction
N	Number of harmonics in circumferential direction
$N_{\theta r}$	Ring circumferential force
N_{xs}	Stringer axial force
N_{xx}, $N_{\theta\theta}$, $N_{\theta x}$, $N_{x\theta}$	Stress resultants of shell theory
$N^s_{x\theta}$	Stress resultant of Sanders' theory of shells
p	Internal pressure load

Q	Stringer axial load share
$\bar{Q}_{ij}$	Transformed reduced stiffness of lamina
Q_x, Q_θ	Transverse shear resultants for shell
R	Radius to middle surface of shell
R_0	Radius to the reference arc of ring
S	Area of the shell's reference surface
t	Thickness of shell
$2R\Theta$	Stringer spacing
$2l$	Frame, or ring, spacing
T_r	Torque in the ring
u	Axial displacement of middle surface of shell
u_r	Axial displacement of reference arc of ring
u_s	Axial displacement of centroidal axis of stringer
U_x, U_y, U_z	Rigid body displacements
v	Circumferential displacement of middle surface of shell
v_r	Circumferential displacement of reference arc of ring
V_{zs}	Stringer shear force
V_{xr}	Ring in-plane shear force
V_{zr}	Ring out-of-plane shear force
δW	Virtual work
w	Normal displacement of middle surface of shell
w_r	Normal displacement of reference arc of ring
w_s	Normal displacement of centroidal axis of stringer
α_m	Axial frequency
β_n	Circumferential frequency
$\epsilon_{\theta r}$	Normal strains of ring's reference axis

ϵ_{xs}	Normal strains of stringer's centroidal axis
$\epsilon_{xx}, \epsilon_{\theta\theta}$	Normal strains of shell's middle surface
$\sigma_{xx}, \sigma_{\theta\theta}$	Normal stress components
$\sigma_{x\theta}, \sigma_{xz}, \sigma_{\theta z}$	Shear stress components
$\gamma_{xr},\ \gamma_{zr}$	Ring's transverse shear strains
γ_{xs}	Stringer's transverse shear strain
$\gamma_{x\theta}$	In-plane shear strain of shell's middle surface
$\gamma_{xz}, \gamma_{\theta z}$	Transverse shear strains of shell's middle surface
$\kappa_{\theta s}$	Bending curvature of stringer's centroidal axis
κ_{xr}	In-plane bending curvature of ring's reference axis
κ_{zr}	Out-of-plane bending curvature of ring's reference axis
$\kappa_{xx}, \kappa_{\theta\theta}$	Bending strains of shell's middle surface
$\bar{\kappa}_{x\theta}, \tilde{\kappa}_{x\theta}$	Twisting strains of shell's middle surface
$\kappa^s_{x\theta}$	Twisting strain of shell's middle surface in Sanders theory
$\lambda_{xr},\ \lambda_{\theta r},\ \lambda_{zr}$	Shell-ring interacting force intensities (F/L)
$\Lambda_{\theta r},\ \Lambda_{zr}$	Shell-ring interacting moment intensities (F-L/L)
$\lambda_{xs},\ \lambda_{zs}$	Shell-stringer interacting force intensities
ϕ_θ	Rotation of shell's normal about x-axis
$\phi_{\theta r}$	Torsional rotation of ring
$\phi_{\theta s}$	Bending rotation of stringer
ϕ_x	Rotation of shell's normal about θ-axis
ϕ_{xr}	In-plane bending rotation of ring
ϕ_z	Shell's rotation around normal
ϕ_{zr}	Out-of-plane bending rotation of ring
τ_r	Twist rate of ring
$\Omega_x,\ \Omega_y,\ \Omega_z$	Rigid body rotations

APPENDIX A

ELEMENTS OF MATRICES FOR LINEAR ANALYSIS USING TRANSVERSE SHEAR DEFORMATION MODEL

The non-zero elements of the submatrices K_{ij}, B_{ij} and F_{11} in Eq. (4.68) for the transverse shear deformation model are listed below. The parameter δ_{ij} is Kronecker delta assuming the values zero for $i \neq j$, and one for $i = j$, respectively.

Elements of $(10MN + 3M + 3N + 2) \times (10MN + 3M + 3N + 2)$ **submatrix** $[K_{11}]$

$$K_{11}\ (1,1) = \frac{A_{11}\Theta R}{l}$$

$$K_{11}\ (1,2) = 2A_{12}\Theta R$$

$$K_{11}\ (2,2) = \frac{4A_{22}\Theta l}{R}$$

$$K_{11}\ (3,3) = 2A_{11}\alpha_m^2 l\Theta R\delta_{mp}$$

$$K_{11}\ (3,4) = 2A_{12}\alpha_m l\Theta\delta_{mp}$$

$$K_{11}\ (3,5) = 2B_{11}\alpha_m^2 l\Theta R\delta_{mp}$$

$$K_{11}\ (4,4) = 2(\frac{A_{22}}{R} + A_{44}\alpha_m^2)l\Theta R\delta_{mp}$$

$$K_{11}\ (4,5) = 2(\frac{B_{12}}{R} - A_{44})\alpha_m l\Theta R\delta_{mp}$$

$$K_{11}\ (5,5) = 2(A_{44} + D_{11}\alpha_m^2)l\Theta R\delta_{mp}$$

$$K_{11}\ (6,6) = 2(\frac{A_{22}}{R}\beta_n^2 + \frac{A_{55}}{R})l\Theta\delta_{nq}$$

$$K_{11}\ (6,7) = 2(\frac{A_{22}}{R} + \frac{A_{55}}{R})\beta_n l\Theta\delta_{nq}$$

$$K_{11}\ (6,8) = 2(\frac{B_{22}}{R}\beta_n^2 - A_{55})l\Theta\delta_{nq}$$

$$K_{11}\ (7,7) = 2(\frac{A_{22}}{R} + \frac{A_{55}}{R}\beta_n^2)l\Theta\delta_{nq}$$

$$K_{11}\ (7,8) = 2(\frac{B_{22}}{R} - A_{55})\beta_n l\Theta\delta_{nq}$$

$$K_{11}\ (8,8) = 2(\frac{D_{22}}{R}\beta_n^2 + A_{55}R)l\Theta\delta_{nq}$$

$$K_{11}\ (9,9) = \left[A_{11}\alpha_m^2 R + \frac{A_{66}}{R}\beta_n^2\right]l\Theta\delta_{mp}\delta_{nq} = K_{11}\ (10,10)$$

$$K_{11}\ (9,12) = -\left[A_{12} + A_{66} + \frac{(B_{66}^1 - B_{66}^2)}{R}\right]\alpha_m\beta_n l\Theta\delta_{mp}\delta_{nq} = -K_{11}\ (10,11)$$

$$K_{11}\ (9,14) = -A_{12}\alpha_m\Theta l\delta_{mp}\delta_{nq} = -K_{11}\ (10,13)$$

$$K_{11}\ (9,15) = \left[B_{11}\alpha_m^2 + \frac{(B_{66}^1 - B_{66}^2)}{R^2}\beta_n^2\right]l\Theta R\delta_{mp}\delta_{nq} = K_{11}\ (10,16)$$

$$K_{11}\ (9,18) = -(B_{12} + B_{66}^1 + B_{66}^2)\alpha_m\beta_n l\Theta\delta_{mp}\delta_{nq} = -K_{11}\ (10,17)$$

$$K_{11}\ (11,11) = \left\{\frac{A_{22}}{R^2}\beta_n^2 + \frac{A_{55}}{R^2} + \left[A_{66} + \frac{2(B_{66}^1 - B_{66}^2)}{R} + \frac{(D_{66}^{11} - 2D_{66}^{12} + D_{66}^{22})}{R^2}\right]\alpha_m^2\right\} *$$

$$Rl\Theta\delta_{mp}\delta_{nq} = K_{11}\ (12,12)$$

$$K_{11}\ (11,13) = \frac{(A_{22} + A_{55})}{R}\beta_n l\Theta\delta_{mp}\delta_{nq} = K_{11}\ (12,14)$$

$$K_{11}\ (11,16) = \left[B_{12} + B_{66}^1 - B_{66}^2 + \frac{(D_{66}^{11} - 2D_{66}^{12} + D_{66}^{22})}{R}\right]\alpha_m\beta_n l\Theta\delta_{mp}\delta_{nq}$$

$$= -K_{11}\ (12,15)$$

$$K_{11}\ (11,17) = \left\{\frac{B_{22}}{R}\beta_n^2 - A_{55} + \left[(B_{66}^1 + B_{66}^2)R + D_{66}^{11} - D_{66}^{22}\right]\alpha_m^2\right\}l\Theta\delta_{mp}\delta_{nq}$$

$$= K_{11}\ (12,18)$$

$$K_{11}\ (13,13) = \left[\frac{A_{22}}{R^2} + \frac{A_{55}}{R^4}\beta_n^2 + A_{44}\alpha_m^2\right]Rl\Theta\delta_{mp}\delta_{nq} = K_{11}\ (14,14)$$

$$K_{11}\ (13,16) = (B_{12} - A_{44}R)\alpha_m l\Theta\delta_{mp}\delta_{nq} = -K_{11}\ (14,15)$$

$$K_{11}\ (13,17) = -(A_{55} - \frac{B_{22}}{R})\beta_n l\Theta\delta_{mp}\delta_{nq} = K_{11}\ (14,18)$$

$$K_{11}\ (15,15) = \left[A_{44} + D_{11}\alpha_m^2 + \frac{(D_{66}^{11} - 2D_{66}^{12} + D_{66}^{22})}{R^2}\beta_n^2\right]Rl\Theta\delta_{mp}\delta_{nq} = K_{11}\ (16,16)$$

$$K_{11}\ (15,18) = -(D_{66}^{11} + D_{12} - D_{66}^{22})\alpha_m\beta_n l\Theta\delta_{mp}\delta_{nq} = -K_{11}\ (16,17)$$

$$K_{11}\ (17,17) = \left[A_{55} + \frac{D_{22}}{R^2}\beta_n^2 + (D_{66}^{11} + 2D_{66}^{12} + D_{66}^{22})\alpha_m^2\right]Rl\Theta\delta_{mp}\delta_{nq} = K_{11}\ (18,18)$$

Elements of $(6M+1)\times(6M+1)$ submatrix $[K_{22}]$

$$K_{22}\ (1,1) = \frac{(EA)_s}{2l}$$

$$K_{22}\ (2,2) = (EA)_s \alpha_m^2 l \delta_{mp}$$

$$K_{22}\ (3,3) = (EA)_s \alpha_m^2 l \delta_{mp}$$

$$K_{22}\ (4,4) = (GA)_s \alpha_m^2 l \delta_{mp}$$

$$K_{22}\ (5,5) = (GA)_s \alpha_m^2 l \delta_{mp}$$

$$K_{22}\ (6,6) = \left[(GA)_s + (EI_{\theta\theta})_s \alpha_m^2\right] l \delta_{mp}$$

$$K_{22}\ (7,7) = \left[(GA)_s + (EI_{\theta\theta})_s \alpha_m^2\right] l \delta_{mp}$$

Elements of $(6N+1)\times(6N+1)$ submatrix $[K_{33}]$

$$K_{33}\ (1,1) = \frac{2EA\Theta}{R_0}$$

$$K_{33}\ (2,2) = GA_{x\theta}\beta_n^2 \frac{\Theta}{R_0}\delta_{nq}$$

$$K_{33}\ (2,7) = -GA_{x\theta}\beta_n \Theta \delta_{nq}$$

$$K_{33}\ (3,3) = (EA\beta_n^2 + GA_{z\theta})\frac{\Theta}{R_0}\delta_{nq}$$

$$K_{33}\ (3,4) = (EA + GA_{z\theta})\beta_n \frac{\Theta}{R_0}\delta_{nq}$$

$$K_{33}\ (3,6) = -GA_{z\theta}\Theta\delta_{nq}$$

$$K_{33}\ (4,4) = (EA + GA_{z\theta}\beta_n^2)\frac{\Theta}{R_0}\delta_{nq}$$

$$K_{33}\ (4,6) = -GA_{z\theta}\beta_n \Theta \delta_{nq}$$

$$K_{33}\ (5,5) = \left[EI_{zz} + (GJ + \frac{2EI_{\omega z}}{R_0} + \frac{EI_{\omega\omega}}{R_0^2}\beta_n^2)\beta_n^2\right]\frac{\Theta}{R_0}\delta_{nq}$$

$$K_{33}\ (5,6) = (EI_{zx} + \frac{EI_{\omega x}}{R_0}\beta_n^2)\frac{\beta_n}{R_0}\Theta\delta_{nq}$$

$$K_{33}\ (5,7) = -\left[(GJ + EI_{zz} + \frac{EI_{\omega z}}{R_0}) + (\frac{EI_{\omega z}}{R_0} + \frac{EI_{\omega\omega}}{R_0^2})\beta_n^2\right]\frac{\beta_n}{R_0}\Theta\delta_{nq}$$

$$K_{33}\ (6,6) = (GA_{z\theta}R_0^2 + EI_{xx}\beta_n^2)\frac{\Theta}{R_0}\delta_{nq}$$

$$K_{33}\ (6,7) = -(EI_{zx} + \frac{EI_{\omega x}}{R_0})\frac{\beta_n^2}{R_0}\Theta\delta_{nq}$$

$$K_{33}\ (7,7) = \left[(GJ + GA_{x\theta}R_0^2) + (EI_{zz} + \frac{2EI_{\omega z}}{R_0} + \frac{EI_{\omega\omega}}{R_0^2})\beta_n^2\right]\frac{\Theta}{R_0}\delta_{nq}$$

Elements of $(10MN + 3M + 3N + 2) \times 4M$ **submatrix** $[B_{11}]$

$$B_{11}\ (1,1) = \frac{(-1)^m}{\alpha_m}$$

$$B_{11}\ (3,1) = -l\delta_{mp}$$

$$B_{11}\ (4,4) = -l\delta_{mp}$$

$$B_{11}\ (5,1) = \frac{t}{2}l\delta_{mp}$$

$$B_{11}\ (9,2) = -l\delta_{mp}$$

$$B_{11}\ (10,1) = -l\delta_{mp}$$

$$B_{11}\ (13,4) = -l\delta_{mp}$$

$$B_{11}\ (14,3) = -l\delta_{mp}$$

$$B_{11}\ (15,1) = \frac{t}{2}l\delta_{mp}$$

$$B_{11}\ (16,2) = \frac{t}{2}l\delta_{mp}$$

Elements of $(10MN + 3M + 3N + 2) \times (5N + 1)$ **submatrix** $[B_{12}]$

$$B_{12}\ (2,1) = -2a\Theta$$

$$B_{12}\ (4,1) = -2a\Theta$$

$$B_{12}\ (6,3) = -a\Theta\delta_{nq}$$

$$B_{12}\ (7,4) = -a\Theta\delta_{nq}$$

$$B_{12}\ (8,3) = \frac{t}{2}a\Theta\delta_{nq}$$

$$B_{12}\ (9,2) = -a\Theta\delta_{nq}$$

$$B_{12}\ (11,3) = -a\Theta\delta_{nq}$$

$$B_{12}\ (12,6) = -\alpha_p a\Theta\delta_{nq}$$

$$B_{12}\ (13,4) = -a\Theta\delta_{nq}$$

$$B_{12}\ (14,5) = \alpha_p a\Theta\delta_{nq}$$

$$B_{12}\ (15,2) = \frac{t}{2} a\Theta\delta_{nq}$$

$$B_{12}\ (17,3) = \frac{t}{2} a\Theta\delta_{nq}$$

$$B_{12}\ (18,6) = \frac{t}{2}\alpha_p a\Theta\delta_{nq}$$

Elements of $(10MN + 3M + 3N + 2) \times 1$ **submatrix** $[B_{13}]$

$$B_{13}\ (1,1) = 1$$

Elements of $(6M + 1) \times 4M$ **submatrix** $[B_{21}]$

$$B_{21}\ (1,1) = \frac{(-1)^{m+1}}{\alpha_m}$$

$$B_{21}\ (2,1) = l\delta_{mp}$$

$$B_{21}\ (3,2) = l\delta_{mp}$$

$$B_{21}\ (4,3) = l\delta_{mp}$$

$$B_{21}\ (5,4) = l\delta_{mp}$$

$$B_{21}\ (6,1) = le_s\delta_{mp}$$

$$B_{21}\ (7,2) = le_s\delta_{mp}$$

Elements of $(6M+1)\times 1$ submatrix $[B_{23}]$

$$B_{23}\ (1,1) = -1$$

Elements of $(6N+1)\times(5N+1)$ submatrix $[B_{32}]$

$$B_{32}\ (1,1) = 2a\Theta$$

$$B_{32}\ (2,2) = a\Theta\delta_{nq}$$

$$B_{32}\ (3,3) = a\Theta\delta_{nq}$$

$$B_{32}\ (4,4) = a\Theta\delta_{nq}$$

$$B_{32}\ (5,2) = e_r a\Theta\delta_{nq}$$

$$B_{32}\ (5,3) = \frac{\omega_0}{R_0}\beta_n a\Theta\delta_{nq}$$

$$B_{32}\ (5,5) = a\Theta\delta_{nq}$$

$$B_{32}\ (5,6) = \frac{\omega_1}{R_0}\beta_n a\Theta\delta_{nq}$$

$$B_{32}\ (6,3) = e_r a\Theta\delta_{nq}$$

$$B_{32}\ (7,3) = -\frac{\omega_0}{R_0}a\Theta\delta_{nq}$$

$$B_{32}\ (7,6) = (1-\frac{\omega_1}{R_0})a\Theta\delta_{nq}$$

Elements of $(10MN+3M+3N+2)\times 1$ submatrix $[F_{11}]$

$$F_{11}\ (1) = pR^2\Theta$$

$$F_{11}\ (2) = 4pl\Theta R$$

APPENDIX B

ELEMENTS OF MATRICES FOR LINEAR ANALYSIS USING CLASSICAL MODEL

The non-zero elements of the submatrices K_{ij}, B_{ij} and F_{11} in Eq. (4.68) for the classical model are listed below. The parameter δ_{ij} is Kronecker delta assuming the values zero for $i \neq j$, and one for $i = j$, respectively.

Elements of $(6MN + 2M + 2N + 2) \times (6MN + 2M + 2N + 2)$ **submatrix** $[K_{11}]$

$$K_{11}\ (1,1) = \frac{A_{11}\Theta R}{l}$$

$$K_{11}\ (1,2) = 2A_{12}\Theta R$$

$$K_{11}\ (2,2) = \frac{4A_{22}\Theta l}{R}$$

$$K_{11}\ (3,3) = 2A_{11}\alpha_m^2 l\Theta R\delta_{mp}$$

$$K_{11}\ (3,4) = 2(\frac{A_{12}}{R} + B_{11}\alpha_m^2)\alpha_m l\Theta R\delta_{mp}$$

$$K_{11}\ (4,4) = 2(\frac{A_{22}}{R^2} + \frac{2B_{12}}{R}\alpha_m^2 + D_{11}\alpha_m^4)l\Theta R\delta_{mp}$$

$$K_{11}\ (5,5) = 2(\frac{A_{22}}{R} + \frac{2B_{22}}{R^2} + \frac{D_{22}}{R^3})\beta_n^2 l\Theta\delta_{nq}$$

$$K_{11}\ (5,6) = 2\big[(\frac{A_{22}}{R} + \frac{B_{22}}{R^2}) + (\frac{B_{22}}{R^2} + \frac{D_{22}}{R^3})\beta_n^2\big]\beta_n l\Theta\delta_{nq}$$

$$K_{11}\ (6,6) = 2\big[\frac{A_{22}}{R} + \frac{2B_{22}}{R^2}\beta_n^2 + \frac{D_{22}}{R^3}\beta_n^4\big]l\Theta\delta_{nq}$$

$$K_{11}\ (7,7) = \big[A_{11}\alpha_m^2 R + (\frac{A_{66}}{R} - \frac{B_{66}}{R^2} + \frac{D_{66}}{4R^3})\beta_n^2\big]l\Theta\delta_{mp}\delta_{nq} = K_{11}\ (8,8)$$

$$K_{11}\ (7,10) = -\big[\frac{A_{12}}{R} + \frac{B_{12}}{R^2} + (\frac{A_{66}}{R} + \frac{B_{66}}{R^2} - \frac{3D_{66}}{4R^3})\big]\alpha_m\beta_n l\Theta R\delta_{mp}\delta_{nq} = -K_{11}\ (8,9)$$

$$K_{11}\ (7,12) = -\big[A_{12} + B_{11}\alpha_m^2 + (\frac{B_{12}}{R} + \frac{2B_{66}}{R} - \frac{D_{66}}{R^2})\beta_n^2\big]\alpha_m\Theta l\delta_{mp}\delta_{nq} = -K_{11}\ (8,11)$$

$$K_{11}\ (9,9) = \left[\left(\frac{A_{22}}{R^2} + \frac{2B_{22}}{R^3} + \frac{D_{22}}{R^4}\right)\beta_n^2 + \left(A_{66} + \frac{3B_{66}}{R} + \frac{9D_{66}}{4R^3}\right)\alpha_m^2\right] Rl\Theta\delta_{mp}\delta_{nq}$$

$$= K_{11}\ (10,10)$$

$$K_{11}\ (9,11) = \left[\frac{A_{22}}{R^2} + \frac{B_{22}}{R^3} + \left(\frac{B_{22}}{R^3} + \frac{D_{22}}{R^4}\right)\beta_n^2 + \left(\frac{B_{12}}{R} + \frac{2B_{66}}{R} + \frac{D_{12}}{R^2} + \frac{3D_{66}}{R^2}\right)\alpha_m^2\right] *$$

$$\beta_n l\Theta R\delta_{mp}\delta_{nq} = K_{11}\ (10,12)$$

$$K_{11}\ (11,11) = \left[\frac{A_{22}}{R} + \frac{2B_{22}}{R^2}\beta_n^2 + \frac{D_{22}}{R^3}\beta_n^4 + \frac{2(D_{12}+2D_{66})}{R}\alpha_m^2\beta_n^2 + (2B_{12} + D_{11}\alpha_m^2 R) *\right.$$

$$\left.\alpha_m^2\right] l\Theta\delta_{mp}\delta_{nq} = K_{11}\ (12,12)$$

Elements of $(4M+1)\times(4M+1)$ submatrix $[K_{22}]$

$$K_{22}\ (1,1) = \frac{(EA)_s}{2l}$$

$$K_{22}\ (2,2) = (EA)_s\alpha_m^2 l\delta_{mp}$$

$$K_{22}\ (3,3) = (EA)_s\alpha_m^2 l\delta_{mp}$$

$$K_{22}\ (4,4) = (EI_{\theta\theta})_s\alpha_m^4 l\delta_{mp}$$

$$K_{22}\ (5,5) = (EI_{\theta\theta})_s\alpha_m^4 l\delta_{mp}$$

Elements of $(4N+1)\times(4N+1)$ submatrix $[K_{33}]$

$$K_{33}\ (1,1) = \frac{2EA\Theta}{R_0}$$

$$K_{33}\ (2,2) = \left[GJ + \left(EI_{zz} + \frac{2EI_{\omega z}}{R_0} + \frac{EI_{\omega\omega}}{R_0^2}\right)\beta_n^2\right]\frac{\beta_n^2}{R_0^3}\Theta\delta_{nq}$$

$$K_{33}\ (2,3) = -\left(EI_{zx} + \frac{EI_{\omega x}}{R_0}\right)\frac{\beta_n^3}{R_0^3}\Theta\delta_{nq}$$

$$K_{33}\ (2,4) = -\left(EI_{zx} + \frac{EI_{\omega x}}{R_0}\right)\frac{\beta_n^4}{R_0^3}\Theta\delta_{nq}$$

$$K_{33}\ (2,5) = -\left[\left(GJ + EI_{zz} + \frac{EI_{\omega z}}{R_0}\right) + \left(\frac{EI_{\omega z}}{R_0} + \frac{EI_{\omega\omega}}{R_0^2}\right)\beta_n^2\right]\frac{\beta_n^2}{R_0^3}\Theta\delta_{nq}$$

$$K_{33}\ (3,3) = (EA + \frac{EI_{xx}}{R_0^2})\frac{\beta_n^2}{R_0}\Theta\delta_{nq}$$

$$K_{33}\ (3,4) = (EA + \frac{EI_{xx}}{R_0^2}\beta_n^2)\frac{\beta_n}{R_0}\Theta\delta_{nq}$$

$$K_{33}\ (3,5) = (EI_{zx} + \frac{EI_{\omega_x}}{R_0}\beta_n^2)\frac{\beta_n}{R_0^2}\Theta\delta_{nq}$$

$$K_{33}\ (4,4) = (EA + \frac{EI_{xx}}{R_0^2}\beta_n^4)\frac{\Theta}{R_0}\delta_{nq}$$

$$K_{33}\ (4,5) = (EI_{zx} + \frac{EI_{\omega_x}}{R_0}\beta_n^2)\frac{\beta_n^2}{R_0^2}\Theta\delta_{nq}$$

$$K_{33}\ (5,5) = \left[EI_{zz} + (GJ + \frac{2EI_{\omega z}}{R_0} + \frac{EI_{\omega\omega}}{R_0^2}\beta_n^2)\beta_n^2\right]\frac{\Theta}{R_0}\delta_{nq}$$

Elements of $(6MN + 2M + 2N + 2) \times 4M$ **submatrix** $[B_{11}]$

$$B_{11}\ (1,1) = \frac{(-1)^m}{\alpha_m}$$

$$B_{11}\ (3,1) = -l\delta_{mp}$$

$$B_{11}\ (4,1) = \frac{t}{2}\alpha_m l\delta_{mp}$$

$$B_{11}\ (4,4) = -l\delta_{mp}$$

$$B_{11}\ (7,2) = -l\delta_{mp}$$

$$B_{11}\ (8,1) = -l\delta_{mp}$$

$$B_{11}\ (11,1) = \frac{t}{2}\alpha_m l\delta_{mp}$$

$$B_{11}\ (11,4) = -l\delta_{mp}$$

$$B_{11}\ (12,2) = -\frac{t}{2}\alpha_m l\delta_{mp}$$

$$B_{11}\ (12,3) = -l\delta_{mp}$$

Elements of $(6MN + 2M + 2N + 2) \times (5N + 1)$ submatrix $[B_{12}]$

$$B_{12}\ (2,1) = -2a\Theta$$

$$B_{12}\ (4,1) = -2a\Theta$$

$$B_{12}\ (5,3) = -(1 - \frac{t}{2R})a\Theta\delta_{nq}$$

$$B_{12}\ (6,3) = \frac{t}{2R}\beta_n a\Theta\delta_{nq}$$

$$B_{12}\ (6,4) = -a\Theta\delta_{nq}$$

$$B_{12}\ (7,2) = -a\Theta\delta_{nq}$$

$$B_{12}\ (9,3) = -(1 - \frac{t}{2R})a\Theta\delta_{nq}$$

$$B_{12}\ (10,6) = -(1 - \frac{t}{2R})\alpha_p a\Theta\delta_{nq}$$

$$B_{12}\ (11,3) = \frac{t}{2R}\beta_n a\Theta\delta_{nq}$$

$$B_{12}\ (11,4) = -a\Theta\delta_{nq}$$

$$B_{12}\ (12,2) = -\frac{t}{2}\alpha_p a\Theta\delta_{nq}$$

$$B_{12}\ (12,5) = \alpha_p a\Theta\delta_{nq}$$

$$B_{12}\ (12,6) = \frac{t}{2R}\beta_n\alpha_p a\Theta\delta_{nq}$$

Elements of $(6MN + 2M + 2N + 2) \times 1$ submatrix $[B_{13}]$

$$B_{13}\ (1,1) = 1$$

Elements of $(4M + 1) \times 1$ submatrix $[B_{23}]$

$$B_{23}\ (1,1) = -1$$

Elements of $(4M+1)\times 4M$ submatrix $[B_{21}]$

$$B_{21}\ (1,1) = \frac{(-1)^{m+1}}{\alpha_m}$$

$$B_{21}\ (2,1) = l\delta_{mp}$$

$$B_{21}\ (3,2) = l\delta_{mp}$$

$$B_{21}\ (4,2) = -\alpha_m l e_s \delta_{mp}$$

$$B_{21}\ (4,3) = l\delta_{mp}$$

$$B_{21}\ (5,1) = \alpha_m l e_s \delta_{mp}$$

$$B_{21}\ (5,4) = l\delta_{mp}$$

Elements of $(4N+1)\times(5N+1)$ submatrix $[B_{32}]$

$$B_{32}\ (1,1) = 2a\Theta$$

$$B_{32}\ (2,2) = a\Theta\delta_{nq}$$

$$B_{32}\ (2,3) = -\frac{\omega_0}{R_0^2}\beta_n a\Theta\delta_{nq}$$

$$B_{32}\ (2,6) = (1-\frac{\omega_1}{R_0})\beta_n a\Theta\delta_{nq}$$

$$B_{32}\ (3,3) = (1+\frac{e_r}{R_0})a\Theta\delta_{nq}$$

$$B_{32}\ (4,3) = \frac{e_r}{R_0}\beta_n a\Theta\delta_{nq}$$

$$B_{32}\ (4,4) = a\Theta\delta_{nq}$$

$$B_{32}\ (5,2) = e_r a\Theta\delta_{nq}$$

$$B_{32}\ (5,3) = \frac{\omega_0}{R_0}(1-\frac{e_r}{R_0})\beta_n a\Theta\delta_{nq}$$

$$B_{32}\ (5,5) = a\Theta\delta_{nq}$$

$$B_{32}\ (5,6) = \left[\frac{e_r}{R_0} + (1-\frac{e_r}{R_0})\frac{\omega_1}{R_0}\right]\beta_n a\Theta\delta_{nq}$$

Elements of $(6MN + 2M + 2N + 2) \times 1$ submatrix $[F_{11}]$

$$F_{11}\ (1) = pR^2\Theta$$

$$F_{11}\ (2) = 4pl\Theta R$$

APPENDIX C

ELEMENTS OF TANGENT STIFFNESS AND LOAD STIFFNESS MATRICES FOR NONLINEAR ANALYSIS

The non-zero elements of the tangent stiffness submatrices K_{ij} and load stiffness submatrix L in Eq. (4.82) for nonlinear analysis are listed below. The parameter δ_{ij} is Kronecker delta assuming the values zero for $i \neq j$, and one for $i = j$, respectively.

Elements of $(3MN + 2M + 2N + 2) \times (3MN + 2M + 2N + 2)$ **submatrix** $[K_{11}(\hat{u}_{shell})]$

$$K_{11}\ (1,1) = \frac{A_{11}\Theta R}{l}$$

$$K_{11}\ (1,2) = 2A_{12}\Theta$$

$$K_{11}\ (1,3) = 0$$

$$K_{11}\ (1,4) = A_{11}\Theta R\alpha_m^2 w_m \delta_{jm}$$

$$K_{11}\ (1,5) = \frac{A_{12}\Theta}{R}(v_n + \beta_n w_n)\delta_{kn}$$

$$K_{11}\ (1,6) = \frac{A_{12}\Theta}{R}\beta_n(v_n + \beta_n w_n)\delta_{kn}$$

$$K_{11}\ (1,7) = 0$$

$$K_{11}\ (1,8) = \frac{A_{12}\Theta}{2R}(v_{mn} + \beta_n w_{mn})\delta_{jm}\delta_{kn}$$

$$K_{11}\ (1,9) = \frac{A_{12}\Theta}{2R}\beta_n(v_{mn} + \beta_n w_{mn})\delta_{jm}\delta_{kn} + 0.5A_{11}\Theta R\alpha_m^2 w_{mn}\delta_{jm}\delta_{kn}$$

$$K_{11}\ (2,2) = \frac{4A_{22}\Theta l}{R}$$

$$K_{11}\ (2,3) = 0$$

$$K_{11}\ (2,4) = 2A_{12}\Theta l\alpha_m^2 w_m \delta_{jm}$$

$$K_{11}\ (2,5) = \frac{2A_{22}\Theta l}{R^2}(v_n + \beta_n w_n)\delta_{kn}$$

$$K_{11}\ (2,6) = \frac{2A_{22}\Theta l}{R^2}\beta_n(v_n + \beta_n w_n)\delta_{kn}$$

$$K_{11}\ (2,7) = 0$$

$$K_{11}\ (2,8) = \frac{A_{22}\Theta l}{R^2}(v_{mn} + \beta_n w_{mn})\delta_{jm}\delta_{kn}$$

$$K_{11}\ (2,9) = \frac{A_{22}\Theta l}{R^2}\beta_n(v_{mn} + \beta_n w_{mn})\delta_{jm}\delta_{kn} + A_{12}\Theta l\alpha_m^2 w_{mn}\delta_{jm}\delta_{kn}$$

$$K_{11}\ (3,3) = 2A_{11}\alpha_m^2\Theta l R\delta_{mp}$$

$$K_{11}\ (3,4) = 2A_{12}\alpha_m\Theta l\delta_{mp} + \sum_{j=1}^{J} 2A_{11}\alpha_m\alpha_p\alpha_j\Theta R w_j I_2$$

$$K_{11}\ (3,5) = \frac{A_{12}\Theta l}{R}\alpha_p(v_{pn} + \beta_n w_{pn})\delta_{jp}\delta_{kn}$$

$$K_{11}\ (3,6) = \frac{A_{12}\Theta l}{R}\alpha_p\beta_n(v_{pn} + \beta_n w_{pn})\delta_{jp}\delta_{kn}$$

$$K_{11}\ (3,7) = 0$$

$$K_{11}\ (3,8) = \frac{A_{12}\Theta l}{R}\alpha_m(v_n + \beta_n w_n)\delta_{mp}\delta_{kn} + \sum_{j=1}^{J}\frac{A_{12}\Theta}{R}\alpha_p(v_{jn} + \beta_n w_{jn})\delta_{kn}I_1$$

$$K_{11}\ (3,9) = \frac{A_{12}\Theta l}{R}\alpha_m\beta_n(v_n + \beta_n w_n)\delta_{mp}\delta_{kn} + \sum_{j=1}^{J}\frac{A_{12}\Theta}{R}\alpha_p\beta_n(v_{jn} + \beta_n w_{jn})\delta_{kn}I_1$$
$$+ \sum_{j=1}^{J} A_{11}\alpha_m\alpha_p\alpha_j\Theta R w_{jn}\delta_{kn}I_2$$

$$K_{11}\ (4,4) = 2(\frac{A_{22}}{R^2} + D_{11}\alpha_m^4)\Theta l R\delta_{mp} + 2A_{12}\alpha_m^2\Theta l w_0\delta_{mp} + A_{11}\alpha_m^2\Theta R q_0\delta_{mp}$$
$$+ \sum_{k=1}^{K}\frac{1}{2}(\frac{A_{12}}{R} + \frac{2A_{66}}{R})\Theta l\alpha_m^2(v_k + \beta_k w_k)^2\delta_{mp} + \sum_{j=1}^{J} 2A_{11}\Theta R\alpha_m\alpha_j\alpha_p u_j I_6$$
$$+ \sum_{j=1}^{J} 2A_{12}\Theta\alpha_m\alpha_j w_j I_2 + \sum_{j=1}^{J}\sum_{k=1}^{K}(\frac{A_{12}}{R} + \frac{2A_{66}}{R})\Theta\alpha_m\alpha_p(v_k + \beta_k w_k)v_{jk}I_6$$
$$+ \sum_{j=1}^{J} 3A_{11}\Theta R\alpha_j^2\alpha_p\alpha_m w_j^2 I_{23} + \sum_{j=1}^{J}\sum_{k=1}^{K} 1.5A_{11}\Theta R\alpha_j^2\alpha_m\alpha_p w_{jk}^2 I_{23}$$
$$+ \sum_{j=1}^{J}\sum_{k=1}^{K}\frac{1}{2}(\frac{A_{12}}{R} + \frac{2A_{66}}{R})\Theta\alpha_m\alpha_p(v_{jk} + \beta_k w_{jk})^2 I_{24} + \sum_{j=1}^{J} 2A_{12}\Theta\alpha_m\alpha_p w_j I_6$$
$$+ \sum_{j=1}^{J}\sum_{k=1}^{K}(\frac{A_{12}}{R} + \frac{2A_{66}}{R})\Theta\alpha_m\alpha_p\beta_k(v_k + \beta_k w_k)w_{jk}I_6 + \sum_{j=1}^{J} 2A_{12}\Theta\alpha_p\alpha_j w_j I_5$$

$$K_{11}(4,5) = (\frac{A_{12}}{R} + \frac{2A_{66}}{R})\Theta l\alpha_m^2(v_q + \beta_q w_q)w_m\delta_{kq}\delta_{jm} + A_{12}\Theta l\alpha_m^2\beta_q w_{mq}\delta_{kq}\delta_{jm}$$
$$- \frac{A_{66}\Theta l}{R}\alpha_m\beta_q u_{mq}\delta_{kq}\delta_{jm} + \frac{A_{22}\Theta l}{R^2}(v_{mq} + \beta_q w_{mq})\delta_{kq}\delta_{jm}$$
$$- A_{66}\Theta l\alpha_m^2 v_{mq}\delta_{kq}\delta_{jm} + \sum_{k=1}^{K}(\frac{A_{12}}{R} + \frac{2A_{66}}{R})l\alpha_m^2(v_k + \beta_k w_k)w_{mk}I_{15}\delta_{jm}$$
$$+ \sum_{j=1}^{J}(\frac{A_{12}}{R} + \frac{2A_{66}}{R})\Theta\alpha_m\alpha_j(v_{jq} + \beta_q w_{jq})w_j I_{14}\delta_{kq}$$
$$+ \sum_{j=1}^{J}\sum_{k=1}^{K}(\frac{A_{12}}{R} + \frac{2A_{66}}{R})\alpha_j\alpha_m(v_{jk} + \beta_k w_{jk})w_{jk}I_{14}I_{15}$$

$$K_{11}(4,6) = (\frac{A_{12}}{R} + \frac{2A_{66}}{R})\Theta l\alpha_p^2\beta_n(v_n + \beta_n w_n)w_p\delta_{kn}\delta_{jp} + A_{12}\Theta l\alpha_p^2 w_{pn}\delta_{kn}\delta_{jp}$$
$$- \frac{A_{66}\Theta l}{R}\alpha_p\beta_n^2 u_{pn}\delta_{kn}\delta_{jp} + \frac{A_{22}\Theta l}{R^2}\beta_n(v_{pn} + \beta_n w_{pn})\delta_{kn}\delta_{jp}$$
$$- A_{66}\Theta l\alpha_p^2\beta_n v_{pn}\delta_{kn}\delta_{jp} + \sum_{k=1}^{K}(\frac{A_{12}}{R} + \frac{2A_{66}}{R})l\alpha_p^2\beta_n(v_k + \beta_k w_k)w_{pk}I_{30}\delta_{jp}$$
$$+ \sum_{j=1}^{J}(\frac{A_{12}}{R} + \frac{2A_{66}}{R})\Theta\alpha_p\alpha_j\beta_n(v_{jn} + \beta_n w_{jn})w_j I_{33}\delta_{kn}$$
$$+ \sum_{j=1}^{J}\sum_{k=1}^{K}(\frac{A_{12}}{R} + \frac{2A_{66}}{R})\alpha_j\alpha_p\beta_n(v_{jk} + \beta_k w_{jk})w_{jk}I_{30}I_{33}$$

$$K_{11}(4,7) = -\frac{A_{66}\Theta l}{R}\alpha_m\beta_n(v_n + \beta_n w_n)\delta_{mp}\delta_{kn} - \sum_{j=1}^{J}\frac{A_{66}\Theta}{R}\alpha_m\beta_n(v_{jn} + \beta_n w_{jn})I_6\delta_{kn}$$
$$+ \sum_{j=1}^{J}A_{11}\Theta R\alpha_m\alpha_p\alpha_j w_{jn}I_2\delta_{kn}$$

$$K_{11}(4,8) = -A_{66}\Theta l\alpha_m^2(v_n + \beta_n w_n)\delta_{mp}\delta_{kn} + \frac{A_{22}\Theta l}{R^2}(v_n + \beta_n w_n)\delta_{mp}\delta_{kn}$$
$$- \sum_{j=1}^{J}\frac{A_{66}\Theta}{R}\alpha_p\beta_n u_{jn}I_5\delta_{kn} + \sum_{j=1}^{J}(\frac{A_{12}}{R} + \frac{2A_{66}}{R})\Theta\alpha_p\alpha_j(v_n + \beta_n w_n)w_j I_5\delta_{kn}$$
$$- \sum_{j=1}^{J}A_{66}\Theta\alpha_p\alpha_j v_{jn}I_5\delta_{kn} + \sum_{j=1}^{J}(\frac{A_{12}}{R} + \frac{2A_{66}}{R})\Theta\alpha_p\alpha_j(v_{jn} + \beta_n w_{jn})w_j I_{34}\delta_{kn}$$
$$+ \sum_{j=1}^{J}\frac{A_{22}\Theta}{R^2}(v_{jn} + \beta_n w_{jn})I_1\delta_{kn} - \sum_{j=1}^{J}A_{66}\Theta\alpha_p\alpha_m(v_{jn} + \beta_n w_{jn})I_6\delta_{kn}$$

$$K_{11}\ (4,8)\ cont'd. = +\sum_{j=1}^{J}\sum_{k=1}^{K}(\frac{A_{12}}{R}+\frac{2A_{66}}{R})\alpha_j\alpha_p(v_{jk}+\beta_k w_{jk})w_{jk}I_{30}I_{34}+\sum_{j=1}^{J}A_{12}\Theta\alpha_j$$

$$*\alpha_p\beta_n w_{jn}I_5\delta_{kn}+\sum_{j=1}^{J}\sum_{k=1}^{K}(\frac{A_{12}}{R}+\frac{2A_{66}}{R})\alpha_j\alpha_p(v_k+\beta_k w_k)w_{jk}I_5I_{30}$$

$$K_{11}\ (4,9) = A_{12}\Theta l\alpha_m^2(\beta_n v_n+w_n)\delta_{mp}\delta_{kn}+\frac{A_{22}\Theta l}{R^2}\beta_n(v_n+\beta_n w_n)\delta_{mp}\delta_{kn}$$

$$+\sum_{j=1}^{J}\frac{A_{22}\Theta}{R^2}\beta_n(v_{jn}+\beta_n w_{jn})I_1\delta_{kn}+\sum_{j=1}^{J}A_{12}\Theta\alpha_m\alpha_p(\beta_n v_{jn}+w_{jn})I_6\delta_{kn}$$

$$+\sum_{j=1}^{J}3A_{11}\Theta R\alpha_j^2\alpha_p\alpha_m w_j w_{jn}I_{23}\delta_{kn}+\sum_{j=1}^{J}A_{11}\Theta R\alpha_j\alpha_p\alpha_m u_{jn}I_6\delta_{kn}$$

$$+\sum_{j=1}^{J}A_{12}\Theta\alpha_j\alpha_p w_{jn}I_5\delta_{kn}+\sum_{k=1}^{K}\frac{1}{2}(\frac{A_{12}}{R}+\frac{2A_{66}}{R})\alpha_m^2 l(v_k+\beta_k w_k)^2\delta_{mp}I_{22}$$

$$-\sum_{j=1}^{J}A_{66}\Theta\alpha_p\alpha_j\beta_n v_{jn}I_5\delta_{kn}+\sum_{j=1}^{J}A_{12}\Theta\alpha_j\alpha_m w_{jn}I_2\delta_{kn}-\sum_{j=1}^{J}\frac{A_{66}\Theta}{R}\alpha_p$$

$$*\beta_n^2 u_{jn}I_5\delta_{kn}+\sum_{j=1}^{J}(\frac{A_{12}}{R}+\frac{2A_{66}}{R})\Theta\alpha_p\alpha_j\beta_n(v_n+\beta_n w_n)w_j I_5\delta_{kn}$$

$$+\sum_{j=1}^{J}(\frac{A_{12}}{R}+\frac{2A_{66}}{R})\Theta\alpha_p\alpha_j\beta_n(v_{jn}+\beta_n w_{jn})w_j I_{34}\delta_{kn}$$

$$+\sum_{j=1}^{J}\sum_{k=1}^{K}\frac{1}{2}(\frac{A_{12}}{R}+\frac{2A_{66}}{R})\alpha_m\alpha_p(v_{jk}+\beta_k w_{jk})^2 I_{22}I_{24}$$

$$+\sum_{j=1}^{J}\sum_{k=1}^{K}(\frac{A_{12}}{R}+\frac{2A_{66}}{R})\alpha_m\alpha_p(v_k+\beta_k w_k)(v_{jk}+\beta_k w_{jk})I_6 I_{22}$$

$$+\sum_{j=1}^{J}\sum_{k=1}^{K}(\frac{A_{12}}{R}+\frac{2A_{66}}{R})\alpha_j\alpha_p\beta_n(v_k+\beta_k w_k)w_{jk}I_5I_{30}$$

$$+\sum_{j=1}^{J}\sum_{k=1}^{K}(\frac{A_{12}}{R}+\frac{2A_{66}}{R})\alpha_j\alpha_p\beta_n(v_{jk}+\beta_k w_{jk})w_{jk}I_{30}I_{34}$$

$$+\sum_{j=1}^{J}\sum_{k=1}^{K}1.5A_{11}R\alpha_j^2\alpha_p\alpha_m w_{jk}^2 I_{23}I_{25}$$

$$
\begin{aligned}
K_{11}(5,5) =& 2\Big(\frac{A_{22}}{R}+\frac{D_{22}}{R^3}\Big)\beta_n^2\Theta l\delta_{nq}+\frac{2A_{22}}{R^2}\Theta l w_0\delta_{nq}+\frac{A_{12}}{R}\Theta q_0\delta_{nq}\\
&+\sum_{k=1}^{K}\frac{2A_{22}}{R^2}l(\beta_k v_k+w_k)I_4+\sum_{k=1}^{K}\frac{2A_{22}}{R^2}\beta_q l(v_k+\beta_k w_k)I_3\\
&+\sum_{k=1}^{K}\frac{2A_{22}}{R^2}\beta_n l(v_k+\beta_k w_k)I_7+\sum_{k=1}^{K}\frac{3A_{22}}{R^3}l(v_k+\beta_k w_k)^2 I_9\\
&+\sum_{j=1}^{J}\frac{1}{2}\Big(\frac{A_{12}}{R}+\frac{2A_{66}}{R}\Big)\alpha_j^2\Theta l w_j^2\delta_{nq}+\sum_{j=1}^{J}\sum_{k=1}^{K}\frac{3A_{22}}{2R^3}l(v_{jk}+\beta_k w_{jk})^2 I_9\\
&+\sum_{j=1}^{J}\sum_{k=1}^{K}\frac{1}{2}\Big(\frac{A_{12}}{R}+\frac{2A_{66}}{R}\Big)\alpha_j^2 l w_{jk}^2 I_{10}+\sum_{j=1}^{J}\sum_{k=1}^{K}\Big(\frac{A_{12}}{R}+\frac{2A_{66}}{R}\Big)\alpha_j^2 l w_j w_{jk}I_4\\
K_{11}(5,6) =& 2\Big(\frac{A_{22}}{R}+\beta_n^2\frac{D_{22}}{R^3}\Big)\beta_n\Theta l\delta_{nq}+\frac{2A_{22}}{R^2}\Theta\beta_n l w_0\delta_{nq}+\frac{A_{12}}{R}\Theta\beta_n q_0\delta_{nq}\\
&+\sum_{k=1}^{K}\frac{2A_{22}}{R^2}l\beta_n(\beta_k v_k+w_k)I_4+\sum_{k=1}^{K}\frac{2A_{22}}{R^2}\beta_n\beta_q l(v_k+\beta_k w_k)I_3\\
&+\sum_{k=1}^{K}\frac{2A_{22}}{R^2}l(v_k+\beta_k w_k)I_7+\sum_{k=1}^{K}\frac{3A_{22}}{R^3}\beta_n l(v_k+\beta_k w_k)^2 I_9\\
&+\sum_{j=1}^{J}\frac{1}{2}\Big(\frac{A_{12}}{R}+\frac{2A_{66}}{R}\Big)\beta_n\alpha_j^2\Theta l w_j^2\delta_{nq}+\sum_{j=1}^{J}\sum_{k=1}^{K}\frac{3A_{22}}{2R^3}\beta_n l(v_{jk}+\beta_k w_{jk})^2 I_9\\
&+\sum_{j=1}^{J}\sum_{k=1}^{K}\frac{1}{2}\Big(\frac{A_{12}}{R}+\frac{2A_{66}}{R}\Big)\alpha_j^2\beta_n l w_{jk}^2 I_{10}+\sum_{j=1}^{J}\sum_{k=1}^{K}\Big(\frac{A_{12}}{R}+\frac{2A_{66}}{R}\Big)\alpha_j^2\beta_n l w_j w_{jk}I_4\\
K_{11}(5,7) =& -\frac{A_{66}\Theta l}{R}\alpha_m\beta_n w_m\delta_{nq}\delta_{jm}-\sum_{k=1}^{K}\frac{A_{66}}{R}l\alpha_m\beta_q w_{mk}I_4\delta_{jm}\\
&+\sum_{k=1}^{K}\frac{A_{12}}{R}\alpha_m l(v_{mk}+\beta_k w_{mk})I_3\delta_{jm}\\
K_{11}(5,8) =& \Big(\frac{A_{22}}{R^2}-A_{66}\alpha_m^2\Big)\Theta l w_m\delta_{jm}\delta_{nq}+\frac{A_{12}}{R}\Theta l\alpha_m u_m\delta_{jm}\delta_{nq}+\sum_{k=1}^{K}\frac{A_{12}}{R}l\alpha_m u_{mk}I_4\delta_{jm}\\
&+\sum_{k=1}^{K}\frac{A_{22}}{R^2}\beta_n l(v_{mk}+\beta_k w_{mk})I_7\delta_{jm}+\sum_{k=1}^{K}\frac{A_{22}}{R^2}\beta_q l(v_{mk}+\beta_k w_{mk})I_3\delta_{jm}
\end{aligned}
$$

$$
\begin{aligned}
K_{11}\ (5,8)\ cont'd. = &+\sum_{k=1}^{K}\frac{A_{22}}{R^2}l(\beta_k v_{mk}+w_{mk})I_4\delta_{jm}+\sum_{j=1}^{J}\frac{1}{2}(\frac{A_{12}}{R}+\frac{2A_{66}}{R})\alpha_j^2\Theta w_j^2 I_{12}\delta_{nq}\\
&+\sum_{k=1}^{K}\frac{3A_{22}}{R^3}l(v_k+\beta_k w_k)(v_{mk}+\beta_k w_{mk})I_9\delta_{jm}-\sum_{k=1}^{K}A_{66}\alpha_m^2 l w_{mk}I_4\delta_{jm}\\
&+\sum_{j=1}^{J}\sum_{k=1}^{K}\frac{1}{2}(\frac{A_{12}}{R}+\frac{2A_{66}}{R})\alpha_j^2 w_{jk}^2 I_{10}I_{12}+\sum_{j=1}^{J}\sum_{k=1}^{K}(\frac{A_{12}}{R}+\frac{2A_{66}}{R})\alpha_j^2 w_j w_{jk}I_4 I_{12}\\
&+\sum_{j=1}^{J}\sum_{k=1}^{K}\frac{3A_{22}}{2R^3}(v_{jk}+\beta_k w_{jk})^2 I_9 I_{11}\\
K_{11}\ (5,9) = &(\frac{A_{22}}{R^2}+A_{12}\alpha_m^2)\Theta l\beta_n w_m\delta_{jm}\delta_{nq}+\frac{A_{12}}{R}\Theta l\alpha_m\beta_n u_m\delta_{jm}\delta_{nq}\\
&+\sum_{k=1}^{K}\frac{A_{22}}{R^2}l(v_{mk}+\beta_k w_{mk})I_7\delta_{jm}+\sum_{k=1}^{K}\frac{A_{22}}{R^2}l\beta_q\beta_n(v_{mk}+\beta_k w_{mk})I_3\delta_{jm}\\
&+\sum_{k=1}^{K}\frac{A_{22}}{R^2}l\beta_n(\beta_k v_{mk}+w_{mk})I_4\delta_{jm}+\sum_{j=1}^{J}\frac{1}{2}(\frac{A_{12}}{R}+\frac{2A_{66}}{R})\alpha_j^2\beta_n\Theta w_j^2 I_{12}\delta_{nq}\\
&+\sum_{k=1}^{K}\frac{3A_{22}}{R^3}\beta_n l(v_k+\beta_k w_k)(v_{mk}+\beta_k w_{mk})I_9\delta_{jm}-\sum_{k=1}^{K}A_{66}\alpha_m^2 l v_{mk}I_7\delta_{jm}\\
&+\sum_{k=1}^{K}A_{12}l\alpha_m^2\beta_q w_{mk}I_8\delta_{jm}+\sum_{k=1}^{K}(\frac{A_{12}}{R}+\frac{2A_{66}}{R})l\alpha_m^2(v_k+\beta_k w_k)w_m I_7\delta_{jm}\\
&-\sum_{k=1}^{K}\frac{A_{66}}{R}\alpha_m\beta_k l u_{mk}I_7\delta_{jm}+\sum_{k=1}^{K}(\frac{A_{12}}{R}+\frac{2A_{66}}{R})l\alpha_m^2(v_k+\beta_k w_k)w_{mk}I_{16}\delta_{jm}\\
&+\sum_{k=1}^{K}\frac{A_{12}}{R}l\alpha_m\beta_n u_{mk}I_4\delta_{jm}+\sum_{j=1}^{J}\sum_{k=1}^{K}\frac{3A_{22}}{2R^3}\beta_n(v_{jk}+\beta_k w_{jk})^2 I_9 I_{11}\\
&+\sum_{j=1}^{J}\sum_{k=1}^{K}\frac{1}{2}(\frac{A_{12}}{R}+\frac{2A_{66}}{R})\alpha_j^2\beta_n w_{jk}^2 I_{10}I_{12}+\sum_{j=1}^{J}\sum_{k=1}^{K}(\frac{A_{12}}{R}+\frac{2A_{66}}{R})\alpha_m\alpha_j\\
&*(v_{jk}+\beta_k w_{jk})w_j I_7 I_{14}+\sum_{j=1}^{J}\sum_{k=1}^{K}(\frac{A_{12}}{R}+\frac{2A_{66}}{R})\alpha_j^2\beta_n w_j w_{jk}I_4 I_{12}\\
&+\sum_{j=1}^{J}\sum_{k=1}^{K}(\frac{A_{12}}{R}+\frac{2A_{66}}{R})\alpha_m\alpha_j(v_{jk}+\beta_k w_{jk})w_{jk}I_{14}I_{16}
\end{aligned}
$$

$$
\begin{aligned}
K_{11}\ (6,6) =& 2(\frac{A_{22}}{R}+\beta_n^4\frac{D_{22}}{R^3})\Theta l\delta_{nq}+\frac{2A_{22}}{R^2}\Theta l\beta_n^2 w_0\delta_{nq}+\frac{A_{12}}{R}\Theta\beta_n^2 q_0\delta_{nq}\\
&+\sum_{k=1}^{K}\frac{2A_{22}}{R^2}l\beta_n\beta_q(\beta_k v_k+w_k)I_4+\sum_{k=1}^{K}\frac{2A_{22}}{R^2}\beta_n l(v_k+\beta_k w_k)I_3\\
&+\sum_{k=1}^{K}\frac{2A_{22}}{R^2}\beta_q l(v_k+\beta_k w_k)I_7+\sum_{k=1}^{K}\frac{3A_{22}}{R^3}l\beta_n\beta_q(v_k+\beta_k w_k)^2 I_9\\
&+\sum_{j=1}^{J}\frac{1}{2}(\frac{A_{12}}{R}+\frac{2A_{66}}{R})\alpha_j^2\beta_n^2\Theta l w_j^2\delta_{nq}+\sum_{j=1}^{J}\sum_{k=1}^{K}\frac{3A_{22}}{2R^3}l(v_{jk}+\beta_k w_{jk})^2\beta_n\beta_q I_9\\
&+\sum_{j=1}^{J}\sum_{k=1}^{K}\frac{1}{2}(\frac{A_{12}}{R}+\frac{2A_{66}}{R})\alpha_j^2\beta_n\beta_q l w_{jk}^2 I_{10}\\
&+\sum_{j=1}^{J}\sum_{k=1}^{K}(\frac{A_{12}}{R}+\frac{2A_{66}}{R})\alpha_j^2\beta_n\beta_q l w_j w_{jk}I_4
\end{aligned}
$$

$$
\begin{aligned}
K_{11}\ (6,7) =& -\frac{A_{66}\Theta l}{R}\alpha_m\beta_q^2 w_m\delta_{nq}\delta_{jm}-\sum_{k=1}^{K}\frac{A_{66}}{R}l\alpha_m\beta_n\beta_q w_{mk}I_4\delta_{jm}\\
&+\sum_{k=1}^{K}\frac{A_{12}}{R}\alpha_m\beta_n l(v_{mk}+\beta_k w_{mk})I_3\delta_{jm}
\end{aligned}
$$

$$
\begin{aligned}
K_{11}\ (6,8) =& (\frac{A_{22}}{R^2}-A_{66}\alpha_m^2)\Theta l\beta_n w_m\delta_{jm}\delta_{nq}+\frac{A_{12}}{R}\Theta l\alpha_m\beta_n u_m\delta_{jm}\delta_{nq}\\
&+\sum_{k=1}^{K}\frac{A_{22}}{R^2}l\beta_q(\beta_k v_{mk}+w_{mk})I_4\delta_{jm}+\sum_{k=1}^{K}\frac{A_{22}}{R^2}l(v_{mk}+\beta_k w_{mk})I_3\delta_{jm}\\
&+\sum_{k=1}^{K}\frac{A_{22}}{R^2}\beta_n\beta_q l(v_{mk}+\beta_k w_{mk})I_7\delta_{jm}-\sum_{k=1}^{K}A_{66}\alpha_m^2\beta_q l w_{mk}I_4\delta_{jm}\\
&+\sum_{k=1}^{K}\frac{A_{12}}{R}l\alpha_m\beta_q u_{mk}I_4\delta_{jm}+\sum_{j=1}^{J}\frac{1}{2}(\frac{A_{12}}{R}+\frac{2A_{66}}{R})\alpha_j^2\beta_n\Theta w_j^2 I_{12}\delta_{nq}\\
&+\sum_{k=1}^{K}\frac{3A_{22}}{R^3}l\beta_q(v_k+\beta_k w_k)(v_{mk}+\beta_k w_{mk})I_9\delta_{jm}\\
&+\sum_{j=1}^{J}\sum_{k=1}^{K}\frac{1}{2}(\frac{A_{12}}{R}+\frac{2A_{66}}{R})\alpha_j^2\beta_q w_{jk}^2 I_{10}I_{12}\\
&+\sum_{j=1}^{J}\sum_{k=1}^{K}(\frac{A_{12}}{R}+\frac{2A_{66}}{R})\alpha_j^2\beta_q w_j w_{jk}I_4 I_{12}\\
&+\sum_{j=1}^{J}\sum_{k=1}^{K}\frac{3A_{22}}{2R^3}\beta_q(v_{jk}+\beta_k w_{jk})^2 I_9 I_{11}
\end{aligned}
$$

$$K_{11}\ (6,9) =(\frac{A_{22}}{R^2}\beta_n^2 + A_{12}\alpha_m^2)\Theta l w_m \delta_{jm}\delta_{nq} + \frac{A_{12}}{R}\Theta l \alpha_m \beta_n^2 u_m \delta_{jm}\delta_{nq}$$
$$+ \sum_{k=1}^{K} \frac{A_{22}}{R^2} l\beta_q (v_{mk} + \beta_k w_{mk}) I_7 \delta_{jm} + \sum_{k=1}^{K} \frac{A_{22}}{R^2} l\beta_n (v_{mk} + \beta_k w_{mk}) I_3 \delta_{jm}$$
$$+ \sum_{k=1}^{K} \frac{A_{22}}{R^2} l\beta_n \beta_q (\beta_k v_{mk} + w_{mk}) I_4 \delta_{jm} + \sum_{j=1}^{J} \frac{1}{2}(\frac{A_{12}}{R} + \frac{2A_{66}}{R})\alpha_j^2 \beta_n^2 \Theta w_j^2 I_{12}\delta_{nq}$$
$$+ \sum_{k=1}^{K} \frac{3A_{22}}{R^3} l\beta_n \beta_q (v_k + \beta_k w_k)(v_{mk} + \beta_k w_{mk}) I_9 \delta_{jm} - \sum_{k=1}^{K} A_{66}\alpha_m^2 \beta_q l v_{mk} I_7 \delta_{jm}$$
$$+ \sum_{k=1}^{K} A_{12} l\alpha_m^2 w_{mk} I_8 \delta_{jm} + \sum_{k=1}^{K} (\frac{A_{12}}{R} + \frac{2A_{66}}{R}) l\alpha_m^2 \beta_q (v_k + \beta_k w_k) w_m I_7 \delta_{jm}$$
$$+ \sum_{k=1}^{K} \frac{A_{12}}{R} l\alpha_m \beta_n \beta_q u_{mk} I_4 \delta_{jm} - \sum_{k=1}^{K} \frac{A_{66}}{R} \alpha_m \beta_q \beta_k l u_{mk} I_7 \delta_{jm}$$
$$+ \sum_{k=1}^{K} (\frac{A_{12}}{R} + \frac{2A_{66}}{R}) l\alpha_m^2 \beta_q (v_k + \beta_k w_k) w_{mk} I_{16} \delta_{jm}$$
$$+ \sum_{j=1}^{J}\sum_{k=1}^{K} \frac{3A_{22}}{2R^3} \beta_n \beta_q (v_{jk} + \beta_k w_{jk})^2 I_9 I_{11}$$
$$+ \sum_{j=1}^{J}\sum_{k=1}^{K} \frac{1}{2}(\frac{A_{12}}{R} + \frac{2A_{66}}{R})\alpha_j^2 \beta_n \beta_q w_{jk}^2 I_{10} I_{12}$$
$$+ \sum_{j=1}^{J}\sum_{k=1}^{K} (\frac{A_{12}}{R} + \frac{2A_{66}}{R})\alpha_j^2 \beta_n \beta_q w_j w_{jk} I_4 I_{12}$$
$$+ \sum_{j=1}^{J}\sum_{k=1}^{K} (\frac{A_{12}}{R} + \frac{2A_{66}}{R}) l\alpha_m \alpha_j \beta_q (v_{jk} + \beta_k w_{jk}) w_j I_7 I_{14}$$
$$+ \sum_{j=1}^{J}\sum_{k=1}^{K} (\frac{A_{12}}{R} + \frac{2A_{66}}{R}) l\alpha_m \alpha_j \beta_q (v_{jk} + \beta_k w_{jk}) w_{jk} I_{14} I_{16}$$

$$K_{11}\ (7,7) =(A_{11}\alpha_m^2 + \frac{A_{66}}{R^2}\beta_n^2) l\Theta R \delta_{mp}\delta_{nq}$$

$$K_{11}\ (7,8) =(A_{12} + A_{66})\alpha_m \beta_n l\Theta \delta_{mp}\delta_{nq} + \sum_{k=1}^{K} \frac{A_{12}}{R} l\alpha_m (v_k + \beta_k w_k) I_3 \delta_{mp}$$
$$- \sum_{j=1}^{J} \frac{A_{66}}{R} \alpha_j \beta_n \Theta w_j I_5 \delta_{nq} + \sum_{j=1}^{J}\sum_{k=1}^{K} \frac{A_{12}}{R} \alpha_p (v_{jk} + \beta_k w_{jk}) I_1 I_3$$
$$- \sum_{j=1}^{J}\sum_{k=1}^{K} \frac{A_{66}}{R} \alpha_j \beta_q w_{jk} I_4 I_5$$

$$K_{11}(7,9) = A_{12}\alpha_m\Theta l\delta_{mp}\delta_{nq} + \sum_{k=1}^{K}\frac{A_{12}}{R}l\alpha_m\beta_n(v_k+\beta_k w_k)I_3\delta_{mp} - \sum_{k=1}^{K}\frac{A_{66}}{R}l\alpha_m\beta_q(v_k$$
$$+\beta_k w_k)I_7\delta_{mp} + \sum_{j=1}^{J}A_{11}\Theta R\alpha_m\alpha_p\alpha_j w_j I_2\delta_{nq} - \sum_{j=1}^{J}\frac{A_{66}}{R}\alpha_j\beta_n^2\Theta w_j I_5\delta_{nq}$$
$$-\sum_{j=1}^{J}\sum_{k=1}^{K}\frac{A_{66}}{R}\alpha_j\beta_n\beta_q w_{jk}I_4I_5 - \sum_{j=1}^{J}\sum_{k=1}^{K}\frac{A_{66}}{R}\alpha_m\beta_q(v_{jk}+\beta_k w_{jk})I_6I_7$$
$$+\sum_{j=1}^{J}\sum_{k=1}^{K}A_{11}R\alpha_m\alpha_p\alpha_j w_{jk}I_2I_8 + \sum_{j=1}^{J}\sum_{k=1}^{K}\frac{A_{12}}{R}\alpha_p\beta_n(v_{jk}+\beta_k w_{jk})I_1I_3$$

$$K_{11}(8,8) = (\frac{A_{22}}{R}+\frac{D_{22}}{R^3})\beta_n^2\Theta l\delta_{mp}\delta_{nq} + (A_{66}+\frac{D_{66}}{R^2})\alpha_m^2 l\Theta R\delta_{mp}\delta_{nq} + \frac{A_{22}}{R^2}\Theta l w_0\delta_{mp}\delta_{nq}$$
$$+\frac{A_{12}}{2R}\Theta q_0\delta_{mp}\delta_{nq} + \sum_{k=1}^{K}\frac{A_{22}}{R^2}l(\beta_k v_k+w_k)I_4\delta_{mp} + \sum_{k=1}^{K}\frac{A_{22}}{R^2}\beta_q l(v_k+\beta_k w_k)$$
$$*I_3\delta_{mp} + \sum_{k=1}^{K}\frac{A_{22}}{R^2}\beta_n l(v_k+\beta_k w_k)I_7\delta_{mp} + \sum_{k=1}^{K}\frac{3A_{22}}{2R^3}l(v_k+\beta_k w_k)^2 I_9\delta_{mp}$$
$$+\sum_{j=1}^{J}\frac{A_{12}}{R}\Theta\alpha_j u_j I_1\delta_{nq} - \sum_{j=1}^{J}A_{66}\Theta\alpha_j(\alpha_m I_2+\alpha_p I_5)w_j\delta_{nq}$$
$$+\sum_{j=1}^{J}\frac{A_{22}}{R^2}\Theta w_j I_1\delta_{nq} + \sum_{j=1}^{J}\frac{1}{2}(\frac{A_{12}}{R}+\frac{2A_{66}}{R})\alpha_j^2\Theta w_j^2 I_{20}\delta_{nq}$$
$$+\sum_{j=1}^{J}\sum_{k=1}^{K}\frac{A_{12}}{R}\alpha_j u_{jk}I_1I_4 + \sum_{j=1}^{J}\sum_{k=1}^{K}\frac{3A_{22}}{2R^3}(v_{jk}+\beta_k w_{jk})^2 I_9I_{19}$$
$$+\sum_{j=1}^{J}\sum_{k=1}^{K}\frac{A_{22}}{R^2}(\beta_k v_{jk}+w_{jk})I_1I_4 + \sum_{j=1}^{J}\sum_{k=1}^{K}\frac{A_{22}}{R^2}\beta_q(v_{jk}+\beta_k w_{jk})I_1I_3$$
$$+\sum_{j=1}^{J}\sum_{k=1}^{K}\frac{A_{22}}{R^2}\beta_n(v_k+\beta_k w_k)I_1I_7 - \sum_{j=1}^{J}\sum_{k=1}^{K}A_{66}\alpha_j(\alpha_m I_2+\alpha_p I_5)w_{jk}I_4$$
$$+\sum_{j=1}^{J}\sum_{k=1}^{K}\frac{1}{2}(\frac{A_{12}}{R}+\frac{2A_{66}}{R})\alpha_j^2 w_{jk}^2 I_{10}I_{20} + \sum_{j=1}^{J}\sum_{k=1}^{K}(\frac{A_{12}}{R}+\frac{2A_{66}}{R})\alpha_j^2 w_j w_{jk}I_4I_{20}$$
$$+\sum_{j=1}^{J}\sum_{k=1}^{K}\frac{3A_{22}}{R^3}(v_k+\beta_k w_k)(v_{jk}+\beta_k w_{jk})I_1I_9$$

$$
\begin{aligned}
K_{11}\ (8,9) = &\Big[\Big(\frac{A_{22}}{R}+\beta_n^2\frac{D_{22}}{R^3}\Big)+\Big(\frac{D_{12}+2D_{66}}{R}\Big)\alpha_m^2\Big]\beta_n\Theta l\delta_{mp}\delta_{nq}+\frac{A_{22}}{R^2}\Theta\beta_n l w_0\delta_{mp}\delta_{nq}\\
&+\frac{A_{12}}{2R}\Theta\beta_n q_0\delta_{mp}\delta_{nq}+\sum_{j=1}^{J}A_{12}\Theta\alpha_j\alpha_m\beta_n w_j I_2\delta_{nq}+\sum_{j=1}^{J}\frac{A_{22}}{R^2}\Theta\beta_n w_j I_1\delta_{nq}\\
&+\sum_{j=1}^{J}\frac{1}{2}\Big(\frac{A_{12}}{R}+\frac{2A_{66}}{R}\Big)\alpha_j^2\Theta\beta_n w_j^2 I_{20}\delta_{nq}-\sum_{j=1}^{J}A_{66}\Theta\alpha_j\alpha_p\beta_n w_j I_5\delta_{nq}\\
&+\sum_{j=1}^{J}\frac{A_{12}}{R}\Theta\alpha_j\beta_n u_j I_1\delta_{nq}-\sum_{k=1}^{K}A_{66}l\alpha_m^2(v_k+\beta_k w_k)I_7\delta_{mp}\\
&+\sum_{k=1}^{K}\frac{A_{22}}{R^2}\beta_n\beta_q l(v_k+\beta_k w_k)I_3\delta_{mp}+\sum_{k=1}^{K}\frac{A_{22}}{R^2}l\beta_n(\beta_k v_k+w_k)I_4\delta_{mp}\\
&+\sum_{k=1}^{K}\frac{A_{22}}{R^2}l(v_k+\beta_k w_k)I_7\delta_{mp}+\sum_{k=1}^{K}\frac{3A_{22}}{2R^3}\beta_n l(v_k+\beta_k w_k)^2 I_9\delta_{mp}\\
&+\sum_{j=1}^{J}\sum_{k=1}^{K}\frac{A_{12}}{R}\alpha_j\beta_n u_{jk}I_1 I_4+\sum_{j=1}^{J}\sum_{k=1}^{K}\frac{3A_{22}}{2R^3}\beta_n(v_{jk}+\beta_k w_{jk})^2 I_9 I_{19}\\
&+\sum_{j=1}^{J}\sum_{k=1}^{K}\frac{A_{22}}{R^2}\beta_n(\beta_k v_{jk}+w_{jk})I_1 I_4+\sum_{j=1}^{J}\sum_{k=1}^{K}\frac{A_{22}}{R^2}\beta_q\beta_n(v_{jk}+\beta_k w_{jk})I_1 I_3\\
&+\sum_{j=1}^{J}\sum_{k=1}^{K}\frac{A_{22}}{R^2}(v_{jk}+\beta_k w_{jk})I_1 I_7-\sum_{j=1}^{J}\sum_{k=1}^{K}A_{66}\alpha_m(\alpha_j I_2+\alpha_p I_6)v_{jk}I_7\\
&-\sum_{j=1}^{J}\sum_{k=1}^{K}\frac{A_{66}}{R}\alpha_m\beta_k u_{jk}I_2 I_7+\sum_{j=1}^{J}\sum_{k=1}^{K}A_{12}\alpha_j\alpha_m\beta_q w_{jk}I_2 I_8\\
&-\sum_{j=1}^{J}\sum_{k=1}^{K}A_{66}\alpha_j\alpha_p\beta_n w_{jk}I_4 I_5+\sum_{j=1}^{J}\sum_{k=1}^{K}\frac{1}{2}\Big(\frac{A_{12}}{R}+\frac{2A_{66}}{R}\Big)\alpha_j^2\beta_n w_{jk}^2 I_{10}I_{20}\\
&-\sum_{j=1}^{J}\sum_{k=1}^{K}A_{66}\alpha_m\alpha_p\beta_k w_{jk}I_6 I_7+\sum_{j=1}^{J}\sum_{k=1}^{K}\Big(\frac{A_{12}}{R}+\frac{2A_{66}}{R}\Big)\alpha_j^2\beta_n w_j w_{jk}I_4 I_{20}\\
&+\sum_{j=1}^{J}\sum_{k=1}^{K}\frac{3A_{22}}{R^3}\beta_n(v_k+\beta_k w_k)(v_{jk}+\beta_k w_{jk})I_1 I_9\\
&+\sum_{j=1}^{J}\sum_{k=1}^{K}\Big(\frac{A_{12}}{R}+\frac{2A_{66}}{R}\Big)\alpha_j\alpha_m(v_k+\beta_k w_k)w_j I_2 I_7
\end{aligned}
$$

$$K_{11}\ (8,9)\ cont'd. = + \sum_{j=1}^{J}\sum_{k=1}^{K}(\frac{A_{12}}{R} + \frac{2A_{66}}{R})\alpha_j\alpha_m(v_{jk} + \beta_k w_{jk})w_j I_7 I_{21}$$

$$+ \sum_{j=1}^{J}\sum_{k=1}^{K}(\frac{A_{12}}{R} + \frac{2A_{66}}{R})\alpha_j\alpha_m(v_k + \beta_k w_k)w_{jk} I_2 I_{16}$$

$$+ \sum_{j=1}^{J}\sum_{k=1}^{K}(\frac{A_{12}}{R} + \frac{2A_{66}}{R})\alpha_j\alpha_m(v_{jk} + \beta_k w_{jk})w_{jk} I_{16} I_{21}$$

$$K_{11}\ (9,9) = [(\frac{A_{22}}{R} + \beta_n^4\frac{D_{22}}{R^3}) + 2(\frac{D_{12} + 2D_{66}}{R})\alpha_m^2\beta_n^2 + D_{11}R\alpha_m^4]\Theta l\delta_{mp}\delta_{nq}$$

$$+ (A_{12}\alpha_m^2 + \frac{A_{22}}{R^2}\beta_n^2)\Theta l w_0\delta_{mp}\delta_{nq} + (\frac{A_{11}}{2}R\alpha_m^2 + \frac{A_{12}}{2R}\beta_n^2)\Theta q_0\delta_{mp}\delta_{nq}$$

$$+ \sum_{j=1}^{J} A_{12}\Theta(\alpha_j\alpha_m I_2 + \alpha_j\alpha_p I_5 + \alpha_p\alpha_m I_6)w_j\delta_{nq} + \sum_{j=1}^{J}\frac{A_{22}}{R^2}\Theta\beta_n^2 w_j I_1\delta_{nq}$$

$$+ \sum_{j=1}^{J}\frac{1}{2}(\frac{A_{12}}{R} + \frac{2A_{66}}{R})\alpha_j^2\Theta\beta_n^2 w_j^2 I_{20}\delta_{nq} + \sum_{j=1}^{J} A_{11}\Theta R\alpha_j\alpha_p\alpha_m u_j I_6\delta_{nq}$$

$$+ \sum_{j=1}^{J} 1.5A_{11}\Theta R\alpha_j^2\alpha_p\alpha_m w_j^2 I_{23}\delta_{nq} + \sum_{k=1}^{K} A_{12}l\alpha_m^2(\beta_k v_k + w_k)I_8\delta_{mp}$$

$$+ \sum_{k=1}^{K}\frac{A_{22}}{R^2}\beta_n l(v_k + \beta_k w_k)I_3\delta_{mp} + \sum_{k=1}^{K}\frac{A_{22}}{R^2}l\beta_q\beta_n(\beta_k v_k + w_k)I_4\delta_{mp}$$

$$+ \sum_{k=1}^{K}\frac{A_{22}}{R^2}l\beta_q(v_k + \beta_k w_k)I_7\delta_{mp} + \sum_{k=1}^{K}\frac{3A_{22}}{2R^3}l\beta_n\beta_q(v_k + \beta_k w_k)^2 I_9\delta_{mp}$$

$$+ \sum_{k=1}^{K}\frac{1}{2}(\frac{A_{12}}{R} + \frac{2A_{66}}{R})\alpha_m^2 l(v_k + \beta_k w_k)^2 I_{28}\delta_{mp} + \sum_{j=1}^{J}\frac{A_{12}}{R}\Theta\alpha_j\beta_n^2 u_j I_1\delta_{nq}$$

$$+ \sum_{j=1}^{J}\sum_{k=1}^{K}\frac{A_{12}}{R}\alpha_j\beta_n\beta_q u_{jk} I_1 I_4 + \sum_{j=1}^{J}\sum_{k=1}^{K}\frac{3A_{22}}{2R^3}\beta_n\beta_q(v_{jk} + \beta_k w_{jk})^2 I_9 I_{19}$$

$$+ \sum_{j=1}^{J}\sum_{k=1}^{K}\frac{A_{22}}{R^2}\beta_n\beta_q(\beta_k v_{jk} + w_{jk})I_1 I_4 + \sum_{j=1}^{J}\sum_{k=1}^{K}\frac{A_{22}}{R^2}\beta_n(v_{jk} + \beta_k w_{jk})I_1 I_3$$

$$+ \sum_{j=1}^{J}\sum_{k=1}^{K}\frac{A_{22}}{R^2}\beta_q(v_{jk} + \beta_k w_{jk})I_1 I_7 - \sum_{j=1}^{J}\sum_{k=1}^{K}\frac{A_{66}}{R}\alpha_p\beta_n\beta_k u_{jk} I_3 I_5$$

$$- \sum_{j=1}^{J}\sum_{k=1}^{K}\frac{A_{66}}{R}\alpha_m\beta_q\beta_k u_{jk} I_2 I_7 - \sum_{j=1}^{J}\sum_{k=1}^{K} A_{66}\alpha_m\alpha_j\beta_q v_{jk} I_2 I_7$$

$$- \sum_{j=1}^{J}\sum_{k=1}^{K} A_{66}\alpha_j\alpha_p\beta_n v_{jk} I_3 I_5 + \sum_{j=1}^{J}\sum_{k=1}^{K}\frac{1}{2}(\frac{A_{12}}{R} + \frac{2A_{66}}{R})\alpha_j^2\beta_n\beta_q w_{jk}^2 I_{10} I_{20}$$

$$
\begin{aligned}
K_{11}\ (9,9) \\ \textit{cont'd.}
&= + \sum_{j=1}^{J}\sum_{k=1}^{K}\left(\frac{A_{12}}{R}+\frac{2A_{66}}{R}\right)\alpha_j^2\beta_n\beta_q w_j w_{jk} I_4 I_{20} \\
&+ \sum_{j=1}^{J}\sum_{k=1}^{K}\frac{3A_{22}}{R^3}\beta_n\beta_q(v_k+\beta_k w_k)(v_{jk}+\beta_k w_{jk})I_1 I_9 \\
&+ \sum_{j=1}^{J}\sum_{k=1}^{K}\left(\frac{A_{12}}{R}+\frac{2A_{66}}{R}\right)\alpha_j\alpha_m\beta_q(v_k+\beta_k w_k)w_j I_2 I_7 \\
&+ \sum_{j=1}^{J}\sum_{k=1}^{K}\left(\frac{A_{12}}{R}+\frac{2A_{66}}{R}\right)\alpha_j\alpha_m\beta_q(v_{jk}+\beta_k w_{jk})w_j I_7 I_{21} \\
&+ \sum_{j=1}^{J}\sum_{k=1}^{K}\left(\frac{A_{12}}{R}+\frac{2A_{66}}{R}\right)\alpha_j\alpha_m\beta_q(v_k+\beta_k w_k)w_{jk} I_2 I_{16} \\
&+ \sum_{j=1}^{J}\sum_{k=1}^{K}\left(\frac{A_{12}}{R}+\frac{2A_{66}}{R}\right)\alpha_j\alpha_m\beta_q(v_{jk}+\beta_k w_{jk})w_j I_{16} I_{21} \\
&+ \sum_{j=1}^{J}\sum_{k=1}^{K}A_{11}R\alpha_j\alpha_p\alpha_m u_{jk} I_6 I_8 + \sum_{j=1}^{J}\sum_{k=1}^{K}1.5A_{11}R\alpha_j^2\alpha_p\alpha_m w_{jk}^2 I_{23} I_{27} \\
&+ \sum_{j=1}^{J}\sum_{k=1}^{K}3A_{11}R\alpha_j^2\alpha_p\alpha_m w_j w_{jk} I_8 I_{23} + \sum_{j=1}^{J}\sum_{k=1}^{K}A_{12}\alpha_p\alpha_m\beta_k v_{jk} I_6 I_8 \\
&+ \sum_{j=1}^{J}\sum_{k=1}^{K}A_{12}(\alpha_j\alpha_m I_2+\alpha_j\alpha_p I_5+\alpha_p\alpha_m I_6)w_{jk} I_8 \\
&+ \sum_{j=1}^{J}\sum_{k=1}^{K}\frac{1}{2}\left(\frac{A_{12}}{R}+\frac{2A_{66}}{R}\right)\alpha_m\alpha_p(v_{jk}+\beta_k w_{jk})^2 I_{24} I_{28} \\
&+ \sum_{j=1}^{J}\sum_{k=1}^{K}\left(\frac{A_{12}}{R}+\frac{2A_{66}}{R}\right)\alpha_p\alpha_m(v_k+\beta_k w_k)(v_{jk}+\beta_k w_{jk})I_6 I_{28} \\
&+ \sum_{j=1}^{J}\sum_{k=1}^{K}\left(\frac{A_{12}}{R}+\frac{2A_{66}}{R}\right)\alpha_j\alpha_p\beta_n(v_k+\beta_k w_k)w_j I_3 I_5 \\
&+ \sum_{j=1}^{J}\sum_{k=1}^{K}\left(\frac{A_{12}}{R}+\frac{2A_{66}}{R}\right)\alpha_j\alpha_p\beta_n(v_{jk}+\beta_k w_{jk})w_j I_3 I_{34} \\
&+ \sum_{j=1}^{J}\sum_{k=1}^{K}\left(\frac{A_{12}}{R}+\frac{2A_{66}}{R}\right)\alpha_j\alpha_p\beta_n(v_k+\beta_k w_k)w_{jk} I_5 I_{26} \\
&+ \sum_{j=1}^{J}\sum_{k=1}^{K}\left(\frac{A_{12}}{R}+\frac{2A_{66}}{R}\right)\alpha_j\alpha_p\beta_n(v_{jk}+\beta_k w_{jk})w_{jk} I_{26} I_{34}
\end{aligned}
$$

Elements of $(3MN + 2M + 2N + 2) \times (3MN + 2M + 2N + 2)$ **submatrix** $[L(\hat{u}_{shell})]$

$$L(1,1) = 0$$

$$L(1,2) = 2\Theta(R + w_0)$$

$$L(1,3) = 0$$

$$L(1,4) = \Theta w_m \delta_{jm}$$

$$L(1,5) = (v_n + \beta_n w_n)\Theta \delta_{kn}$$

$$L(1,6) = (\beta_n v_n + w_n)\Theta \delta_{kn}$$

$$L(1,7) = 0$$

$$L(1,8) = \frac{1}{2}(v_{mn} + \beta_n w_{mn})\Theta \delta_{jm}\delta_{kn}$$

$$L(1,9) = \frac{1}{2}(\beta_n v_{mn} + w_{mn})\Theta \delta_{jm}\delta_{kn}$$

$$L(2,2) = 2\Theta(2l + q_0)$$

$$L(2,3) = 2\alpha_m \Theta l w_m \delta_{jm}$$

$$L(2,4) = 2\alpha_m \Theta l u_m \delta_{jm}$$

$$L(2,5) = 0$$

$$L(2,6) = 0$$

$$L(2,7) = \alpha_m \Theta l w_{mn} \delta_{jm}\delta_{kn}$$

$$L(2,8) = 0$$

$$L(2,9) = \alpha_m \Theta l u_{mn} \delta_{jm}\delta_{kn}$$

$$L(3,3) = 0$$

$$L(3,4) = 2\alpha_m \Theta l(R + w_0)\delta_{mp} + \sum_{j=1}^{J} 2\alpha_p \Theta w_j I_1$$

$$L(3,5) = \alpha_p \Theta l(v_{pn} + \beta_n w_{pn})\delta_{jp}\delta_{kn}$$

$$L(3,6) = \alpha_p \Theta l(\beta_n v_{pn} + w_{pn})\delta_{jp}\delta_{kn}$$

$$L(3,7) = 0$$

$$L(3,8) = \alpha_m \Theta l(v_n + \beta_n w_n)\delta_{mp}\delta_{kn} + \sum_{j=1}^{J} \frac{2}{3}\alpha_p \beta_n \Theta w_{jn} I_1 \delta_{kn}$$
$$+ \sum_{j=1}^{J} \alpha_p \Theta v_{jn} I_1 \delta_{kn} + \sum_{j=1}^{J} \frac{1}{3}\beta_n \Theta(\alpha_j I_5 + \alpha_m I_6) w_{jn}\delta_{kn}$$

$$L(3,9) = \alpha_m \Theta l(\beta_n v_n + w_n)\delta_{mp}\delta_{kn} + \sum_{j=1}^{J} \frac{2}{3}\alpha_p \beta_n \Theta v_{jn} I_1 \delta_{kn}$$
$$+ \sum_{j=1}^{J} \alpha_p \Theta w_{jn} I_1 \delta_{kn} + \sum_{j=1}^{J} \frac{1}{3}\beta_n \Theta(\alpha_j I_5 + \alpha_m I_6) v_{jn}\delta_{kn}$$

$$L(4,4) = \Theta(2l + q_0)\delta_{mp} + \sum_{j=1}^{J} 2\alpha_j \Theta u_j I_1$$

$$L(4,5) = \alpha_p \beta_n \Theta l u_{pn}\delta_{jp}\delta_{kn}$$

$$L(4,6) = \alpha_p \Theta l u_{pn}\delta_{jp}\delta_{kn}$$

$$L(4,7) = \alpha_m \Theta l(\beta_n v_n + w_n)\delta_{mp}\delta_{kn} + \sum_{j=1}^{J} \frac{2}{3}\alpha_p \beta_n \Theta v_{jn} I_6 \delta_{kn}$$
$$+ \sum_{j=1}^{J} \alpha_m \Theta w_{jn} I_1 \delta_{kn} + \sum_{j=1}^{J} \frac{1}{3}\beta_n \Theta(\alpha_m I_1 - \alpha_j I_2) v_{jn}\delta_{kn}$$

$$L(4,8) = \sum_{j=1}^{J} \frac{2}{3}\alpha_p \beta_n \Theta u_{jn} I_5 \delta_{kn} + \sum_{j=1}^{J} \frac{1}{3}\beta_n \Theta(\alpha_j I_1 - \alpha_m I_2) u_{jn}\delta_{kn}$$

$$L(4,9) = \sum_{j=1}^{J} \alpha_j \Theta u_{jn} I_1 \delta_{kn}$$

$$L(5,5) = \Theta(2l + q_0)\delta_{nq}$$

$$L(5,6) = \beta_n \Theta(2l + q_0)\delta_{nq}$$

$$L(5,7) = \alpha_m \beta_n \Theta l w_m \delta_{nq} + \sum_{k=1}^{K} \frac{1}{3}\alpha_m l(3v_{mk} + \beta_k w_{mk}) I_7 \delta_{jm}$$
$$+ \sum_{k=1}^{K} \frac{2}{3}\alpha_m \beta_q l w_{mk} I_8 \delta_{jm} + \sum_{k=1}^{K} \frac{1}{3}\alpha_m \beta_n l w_{mk} I_4 \delta_{jm}$$

$$L(5,8) = \alpha_m \Theta l u_m \delta_{nq} + \sum_{k=1}^{K} \alpha_m l u_{mk} I_4 \delta_{jm}$$

$$L(5,9) = \alpha_m\beta_n\Theta l u_m\delta_{nq} + \sum_{k=1}^{K}\frac{2}{3}\alpha_m\beta_q l u_{mk}I_8\delta_{jm} + \sum_{k=1}^{K}\frac{1}{3}\alpha_m l(\beta_n I_4 + \beta_k I_7)u_{mk}\delta_{jm}$$

$$L(6,6) = \Theta(2l + q_0)\delta_{nq}$$

$$L(6,7) = \alpha_m\Theta l w_m\delta_{nq} + \sum_{k=1}^{K}\frac{1}{3}\alpha_m l(\beta_k I_8 - \beta_n I_3)v_{mk}\delta_{jm}$$
$$+ \sum_{k=1}^{K}\frac{2}{3}\alpha_m\beta_q l v_{mk}I_7\delta_{jm} + \sum_{k=1}^{K}\alpha_m l w_{mk}I_8\delta_{jm}$$

$$L(6,8) = \alpha_m\beta_n\Theta l u_m\delta_{nq} + \sum_{k=1}^{K}\frac{2}{3}\alpha_m\beta_q l u_{mk}I_4\delta_{jm} + \sum_{k=1}^{K}\frac{1}{3}\alpha_m l(\beta_n I_8 - \beta_k I_3)u_{mk}\delta_{jm}$$

$$L(6,9) = \alpha_m\Theta l u_m\delta_{nq} + \sum_{k=1}^{K}\alpha_m l u_{mk}I_8\delta_{jm}$$

$$L(7,7) = 0$$

$$L(7,8) = \sum_{k=1}^{K}\frac{1}{3}\alpha_m l(\beta_n I_8 - \beta_q I_4)w_k\delta_{mp} + \sum_{k=1}^{K}\frac{2}{3}\alpha_m\beta_k l w_k I_3\delta_{mp} + \sum_{k=1}^{K}\alpha_m l v_k I_3\delta_{mp}$$
$$+ \sum_{j=1}^{J}\frac{2}{3}\alpha_j\beta_n\Theta w_j I_5\delta_{nq} + \sum_{j=1}^{J}\frac{1}{3}\beta_n\Theta(\alpha_p I_1 - \alpha_m I_6)w_j\delta_{nq} + \sum_{j=1}^{J}\sum_{k=1}^{K}\alpha_p v_{jk}I_1 I_3$$
$$+ \sum_{j=1}^{J}\sum_{k=1}^{K}\frac{1}{3}\beta_k(\alpha_p I_1 + \alpha_m I_6)w_{jk}I_3 + \sum_{j=1}^{J}\sum_{k=1}^{K}\frac{1}{3}\beta_n(\alpha_p I_1 + \alpha_j I_5)w_{jk}I_8$$
$$+ \sum_{j=1}^{J}\sum_{k=1}^{K}\frac{1}{3}\beta_q(\alpha_j I_5 - \alpha_m I_6)w_{jk}I_4$$

$$L(7,9) = \alpha_m\Theta l(R + w_0)\delta_{mp}\delta_{nq} + \sum_{j=1}^{J}\alpha_p\Theta w_j I_1\delta_{nq} + \sum_{k=1}^{K}\frac{2}{3}\alpha_m l v_k I_8\delta_{mp}$$
$$+ \sum_{k=1}^{K}\frac{1}{3}\alpha_m l(\beta_n I_3 + \beta_q I_7)v_k\delta_{mp} + \sum_{k=1}^{K}\alpha_m l w_k I_8\delta_{mp} + \sum_{j=1}^{J}\sum_{k=1}^{K}\alpha_p w_{jk}I_1 I_8$$
$$+ \sum_{j=1}^{J}\sum_{k=1}^{K}\frac{1}{3}\beta_k(\alpha_p I_1 + \alpha_m I_6)v_{jk}I_8 + \sum_{j=1}^{J}\sum_{k=1}^{K}\frac{1}{3}\beta_n(\alpha_p I_1 + \alpha_j I_5)v_{jk}I_3$$
$$+ \sum_{j=1}^{J}\sum_{k=1}^{K}\frac{1}{3}\beta_q(\alpha_m I_6 - \alpha_j I_5)v_{jk}I_7$$

$$L(8,8) = \frac{1}{2}\Theta(2l + q_0)\delta_{mp}\delta_{nq} + \sum_{j=1}^{J}\alpha_j\Theta u_j I_1\delta_{nq} + \sum_{j=1}^{J}\sum_{k=1}^{K}\alpha_j u_{jk}I_1 I_4$$

$$L(8,9) = \frac{1}{2}\beta_n\Theta(2l+q_0)\delta_{mp}\delta_{nq} + \sum_{j=1}^{J}\frac{2}{3}\alpha_j\beta_n\Theta u_j I_1\delta_{nq} + \sum_{j=1}^{J}\frac{1}{3}\beta_n\Theta(\alpha_p I_5 + \alpha_m I_2)u_j\delta_{nq}$$
$$+ \sum_{j=1}^{J}\sum_{k=1}^{K}\frac{1}{3}\beta_k(\alpha_m I_2 - \alpha_p I_5)u_{jk}I_7 + \sum_{j=1}^{J}\sum_{k=1}^{K}\frac{1}{3}\beta_n(\alpha_j I_1 + \alpha_p I_5)u_{jk}I_4$$
$$+ \sum_{j=1}^{J}\sum_{k=1}^{K}\frac{1}{3}\beta_q(\alpha_m I_2 + \alpha_j I_1)u_{jk}I_8$$

$$L(9,9) = \frac{1}{2}\Theta(2l+q_0)\delta_{mp}\delta_{nq} + \sum_{j=1}^{J}\alpha_j\Theta u_j I_1\delta_{nq} + \sum_{j=1}^{J}\sum_{k=1}^{K}\alpha_j u_{jk}I_1 I_8$$

Elements of $(2M+1)\times(2M+1)$ submatrix $[K_{22}(\hat{u}_{str})]$

$$K_{22}\ (1,1) = \frac{(EA)_s}{2l}$$

$$K_{22}\ (1,2) = 0$$

$$K_{22}\ (1,3) = 0.5(EA)_s\alpha_m^2 w_{sm}$$

$$K_{22}\ (2,2) = (EA)_s\alpha_m^2 l\delta_{mp}$$

$$K_{22}\ (2,3) = \sum_{j=1}^{J}(EA)_s\alpha_m\alpha_j\alpha_p w_{sj}I_2$$

$$K_{22}\ (3,3) = \left[0.5(EA)_s q_1 + (EI)_s\alpha_m^2 l\right]\alpha_m^2\delta_{mp} + \sum_{j=1}^{J}(EA)_s\alpha_m\alpha_j\alpha_p u_{sj}I_6$$
$$+ \sum_{j=1}^{J}1.5(EA)_s\alpha_m\alpha_j^2\alpha_p w_{sj}^2 I_{23}$$

Elements of $(2N+1)\times(2N+1)$ submatrix $[K_{33}(\hat{u}_r)]$

$$K_{33}\ (1,1) = 2\frac{(EA)_r}{R_0}\Theta$$

$$K_{33}\ (1,2) = \frac{(EA)_r}{R_0^2}\Theta(v_{rn}+\beta_n w_{rn})$$

$$K_{33}\ (1,3) = \frac{(EA)_r}{R_0^2}\Theta\beta_n(v_{rn}+\beta_n w_{rn})$$

$$\begin{aligned}K_{33}\ (2,2) = &\Big[\frac{(EA)_r}{R_0}+\frac{(EI)_r}{R_0^3}\Big]\beta_n^2\Theta\delta_{nq}+\frac{(EA)_r}{R_0^2}\Theta w_{r0}\delta_{nq}\\ &+\sum_{k=1}^{K}\frac{(EA)_r}{R_0^2}\beta_q(v_{rk}+\beta_k w_{rk})I_3+\sum_{k=1}^{K}\frac{(EA)_r}{R_0^2}\beta_n(v_{rk}+\beta_k w_{rk})I_7\\ &+\sum_{k=1}^{K}\frac{3(EA)_r}{2R_0^3}(v_{rk}+\beta_k w_{rk})^2 I_9+\sum_{k=1}^{K}\frac{(EA)_r}{R_0^2}(\beta_k v_{rk}+w_{rk})I_4\end{aligned}$$

$$\begin{aligned}K_{33}\ (2,3) = &\Big[\frac{(EA)_r}{R_0}+\beta_n^2\frac{(EI)_r}{R_0^3}\Big]\beta_n\Theta\delta_{nq}+\frac{(EA)_r}{R_0^2}\beta_n\Theta w_{r0}\delta_{nq}\\ &+\sum_{k=1}^{K}\frac{(EA)_r}{R_0^2}\beta_n\beta_q(v_{rk}+\beta_k w_{rk})I_3+\sum_{k=1}^{K}\frac{(EA)_r}{R_0^2}(v_{rk}+\beta_k w_{rk})I_7\\ &+\sum_{k=1}^{K}\frac{3(EA)_r}{2R_0^3}\beta_n(v_{rk}+\beta_k w_{rk})^2 I_9+\sum_{k=1}^{K}\frac{(EA)_r}{R_0^2}\beta_n(\beta_k v_{rk}+w_{rk})I_4\end{aligned}$$

$$\begin{aligned}K_{33}\ (3,3) = &\Big[\frac{(EA)_r}{R_0}+\beta_n^4\frac{(EI)_r}{R_0^3}\Big]\Theta\delta_{nq}+\frac{(EA)_r}{R_0^2}\beta_n^2\Theta w_{r0}\delta_{nq}\\ &+\sum_{k=1}^{K}\frac{(EA)_r}{R_0^2}\beta_n(v_{rk}+\beta_k w_{rk})I_3+\sum_{k=1}^{K}\frac{(EA)_r}{R_0^2}\beta_q(v_{rk}+\beta_k w_{rk})I_7\\ &+\sum_{k=1}^{K}\frac{3(EA)_r}{2R_0^3}\beta_n\beta_q(v_{rk}+\beta_k w_{rk})^2 I_9+\sum_{k=1}^{K}\frac{(EA)_r}{R_0^2}\beta_n\beta_q(\beta_k v_{rk}+w_{rk})I_4\end{aligned}$$

The integrals I_1 to I_{34} in the elements of the submatrices K_{ij} and L are given by

$$I_1 = \int_{-l}^{l} Cos(\alpha_j x)Cos(\alpha_m x)Cos(\alpha_p x)dx$$

$$I_2 = \int_{-l}^{l} Sin(\alpha_j x)Sin(\alpha_m x)Cos(\alpha_p x)dx$$

$$I_3 = \int_{-\Theta}^{\Theta} Sin(\beta_k \theta)Sin(\beta_n \theta)Cos(\beta_q \theta)d\theta$$

$$I_4 = \int_{-\Theta}^{\Theta} Cos(\beta_k \theta)Sin(\beta_n \theta)Sin(\beta_q \theta)d\theta$$

$$I_5 = \int_{-l}^{l} Cos(\alpha_m x)Sin(\alpha_j x)Sin(\alpha_p x)dx$$

$$I_6 = \int_{-l}^{l} Cos(\alpha_j x)Sin(\alpha_m x)Sin(\alpha_p x)dx$$

$$I_7 = \int_{-\Theta}^{\Theta} Cos(\beta_n \theta)Sin(\beta_k \theta)Sin(\beta_q \theta)d\theta$$

$$I_8 = \int_{-\Theta}^{\Theta} Cos(\beta_n \theta)Cos(\beta_k \theta)Cos(\beta_q \theta)d\theta$$

$$I_9 = \int_{-\Theta}^{\Theta} Sin^2(\beta_k \theta)Sin(\beta_n \theta)Sin(\beta_q \theta)d\theta$$

$$I_{10} = \int_{-\Theta}^{\Theta} Cos^2(\beta_k \theta)Sin(\beta_n \theta)Sin(\beta_q \theta)d\theta$$

$$I_{11} = \int_{-l}^{l} Cos^2(\alpha_j x)Cos(\alpha_m x)dx$$

$$I_{12} = \int_{-l}^{l} Sin^2(\alpha_j x)Cos(\alpha_m x)dx$$

$$I_{13} = \int_{-\Theta}^{\Theta} Sin(\beta_k\theta)Sin(\beta_n\theta)Sin(\beta_q\theta)d\theta$$

$$I_{14} = \int_{-l}^{l} Cos(\alpha_j x)Sin(\alpha_j x)Sin(\alpha_m x)dx$$

$$I_{15} = \int_{-\Theta}^{\Theta} Cos(\beta_k\theta)Sin(\beta_k\theta)Sin(\beta_q\theta)d\theta$$

$$I_{16} = \int_{-\Theta}^{\Theta} Cos(\beta_k\theta)Cos(\beta_n\theta)Sin(\beta_k\theta)Sin(\beta_q\theta)d\theta$$

$$I_{17} = \int_{-l}^{l} Cos^2(\alpha_j x)Cos(\alpha_p x)dx$$

$$I_{18} = \int_{-l}^{l} Sin^2(\alpha_j x)Cos(\alpha_p x)dx$$

$$I_{19} = \int_{-l}^{l} Cos^2(\alpha_j x)Cos(\alpha_m x)Cos(\alpha_p x)dx$$

$$I_{20} = \int_{-l}^{l} Sin^2(\alpha_j x)Cos(\alpha_m x)Cos(\alpha_p x)dx$$

$$I_{21} = \int_{-l}^{l} Sin(\alpha_j x)Cos(\alpha_j x)Sin(\alpha_m x)Cos(\alpha_p x)dx$$

$$I_{22} = \int_{-\Theta}^{\Theta} Sin^2(\beta_k\theta)Cos(\beta_n\theta)d\theta$$

$$I_{23} = \int_{-l}^{l} Sin^2(\alpha_j x)Sin(\alpha_m x)Sin(\alpha_p x)dx$$

$$I_{24} = \int_{-l}^{l} Cos^2(\alpha_j x)Sin(\alpha_m x)Sin(\alpha_p x)dx$$

$$I_{25} = \int_{-\Theta}^{\Theta} Cos^2(\beta_k\theta)Cos(\beta_n\theta)d\theta$$

$$I_{26} = \int_{-\Theta}^{\Theta} Cos(\beta_k\theta)Sin(\beta_k\theta)Sin(\beta_n\theta)Cos(\beta_q\theta)d\theta$$

$$I_{27} = \int_{-\Theta}^{\Theta} Cos^2(\beta_k\theta)Cos(\beta_n\theta)Cos(\beta_q\theta)d\theta$$

$$I_{28} = \int_{-\Theta}^{\Theta} Sin^2(\beta_k\theta)Cos(\beta_n\theta)Cos(\beta_q\theta)d\theta$$

$$I_{29} = \int_{-l}^{l} Sin(\alpha_j x)Sin(\alpha_m x)Sin(\alpha_p x)dx$$

$$I_{30} = \int_{-\Theta}^{\Theta} Cos(\beta_k\theta)Sin(\beta_k\theta)Sin(\beta_n\theta)d\theta$$

$$I_{31} = \int_{-\Theta}^{\Theta} Cos^2(\beta_k\theta)Cos(\beta_q\theta)d\theta$$

$$I_{32} = \int_{-\Theta}^{\Theta} Sin^2(\beta_k\theta)Cos(\beta_q\theta)d\theta$$

$$I_{33} = \int_{-l}^{l} Cos(\alpha_j x)Sin(\alpha_j x)Sin(\alpha_p x)dx$$

$$I_{34} = \int_{-l}^{l} Cos(\alpha_j x)Sin(\alpha_j x)Cos(\alpha_m x)Sin(\alpha_p x)dx$$

APPENDIX D

ELEMENTS OF RESIDUAL FORCE VECTORS FOR NONLINEAR ANALYSIS

The non-zero elements of the residual force subvectors R_{shell}, R_{str} and R_r in Eq. (4.81) for nonlinear analysis are listed below. The parameter δ_{ij} is Kronecker delta assuming the values zero for $i \neq j$, and one for $i = j$, respectively.

Elements of $(3MN + 2M + 2N + 2) \times 1$ residual force subvector $[R_{shell}(u_{\hat{shell}}; p)]$

For the sake of simplicity the residual force subvector $[R_{shell}]$ is written as

$$R_{shell} = p\, F^{ext.}_{shell} - F^{int.}_{shell}$$

in which the elements of $[F^{int.}_{shell}]$ are

$$\begin{aligned}
F^{int.}_{shell}\,(1) =& \frac{A_{11}\Theta R}{l} q_0 + 2A_{12}\Theta w_0 + \sum_{n=1}^{N} \frac{A_{12}\Theta}{2R}(v_n + \beta_n w_n)^2 + \sum_{m=1}^{M} \frac{A_{11}\Theta R}{2}\alpha_m^2 w_m^2 \\
&+ \sum_{m=1}^{M}\sum_{n=1}^{N} \frac{A_{11}\Theta R}{4}\alpha_m^2 w_{mn}^2 + \sum_{m=1}^{M}\sum_{n=1}^{N} \frac{A_{12}\Theta}{4R}(v_{mn} + \beta_n w_{mn})^2 \\
F^{int.}_{shell}\,(2) =& 2A_{12}\Theta q_0 + \frac{4A_{22}\Theta l}{R} w_0 + \sum_{n=1}^{N} \frac{A_{22}\Theta l}{R^2}(v_n + \beta_n w_n)^2 + \sum_{m=1}^{M} A_{12}\Theta l \alpha_m^2 w_m^2 \\
&+ \sum_{m=1}^{M}\sum_{n=1}^{N} \frac{A_{12}\Theta l}{2}\alpha_m^2 w_{mn}^2 + \sum_{m=1}^{M}\sum_{n=1}^{N} \frac{A_{22}\Theta l}{2R^2}(v_{mn} + \beta_n w_{mn})^2 \\
F^{int.}_{shell}\,(3) =& 2A_{11}\alpha_m^2 \Theta l R u_m \delta_{mp} + 2A_{12}\alpha_m \Theta l w_m \delta_{mp} + \sum_{n=1}^{N} \frac{A_{12}\alpha_m \Theta l}{R}(v_{mn} + \beta_n w_{mn}) \\
&* (v_n + \beta_n w_n)\delta_{mp} + \sum_{m=1}^{M} A_{11}\Theta R \alpha_m^2 \alpha_p w_m^2 I_2 + \sum_{m=1}^{M}\sum_{n=1}^{N} \frac{A_{11}\Theta R}{2}\alpha_m^2 \alpha_p w_{mn}^2 I_2 \\
&+ \sum_{m=1}^{M}\sum_{n=1}^{N} \frac{A_{12}\Theta \alpha_p}{2R}(v_{mn} + \beta_n w_{mn})^2 I_1
\end{aligned}$$

$$F^{int.}_{shell}(4) = 2A_{12}\alpha_m\Theta l u_m\delta_{mp} + 2(\frac{A_{22}}{R^2} + D_{11}\alpha_m^4)\Theta l R w_m\delta_{mp} + 2A_{12}\alpha_m^2\Theta l w_0 w_m\delta_{mp}$$
$$+ A_{11}\alpha_m^2\Theta R q_0 w_m\delta_{mp} + \sum_{n=1}^{N}\frac{1}{2}(\frac{A_{12}}{R} + \frac{2A_{66}}{R})\Theta l\alpha_m^2(v_n + \beta_n w_n)^2 w_m\delta_{mp}$$
$$- \sum_{n=1}^{N}\frac{A_{66}\Theta l}{R}\alpha_m\beta_n(v_n + \beta_n w_n)u_{mn}\delta_{mp} + \sum_{n=1}^{N}A_{12}\Theta l\alpha_m^2(\beta_n v_n + w_n)w_{mn}\delta_{mp}$$
$$+ \sum_{n=1}^{N}\frac{A_{22}\Theta l}{R^2}(v_n + \beta_n w_n)(v_{mn} + \beta_n w_{mn})\delta_{mp} + \sum_{m=1}^{M}2A_{11}\Theta R\alpha_m^2\alpha_p u_m w_m I_4$$
$$- \sum_{n=1}^{N}A_{66}\Theta l\alpha_m^2(v_n + \beta_n w_n)v_{mn}\delta_{mp} + \sum_{m=1}^{M}A_{11}\Theta R\alpha_m^3\alpha_p w_m^3 I_{13} + \sum_{m=1}^{M}A_{12}\alpha_m^2$$
$$*\Theta w_m^2 I_2 + \sum_{m=1}^{M}2A_{12}\Theta\alpha_m\alpha_p w_m^2 I_4 - \sum_{m=1}^{M}\sum_{n=1}^{N}A_{66}\Theta\alpha_p\alpha_m(v_{mn} + \beta_n w_{mn})v_{mn}I_4$$
$$+ \sum_{m=1}^{M}\sum_{n=1}^{N}(\frac{A_{12}}{R} + \frac{2A_{66}}{R})\Theta\alpha_m\alpha_p(v_n + \beta_n w_n)w_m v_{mn}I_4$$
$$+ \sum_{m=1}^{M}\sum_{n=1}^{N}\frac{1}{2}(\frac{A_{12}}{R} + \frac{2A_{66}}{R})\Theta\alpha_m\alpha_p(v_{mn} + \beta_n w_{mn})^2 w_m I_{15} + \sum_{m=1}^{M}\sum_{n=1}^{N}\frac{A_{22}\Theta}{2R^2}$$
$$*(v_{mn} + \beta_n w_{mn})^2 I_1 + \sum_{m=1}^{M}\sum_{n=1}^{N}(\frac{A_{12}}{R} + \frac{2A_{66}}{R})\Theta\alpha_m\alpha_p\beta_n(v_n + \beta_n w_n)w_m w_{mn}I_4$$
$$+ \sum_{m=1}^{M}\sum_{n=1}^{N}A_{12}\Theta\alpha_m\alpha_p(\beta_n v_{mn} + w_{mn})w_{mn}I_4 + \sum_{m=1}^{M}\sum_{n=1}^{N}\frac{A_{12}\Theta}{2}\alpha_m^2 w_{mn}^2 I_2$$
$$+ \sum_{m=1}^{M}\sum_{n=1}^{N}1.5A_{11}\Theta R\alpha_m^3\alpha_p w_m w_{mn}^2 I_{13} + \sum_{m=1}^{M}\sum_{n=1}^{N}A_{11}\Theta R\alpha_m^2\alpha_p u_{mn}w_{mn}I_4$$
$$- \sum_{m=1}^{M}\sum_{n=1}^{N}\frac{A_{66}\Theta}{R}\alpha_p\beta_n(v_{mn} + \beta_n w_{mn})u_{mn}I_4$$

$$F^{int.}_{shell}(5) = 2(\frac{A_{22}}{R} + \frac{D_{22}}{R^3})\beta_n^2\Theta l v_n\delta_{nq} + 2(\frac{A_{22}}{R} + \beta_n^2\frac{D_{22}}{R^3})\beta_n\Theta l w_n\delta_{nq} + \frac{A_{12}}{R}\Theta q_0(v_n + \beta_n$$
$$* w_n)\delta_{nq} + \frac{2A_{22}}{R^2}\Theta l w_0(v_n + \beta_n w_n)\delta_{nq} + \sum_{m=1}^{M}\frac{A_{12}}{R}\alpha_m\Theta l(v_{mn} + \beta_n w_{mn})u_m\delta_{nq}$$
$$+ \sum_{m=1}^{M}\frac{1}{2}(\frac{A_{12}}{R} + \frac{2A_{66}}{R})\alpha_m^2\Theta l(v_n + \beta_n w_n)w_m^2\delta_{nq} + \sum_{m=1}^{M}A_{12}\alpha_m^2\beta_n\Theta l w_m w_{mn}\delta_{nq}$$
$$- \sum_{m=1}^{M}\frac{A_{66}}{R}\Theta l\alpha_m\beta_n w_m u_{mn}\delta_{nq} - \sum_{m=1}^{M}A_{66}\Theta l\alpha_m^2 w_m v_{mn}\delta_{nq} + \sum_{m=1}^{M}\frac{A_{22}}{R^2}\Theta l w_m$$

$$F^{int.}_{shell}\ (5)\ cont'd. = *(v_{mn}+\beta_n w_{mn})\delta_{nq} + \sum_{n=1}^{N}\frac{A_{22}}{R^2}\beta_q l(v_n+\beta_n w_n)^2 I_3 + \sum_{n=1}^{N}\frac{A_{22}l}{R^3}(v_n+\beta_n w_n)^3 I_7$$

$$+ \sum_{n=1}^{N}\frac{2A_{22}l}{R^2}(v_n+\beta_n w_n)(\beta_n v_n + w_n)I_5 + \sum_{m=1}^{M}\sum_{n=1}^{N}\frac{A_{22}l}{2R^2}\beta_q(v_{mn}+\beta_n w_{mn})^2 I_3$$

$$+ \sum_{m=1}^{M}\sum_{n=1}^{N}\Big[\frac{A_{12}}{R}l\alpha_m(v_{mn}+\beta_n w_{mn})u_{mn} - A_{66}\alpha_m^2 l v_{mn}w_{mn} + (\frac{A_{12}}{R}+\frac{2A_{66}}{R})l$$

$$*\alpha_m^2(v_n+\beta_n w_n)w_m w_{mn} - \frac{A_{66}}{R}\alpha_m\beta_n l u_{mn}w_{mn} + \frac{A_{22}l}{R^2}(v_{mn}+\beta_n w_{mn})(\beta_n v_{mn}$$

$$+ w_{mn})\Big]I_5 + \sum_{m=1}^{M}\sum_{n=1}^{N}\frac{1.5A_{22}l}{R^3}(v_n+\beta_n w_n)(v_{mn}+\beta_n w_{mn})^2 I_7 + \sum_{m=1}^{M}\sum_{n=1}^{N}\frac{1}{2}(\frac{A_{12}}{R}$$

$$+\frac{2A_{66}}{R})\alpha_m^2 l(v_n+\beta_n w_n)w_{mn}^2 I_8 + \sum_{m=1}^{M}\sum_{n=1}^{N}0.5A_{12}\alpha_m^2\beta_q l w_{mn}^2 I_6$$

$$F^{int.}_{shell}\ (6) = 2(\frac{A_{22}}{R}+\beta_n^2\frac{D_{22}}{R^3})\beta_n\Theta l v_n\delta_{nq} + 2(\frac{A_{22}}{R}+\beta_n^4\frac{D_{22}}{R^3})\Theta l w_n\delta_{nq} + \frac{A_{12}}{R}\Theta\beta_n q_0(\beta_n w_n$$

$$+ v_n)\delta_{nq} + \frac{2A_{22}}{R^2}\Theta l\beta_n w_0(v_n+\beta_n w_n)\delta_{nq} - \sum_{m=1}^{M}\frac{A_{66}}{R}\Theta l\alpha_m\beta_n^2 w_m u_{mn}\delta_{nq}$$

$$+ \sum_{m=1}^{M}\frac{A_{12}}{R}\alpha_m\beta_n\Theta l(v_{mn}+\beta_n w_{mn})u_m\delta_{nq} - \sum_{m=1}^{M}A_{66}\Theta l\alpha_m^2\beta_n w_m v_{mn}\delta_{nq}$$

$$+ \sum_{m=1}^{M}\frac{1}{2}(\frac{A_{12}}{R}+\frac{2A_{66}}{R})\alpha_m^2\beta_n\Theta l(v_n+\beta_n w_n)w_m^2\delta_{nq} + \sum_{m=1}^{M}A_{12}\alpha_m^2\Theta l w_m w_{mn}\delta_{nq}$$

$$+ \sum_{m=1}^{M}\frac{A_{22}}{R^2}\beta_n\Theta l w_m(v_{mn}+\beta_n w_{mn})\delta_{nq} + \sum_{n=1}^{N}\frac{A_{22}l}{R^3}\beta_q(v_n+\beta_n w_n)^3 I_7 + \sum_{n=1}^{N}\frac{A_{22}l}{R^2}$$

$$*(v_n+\beta_n w_n)^2 I_3 + \sum_{n=1}^{N}\frac{2A_{22}l}{R^2}\beta_q(v_n+\beta_n w_n)(\beta_n v_n+w_n)I_5 + \sum_{m=1}^{M}\sum_{n=1}^{N}\Big[\frac{A_{12}}{R}l$$

$$*\alpha_m(v_{mn}+\beta_n w_{mn})u_{mn} - A_{66}\alpha_m^2 l v_{mn}w_{mn} + (\frac{A_{12}}{R}+\frac{2A_{66}}{R})\alpha_m^2 l w_m w_{mn}(v_n$$

$$+ \beta_n w_n) - \frac{A_{66}}{R}\alpha_m\beta_n l u_{mn}w_{mn} + \frac{A_{22}l}{R^2}(v_{mn}+\beta_n w_{mn})(\beta_n v_{mn}+w_{mn})\Big]\beta_q I_5$$

$$+ \sum_{m=1}^{M}\sum_{n=1}^{N}\frac{1.5A_{22}l}{R^3}\beta_q(v_n+\beta_n w_n)(v_{mn}+\beta_n w_{mn})^2 I_7 + \sum_{m=1}^{M}\sum_{n=1}^{N}\frac{1}{2}(\frac{A_{12}}{R}$$

$$+\frac{2A_{66}}{R})\alpha_m^2\beta_q l(v_n+\beta_n w_n)w_{mn}^2 I_8 + \sum_{m=1}^{M}\sum_{n=1}^{N}0.5A_{12}\alpha_m^2 l w_{mn}^2 I_6$$

$$F^{int.}_{shell}\ (7) = \Big[(A_{11}\alpha_m^2 + \beta_n^2\frac{A_{66}}{R^2})\Theta l R u_{mn} + (A_{12}+A_{66})\alpha_m\beta_n\Theta l v_{mn} + A_{12}\alpha_m\Theta l w_{mn}$$

$$- \frac{A_{66}}{R}\alpha_m\beta_n\Theta l(v_n+\beta_n w_n)w_m\Big]\delta_{mp}\delta_{nq} + \sum_{n=1}^{N}\frac{A_{12}}{R}\alpha_m l(v_n+\beta_n w_n)(v_{mn}+\beta_n$$

$$*w_{mn})\delta_{mp}I_3 - \sum_{n=1}^{N}\frac{A_{66}}{R}\alpha_m\beta_q l(v_n+\beta_n w_n)w_{mn}\delta_{mp}I_5 - \sum_{m=1}^{M}\frac{A_{66}}{R}\alpha_m\beta_n\Theta$$

$$*(v_{mn}+\beta_n w_{mn})w_m\delta_{nq}I_4 + \sum_{m=1}^{M}A_{11}\alpha_m^2\alpha_p\Theta R w_m w_{mn}\delta_{nq}I_2 + \sum_{m=1}^{M}\sum_{n=1}^{N}\frac{A_{12}}{2R}$$

$$*\alpha_p(v_{mn}+\beta_n w_{mn})^2 I_1 I_3 - \sum_{m=1}^{M}\sum_{n=1}^{N}\frac{A_{66}}{R}\alpha_m\beta_q(v_{mn}+\beta_n w_{mn})w_{mn}I_4 I_5$$

$$+ \sum_{m=1}^{M}\sum_{n=1}^{N}0.5A_{11}\alpha_m^2\alpha_p R w_{mn}^2 I_2 I_6$$

$$F^{int.}_{shell}\ (8) = \Big\{(A_{12}+A_{66})\alpha_m\beta_n\Theta l u_{mn} + \Big[(\frac{A_{22}}{R}+\frac{D_{22}}{R^3})\beta_n^2 + (A_{66}+\frac{D_{66}}{R^2})\alpha_m^2 R\Big]\Theta l v_{mn}$$

$$+ \Big[\frac{A_{22}}{R} + \beta_n^2\frac{D_{22}}{R^3} + \alpha_m^2\frac{(D_{12}+2D_{66})}{R}\Big]\beta_n\Theta l w_{mn} + (\frac{A_{12}}{R}\alpha_m u_m - A_{66}\alpha_m^2 w_m$$

$$+ \frac{A_{22}}{R^2}w_m)(v_n+\beta_n w_n)\Theta l + (\frac{0.5A_{12}}{R}q_0 + \frac{A_{22}}{R^2}l w_0)(v_{mn}+\beta_n w_{mn})\Theta\Big\}\delta_{mp}\delta_{nq}$$

$$+ \sum_{n=1}^{N}\Big\{(\frac{A_{12}}{R}u_{mn} - A_{66}\alpha_m w_{mn})l\alpha_m(v_n+\beta_n w_n) + \frac{A_{22}l}{R^2}\big[(1+\beta_n^2)(w_n v_{mn}$$

$$+v_n w_{mn}) + 2\beta_n(v_n v_{mn} + w_n w_{mn})\big]\Big\}\delta_{mp}I_5 + \sum_{n=1}^{N}\frac{A_{22}}{R^2}\beta_q l(v_n+\beta_n w_n)$$

$$*\,(v_{mn}+\beta_n w_{mn})\delta_{mp}I_3 + \sum_{n=1}^{N}\frac{1.5A_{22}}{R^3}l(v_n+\beta_n w_n)^2(v_{mn}+\beta_n w_{mn})\delta_{mp}I_7$$

$$+ \sum_{m=1}^{M}(\frac{A_{12}}{R}\alpha_m u_m + \frac{A_{22}}{R^2}w_m)(v_{mn}+\beta_n w_{mn})\Theta\delta_{nq}I_1 + \sum_{m=1}^{M}\Big[A_{12}\alpha_m^2\beta_n w_{mn}$$

$$+ \frac{1}{2}(\frac{A_{12}}{R}+\frac{2A_{66}}{R})\alpha_m^2 w_m(v_n+\beta_n w_n) - A_{66}\alpha_m^2 v_{mn} - \frac{A_{66}}{R}\alpha_m\beta_n u_{mn}\Big]\Theta w_m\delta_{nq}I_2$$

$$+ \sum_{m=1}^{M}\frac{1}{2}(\frac{A_{12}}{R}+\frac{2A_{66}}{R})\alpha_m^2\Theta(v_{mn}+\beta_n w_{mn})w_m^2\delta_{nq}I_{11} - \sum_{m=1}^{M}A_{66}\alpha_m\alpha_p\Theta(v_{mn}$$

$$+\beta_n w_{mn})w_m\delta_{nq}I_4 + \sum_{m=1}^{M}\sum_{n=1}^{N}\Big[\frac{A_{12}}{R}\alpha_m u_{mn} + \frac{A_{22}}{R^2}(\beta_n v_{mn} + w_{mn})\Big](v_{mn}$$

C-3

$$F^{int.}_{shell}\ (8)\ cont'd. = +\beta_n w_{mn})I_1 I_5 + \sum_{m=1}^{M}\sum_{n=1}^{N}\frac{0.5A_{22}}{R^2}\beta_q(v_{mn}+\beta_n w_{mn})^2 I_1 I_3 + \sum_{m=1}^{M}\sum_{n=1}^{N}\frac{1.5A_{22}}{R^3}$$

$$*(v_n+\beta_n w_n)(v_{mn}+\beta_n w_{mn})^2 I_1 I_7 + \sum_{m=1}^{M}\sum_{n=1}^{N}\frac{0.5A_{22}}{R^3}(v_{mn}+\beta_n w_{mn})^3 I_7 I_{12}$$

$$+\sum_{m=1}^{M}\sum_{n=1}^{N}\left[(\frac{A_{12}}{R}+\frac{2A_{66}}{R})\alpha_m^2(v_n+\beta_n w_n)w_m - A_{66}\alpha_m^2 v_{mn} - \frac{A_{66}}{R}\alpha_m\beta_n u_{mn}\right]$$

$$*w_{mn}I_2 I_5 + \sum_{m=1}^{M}\sum_{n=1}^{N}0.5A_{12}\alpha_m^2\beta_q w_{mn}^2 I_2 I_6 - \sum_{m=1}^{M}\sum_{n=1}^{N}A_{66}\alpha_m\alpha_p\beta_n w_{mn}^2 I_4 I_5$$

$$+\sum_{m=1}^{M}\sum_{n=1}^{N}\frac{1}{2}(\frac{A_{12}}{R}+\frac{2A_{66}}{R})\alpha_m^2(v_n+\beta_n w_n)w_{mn}^2 I_2 I_8$$

$$+\sum_{m=1}^{M}\sum_{n=1}^{N}(\frac{A_{12}}{R}+\frac{2A_{66}}{R})\alpha_m^2(v_{mn}+\beta_n w_{mn})w_m w_{mn} I_5 I_{11}$$

$$+\sum_{m=1}^{M}\sum_{n=1}^{N}\frac{1}{2}(\frac{A_{12}}{R}+\frac{2A_{66}}{R})\alpha_m^2(v_{mn}+\beta_n w_{mn})w_{mn}^2 I_8 I_{11}$$

$$F^{int.}_{shell}\ (9) = \Big\{A_{12}\alpha_m l u_{mn} + \Big[\frac{A_{22}}{R}+\beta_n^2\frac{D_{22}}{R^3}+\alpha_m^2\frac{(D_{12}+2D_{66})}{R}\Big]\beta_n l v_{mn}$$

$$+\Big[\frac{A_{22}}{R}+\beta_n^4\frac{D_{22}}{R^3}+2\frac{(D_{12}+2D_{66})}{R}\alpha_m^2\beta_n^2+D_{11}\alpha_m^4 R\Big]l w_{mn} + (\frac{0.5A_{12}}{R}q_0$$

$$+\frac{A_{22}}{R^2}l w_0)(v_{mn}+\beta_n w_{mn})\beta_n + (0.5A_{11}q_0 R + A_{12}w_0 l)\alpha_m^2 w_{mn}$$

$$+(\frac{A_{12}}{R}\alpha_m u_m + \frac{A_{22}}{R^2}w_m)(v_n+\beta_n w_n)\beta_n l + A_{12}\alpha_m^2 l(\beta_n v_n + w_n)w_m\Big\}\Theta\delta_{mp}\delta_{nq}$$

$$-\sum_{n=1}^{N}A_{66}\alpha_m^2 l(v_n+\beta_n w_n)v_{mn}I_3\delta_{mp} - \sum_{n=1}^{N}\frac{A_{66}}{R}\alpha_m\beta_n l(v_n+\beta_n w_n)u_{mn}I_3\delta_{mp}$$

$$+\sum_{n=1}^{N}\Big\{\frac{A_{12}}{R}\alpha_m u_{mn}(v_n+\beta_n w_n) + \frac{A_{22}l}{R^2}\big[(1+\beta_n^2)(w_n v_{mn}+v_n w_{mn}) + 2\beta_n$$

$$*(v_n v_{mn}+w_n w_{mn})\big]\Big\}\beta_q l\delta_{mp}I_5 + \sum_{n=1}^{N}\frac{A_{22}l}{R^2}(v_n+\beta_n w_n)(v_{mn}+\beta_n w_{mn})\delta_{mp}I_3$$

$$+\sum_{n=1}^{N}\frac{1.5A_{22}l}{R^3}(v_n+\beta_n w_n)^2(v_{mn}+\beta_n w_{mn})\beta_q\delta_{mp}I_7 + \sum_{n=1}^{N}A_{12}\alpha_m^2 l w_{mn}(\beta_n v_n$$

$$+w_n)\delta_{mp}I_6 + \sum_{n=1}^{N}\frac{1}{2}(\frac{A_{12}}{R}+\frac{2A_{66}}{R})\alpha_m^2 l(v_n+\beta_n w_n)^2 w_m\delta_{mp}I_3 + \sum_{n=1}^{N}\frac{1}{2}(\frac{A_{12}}{R}$$

$F^{int.}_{shell}$ (9) cont'd.

$$= +\frac{2A_{66}}{R})\alpha_m^2 l(v_n+\beta_n w_n)^2 w_{mn}\delta_{mp} I_{17} + \sum_{m=1}^{M}\frac{A_{12}}{R}\alpha_m\beta_n\Theta u_m(v_{mn}+\beta_n w_{mn})\delta_{nq}$$

$$* I_1 + \sum_{m=1}^{M}\Big[A_{12}\alpha_m^2 w_{mn} + \frac{1}{2}(\frac{A_{12}}{R}+\frac{2A_{66}}{R})\alpha_m^2\beta_n w_m(v_n+\beta_n w_n) - A_{66}\alpha_m^2\beta_n v_{mn}$$

$$-\frac{A_{66}}{R}\alpha_m\beta_n^2 u_{mn}\Big]\Theta w_m\delta_{nq} I_2 + \sum_{m=1}^{M} A_{12}\Theta\alpha_m\alpha_p(\beta_n v_{mn}+2w_{mn})w_m\delta_{nq} I_4$$

$$+\sum_{m=1}^{M}\frac{A_{22}}{R^2}\beta_n\Theta w_m(v_{mn}+\beta_n w_{mn})\delta_{nq} I_1 + \sum_{m=1}^{M} 1.5A_{11}\Theta R\alpha_m^3\alpha_p w_m^2 w_{mn}\delta_{nq} I_{13}$$

$$+\sum_{m=1}^{M}\frac{1}{2}(\frac{A_{12}}{R}+\frac{2A_{66}}{R})\alpha_m^2\beta_n\Theta(v_{mn}+\beta_n w_{mn})w_m^2\delta_{nq} I_{11} + \sum_{m=1}^{M} A_{11}\Theta R\alpha_m^2\alpha_p$$

$$*(w_m u_{mn}+u_m w_{mn})\delta_{nq} I_4 + \sum_{m=1}^{M}\sum_{n=1}^{N}\Big[\frac{A_{12}}{R}\alpha_m u_{mn} + \frac{A_{22}}{R^2}(\beta_n v_{mn}+w_{mn})\Big](v_{mn}$$

$$+\beta_n w_{mn})\beta_q I_1 I_5 + \sum_{m=1}^{M}\sum_{n=1}^{N} A_{12}\alpha_m\alpha_p(\beta_n v_{mn}+w_{mn})w_{mn} I_4 I_6 + \sum_{m=1}^{M}\sum_{n=1}^{N}\frac{1.5A_{22}}{R^3}$$

$$*(v_n+\beta_n w_n)(v_{mn}+\beta_n w_{mn})^2\beta_q I_1 I_7 + \sum_{m=1}^{M}\sum_{n=1}^{N}\frac{0.5A_{22}}{R^3}(v_{mn}+\beta_n w_{mn})^3\beta_q I_7 I_{12}$$

$$+\sum_{m=1}^{M}\sum_{n=1}^{N}\Big[(\frac{A_{12}}{R}+\frac{2A_{66}}{R})\alpha_m^2(v_n+\beta_n w_n)w_m - A_{66}\alpha_m^2 v_{mn} - \frac{A_{66}}{R}\alpha_m\beta_n u_{mn}\Big]$$

$$*\beta_q w_{mn} I_2 I_5 + \sum_{m=1}^{M}\sum_{n=1}^{N} 1.5A_{11}\alpha_m^3\alpha_p R w_m w_{mn}^2 I_6 I_{13} + \sum_{m=1}^{M}\sum_{n=1}^{N} 0.5A_{12}\alpha_m^2 w_{mn}^2 I_2 I_6$$

$$+\sum_{m=1}^{M}\sum_{n=1}^{N}\frac{0.5A_{22}}{R^2}(v_{mn}+\beta_n w_{mn})^2 I_1 I_3 + \sum_{m=1}^{M}\sum_{n=1}^{N} 0.5A_{11}\alpha_m^3\alpha_p R w_{mn}^3 I_{13} I_{18}$$

$$+\sum_{m=1}^{M}\sum_{n=1}^{N} A_{11}\alpha_m^2\alpha_p R u_{mn} w_{mn} I_4 I_6 - \sum_{m=1}^{M}\sum_{n=1}^{N}\frac{A_{66}}{R}\alpha_p\beta_n(v_{mn}+\beta_n w_{mn})u_{mn} I_3 I_4$$

$$+\sum_{m=1}^{M}\sum_{n=1}^{N}(\frac{A_{12}}{R}+\frac{2A_{66}}{R})\alpha_m^2(v_{mn}+\beta_n w_{mn})w_m w_{mn}\beta_q I_5 I_{11} - \sum_{m=1}^{M}\sum_{n=1}^{N} A_{66}\alpha_m\alpha_p$$

$$*(v_{mn}+\beta_n w_{mn})v_{mn} I_3 I_4 + \sum_{m=1}^{M}\sum_{n=1}^{N}\frac{1}{2}(\frac{A_{12}}{R}+\frac{2A_{66}}{R})\alpha_m^2(v_n+\beta_n w_n)w_{mn}^2\beta_q I_2 I_8$$

$$+\sum_{m=1}^{M}\sum_{n=1}^{N}(\frac{A_{12}}{R}+\frac{2A_{66}}{R})\alpha_m\alpha_p(v_n+\beta_n w_n)(v_{mn}+\beta_n w_{mn})w_m I_3 I_4$$

$$
\begin{aligned}
F^{int.}_{shell}\ (9) \\ cont'd.
&= +\sum_{m=1}^{M}\sum_{n=1}^{N}\frac{1}{2}\left(\frac{A_{12}}{R}+\frac{2A_{66}}{R}\right)\alpha_m\alpha_p(v_{mn}+\beta_n w_{mn})^2 w_m I_3 I_{15} \\
&\quad+\sum_{m=1}^{M}\sum_{n=1}^{N}\left(\frac{A_{12}}{R}+\frac{2A_{66}}{R}\right)\alpha_m\alpha_p(v_n+\beta_n w_n)(v_{mn}+\beta_n w_{mn})w_{mn} I_4 I_{17} \\
&\quad+\sum_{m=1}^{M}\sum_{n=1}^{N}\frac{1}{2}\left(\frac{A_{12}}{R}+\frac{2A_{66}}{R}\right)\alpha_m\alpha_p(v_{mn}+\beta_n w_{mn})^2 w_{mn} I_{15} I_{17} \\
&\quad+\sum_{m=1}^{M}\sum_{n=1}^{N}\frac{1}{2}\left(\frac{A_{12}}{R}+\frac{2A_{66}}{R}\right)(v_{mn}+\beta_n w_{mn})\alpha_m^2 w_{mn}^2\beta_q I_8 I_{11},
\end{aligned}
$$

and the elements of $[F^{ext.}_{shell}]$ are given by

$$
\begin{aligned}
F^{ext.}_{shell}\ (1) &= (R+w_0)^2\Theta+\sum_{m=1}^{M}\frac{1}{2}\Theta w_m^2+\sum_{n=1}^{N}\frac{1}{2}\Theta(v_n^2+w_n^2)+\sum_{n=1}^{N}\Theta\beta_n v_n w_n \\
&\quad+\sum_{m=1}^{M}\sum_{n=1}^{N}\frac{1}{4}\Theta(v_{mn}^2+w_{mn}^2)+\sum_{m=1}^{M}\sum_{n=1}^{N}\frac{1}{2}\Theta\beta_n v_{mn} w_{mn} \\
F^{ext.}_{shell}\ (2) &= 4(R+w_0)\Theta l+2(R+w_0)\Theta q_0+\sum_{m=1}^{M}2\alpha_m\Theta l u_m w_m+\sum_{m=1}^{M}\sum_{n=1}^{N}\alpha_m\Theta l u_{mn} w_{mn} \\
F^{ext.}_{shell}\ (3) &= 2(R+w_0)\alpha_m\Theta l w_m\delta_{mp}+\sum_{m=1}^{M}\alpha_p\Theta w_m^2 I_1+\sum_{n=1}^{N}\alpha_m\Theta l(v_n+\beta_n w_n)v_{mn}\delta_{mp} \\
&\quad+\sum_{n=1}^{N}\alpha_m\Theta l(\beta_n v_n+w_n)w_{mn}\delta_{mp}+\sum_{m=1}^{M}\sum_{n=1}^{N}\frac{1}{2}\alpha_p\Theta(v_{mn}^2+w_{mn}^2)I_1 \\
&\quad+\sum_{m=1}^{M}\sum_{n=1}^{N}\frac{2}{3}\alpha_m\beta_n\Theta v_{mn} w_{mn} I_4+\sum_{m=1}^{M}\sum_{n=1}^{N}\frac{2}{3}\alpha_p\beta_n\Theta v_{mn} w_{mn} I_1 \\
F^{ext.}_{shell}\ (4) &= 2(R+w_0)\alpha_m\Theta l u_m\delta_{mp}+(2l+q_0)\Theta w_m\delta_{mp}+\sum_{m=1}^{M}2\alpha_m\Theta u_m w_m I_1 \\
&\quad+\sum_{n=1}^{N}\alpha_m\Theta l(\beta_n v_n+w_n)u_{mn}\delta_{mp}+\sum_{m=1}^{M}\sum_{n=1}^{N}\alpha_m\Theta u_{mn} w_{mn} I_1 \\
&\quad+\sum_{m=1}^{M}\sum_{n=1}^{N}\frac{1}{3}\Theta\beta_n\left[\alpha_m(I_1-I_2)+2\alpha_p I_4\right]u_{mn} v_{mn}
\end{aligned}
$$

$$F^{ext.}_{shell}\ (5) = (2l+q_0)(v_n+\beta_n w_n)\Theta\delta_{nq} + \sum_{m=1}^{M}\alpha_m\Theta l\beta_n w_m u_{mn}\delta_{nq} + \sum_{m=1}^{M}\sum_{n=1}^{N}\alpha_m l u_{mn}v_{mn}I_5$$
$$+ \sum_{m=1}^{M}\alpha_m\Theta l(v_{mn}+\beta_n w_{mn})u_m\delta_{nq} + \sum_{m=1}^{M}\sum_{n=1}^{N}\frac{2}{3}\alpha_m l(\beta_n I_5+\beta_q I_6)u_{mn}w_{mn}$$

$$F^{ext.}_{shell}\ (6) = (2l+q_0)(\beta_n v_n+w_n)\Theta\delta_{nq} + \sum_{m=1}^{M}\alpha_m\Theta l w_m u_{mn}\delta_{nq}$$
$$+ \sum_{m=1}^{M}\alpha_m\Theta l(\beta_n v_{mn}+w_{mn})u_m\delta_{nq} + \sum_{m=1}^{M}\sum_{n=1}^{N}\alpha_m l u_{mn}w_{mn}I_6$$
$$+ \sum_{m=1}^{M}\sum_{n=1}^{N}\frac{1}{3}\alpha_m l\left[\beta_n(I_6-I_3)+2\beta_q I_5\right]u_{mn}v_{mn}$$

$$F^{ext.}_{shell}\ (7) = (R+w_0)\alpha_m\Theta l w_{mn}\delta_{mp}\delta_{nq} + (\beta_n v_n+w_n)\alpha_m\Theta l w_m\delta_{mp}\delta_{nq}$$
$$+ \sum_{m=1}^{M}\alpha_p\Theta w_m w_{mn}I_1\delta_{nq} + \sum_{m=1}^{M}\frac{1}{3}\beta_n\Theta(\alpha_m I_4+\alpha_p I_1)w_m v_{mn}\delta_{nq}$$
$$+ \sum_{n=1}^{N}\alpha_m l w_n w_{mn}I_6\delta_{mp} + \sum_{n=1}^{N}\frac{1}{3}\alpha_m l(\beta_n I_6-\beta_q I_5)w_n v_{mn}\delta_{mp}$$
$$+ \sum_{n=1}^{N}\alpha_m l v_n v_{mn}I_3\delta_{mp} + \sum_{n=1}^{N}\frac{2}{3}\alpha_m\beta_n l(w_n v_{mn}I_3+v_n w_{mn}I_6)\delta_{mp}$$
$$+ \sum_{n=1}^{N}\frac{1}{3}\alpha_m l(\beta_n I_3+\beta_q I_5)v_n w_{mn}\delta_{mp} + \sum_{m=1}^{M}\sum_{n=1}^{N}\frac{1}{2}\alpha_p(v^2_{mn}I_3+w^2_{mn}I_6)I_1$$
$$+ \sum_{m=1}^{M}\sum_{n=1}^{N}\frac{1}{3}\beta_n(\alpha_m I_4+\alpha_p I_1)(I_3+I_6)v_{mn}w_{mn}$$

$$F^{ext.}_{shell}\ (8) = (v_n+\beta_n w_n)\alpha_m\Theta l u_m\delta_{mp}\delta_{nq} + (v_{mn}+\beta_n w_{mn})\Theta l\delta_{mp}\delta_{nq}$$
$$+ \frac{1}{2}\Theta(v_{mn}+\beta_n w_{mn})q_0\delta_{mp}\delta_{nq} + \sum_{n=1}^{N}\alpha_m l v_n u_{mn}I_5\delta_{mp}$$
$$+ \sum_{m=1}^{M}\alpha_m\Theta u_m v_{mn}I_1\delta_{nq} + \sum_{m=1}^{M}\frac{1}{3}\beta_n\Theta(\alpha_m I_2+\alpha_p I_4)u_m w_{mn}\delta_{nq}$$
$$+ \sum_{m=1}^{M}\frac{2}{3}\alpha_m\beta_n\Theta w_m u_{mn}I_2\delta_{nq} + \sum_{m=1}^{M}\frac{1}{3}\beta_n\Theta(\alpha_m I_1-\alpha_p I_4)w_m u_{mn}\delta_{nq}$$
$$+ \sum_{m=1}^{M}\frac{2}{3}\alpha_m\beta_n\Theta u_m w_{mn}I_1\delta_{nq} + \sum_{n=1}^{N}\frac{1}{3}\alpha_m l(\beta_n I_5+\beta_q I_6)w_n u_{mn}\delta_{mp}$$
$$+ \sum_{m=1}^{M}\sum_{n=1}^{N}\alpha_m u_{mn}v_{mn}I_1I_5 + \sum_{m=1}^{M}\sum_{n=1}^{N}\frac{1}{3}\alpha_m(\beta_n I_5+\beta_q I_6)(I_1+I_2)u_{mn}w_{mn}$$

$$
\begin{aligned}
F^{ext.}_{shell}\ (9) =& (\beta_n v_n + w_n)\alpha_m \Theta l u_m \delta_{mp}\delta_{nq} + (\beta_n v_{mn} + w_{mn})\Theta l \delta_{mp}\delta_{nq} \\
&+ \frac{1}{2}\Theta(\beta_n v_{mn} + w_{mn}) q_0 \delta_{mp}\delta_{nq} + (R + w_0)\alpha_m \Theta l u_{mn}\delta_{mp}\delta_{nq} \\
&+ \sum_{m=1}^{M} \alpha_m \Theta u_m w_{mn} I_1 \delta_{nq} + \sum_{m=1}^{M} \frac{1}{3}\beta_n \Theta(\alpha_m I_2 + \alpha_p I_4) u_m v_{mn}\delta_{nq} \\
&+ \sum_{m=1}^{M} \frac{2}{3}\alpha_m \beta_n \Theta u_m v_{mn} I_1 \delta_{nq} + \sum_{n=1}^{N} \frac{1}{3}\alpha_m l(\beta_n I_3 + \beta_q I_5) v_n u_{mn}\delta_{mp} \\
&+ \sum_{m=1}^{M} \alpha_m \Theta w_m u_{mn} I_1 \delta_{nq} + \sum_{n=1}^{N} \frac{2}{3}\alpha_m \beta_n l v_n u_{mn} I_6 \delta_{mp} + \sum_{n=1}^{N} \alpha_m l w_n u_{mn} I_6 \delta_{mp} \\
&+ \sum_{m=1}^{M}\sum_{n=1}^{N} \frac{1}{3}\beta_n(\alpha_m I_2 + \alpha_p I_4) u_{mn} v_{mn} I_3 + \sum_{m=1}^{M}\sum_{n=1}^{N} \alpha_m u_{mn} w_{mn} I_1 I_6 \\
&+ \sum_{m=1}^{M}\sum_{n=1}^{N} \frac{1}{3}\beta_n(\alpha_m I_1 + \alpha_p I_4) u_{mn} v_{mn} I_6 + \sum_{m=1}^{M}\sum_{n=1}^{N} \frac{1}{3}\alpha_m \beta_q (I_1 + I_2) u_{mn} v_{mn} I_5
\end{aligned}
$$

Elements of $(2M+1)\times 1$ residual force subvector $[R_{str}(\hat{u_{str}})]$

$$
R_{str}\ (1) = \frac{(EA)_s}{2l} q_1 + \sum_{m=1}^{M} 0.25(EA)_s \alpha_m^2 w_{sm}^2
$$

$$
R_{str}\ (2) = (EA)_s \alpha_m^2 l u_{sm}\delta_{mp} + \sum_{m=1}^{M} 0.5(EA)_s \alpha_m^2 \alpha_p w_{sm}^2 I_2
$$

$$
\begin{aligned}
R_{str}\ (3) =& \left[0.5(EA)_s q_1 + (EI)_s \alpha_m^2 l\right]\alpha_m^2 w_{sm}\delta_{mp} + \sum_{m=1}^{M} 0.5(EA)_s \alpha_m^3 \alpha_p w_{sm}^3 I_{13} \\
&+ \sum_{m=1}^{M} (EA)_s \alpha_m^2 \alpha_p u_{sm} w_{sm} I_4
\end{aligned}
$$

Elements of $(2N+1)\times 1$ residual force subvector $[R_r(\hat{u}_r)]$

$$R_r\ (1) = 2\frac{(EA)_r}{R_0}\Theta w_{r0} + \sum_{n=1}^{N}\frac{(EA)_r}{2R_0^2}\Theta(v_{rn}+\beta_n w_{rn})^2$$

$$\begin{aligned}R_r\ (2) =& \Big[\frac{(EA)_r}{R_0}+\frac{(EI)_r}{R_0^3}\Big]\beta_n^2\Theta v_{rn}\delta_{nq} + \Big[\frac{(EA)_r}{R_0}+\beta_n^2\frac{(EI)_r}{R_0^3}\Big]\beta_n\Theta w_{rn}\delta_{nq}\\ &+\frac{(EA)_r}{R_0^2}\Theta(v_{rn}+\beta_n w_{rn})w_{r0}\delta_{nq} + \sum_{n=1}^{N}\frac{(EA)_r}{2R_0^2}\beta_q(v_{rn}+\beta_n w_{rn})^2 I_3\\ &+\sum_{n=1}^{N}\frac{(EA)_r}{2R_0^3}(v_{rn}+\beta_n w_{rn})^3 I_7 + \sum_{n=1}^{N}\frac{(EA)_r}{R_0^2}(v_{rn}+\beta_n w_{rn})(\beta_n v_{rn}+w_{rn})I_5\end{aligned}$$

$$\begin{aligned}R_r\ (3) =& \Big[\frac{(EA)_r}{R_0}+\beta_n^2\frac{(EI)_r}{R_0^3}\Big]\beta_n\Theta v_{rn}\delta_{nq} + \Big[\frac{(EA)_r}{R_0}+\beta_n^4\frac{(EI)_r}{R_0^3}\Big]\Theta w_{rn}\delta_{nq}\\ &+\frac{(EA)_r}{R_0^2}\beta_n\Theta(v_{rn}+\beta_n w_{rn})w_{r0}\delta_{nq} + \sum_{n=1}^{N}\frac{(EA)_r}{2R_0^3}\beta_q(v_{rn}+\beta_n w_{rn})^3 I_7\\ &+\sum_{n=1}^{N}\frac{(EA)_r}{2R_0^2}(v_{rn}+\beta_n w_{rn})^2 I_3 + \sum_{n=1}^{N}\frac{(EA)_r}{R_0^2}\beta_q(v_{rn}+\beta_n w_{rn})(\beta_n v_{rn}+w_{rn})I_5\end{aligned}$$

The integrals I_1 to I_{18} in the elements of the residual force subvectors are given by

$$I_1 = \int_{-l}^{l} Cos^2(\alpha_m x)Cos(\alpha_p x)dx$$

$$I_2 = \int_{-l}^{l} Sin^2(\alpha_m x)Cos(\alpha_p x)dx$$

$$I_3 = \int_{-\Theta}^{\Theta} Sin^2(\beta_n\theta)Cos(\beta_q\theta)d\theta$$

$$I_4 = \int_{-l}^{l} Cos(\alpha_m x)Sin(\alpha_m x)Sin(\alpha_p x)dx$$

$$I_5 = \int_{-\Theta}^{\Theta} Cos(\beta_n\theta)Sin(\beta_n\theta)Sin(\beta_q\theta)d\theta$$

$$I_6 = \int_{-\Theta}^{\Theta} Cos^2(\beta_n\theta)Cos(\beta_q\theta)d\theta$$

$$I_7 = \int_{-\Theta}^{\Theta} Sin^3(\beta_n\theta)Sin(\beta_q\theta)d\theta$$

$$I_8 = \int_{-\Theta}^{\Theta} Cos^2(\beta_n\theta)Sin(\beta_n\theta)Sin(\beta_q\theta)d\theta$$

$$I_9 = \int_{-l}^{l} Cos^3(\alpha_m x)dx$$

$$I_{10} = \int_{-l}^{l} Sin^2(\alpha_m x)Cos(\alpha_m x)dx$$

$$I_{11} = \int_{-l}^{l} Sin^2(\alpha_m x)Cos(\alpha_m x)Cos(\alpha_p x)dx$$

$$I_{12} = \int_{-l}^{l} Cos^3(\alpha_m x)Cos(\alpha_p x)dx$$

$$I_{13} = \int_{-l}^{l} Sin^3(\alpha_m x)Sin(\alpha_p x)dx$$

$$I_{14} = \int_{-\Theta}^{+\Theta} Sin^2(\beta_n\theta)Cos(\beta_n\theta)d\theta$$

$$I_{15} = \int_{-l}^{l} Cos^2(\alpha_m x)Sin(\alpha_m x)Sin(\alpha_p x)dx$$

$$I_{16} = \int_{-\Theta}^{\Theta} Cos^3(\beta_n\theta)d\theta$$

$$I_{17} = \int_{-\Theta}^{\Theta} Sin^2(\beta_n\theta)Cos(\beta_n\theta)Cos(\beta_q\theta)d\theta$$

$$I_{18} = \int_{-\Theta}^{\Theta} Cos^3(\beta_n\theta)Cos(\beta_q\theta)d\theta$$